THE INVESTIGATION OF OSCILLATORY CHANGES IN THE VISUAL CORTEX USING SYNTHETIC APERTURE MAGNETOMETRY

IAN FAWCETT

Doctor of Philosophy

ASTON UNIVERSITY

September 2004

ASTON UNIVERSITY

THE INVESTIGATION OF OSCILLATORY CHANGES IN THE VISUAL CORTEX USING SYNTHETIC APERTURE MAGNETOMETRY

IAN FAWCETT

Doctor of Philosophy

2004

This thesis is an exploration of the oscillatory changes occurring in the visual cortex as measured by a functional imaging technique known as Synthetic Aperture Magnetometry (SAM), and how these compare to the BOLD response, across a number of different experimental paradigms.
In chapter one the anatomy and physiology of the visual pathways and cortex are outlined, introducing the reader to structures and terms used throughout the thesis whilst chapter two introduces both the technology and analysis techniques required to record MEG and fMRI and also outlines the theory behind SAM. In chapter three the temporal frequency tuning of both striate and extrastriate cortex is investigated, showing fundamental differences in both tuning characteristics and oscillatory power changes between the two areas. Chapter four introduces the concept of implied-motion and investigates the role of area V5 / MT in the perception of such stimuli and shows, for the first time, the temporal evolution of the response in this area. Similarly a close link is shown between the early evoked potential, produced by the stimulus, and previous BOLD responses. Chapter five investigates the modulation of cortical oscillations to both shifts in attention and varying stimulus contrast. It shows that there are both induced and evoked modulation changes with attention, consistent with areas previously known to show BOLD responses. Chapter six involves a direct comparison of cortical oscillatory changes with those of the BOLD response in relation to the parametric variation of a motion coherence stimulus. It is shown that various cortical areas show a linear BOLD response to motion coherence and, for the first time, that both induced oscillatory and evoked activity also vary linearly in areas coincidental with the BOLD response. The final chapter is a summary of the main conclusions and suggests further work.

Keywords: Synthetic Aperture Magnetometry (SAM); visual cortex; BOLD; temporal frequency tuning; implied-motion; motion coherence; attentional modulation

Acknowledgements

The work in this thesis was carried out by the author with the following exceptions:

Chapter 2: Figure 2-13. is an adaptation from a handout by Dr Gareth Barnes

Chapter 3: The programming of the visual stimulus was performed by Dr K.D. Singh.

Chapter 5: The stimulus used was an adaptation of one supplied by Dr A.Williams, Royal Holloway College, University of London.

Chapter 6: The stimulus used in the fMRI and MEG experiment was programmed by Dr K.D. Singh. The setting up of the event related fMRI design was assisted by Dr K.D. Singh. The linear analysis program was devised by Dr K.D. Singh.

Signed:

This thesis would not have reached fruition without the assistance of a number of people:

To my supervisor, Dr Krish Singh, who was brave enough to take me on as a very mature student and has always been there with assistance, words of wisdom and computer programming skills when required. Similarly I would like to thank the Neuroscience Research Institute at Aston University who provided the maintenance grant that helped to fund my way through this research.

My journey into neuroscience has relied on the invaluable support of the MEG team at Aston University. Particular thanks go to Dr Gareth Barnes and Dr Arjan Hillebrand who have written scripts and provided support to assist the countless hours of analysis that have gone into the work detailed in this thesis.

To my fellow postgraduate students, I have enjoyed your friendship over the past three years and hope that our paths continue to cross in the coming years.

Last, but most definitely not least, to my wife. Kay, you have given me the financial and emotional support to make this thesis a reality. Throughout the past three years you have experienced my highs and lows, my insecurities and my anxieties but have always been there with uplifting words of support. I will never forget what you have allowed me to achieve and am forever in your debt. I promise, now that this thesis is written, that all those DIY jobs around the house will be completed, that we will rekindle our social life and most importantly of all have a holiday.

TABLE OF CONTENTS

FIGURES

Chapter 1

Chapter 2

Chapter 3

Chapter 4

Chapter 5

Chapter 6

TABLES

1. THE ANATOMY AND PHYSIOLOGY OF THE VISUAL SYSTEM

1.1 Overview

Chapter one is a basic introduction to the human visual system. It begins with a description of the anatomy and physiology of the visual structures that are initially encountered by signals as they enter the visual system on route to the visual cortex; the retina and lateral geniculate nucleus (LGN) and explains how the light received by the eye is converted to electrical signals and conducted to the brain. The anatomy and physiology of the primary visual cortex and extrastriate visual areas is then described, including details of their cellular arrangements, psychophysical properties and projections to other areas. The chapter continues with an introduction to the magnocellular and parvocellular pathways and ends with an overview of the visual motion system.

The aim of this chapter is to provide an overview of the structure of the human visual system and introduce the reader to terms used in the experimental chapters.

1.2 Introduction

Vision is the dominant sense in humans and other primates, with approximately 30% of the cortical surface representing information that is predominantly visual. The human visual system is designed to take information from the environment in the form of light and then analyse and interpret it so that we see a three-dimensional, moving, colour panorama within our field of view. What is remarkable about this feat is how seemingly simple the brain makes this incredibly complex task appear. This process of visual perception involves the complex interaction of many structures that are organised into hierarchical and parallel systems.

1.3 The Retina

The retina is a thin layer (100 to 250μm) of neurons and glial cells on the posterior inner surface of the eyeball. Although lying in the periphery of the body the retina is classed as a part of the central nervous system, developing as an extension of the diencepalon during early maturation of the nervous system. It is a highly organised structure consisting of multiple layers of cell bodies and synaptic interactions. The retina is not simply a passive receiver of information, in the form of light, but selectively processes the visual signals before the information is sent to the brain where it is further analysed as part of the process of conscious perception.

1.3.1 The histological structure of the Retina

The synaptic organisation of the retina contains five major classes of neurones (see Figure 1-1A); photoreceptors (rods and cones), bipolar cells, horizontal cells, amacrine cells and ganglion cells. As with many components of the visual system the retina has a laminated structure with neurons of a particular type and function being located together (see Figure 1-1B). The structural layout of the retina is not immediately intuitive as the light sensitive photoreceptors are located in the outer layers (located deep in the retina itself) meaning that light has to pass through the retinal layers that contain the projection neurons and interneurons before reaching the rods and cones (see Figure 1-1B). However, at the fovea the interneurons and ganglion cells are displaced exposing the photoreceptors directly to visual stimulation and thus optimising the visual image obtained.

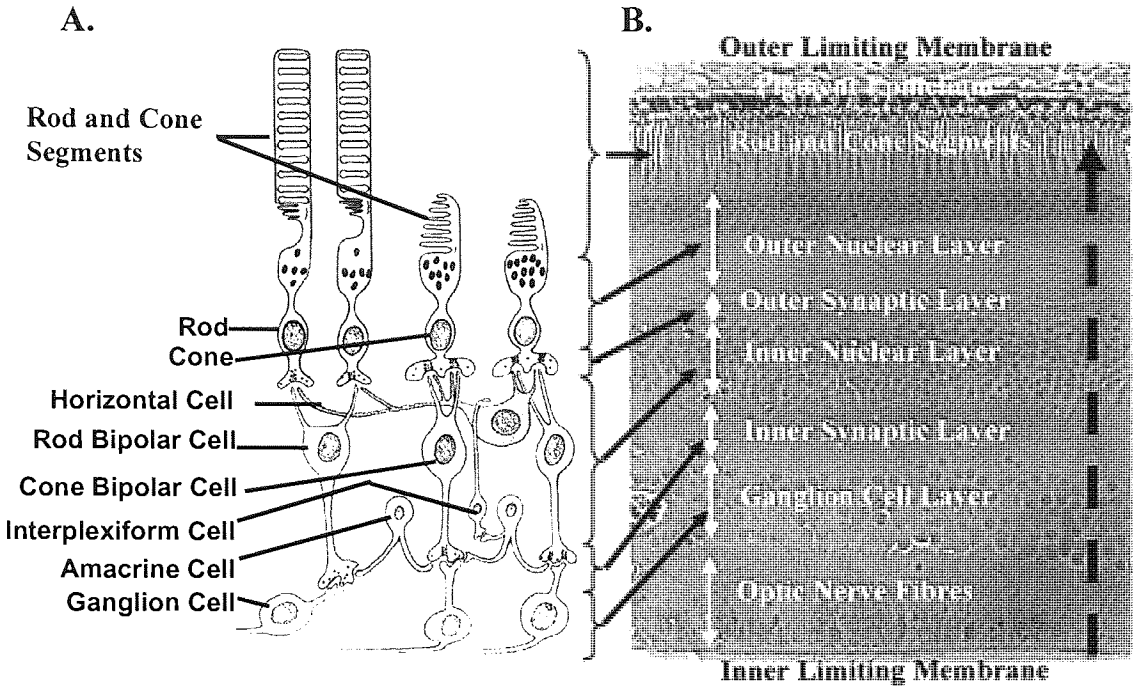

Figure 1-1. The histology of the retina. A). Schematic representation of the cellular structure and connectivity within the retina. B). A transverse section through the retina showing the laminated structure. The dashed black line indicates the direction of light through the retina when it first enters the eye. The black arrows from A) to B) indicate the layers in which the particular retinal cells are found. Adapted from Martin 2000.

1.3.2 The laminations of the retina

The retina contains five principle layers (see Figure 1-1) with cell bodies being found in three layers and synapses in two. The outer nuclear layer contains the cell bodies of the photoreceptors whilst the connections between the photoreceptors and the retinal interneurons are made in the outer synaptic layer. Similarly the inner nuclear layer contains the cell bodies of the retinal interneurons; bipolar, horizontal and amacrine cells and the inner synaptic layer is where synapses occur between the bipolar cells and the ganglion cells. Finally the cells that produce the retinal output are found in the ganglion cell layer where the ganglion cell axons collect along the inner retinal surface. These axons are initially unmyelinated thus increasing the transparency of the retina to light passing through to the deeper photoreceptors, although as they leave the eye at the optic disk to form the optic nerve they become myelinated.

1.3.3 The function of retinal cells

There are both vertical and lateral pathways within the retinal cell structure. The photoreceptors, bipolar and ganglion cells provide direct vertical communication with one another while horizontal and amacrine cells provide lateral communication across the retina between the different cell types. Below is an outline of the function of the various retinal cells.

1.3.3.1 Photoreceptors

There are two types of detector in the retina which enable detection of light over the full range of environmental wavelengths and intensities. The human retina consists of an average of 57.4 million rods and 3.3 million cones. When light strikes the photoreceptor cells, energy is transferred from photons to photopigments. The absorption of light by the latter causes hyperpolarisation of the cell membrane leading to an electrical impulse that begins the chain of neural events that ends with the perception of an image in the brain. Furthermore, unlike neurons in the central nervous system whose action potentials occur as all-or-none phenomena, the impulses of the retinal neurons are graded slow potentials that depend upon stimulus properties such as luminance, colour, and shape.

1.3.3.1.1 Cones

These are densest in the fovea where they number approximately 200,000 per square mm although this density falls off rapidly with distance from the fovea. Cones are the photoreceptors that mediate high visual acuity and colour vision which occurs due to the presence of trichromatic pigments. Each type of cone contains one of three different

iodopsin molecules that absorbs light at three distinct wavelengths; short wavelength, or S, cones absorb light in the blue spectrum (440nm), medium wavelength, or M, cones absorb light in the green spectrum (540nm) and long wavelength, or L, cones absorb light in the red spectrum (577nm). The cones are capable of responding rapidly to stimulation and consequently can detect flicker changes up to 55Hz meaning that the cone system has a far higher temporal resolution than the rod system (Dowling 1987).

1.3.3.1.2 Rods

Rods are absent in the fovea but predominate around the peripheral retina where the maximum density is approximately 175,000 per square mm. They contain rhodopsin and are optimally suited for detecting low level illumination although as they contain no colour pigments they play no role in colour vision. Rods have a poor resolution of temporal frequency being unable to resolve flicker frequencies greater than 12Hz.

1.3.3.2 Bipolar Cells

Bipolar cells link photoreceptor cells with ganglion cells. The term bipolar refers to the fact that the cell body is situated between the dendritic end and the axon terminal end (see Figure 1-1) . Nine types of bipolar cell have been classified in accordance with their morphology and synaptic connectivity (Kolb *et al.* 1992) although only one type is associated with the rod photoreceptor with the rest being associated with cone function. Cone bipolar cells receive direct synaptic input from only a small number of cone cells thus providing high visual acuity and colour vision whilst rod bipolar cells receive input from many rod cells thus reducing acuity but increasing sensitivity. Thus, the bipolar cells provide an array of parallel channels that conduct information from the photoreceptors to the ganglion cells.

1.3.3.3 Horizontal cells

Horizontal cells are the interneurons of the retina, forming a connecting layer between neighbouring photoreceptors (Boycott and Kolb 1973). As the name suggests, unlike bipolar cells that relay information radially through the retina, horizontal cells form a network that integrate the activity of the photoreceptor cells horizontally. The concentration of these cells is maximal at the fovea decreasing towards the periphery of the retina. Their function is to transform the visual information received from the photoreceptors. By synapsing with bipolar cells other than those directly connected to the photoreceptors that stimulated the horizontal cell, these cells play an important role in the complex process of visual integration (Wu 1991, Wu 1994).

1.3.3.4 Amacrine cells

The amacrine cells in the inner retina form the second of the lateral pathways. They form complex pre and post synaptic connections with bipolar cells, ganglion cells and other amacrine cells. They are the most diverse of all the retinal cells with up to 29 different forms of the cell being isolated, reflecting their wide variety of synaptic connections. Due to their complex synaptic links it has been proposed that these cells play an important role in the inhibitory feedback system of the visual pathway (Dowling and Boycott 1966). Recent research suggests that these cells also play a role in differentiating coherent motion across the retina as opposed to the movement of an object against a stationary background (Olveczky *et al.* 2003). Thus the cells regulate the output to the ganglion cells based on the nature of the visual input they receive.

1.3.3.5 Ganglion cells

The neural signals produced by the photoreceptors and modified by the complex synaptic connections of the retina finally reach the ganglion cells. These are the output neurons of the retina and are the last stage of processing before signals are sent to the brain. Ganglion cells receive specific synaptic connections from the bipolar cells such that they form two major pathways, which remain segregated through to the lateral geniculate nucleus (LGN) (Schiller and Malpeli 1977, Schiller *et al.* 1986).

Ganglion cells are multipolar with dendrites that extend horizontally in the retina and radially into the inner plexiform layer. Up to 18 different types of ganglion cell have been isolated (Boycott and Dowling 1969, Kolb *et al.* 1992) although the most important are the midget (Pβ) and the parasol (Pα) types that dominate the primate retina (Polyak 1941). These constitute about 80% and 10% of the total ganglion cells respectively (Watanabe and Rodieck 1989) and differ in the size and the spread of their dendrites (see Figure 1-2).

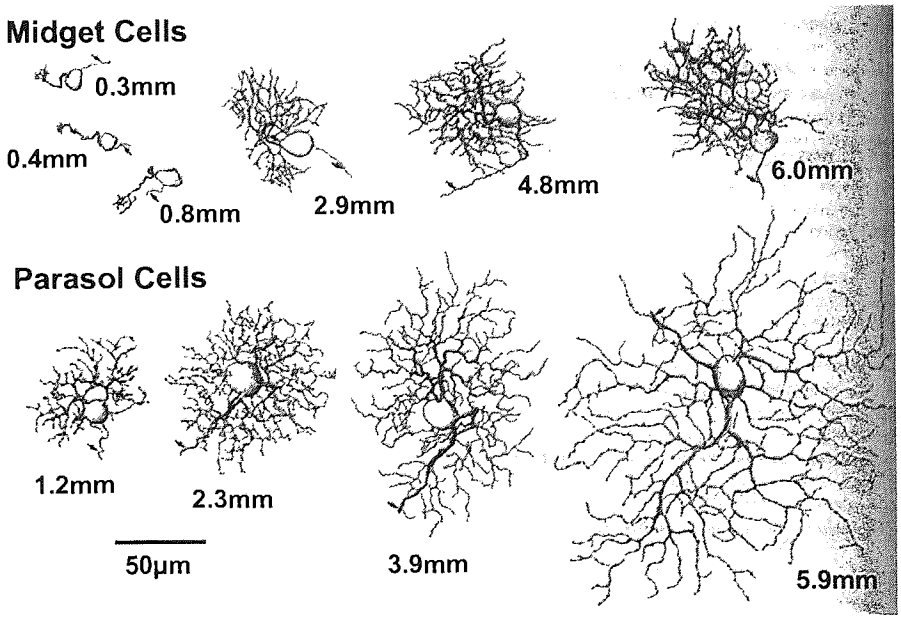

Figure 1-2. Overleaf. Schematic drawings of midget and parasol ganglion cells in the primate retina. Numbers indicate the distance from the fovea. It can be seen that there is an eccentricity dependence on the morphology of ganglion cells. Dendritic diameter of both cell classes increases with distance from the fovea. Modified from Ghosh et al. 1996).

1.3.3.5.1 Centre-surround organisation

Both midget and parasol retinal ganglion cells have a concentric, antagonistic centre-surround organisation (see Figure 1-3B). The receptive field (RF) of the cell is the area of retina over which the impulse activity of that particular cell can be influenced by stimulation. In the fovea of the retina, where visual acuity is greatest, the RF's are smaller with centres that are only a few minutes of arc whilst in the periphery, where acuity is low, the RF's are larger.

Midget cells show a property called colour-opponency (de Montaserio and Gouras 1975). That is the antagonistic centre and surround regions show peak sensitivities that are at different wavelengths meaning that if coloured light fills the whole receptive field the centre and surround are excited differently and the cells response will be a function of the wavelength of the light (see Figure 1-3A). The cells firing will be excited at some frequencies and inhibited at others. The colour-opponent cell therefore carries information about both the wavelength of light and differences in luminance between the centre and surround.

Parasol cells lack colour opponency as the peak sensitivities of their centre and surround are at the same wavelength so that the cells respond weakly to isoluminant monochromatic light but strongly to a difference in luminance between the centre and surround across a broad band of wavelengths. Due to the differences in their responses

to colour stimuli the two types of cells have been termed colour-opponent and broad-band respectively.

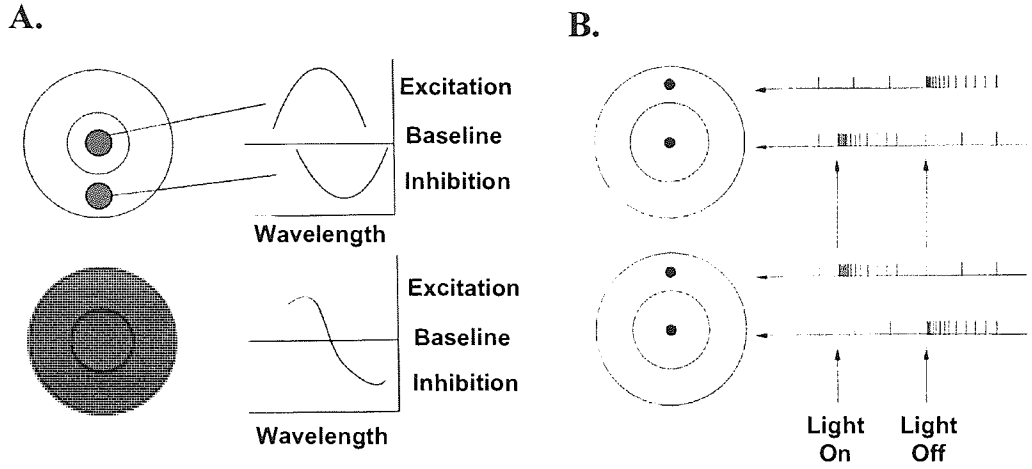

Figure 1-3. A). Top: schematic representation of the response of a colour-opponent retinal ganglion cell to the onset of small spots of light of different wavelengths. The peak excitation by light in the centre of the field, and the peak inhibition by light in the surround, occur at different wavelengths. Bottom: response of the same cell to light filling the receptive field. Excitation occurs at some wavelengths and inhibition at others. B). The response of cat ganglion cells to spots of light. Top: A centre-on cell responds with a burst of impulses to the onset of a spot of light in the centre of its field or to the offset of a spot of light in the surround area. Bottom: a centre-off cell responds in the opposite fashion. Adapted from Bruce et al. 2003.

The centre-surround organisation of the ganglion cells means that they can exhibit two modes of response when stimulated . ON-centre cells are excited (depolarised) when light is directed to the centre of their receptive field, and they are inhibited when light hits their surround. By contrast, OFF-centre cells are inhibited (hyperpolarised) when light is directed to the centre of their receptive field, and are excited when light is directed at their surround. Thus it would appear that the ganglion cells are organised in such a way so as to convert the information from the photoreceptors into information about spatial discontinuities in light patterns (see section 1.4 for a more detailed overview of the on-off pathways).

Each subgroup of ganglion cells projects to a different layer of the LGN and subserves different functional roles: parasol cells play an important role in the perception of fast flicker and motion, whereas the midget cells are important in form and colour perception (Schiller and Logothetis 1990, Schiller *et al.* 1990a, Schiller *et al.* 1990b). The parasol and midget ganglion cells initiate two major channels mentioned previously, the broadband and the colour-opponent channels respectively (Schiller and Logothetis 1990). These pathways project to different laminae of LGN; the broadband cells connect to the magnocellular (M) layers, whereas the colour-opponent pathway projects to the parvocellular (P) layers. For this reason they are also referred to as magnocellular (M) and parvocellular (P) pathways respectively. This however is somewhat misleading as the characteristics of the two channels are influenced at the retinal level and not at the LGN. However the channels will from now on be referred to by their common names of M and P (see section 1.8 for an overview of the functional differences between the M and P pathways). The retinal coverage of the two cell types is the same. It is the lower density of the parasol cells which explains why the spatial resolution of the M system is much lower than the P system and is the case even though the spatial resolution of individual M and P cells are virtually identical (Crook *et al.* 1988).

However, not all ganglion cells fall into these two groups. Some do not have concentric receptive fields but respond to light onset, offset or both in any part of the visual field (de Monasterio and Gouras 1975). Others have colour opponent responses but without a concentric field (de Monasterio 1978). These various types of ganglion cell form a third distinct pathway to the brain known as the koniocellular (K) pathway (Hendry and Reid 2000).

1.3.3.6 Muller cells

Muller cells are the principle neuroglial cells with their nuclei being located in the inner nuclear layer. They play an important role in maintaining the structure and metabolism of the retina. The Muller cells stretch from the inner to the outer limiting membrane (see Figure 1-1B).

1.3.3.7 Pigment Epithelium

The pigment epithelium plays an important role in photoreceptor renewal. Rod segments that are constantly being replaced as part of the normal functional process are removed by this layer. In addition this layer is involved in the recycling of vitamin A as well as the transportation of nutrients and metabolites through the extraretinal-blood barrier.

1.4 On and off pathways in the retina.

A key function in the visual system is that of feature detection. Images that are viewed by the eye are made up of highlights and shadows and the representation of these image features occurs not only as a result of separate sets of ganglion cells but by separate systems of cells throughout the retina.

The photoreceptors are the first neurons to decompose the image into separate parts and this information is differentiated further into its component elements at the synapse with the bipolar cells. There are various bipolar cells that respond to different aspects of the visual signal with some responding to fast fluctuations in the image and some tuned to slower fluctuations in the signal. These kinetic differences in response allow the bipolar

cells to respond to the temporal fluctuations in the visual signal (DeVries 2000). Some bipolar cells are excitatory and others are inhibitory leading to off-centre and on-centre bipolar cell responses. Thus two separate pathways for the detection of shadow and highlights are initiated and these are the beginnings of the on- and the off-centre pathways.

These pathways are maintained through to the ganglion cells. Pioneering work found that there were different classes of ganglion cells; On cells that produce heightened discharges at stimulus onset and maintain a steady stream of impulses whilst the stimulus is present; Off cells that produce discharges at stimulus offset whilst on-off cells produce discharges only at the beginning and end of stimulus presentation (Hartline 1938). These different classes of ganglion cell are bundled together to form the optic nerve which travels to the LGN (see section 1.5). The neurons of the LGN are all on-centre or off-centre types. From here the on-off pathway travels from the LGN to layer 4 of the visual cortex (see section 1.6.2). Here simple and complex cells are found. Simple cells are either on-centre or off-centre types although they contain different receptive field sizes to the ganglion cells (Hubel 1988). The complex cells are often difficult to classify as either on or off types (Hubel 1988, Hubel and Wiesel 1959) and therefore seem to combine signals from both pathways. Thus the on and off emphasis remains distinct through to the early stages of visual cortical processing in the occipital lobe.

1.5 Lateral Geniculate Nucleus (LGN)

The major retinal output exits the eye via the optic nerve and crosses over at the optic chiasm to form the optic tract. Around 10% of retinal ganglion cell outputs enter a

nucleus in the midbrain known as the superior colliculus, which helps to orient the eyes and head to salient stimuli in the environment by combining the visual information from the retina with somatic and auditory information, thus producing a spatial map of the external world. The remainder of the ganglion cell axons terminate in the lateral geniculate nucleus (LGN). Virtually all the outputs from the parasol and midget ganglion cells enter the LGN, with none going to the superior colliculus (Cowey and Perry 1980).

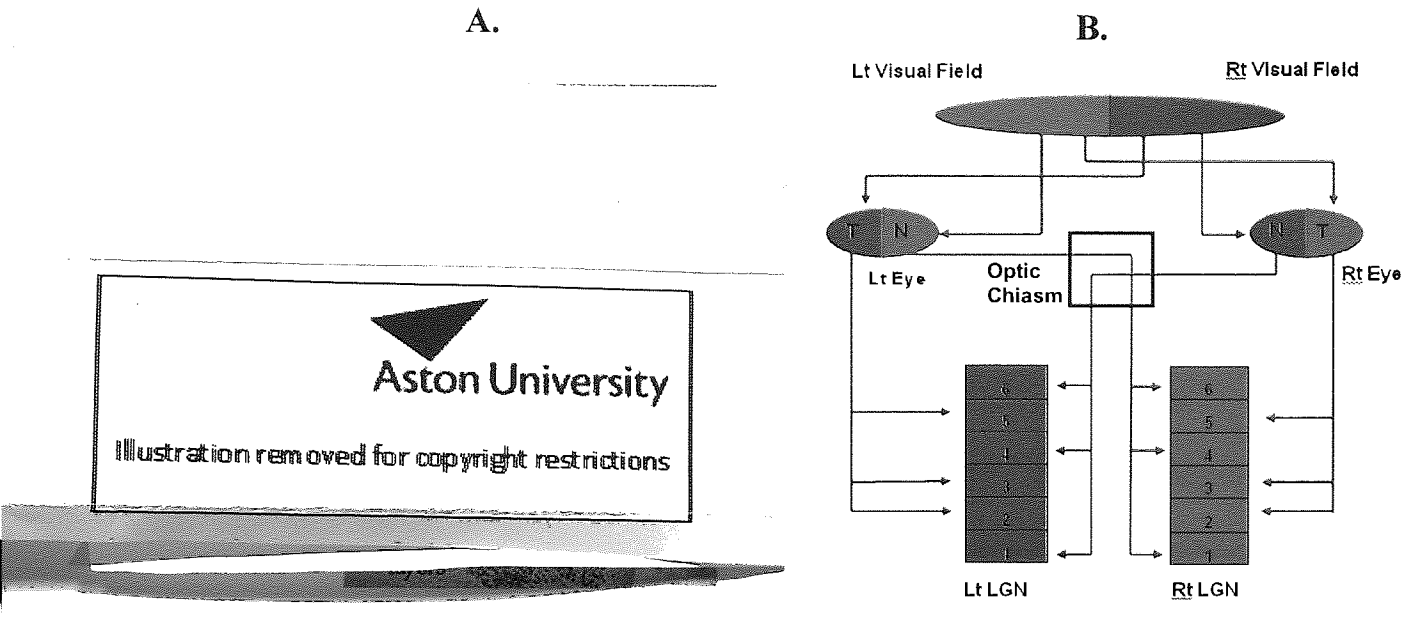

Figure 1-4. A). The parvocellular and magnocellular layers of the lateral geniculate nucleus. The nerve fibres from each eye terminate at different layers. From Merigan and Maunsell 1990. B). A schematic diagram of the LGN showing how the right and left visual fields are represented on the contralateral side. Note how the ipsilateral and the contralateral terminations in each LGN occur in different layers.

The LGN is a complex structure containing six major layers of cells (see Figure 1-4A) which show remarkable specificity of connections with the eyes. Optic nerve fibres coming from the ipsilateral eye (temporal retina) terminate in layers 5, 3 and 2 whilst optic nerve fibres from the contralateral eye (nasal retina) terminate in layers 6, 4 and 1. As information in the ipsilateral temporal retina contains information from the contralateral visual field (see Figure 1-4B) this means that the LGN in each hemisphere contains all the information from the opposite visual field..

The layers of the LGN are stacked in precise registration in terms of retinal representation meaning that there is a very detailed point to point projection from the retina. Adjacent points in the retina project to adjacent points in each layer of the LGN, which means that if a point in layer 6 receives input from a particular point in the left

retina the corresponding point in the layer below will receive information from the same area of the right retina.

The upper four layers of the LGN contain cells with small cell bodies and are therefore termed the parvocellular (P) layers. The two lower layers contain cells with large cell bodies and are termed the magnocellular (M) layers (see section 1.8 for an explanation of the functional disparity between the two types of layers). In addition, the retinal K cells project to six koniocellular layers each just below one of the magno- or parvo-layers and containing cells smaller again than the P cells (Hendry and Reid 2000).

The receptive fields of LGN cells are similar to those of the retinal ganglion cells that drive them (Derrington and Lennie 1984). This would suggest that little further processing takes place in the LGN and that it simply acts as a relay between the retina and the visual cortex. However, a more complex role for the LGN is suggested by the fact that axons also run from the visual cortex back to the LGN. It has been found that the response of pairs of LGN cells are more highly correlated when they are stimulated by a drifting grating that extends over both receptive fields simultaneously than if the receptive fields are stimulated separately by the same stimulus. This effect disappears if feedback from V1 is blocked (Sillito *et al.* 1994) suggesting that feedback from V1 affects the activity of LGN cells which in turn affects the responses to V1. This suggests a role for the LGN in sharpening and amplifying responses in V1.

1.6 The visual cortex

The neurons in all six layers of the LGN send their axons, via the optic radiations, to terminate in the primary visual cortex (V1). The projection from the LGN to the cortex

is in an orderly point to point fashion. Thus the segregation of the visual fields is maintained, with the visual cortex of each hemisphere receiving information from the contralateral eye. Similarly adjacent points in the retina are mapped at adjacent points in the cortex just as they are in the LGN, generating a retinotopic map of visual space in primary visual cortex.

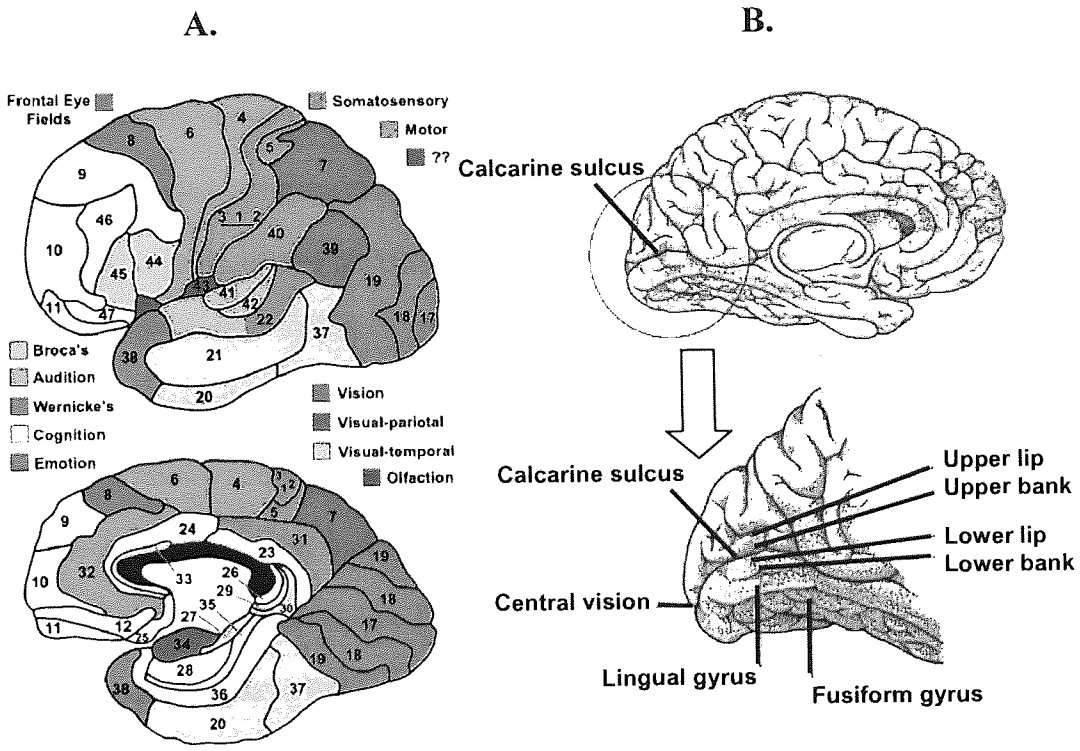

Figure 1-5. A). Illustration showing the different Brodmann areas of the cerebral cortex. The areas are coloured in relation to their function. B). Illustration showing the relative position of the calcarine sulcus. The lower part of the field of view is represented in the upper calcarine cortex and the upper part of the visual field is represented in the lower calcarine sulcus. Central vision is represented at the occipital pole. Adapted from Zeki 1993.

The right striate cortex receives projections (via the LGN) from the left visual hemifield whilst the right hemifield projects to the left striate cortex. Similarly the upper retina, which registers the lower field of view, is represented in the upper lip of the calcarine cortex (see Figure 1-5B) whilst the lower retina, registering the upper field of view, is

represented in the lower lip. This produces a complete topographic map of the retina within the primary visual cortex (Hubel and Wiesel 1977).

1.6.1 Methods of differentiating cellular architecture

Several methods have been used to differentiate the anatomical and functional characteristics of the visual cortex. Firstly, by staining with appropriate agents the cytoarchitecture of the cortex can be revealed whilst myeloarchitecture, a method of studying the patterns of myelination in the cortex, has proved useful in indicating the functional boundaries between areas. Most importantly the differences in metabolic activity can be revealed using the cytochrome oxidase method allowing discrimination of the functional organisation of the striate cortex.

1.6.2 Architecture of primary visual cortex

Much of what is known about the architecture of the visual cortex comes from studies of animals such as the macaque monkey. The primary visual cortex (V1) is a multi-layered structure about 2mm thick that lies at the pole of the occipital lobe and approximately corresponds to Brodmann area 17 (see Figure 1-5A). It has six principle layers, with layer 4 being further subdivided into sublaminae with the cells in the different layers being distinguished by different physiological properties, cellular structure and connections. One of these sublamina contains the stria of Gennari, a dense plexus of myelinated fibres, and it is due to this feature that the area is commonly known as the striate cortex. Much of the striate cortex is buried within the medial surface of the hemisphere in the calcarine sulcus (see Figure 1-5B) with only a small part, located at the occipital pole, being visible from the external surface.

The major projection from the LGN to the visual cortex is to layer 4 with neurons in the magnocellular and parvocellular streams projecting to different sublaminae; the magnocellular system projects primarily to layer 4Cα whilst the parvocellular system projects mainly to layers 4A and 4Cβ (Hendrickson *et al.* 1978, Hubel and Wiesel 1972). Interneurons in the layer 4 sublaminae connect with neurons in superficial and deeper cortical layers which, in turn, distribute visual information to other cortical and subcortical regions. Cells of layer 4Cβ send connections to layers 2 and 3 (Hendry and Yoshioka 1994) whilst layer 4B receives significant input from 4Cα (Felleman and Van Essen 1991) and sends its output to extrastriate areas. Layer 5, which contains less cell bodies compared to the other layers, sends its input back to the superior colliculus whilst layer 6, which is densely populated with cells, sends significant output back to the LGN (Lund 1988).

The primary visual cortex also contains columns running at right angles to the surface (Hubel and Wiesel 1962). Ocular dominance columns receive visual input from either the ipsilateral or contralateral eye, whilst orientation columns contain neurons that are maximally sensitive to simple visual stimuli with similar spatial orientations (Hubel and Wiesel 1977). In addition, there are vertically orientated aggregates of neurons in layers 2 and 3, which although columnar in shape are not thought of as columns as they are only located in the superficial layers of the cortex.

As stated earlier (section 1.5), the LGN in each hemisphere, although receiving data from only one hemifield, contain information from both ipsilateral and contralateral retinas. However, these are segregated in the different layers of the LGN and this segregation of ipsilateral and contralateral neurons is maintained through the

connections to the visual cortex (Casagrande and Kaas 1994). Thus in layer 4, LGN axon terminals transmitting input from one eye alternate with terminals transmitting inputs from the other eye meaning that neurons in layer 4 are therefore monocular, receiving visual input from only one eye. Binocular vision occurs due to the mixing of information from both eyes in neurons located above and below layer 4 and is mediated by the action of cortical interneurons (Freeman and Ohzawa 1990). This blending of information from layer 4 with connections above and below layer 4 forms the anatomical basis of the ocular dominance columns, with any given retinal location in each eye being represented by a pair of these columns.

Distinct from the ocular dominance columns are areas of darkly staining tissue most evident in the upper cortical areas (layers 2 and 3) which consist of cytochrome oxidase blobs (Horton 1984). These blobs are approximately 300μm in diameter separated by lightly stained regions known as interblobs. Although much of the early work was done on monkeys, the findings hold true for human visual cortex although the dimensions of the blobs are different (Horton and Hedley-Whyte 1984, BurkHalter and Bernardo 1989). There is a functional disparity between the blobs and interblobs. Cells in the blobs, unlike the majority of cells in V1, are not orientation specific. About half are wavelength specific whilst the others are broadband, responding to light of all wavelengths without being orientation specific. In contrast the cells of the interblobs are orientation specific without being concerned with the colour of the stimulus (Livingstone and Hubel 1984).

1.6.3 Anatomy of extrastriate areas

Higher-order visual areas are collectively termed the extrastriate cortex because they lack the stripe of Gennari that characterises the primary visual cortex. The existence of these areas was first confirmed by Clare and Bishop 1954 and was expanded on by Hubel and Wiesel 1962 who recorded from the cat's visual cortex and specifically Brodmann areas 18 and 19, which lie adjacent to V1, and found a highly complex variety of cells similar in architecture to V1. This indicated a hierarchical organisation for visual processing. Further studies in many species have shown that the extrastriate cortex comprises a mosaic of visual areas that can be distinguished by several anatomical, functional, and physiological criteria (reviewed by Zeki 1978a, Cowey 1979, Van Essen 1985). Many different visual areas have been identified over the past two decades (Figure 1-6), below is an outline of some of the major areas.

Figure 1-6. Overleaf. A two-dimensional, unfolded map of cerebral cortex in the right hemisphere of the macaque monkey. The coloured regions on the map and on the lateral and medial brain views include 32 visual areas, 25 of which are predominantly or exclusively visual in function while the other 7 are involved in other functions such as polysensory or visuomotor functions. They occupy an estimated 54% of the cerebral neocortex. Taken from Van Essen et al. 1990.

1.6.3.1 Area V2

V2 lies within Brodmann area 18 (see Figure 1-6). Anatomically, as revealed by the cytochrome oxidase architecture, it consists of alternate thick and thin dark stripes, separated from each other by lightly staining, or pale interstripes that run perpendicular to the border between V1 and V2. This structure is unique to area V2 and has important functional implications (see section 1.7.2). The striped regions are relay points for the three major pathways that pass through V1, projecting to different extrastriate areas (Zeki and Shipp 1988, Van Essen *et al.* 1992) and form systems that appear to process distinct types of visual information.

Just as adjacent retinal points connect with adjacent points in V1, resulting in a detailed point-to-point map of the visual scene in the latter, adjacent points in V2 also receive detailed connections from adjacent points in V1, resulting in a detailed topographical map of the visual scene in V2 (Zeki 1969, Cragg 1969). This pattern of connectivity from V1 to V2 is such that the upper field of view, or the lower contralateral retinal quadrant, is mapped in the lower part of V2 while the lower field of view, or the upper contralateral retinal quadrant, is mapped in its upper part (Van Essen and Zeki 1978). In man, much of area V2 lies on the medial surface that surrounds the striate cortex. The part of V2 on which the upper retina (or the lower visual field) is mapped borders the upper lip of the calcarine sulcus. Similarly, the part of V2 on which the lower retina (or the upper visual field) is represented lies on the border of the lingual gyrus.

1.6.3.2 Area V3

Area V3 lies on the medial side of the brain surrounding area V2 and has both a ventral and a dorsal part (see Figure 1-6). In the macaque, V3 lies on the cuneus and the lingual gyrus where the latter represents the upper visual field and the former representing the lower visual field (Van Essen and Zeki 1978). Area V3A extends dorsally across the brain and it shares certain functional characteristics with V3. It does not receive a direct input from V1, but instead it receives strong input from V3 (See section 4.3.2 for further details).

1.6.3.3 Area V4

In the macaque, area V4 is situated on the lateral side of the brain bordering area V3A (see Figure 1-6). The main input into V4 arrives from V2 although it also receives direct input from that region of V1 with foveal representation (Zeki 1978b).

1.6.3.4 Area V5/MT

Lying buried within the superior temporal sulcus on the anterior side of V4 (see Figure 1-6) and extending laterally on the side of the brain is area V5/MT (Dubner and Zeki 1971). It receives direct input from V1 and projects to a number of locations in its immediate surrounding such as the ventral intraparietal sulcus (VIP), middle superior temporal sulcus (MST) and the floor of the superior temporal sulcus (FST). These areas do not have inputs from V1 and share certain physiological characteristics with V5 itself, such as specific response to certain kinds of motion (Dubner and Zeki 1971).

1.7 Physiological and functional characteristics of the visual areas.

As highlighted above the visual cortex is composed of numerous functional areas. Once information reaches the striate cortex it is initially relayed to those cortical areas close

by, which in turn transmit the information to additional cortical areas. These different areas contain a more or less complete representation of the contralateral visual hemifield. In this section the connections between the different functional areas and the characteristics of each functional area are highlighted.

1.7.1 V1

The primary visual cortex receives most of the visual input to the brain and sends parallel outputs to a number of specialised visual areas (Zeki 1978a, Zeki 1978c). Confirmation of the role of V1 in segregating the various kinds of visual information relating to colour, form, motion, and depth has come from a number of anatomical studies (Zeki 1978a, Livingstone and Hubel 1984, Shipp and Zeki 1985a).

Highly specific connections exist between the functionally distinct groups of cells of V1 and V2. In particular, the blobs in layers 2 and 3 of V1 connect to the thin stripes of V2 while layer 4B connects with the thick stripes, and the interblobs connect with interstripes (Livingstone and Hubel 1987a).

1.7.2 V2

V2 receives point-to-point projections from V1 (De Yoe and Van Essen 1985) and consists of three functionally distinct areas. As with the blob cells of V1 and the cells of area V4 to which they project, the thin stripes of V2 are primarily wavelength selective (Shipp and Zeki 1985b). Moreover, as in layer 4B of V1, cells in the thick stripes of V2 to which they connect are also direction as well as orientation selective, whilst the interstripes of V2 are orientation but not wavelength selective as are the interblobs of V1 from which they receive their input (Shipp and Zeki 1985b). Studies

have shown that the thick stripes project to V3 and V5 where cells are predominantly orientation and direction selective respectively (Shipp and Zeki 1985a, De Yoe and Van Essen 1985, Livingstone and Hubel 1987a). Similarly it has been shown that the thin stripes connect with area V4 (Shipp and Zeki 1989a, Shipp and Zeki 1989b).

As with V1, V2 can be thought of as a segregator that sends separate and distinct signals to different specialised areas each of which attends to different attributes of the visual scene (Zeki 1993). Furthermore, since V1 and V2 contain representations of the same submodalities of vision, it can be logically inferred that cells processing particular types of signals in each area are connected with each other in such a way that wavelength selective cells of V1 connect specifically with wavelength selective cells in V2 and so on.

1.7.3 Area V3

V3 has been identified as an area whose cells respond to lines of specific orientation regardless of both the colour of the lines and the colour of the background on which these lines were presented (Zeki 1978c). It has been speculated, that since orientated lines are important components of the form of objects, that V3 is involved in processing of the form of visual stimuli (Zeki 1978c) (see section 4.3.2. for further details).

1.7.4 Area V4

The mapping of the retina in V4 occurs differently to that in all other visual areas. In V4, only the central 40 degrees of retina is mapped which corresponds to the foveal region where the cones required for colour vision are concentrated (Van Essen and Zeki 1978).

Cells in area V4 of the macaque are colour selective (Zeki 1973, Zeki 1977), in that they respond to some wavelengths better than others. V4 contains few cells that are involved in detecting the direction of motion and further studies have confirmed that form, colour, and wavelength selectivity are overwhelmingly emphasised within area V4 (Desimone and Schein 1987). The human homologue of V4 appears to be in the lingual and fusiform gyri (Zeki 1993)

1.7.5 Area V5

It has been found that a region of cortex in the superior temporal sulcus contains an abundance of neurons that are selective for the direction of stimulus motion rather than for colour or form (Dubner and Zeki 1971). This area was first identified in the owl monkey and was referred to as the middle temporal visual area (MT), with its homologue being area V5 in humans (Zeki 1993) and the macaque monkey (Zeki 1983b, Zeki 1983a).

V5/MT was the first visual area whose function was studied in some detail (Zeki 1974). It was found that 90% of the cells in area V5 of the rhesus monkey respond to motion in a particular direction but not to its opposite or a null direction. In other words the majority of cells in area V5 were directionally selective and neither the intensity nor the colour of the spots of light seemed to alter the response of cells in this area. The cell's response depended solely upon the direction of movement within its receptive field independent of other attributes.

The receptive fields of cells in areas V4 and V5 are much larger than cells in V1 or V2 (Maunsell and Van Essen 1983) with recordings from successive cells in V4 and V5 showing that the receptive fields of most cells are in roughly the same region of visual space. This fact, in addition to the large size of receptive fields in these areas, indicates that the retinal maps created in them are not as clear as those in V1 or V2. The maps in V4 and V5 (if they are topographic maps at all) are less precise and represent particular types of activity, namely colour and motion processing that occur in the field of view (Zeki 1993).

1.8 Parallel visual pathways

The idea that the primate visual cortex consists of two separate functional pathways was first suggested by Ungerleider and Mishkin (1982) who described two streams of processing, the M and P pathways, that diverge on exit from V2 with one leading to the temporal lobe and the other to the parietal lobe. As mentioned earlier (section 1.3.3.5), there is now known to be a third major information stream in the primate visual system. The K system has only recently been discovered and far less is known about it than the other streams although it is thought to be involved in colour vision (Hendry and Reid 2000, White *et al.* 2001, Xu *et al.* 2001). As a consequence this review will concentrate on the two major visual streams that have been extensively studied over many years.

The M and P pathways have different destinations in the visual cortex (see Figure 1-7 for clarification). The magnocellular pathway arrives at layer 4Cα of V1 and then projects to layers 4B and 6 from where it leads to the thick stripes of V2 and then to V3 and V5/MT. The parvocellular system subdivides to form two distinct patterns of connectivity. The first of these enters V1 through layer 4Cβ and projects to the

interblobs of layer 2 and 3 then to the pale stripes of V2 and to V4 before finally reaching the inferior temporal cortex (ITC). The second subdivision projects to the blobs of layers 2 and 3 in V1, then to the thin stripes of V2, and then to area V4 and eventually terminating within ITC (Livingstone and Hubel 1988).

Due to their cell properties it has been suggested that the major destination of the P pathway is to the colour and form areas of the visual cortex whereas the M pathway carries motion information (Maunsell and Newsome 1987, Livingstone and Hubel 1988). The parvocellular-interblob system is characterised by a high incidence of orientation selectivity (De Yoe and Van Essen 1988). However, the system also contains many cells that are wavelength selective and is seemingly specialised for the detection of high-resolution static form and shape with the ability to see details of stationary objects and scenes (Merigan and Maunsell 1990). The parvocellular-blob system is characterised by cells that are predominantly wavelength selective meaning that it is specialised for colour but not movement, stereopsis, or shape discrimination (Livingstone and Hubel 1988). Finally, the magnocellular-thick stripe system is characterised by cells that are direction selective but includes many cells that are selective for orientation and disparity. This system is therefore specialised for motion and spatial relationships and contributes to detection of stereoscopic depth. The cells in this pathway are insensitive to colour and therefore respond poorly to borders and contours that are only perceived based on colour contrast (Zeki 1983b).

It has been proposed that the visual system consists of the two M and P pathways with two subdivisions of each thus creating 4 pathways: a motion pathway, a colour pathway, and two form pathways (Zeki 1993). More specifically there exists a motion pathway

(see section 1.9 for more detail) which originates in the parasol (Pα) ganglion cells of the retina and is relayed to the magnocellular layers of the LGN from where it projects to layer 4B of V1 followed by the thick stripes of V2, eventually ending in area V5/MT. The dynamic form pathway also originates in the parasol ganglion cells and passes through the magnocellular division of LGN, projecting to orientation selective cells of layer 4B and from there to area V3, both directly and via the thick stripes of V2. These are both subdivisions of the M pathway. Within this model, the two subdivisions of the P pathway originate in the midget ganglion cells of the retina and pass through the parvocellular layers of LGN and from layer 4C. One feeds the blobs and the other the interblobs of layers 2 and 3 to create a colour pathway and a form pathway respectively. They relay to area V4 both directly and via the thin stripes and interstripes of area V2. The form subdivision of the P pathway is concerned with form in association with colour (Zeki 1993).

The two streams have different visual capabilities: the temporal system analyses the physical properties of a visual scene and is therefore involved in identification of objects and is referred to as the 'what', or the ventral stream because it is thought to lie more ventrally (Schneider 1969, Ungerleider and Mishkin 1982). The parietal stream is believed to be involved in analysing the spatial relationship of objects in a visual scene and is therefore concerned with the position of an object. It is also referred to as the 'where', or the dorsal stream because it is thought to lie dorsally (Schneider 1969, Ungerleider and Mishkin 1982). The differences between the two pathways are outlined in Table 1-1 and summarised in the following sections.

Property	P	M
Clear spectral opponency / selectivity	Yes	No
Luminance contrast gain	Low	High
Receptive field size	Small	Large
Spatial resolution of individual cell	Similar to M	Similar to P
Ganglion cells/mm^2 (Acuity of cell group)	Many (high)	Few (low)
Retinal source	Midget cells	Parasol cells
LGN projection target	Parvocellular	Magnocellular
V1 projection target	Layer 4Cβ	Layer 4Cα
Cell size	Small	Large
Conduction velocity of axons	Low	High
Response to light steps	Tonic	Phasic
Contrast sensitivity at scotopic luminance	Poor	Good
Fraction of LGN population	~80%	~10%

Table 1-1. Summary of the physiological and functional differences between the M and P pathways.

1.8.1 Colour Vision

The receptive field centres of the P pathway ganglion cells receive input from only one cone type whereas the M ganglion cells have a receptive field that receives input from all three cone types. The P cells have small receptive fields and have colour coding properties whilst their colour-opponent organisation means that while the centre may be stimulated by one colour, another activates the surround. This interaction is based on the three types of cone inputs introduced earlier (see section 1.3.3.1.1): the S, M, and L wavelength receptors.

In contrast, M cells have larger receptive fields and do not discriminate colour. The RF centre region of the M cells is believed to receive input from all three types of cone

photoreceptors, whereas the P cells receive their input from only one cone type (Wiesel and Hubel 1966, Gouras 1968). On the other hand, the RF surround of both types of cells receives equal input from all cones (Wassle *et al.* 1989). The RF of M cells is much larger than the P cells, and they are much more sensitive to slight differences in luminance information. The response latencies of these cells also differ from each other; whereas P cells respond in a sustained fashion to the stimulation, the response of the M cells is transient.

The RF properties of single cells at different levels of the visual system suggest that the P channel is involved in colour vision as well as the perception of high spatial frequency patterns, whereas the M system is involved in the perception of motion and low contrast stimuli (Livingstone and Hubel 1987b, Schiller and Logothetis 1990, Schiller *et al.* 1990a).

1.8.2 Visual Acuity

M and P cells differ in the size of their field centres. Although receptive field size increases with distance from the fovea in both classes, at any given eccentricity M cells have larger receptive fields than P cells by a factor of two or three.

1.8.3 Speed

M cells respond faster and more transiently than P cells. Due to this sensitivity to the temporal nature of a stimulus, M cells play an important role in detecting visual motion.

1.8.4 Contrast

M cells are much more sensitive than P cells to low contrast stimuli. M cell responses increase rapidly with increasing contrast and saturate at approximately 10% contrast. P cells, however, respond much more slowly to the contrast of a visual input and saturate at far higher contrasts.

1.9 The Visual motion system

Moving stimuli can be classed according to the spatial characteristics of their defining cues (Cavanagh and Mather 1989). First-order stimuli are those that can be perceived on the basis of their luminance contrast whilst second-order stimuli are perceived through changes in texture, motion or disparity (Schofield 2000, Smith 1994). Experimental work into the detection of visual motion has shown that there are specific neural mechanisms that are tuned to the basic properties of motion such as the direction or speed of a moving object. The most notable property of area MT is the very high proportion of directionally selective cells (Dubner and Zeki 1971).

As mentioned previously the main projection of the LGN is into layer 4C of the striate cortex. The P pathway connects to layer 4Cβ and the M pathway to layer 4Cα (Hubel and Wiesel 1972). Layer 4Cα projects to layer 4b which projects to area MT (Shipp and Zeki 1985a, Shipp and Zeki 1989a). There are also interconnections between layer 4Cα and layer 6 which has connections with MT (Shipp and Zeki 1989a). Layer 4b projects to thick stripes of area V2 which also connect with MT (see Figure 1-7).

The pulvinar is a large nuclear mass in the thalamus. It receives input from the superior colliculus and in turn projects to area MT (Beneveto and Standage 1983). Lesions of

striate cortex have been shown not to completely silence area MT (Rodman *et al.* 1989) although combined lesions of striate cortex and superior colliculus do suppress activity in MT (Rodman *et al.* 1990).

Area V2 contains three architecturally distinct areas that show functional differences based on their inputs from the different layers of the striate cortex. Cells in the thick stripes are selective for disparity, orientation or direction (Zeki 1978d). Studies on the cells of V3 have shown that about 40% of them are selective for orientation or direction (Felleman and Van Essen 1987). More than 90% of the cells are tuned to the speed of the moving stimulus. Both the thick stripes of V2 and V3 project to areas MT, medial superior temporal sulcus, the floor of the superior temporal sulcus and the ventral intraparietal area (see section 4.3.2. for further details about V3)

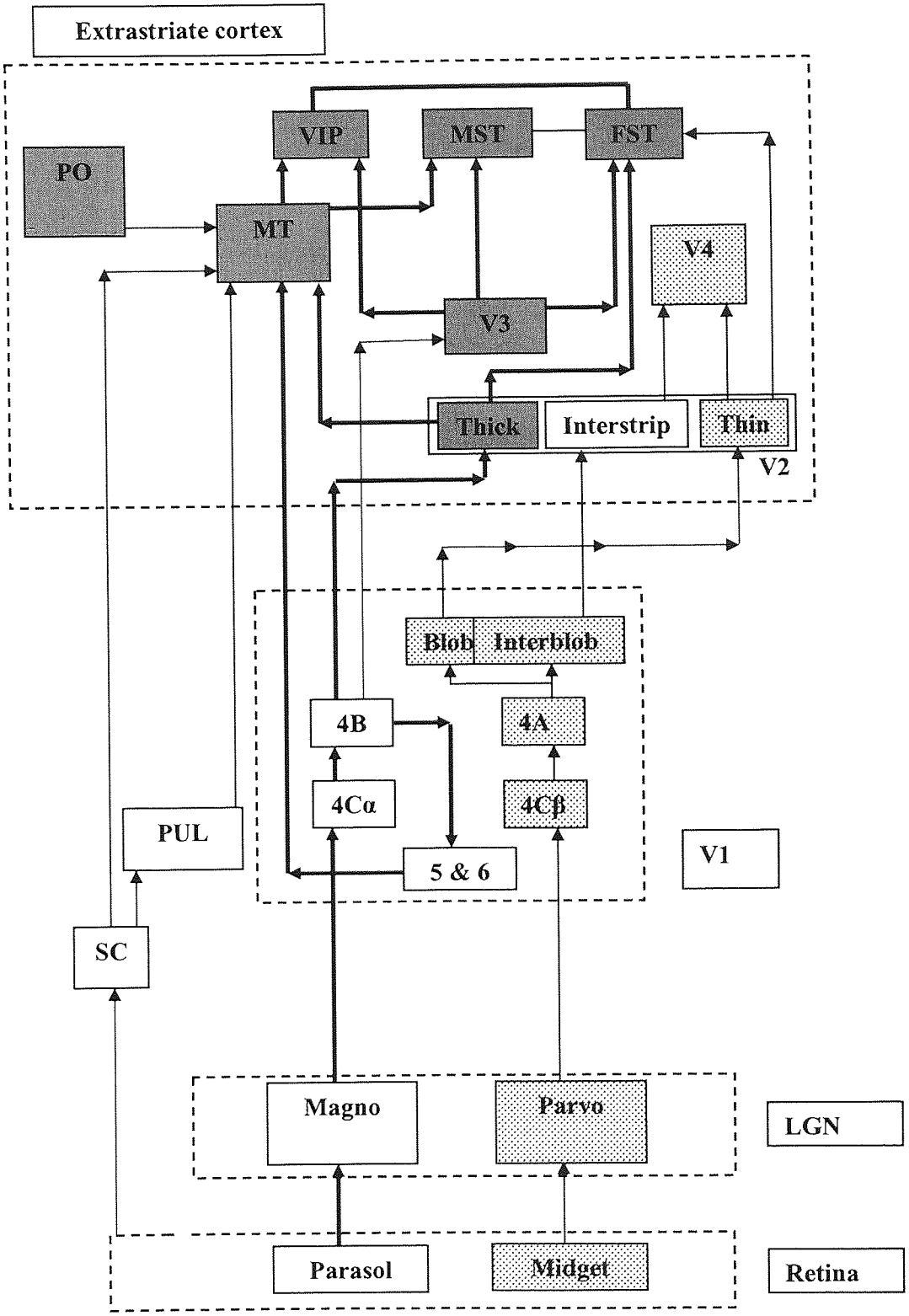
Extrastriate cortex
VIP
MST
FST
PO
MT
V4
V3
Thick
Interstrip
Thin
V2
Blob
Interblob
4B
4A
4Cα
4Cβ
PUL
5 & 6
V1
SC
Magno
Parvo
LGN
Parasol
Midget
Retina

Figure 1-7. Overleaf. Visual areas related to motion processing. The grey rectangles correspond to areas with high proportions of direction-selective neurons. The spotted rectangles are areas mostly associated with form and colour vision. Black, thick lines show the commonly accepted motion pathways. Note that the arrows imply the direction of information in one direction only. The feedback connections between areas are not shown. SC, superior colliculus; PUL, pulvinar; MT, middle temporal; PO, parieto-occipital area; MST, middle superior temporal; FST, floor of superior temporal; VIP, ventral intraparietal.

Area V5/MT is located within the posterior bank and fundus of the superior temporal sulcus (STS) (Dubner and Zeki 1971). Anatomically it is characterised by areas of dense myelination and reciprocal connections with V1 (Ungerleider and Mishkin 1979, Zeki 1974). V5/MT contains a complete representation of the contralateral visual field (Van Essen *et al.* 1981) but, due to its large receptive field sizes, also includes some ipsilateral representation (Tootell *et al.* 1998). The receptive field sizes increase linearly with eccentricity and are about 10 times larger than in the striate cortex at any given eccentricity (Albright and Desimone 1987). The area is organised in a columnar fashion with blocks of cortical tissue containing neurons of similar directional selectivity (Albright 1984). In addition to its input from V1, V5/MT receives ascending input from V2, V3 and the pulvinar complex (Ungerleider and Mishkin 1979, Van Essen *et al.* 1981, Zeki 1974) and is connected with a wide variety of other areas in the superior temporal sulcus, the parietal lobe and the frontal lobe (Van Essen *et al.* 1981, Zeki 1974). Lesion studies of area MT have shown substantially elevated thresholds for speed discrimination (Orban *et al.* 1995) and direction discrimination (Lauwers *et al.* 2000). Although these studies show that area MT has an important functional role in motion related tasks, the necessity is not absolute as the results of lesion studies show that performance can improve over time and be dependent on the type of motion being tested (Pasternak and Merigan 1994, Rudolph and Pasternak 1999). However, where performance after lesioning was poor, it was shown that the lesion incorporated area MST showing that the two areas are more necessary for the normal discrimination of

motion than V5/MT by itself (Rudolph and Pasternak 1999). See section 3.2 for an overview of speed and temporal frequency selectivity.

1.10 Feedforward and feedback mechanisms in the visual cortex

After processing in area V1, activity is relayed to areas close by which in turn transmit activity to additional cortical areas. Cortical neurons do not simply transfer information to other visual areas with feedforward connections, they also process it. This is done by means of intrinsic or horizontal connections that connect neighbouring neurons in a cortical area and feedback connections that connect cortical areas in the direction opposite to feedforward connections (Callaway 1998). Thus processing between areas and processing within areas are related by the fact that any information sent by a cortical neuron to a neighbouring visual area is transmitted by horizontal connections to neurons within the same area.

One of the major organising principles of the visual cortex is that each area contains a retinotopic representation of the contralateral visual field. In addition, receptive field sizes increase greatly as one moves up the visual cortical hierarchy. As a consequence of this there is an important degree of convergence and divergence in cortico-cortico connections. In other words a cortical zone a few microns wide will project and receive information from a much bigger part of a connected area. This convergence and divergence means that feedforward connections between areas are retinotopically organised such that the receptive field centres of the afferent neurons are included in the receptive field centres of the recipient cell (Girard and Bullier 1989, Girard *et al.* 1991a, Girard *et al.* 1991b). However this is not the case for feedback connections. Due to the

much larger receptive fields in areas distant from V1 this means that neurons in V1 are influenced by information concerning large portions of the visual field.

Inactivation or lesioning of area V1 in the macaque leads to a complete cessation of activity in a number of visual areas (Bullier *et al.* 1994). This would suggest that feedforward connections are important for carrying the visual drive from one neuronal population to the next. However, when similar lesions are produced in area V2 only one third of the neurons in V1 were shown to be affected (Sandell and Schiller 1982) showing that feedback connections have a weaker effect on their target neurons than feedforward connections. Studies have also shown that these feedback connections are unable to drive neurons in the absence of a feedforward drive (Girard and Bullier 1989). The feedforward connections to area MT have been described in section 1.9. Feedback connections from layers 3 and 6 in MT target layers 1, 4B and 6 in V1 (Orban 1997).

1.11 Conclusion

Although anatomical and physiological studies of the monkey cortex provide important information regarding the cytoarchitecture and patterns of connectivity between the visual areas they are nevertheless limited in what they can tell us about the precise location and functionality of each area within the visual cortex of man. Much less is known about the organisation of visual areas in humans compared to that of other primates. In terms of their function, it has been shown that at least areas V1 and V2 of man show striking similarities with other primates, particularly in cytochrome oxidase patterns, revealing blobs and stripes, retinal projections, and visual field representations (Van Essen *et al.* 1993). Post-mortem studies have also revealed similarities in the patterns of connectivity between the visual areas of man and other primates (BurkHalter

and Bernardo 1989). In man, the most advanced and often non-invasive technique in distinguishing the visual areas is the use of functional imaging modalities. With the technological advancement in functional imaging techniques such as Positron Emission Tomography (PET), functional Magnetic Resonance Imaging (fMRI) and Magnetoencephalography (MEG) it has become possible to estimate spatially and temporally localised activity in the human brain given our knowledge of the functional interconnectivity and specificity of the visual areas (Zeki *et al.* 1991, Wandell *et al.* 1996). In the following chapter the techniques of MEG and fMRI are outlined.

2. THE ORIGIN, RECORDING AND ANALYSIS OF MAGNETOENCEPHALOGRAPHY (MEG) AND FUNCTIONAL MAGNETIC RESONANCE (FMRI) SIGNALS

2.1 Overview

This chapter forms an introduction to the methodologies of Magnetoencephalography (MEG) and Functional Magnetic Resonance Imaging (fMRI) used in this thesis.

It begins by outlining the neuronal source of the magnetic fields as measured by MEG and electroencephalography (EEG) signals. The next section introduces the hardware required to perform MEG recording including the super conducting quantum interference device (SQUID), the dewar required to maintain temperatures at superconducting levels and the design of the flux transformers that detect the magnetic fields. This leads to an overview of the technical details of MEG localisation including details of the forward and inverse problems and outlines several possible solutions to this inverse problem, including an introduction to synthetic aperture magnetometry (SAM). The section on MEG concludes with details of how the MEG signals are co-registered with the subject's MRI scan.

The chapter ends by introducing the principles of fMRI recording. Firstly, the neuronal origins of the fMRI signal and the BOLD response are described. This is followed by a discussion of experimental design as related to fMRI and the chapter ends with a review of how the fMRI signals are analysed to produce data.

2.2 The physiological source of MEG signals

The cerebral cortex consists of up to 10^{10} neurons (Hamalainen *et al.* 1993) and is made up of six main layers containing principally stellate and pyramidal cells (Wikswo 1989). These cortical neurons communicate by means of electrical signals that result in the formation of intracellular ionic currents and lead to the production of magnetic fields (Okada 1982), which can be measured outside of the head if sufficient numbers of neurons are simultaneously activated (Hamalainen *et al.* 1993). What follows is an overview of how these electrical and magnetic fields are produced.

2.2.1 Action potentials

A neuron consists of the cell body (soma), which contains the nucleus, the dendrites which receive information from other cells and the axon, a single long fibre that carries the nerve impulse away from the soma to other cells (see Figure 2-1). Electrical charge is unevenly distributed across the neuronal membrane with the inside of the neuron being negative with respect to the outside. This negativity occurs due to the fact that sodium (Na^+) is over ten times more concentrated on the outside than on the inside of the neuronal membrane whilst potassium (K^+) is over twenty times more concentrated inside the neuron than outside. This yields a negative resting potential, across the cell membrane, of approximately -70mV and this negativity is emphasised further by an abundance of chloride (Cl^-) ions inside the neuronal membrane. The negative resting potential means that the neuron is able to respond rapidly to a stimulus and it is maintained through a protein complex known as the sodium-potassium pump (Cantley 1986).

An action potential occurs when the axon depolarises sufficiently to reach a threshold level. When this occurs, voltage gated sodium channels open leading to a dramatic redistribution of electrical charge across the neural membrane and an action potential is initiated. The influx of positive charges depolarises the segment of membrane immediately adjacent to it until it to reaches threshold and generates its own action potential (Wikswo 1989). In this way the action potential works its way down the axon until it reaches the axon terminal thereby initiating synaptic transmission. The speed with which the action potential propagates down the axon depends on the characteristics of the neuron, with many having their axons sheathed in myelin to increase conduction velocity. The myelin does not extend continuously along the entire length of the axon but has breaks in the insulation known as nodes of Ranvier which contain concentrated levels of voltage gated sodium channels so allowing ions to cross the membrane in order to generate action potentials. As a result of this, action potentials skip along the axon, from node to node, in a process known as saltatory conduction. Action potentials are a feature mainly of axons as the membranes of dendrites and neuronal cell bodies are not able to generate sodium dependent action potentials because they have few voltage gated sodium channels (Wikswo 1989).

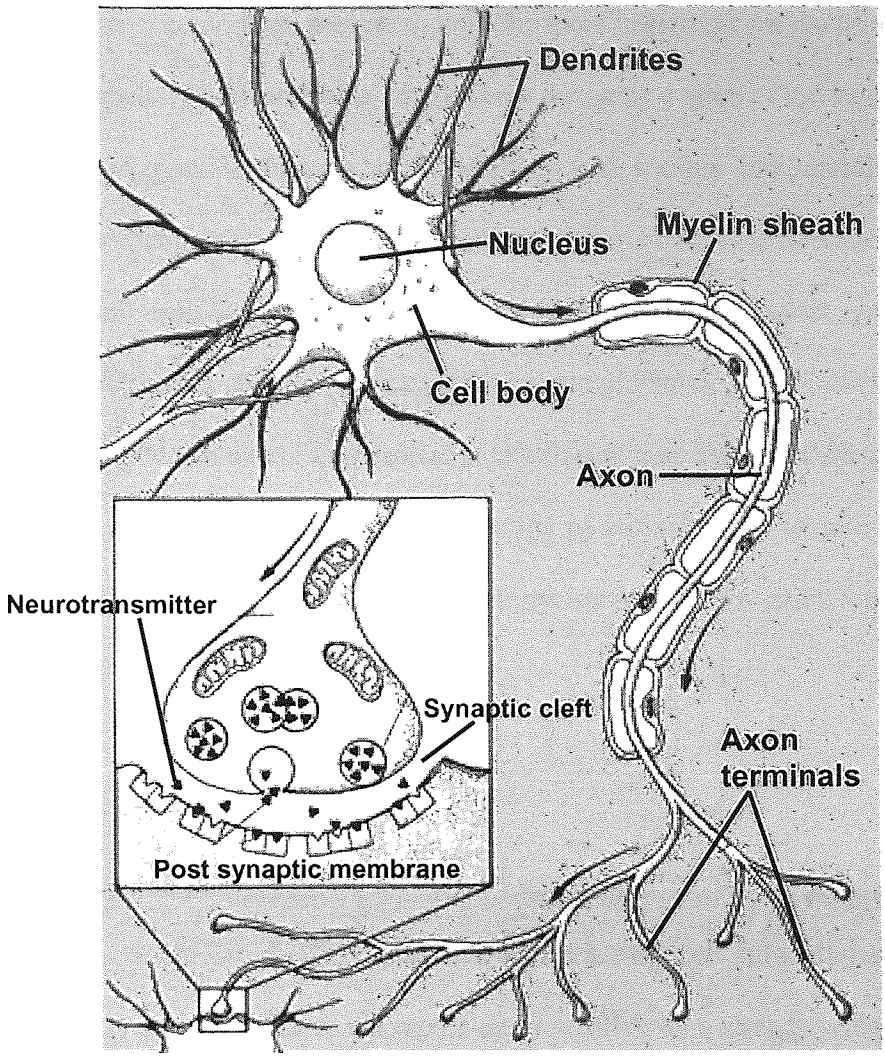

Figure 2-1. A schematic representation of a cortical neuron and its synapse. Adapted from image on Society for Neuroscience website (http://web.sfn.org/Template.cfm?Section=PublicResources&Template=PublicResources/SubCategory.cfm&cat_id=6). Accessed 1/7/04.

2.2.2 Post synaptic potentials

When the action potential reaches the axon terminal it causes depolarisation of the terminal membrane which opens gated calcium channels resulting in a large inward driving force of calcium ions into the cytoplasm of the axon terminal which causes neurotransmitter to be released from the synaptic vesicles. Neurotransmitter released into the synaptic cleft affects the postsynaptic neuron by binding to specific receptor proteins that are embedded in the postsynaptic membrane. Many different

neurotransmitter receptors are present though the most important are the transmitter-gated ion channels. These channels do not show the same degree of ion selectivity as do voltage-gated channels and can be permeable to both sodium and potassium ions, although if the channels are permeable to sodium the net effect is to depolarise the postsynaptic cell from its resting potential resulting in an excitatory post synaptic potential (EPSP) and is common in acetylcholine and glutamate gated ion channels. If the transmitter gated channels are permeable to chloride ions the net effect is to hyperpolarise the postsynaptic cell from its resting potential leading to an inhibitory post synaptic potential (IPSP) and is typical of glycine and GABA gated ion channels (Wikswo 1989).

2.2.3 The source of MEG signals

The ionic processes described in sections 2.2.1 and 2.2.2 give rise to three types of current. As the positively charged potassium ions enter the cell intracellular currents (see Figure 2-2) are set up due to the repulsion of positive ions already within the cell. This movement of positive charge gives rise to transmembrane displacement currents (see Figure 2-2) which only make a negligible contribution to the field measured far from the neuron, due to their radial symmetry (Okada 1982). These transmembrane currents in turn repel positive ions, that return to the point of depolarisation, in the extracellular space, which produces extracellular (volume) currents which close the current loop (Swinney and Wikswo Jr 1980).

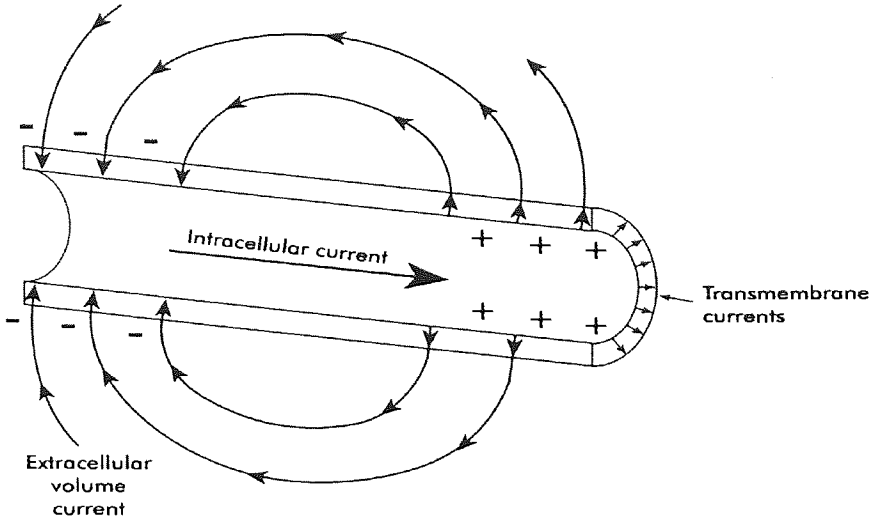

Figure 2-2. A schematic diagram of the currents produced by an action potential in a cortical neuron. Adapted from Lewine and Orrison 1995

When action potentials are propagated, bidirectional currents occur (see Figure 2-3) which can be modelled as two opposing dipoles, producing a quadrupole, the magnetic field of which falls off more rapidly than for a single dipole so producing only a small magnetic field.

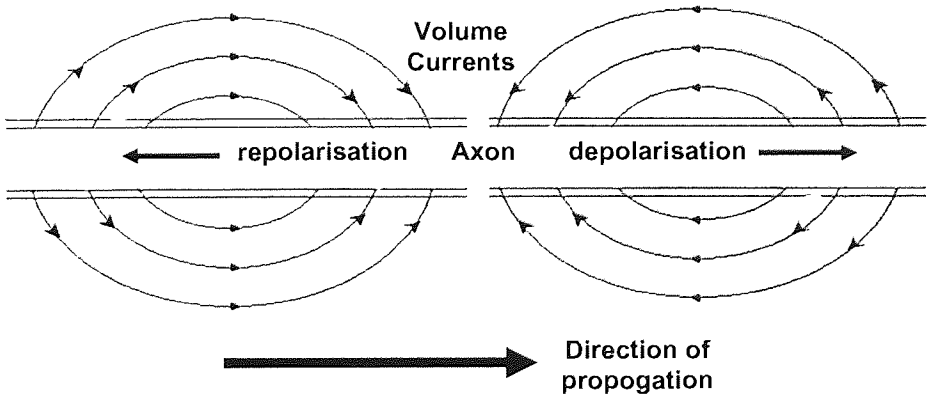

Figure 2-3. A schematic diagram illustrating the current flow during the propogation of an action potential. Bidirectional currents are produced leading to opposing dipoles which cancel each other out. At the post synaptic membrane current flows in only one direction which produces a dipole which is not cancelled. The MEG signals recorded at the scalp are therefore the result of primary currents produced by post synaptic potentials.

Conversely, at the post synaptic membranes current flows in only one direction thus producing a single dipole which is not cancelled (see Figure 2-4).

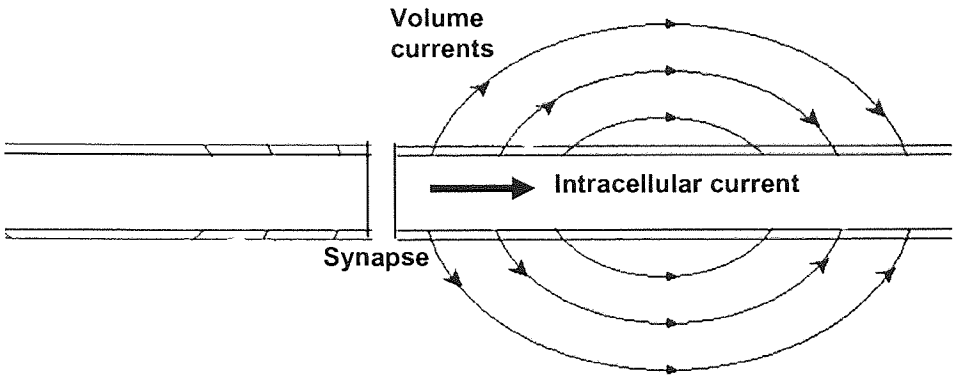

Figure 2-4. A schematic diagram of a synapse illustrating the current flow resulting from the post synaptic potential

The magnetic field produced by a single neuron is to small to be measured outside of the skull therefore the temporal summation of many neurons is required for a measurable signal to be obtained. The temporal summation of post synaptic potentials is greater than that of action potentials, given that post synaptic potentials last tens of milliseconds compared to action potentials which last approximately 1ms (Romani 1989). Thus electrical signals within the brain occur largely as the result of post synaptic potentials and the magnetic fields measured outside of the skull are the result of the net primary current.

How cells contribute to the measured magnetic field is determined by their morphology. Stellate cells consist of a central soma, from which dendrites extend radially and are said to have a closed field morphology, the net effect being the cancellation of magnetic fields produced by the cell (Okada 1982). Conversely pyramidal cells have dendrites

that reach out parallel to each other so that they tend to lie perpendicular to the cortical surface and are said to have an open field morphology thus generating magnetic fields (Okada 1982).

All the moving electrical charges within the neurons of the brain are accompanied by magnetic fields which, according to the right hand rule are perpendicular to the current direction (see Figure 2-5).

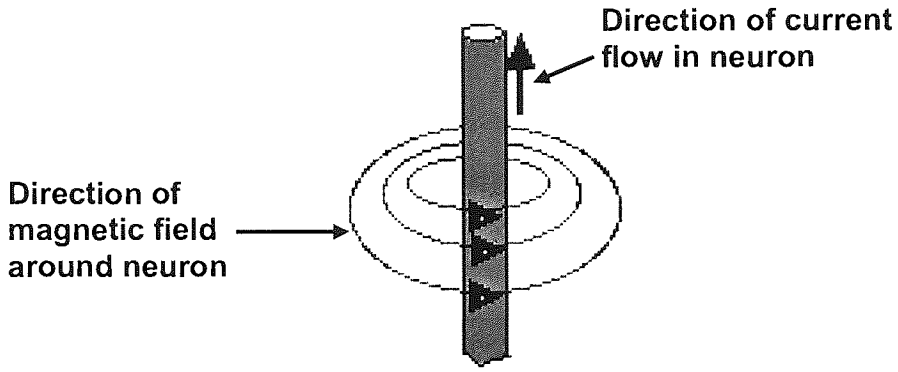

Figure 2-5. A schematic representation of current flow along a neuronal axon and the resulting magnetic field that is produced. Note that according to the right hand rule the magnetic field is perpendicular to the current flow and rotates anticlockwise around the neuron.

2.2.4 Source orientation

The cerebral cortex consists of a two-dimensional sheet of grey matter which is 2-4mm thick and is the main source of the MEG signal (Wikswo 1989). The cortex has a surface area of approximately 2500cm^2 and has an extremely convoluted surface consisting of many sulci and gyri. Spatial and temporal summation is possible when sufficient synapses (about 10^6) are activated in relative synchrony and with common orientations (Nunez 1986) and this summed activity creates a change in the magnetic field that is strong enough for detection by both EEG and MEG. It is known that in a spherically symmetrical volume conductor, a radially orientated current source produces

no external magnetic field (Sarvas 1987) suggesting that only the tangential component of the current dipole produces a net magnetic field outside of the skull, meaning that MEG is more sensitive to sources located in the sulci rather than in the gyri (see Figure 2-6). However, recent research suggests that only very small strips of neocortex at the crest of gyri are poorly resolved by MEG and it is source depth, not orientation, that effects the sensitivity of MEG (Hillebrand and Barnes 2002).

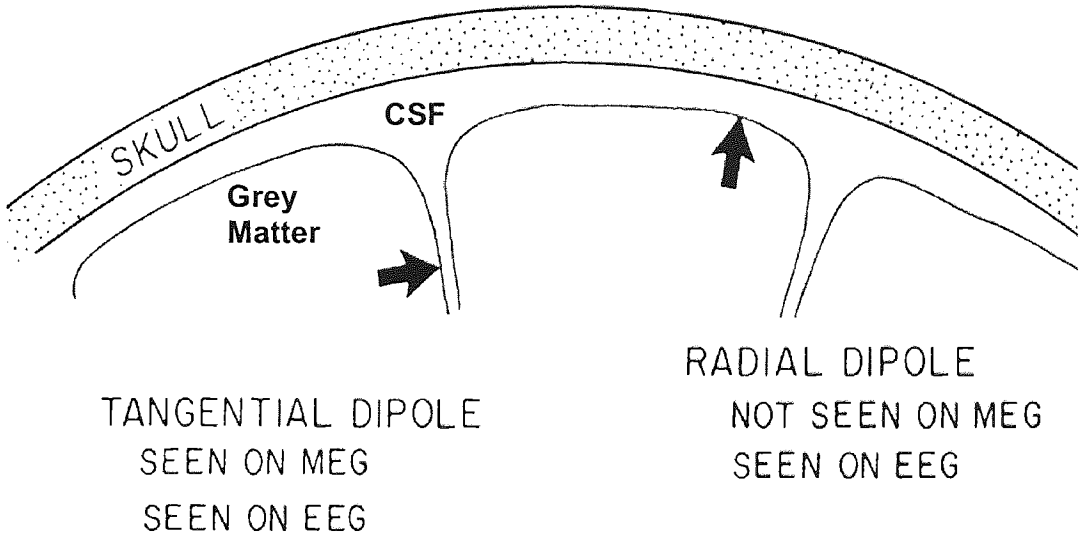

Figure 2-6. Two sources in the cortex; one is oriented tangentially to the skull, and the other is oriented radially. Each is represented as a current dipole, shown as a heavy arrow. Because sources in the cortex are generally oriented perpendicularly to the cortical surface, tangential sources are located in the sulci while radial sources are in the gyri. Although the EEG sees both sources, it is dominated by the radial sources in the gyri (Adapted from Cohen and Halgren 2003).

2.3 MEG v EEG

MEG and EEG field distributions are mutually orthogonal meaning that the data produced by the two techniques compliments the other. As stated in section 2.2.4, MEG is most sensitive to sources tangential to the skull, which differs from EEG which is sensitive to both radial and tangential sources. However EEG has a tendency to be

more sensitive to radial sources as these arise from the gyri which lie closer to the EEG electrodes placed onto the scalp. Differences between the two techniques are seen if one studies the field map patterns produced in response to a theoretical tangential source in a spherical model (see Figure 2-7). It is evident that the field maps lie orthogonal to one another due to the nature of the magnetic and electrical fields. As a consequence of this MEG localises the source best in the Y direction whilst the EEG localises it best in the X direction. Furthermore it can be seen that the field pattern is tighter in the MEG model than the EEG model. This is due to smearing of the EEG signal by the skull and scalp. Note that these simulated results are based on a model that assumes a spherical conductivity profile for the head. In reality the EEG signal must leak to the surface through a complex undetermined path, making source localisation difficult. The magnetic field by contrast is not affected by the conductivity profile and so is not affected by surface smearing.

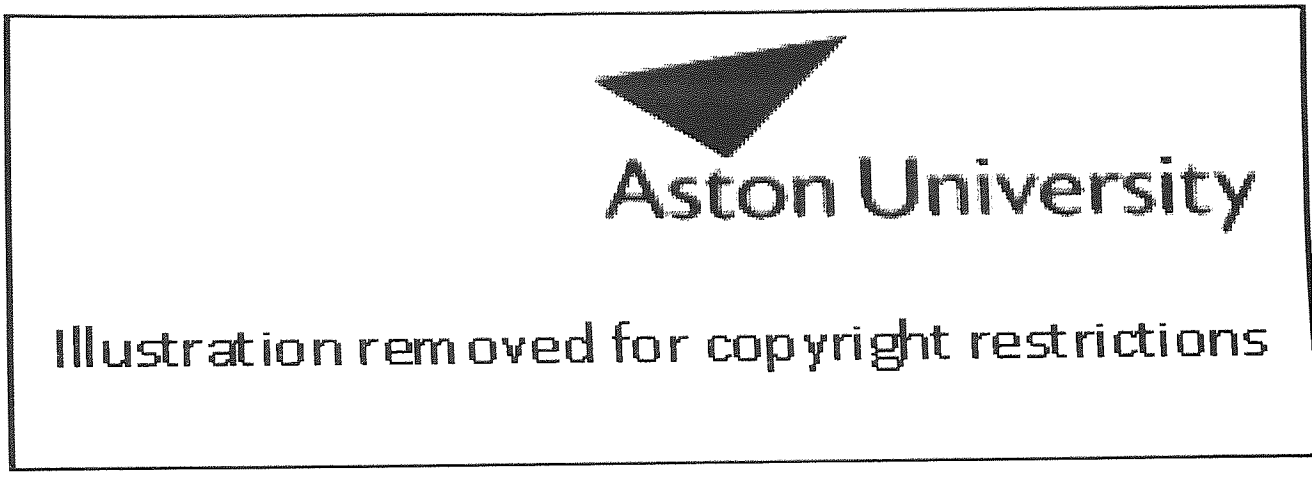

Figure 2-7. Computed theoretical MEG and EEG maps, shown as contour maps, due to a tangential dipole source in a spherical model of the head (Cohen and Cuffin 1983). They are shown on a spherical "cap", which has x and y coordinates with ticks at each cm. The EEG map is of the surface potential with contour lines every 20% while the MEG map is of the component of magnetic field vector normal to the scalp, also with 20% lines. The neural source generating the MEG and EEG is approximated as a tangential dipole at a depth of 2.7 cm. It is seen that the MEG pattern is oriented at 90o to that of the EEG, and is somewhat tighter.

2.4 MEG Technology

Current flow within a single neuron is to small to produce an observable magnetic field outside of the skull which requires the simultaneous activation of approximately 10^6 neurons (Nunez 1986). Even when such large numbers of neurons are activated the magnetic field produced is only in the region of 10^{-12} Tesla (see Figure 2-8 for how this compares to environmental and physiological noise). To overcome this problem highly sensitive recording apparatus is required as well as the implementation of noise reduction techniques. What follows is a description of the technical requirements necessary for MEG recording.

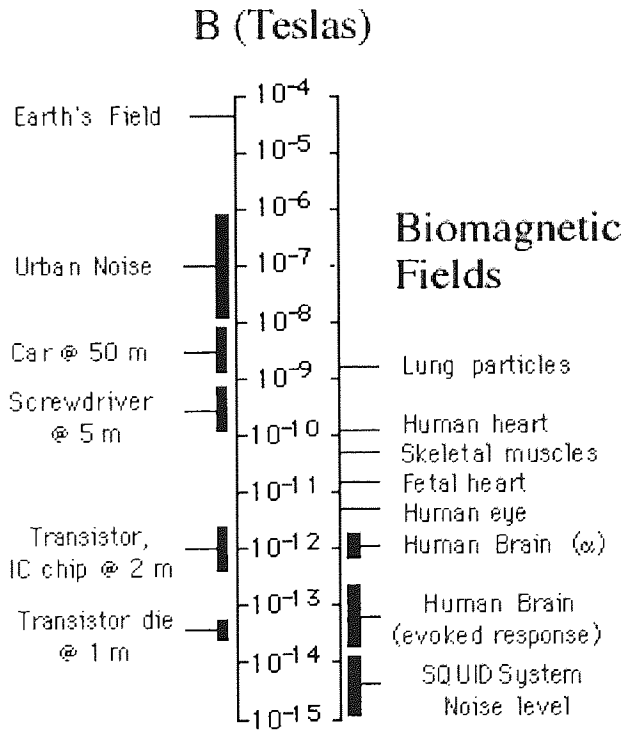

Figure 2-8. Comparison of magnetic field strengths produced by both physiological and environmental sources. Note that the magnetic field produced by the brain is several orders of magnitude smaller than the Earth's magnetic field. Similarly, the brain's magnetic field is smaller than other physiological magnetic fields produced in the body. These sources of "noise" have to be removed for clear MEG signals to be recorded.

2.4.1 The SQUID

The MEG signals are so weak (see Figure 2-8) that highly sensitive detection systems are required. The heart of the recording system is the superconducting quantum interference device (SQUID) consisting of a superconducting ring interrupted by one or two weak links, or Josephson junctions, which give the device its great sensitivity enabling very small variations in the magnetic field to be detected (see Figure 2-9). Magnetic flux from the brain is inductively coupled to the SQUID via a pickup coil (see section 2.4.2) with the voltage across the device changing in a non linear, periodic fashion, with changes in magnetic flux. This output voltage is used to generate a feedback current which is coupled back into the SQUID loop to null the applied signal flux, with the feedback current being proportional to the change in magnetic flux applied to the SQUID (Hamalainen *et al.* 1993).

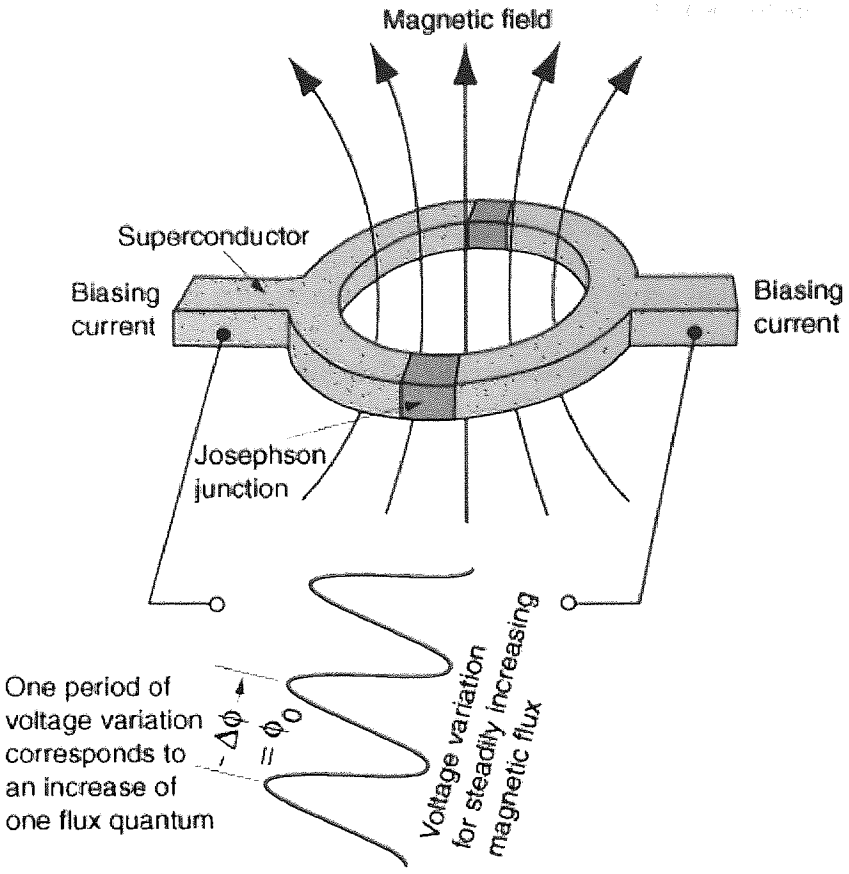

Figure 2-9. A schematic representation of a SQUID. A constant biasing current is maintained within the device such that any change in phase at the two Josephson junctions is proportional to the change in magnetic flux measured by the device. The SQUID is an extremely sensitive measuring device capable of recording magnetic field changes as small as one flux quantum in magnitude. Adapted from http://hyperphysics.phy-astr.gsu.edu/hbase/solids/squid.html#c1 accessed 25/5/04

2.4.2 Flux Transfomers (gradiometers)

SQUIDs are so sensitive to changes in the magnetic field that flux transforming devices, known as gradiometers, are used to feed the flux to the SQUIDs and shield them from unwanted noise. Gradiometers consist of two or more coils wound in opposition so that they approximately measure the gradient of the magnetic field and not the magnetic field itself (Vrba 1997).

Various configurations of gradiometer are available but the principle behind their function is the same (see Figure 2-10). A first-order gradiometer consists of a detection

coil attached to an adjacent coil, which are wound in opposition to each other, with the distance between the coils being known as the baseline. Noise rejection occurs because the fields of distant sources tend to appear uniform, which causes current of equal magnitude to flow in opposing directions in each coil thus cancelling each other out. However, as magnetic fields fall off with distance according to the inverse-square law, fields from nearby sources, such as the brain, induce a larger signal in the detection coil, compared to the other coils, which means that there is a net change in current flow within the entire gradiometer. At the top end of the gradiometer a small coil is placed adjacent to the SQUID, within a superconducting shield. This coil allows the current within the gradiometer to be inductively coupled into the SQUID itself.

Higher order gradiometers tend to be quite large meaning that they are unsuitable for systems containing a large number of channels. The Aston system consists of magnetometers, 1^{st} and 2^{nd} order gradiometers which can be combined, using software, to form synthetic 3^{rd} order gradiometers.

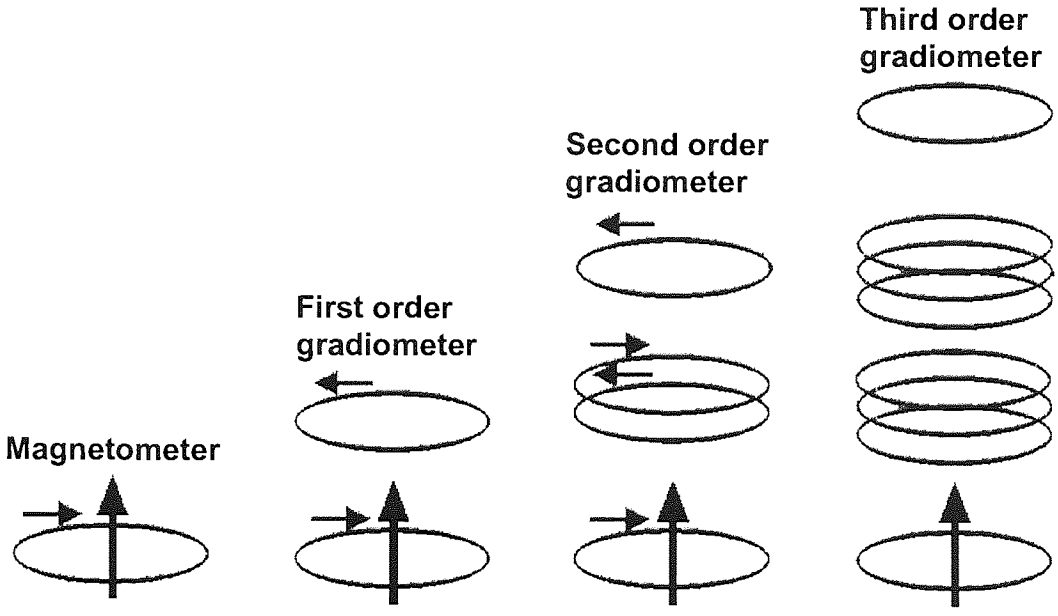

Figure 2-10. The construction of various types of gradiometer. The direction of magnetic field is shown by the large arrow. The small arrows indicate the direction of current flow in a particular coil. The magnetic fields of distant sources tend to have small spatial gradients thus causing current to flow in opposing coils that cancel each other out. The greater the number of coils in the gradiometer the greater the rejection of noise. For illustration purposes the connections between coils are not shown.

2.4.3 Cryogenics

The SQUIDS, flux transformers and their interconnections are superconducting and therefore must be maintained at very low temperatures using liquid helium (He). The cooling of the components is achieved by means of a liquid He bath contained in a dewar (see Figure 2-11 for a schematic diagram of a dewar). The construction of the helium dewar is similar to that of a thermos flask. However, as the temperature differential between the He and the environment is in the region of 300°C, in order to reduce thermal radiation losses, the insulation required in a He dewar is much more rigorous than that of a thermos flask. The dewar is a double walled vacuum vessel with

multiple layers of superinsulation (mylar foil) placed onto the walls of the vacuum space. At the neck of the dewar heat shields take energy from the evaporating He and conduct it back into the vacuum space to reduce the thermal gradient between the liquid He and the environment. Thus the dewar minimises heat losses by conduction, radiation and convection by using reflectivity, insulation and energy extraction (Vrba and Robinson 2001b). The Aston dewar has a He capacity of approximately 85L and consumes He at the rate of approximately10L per day meaning that the cryogenic container needs to be refilled at least once a week.

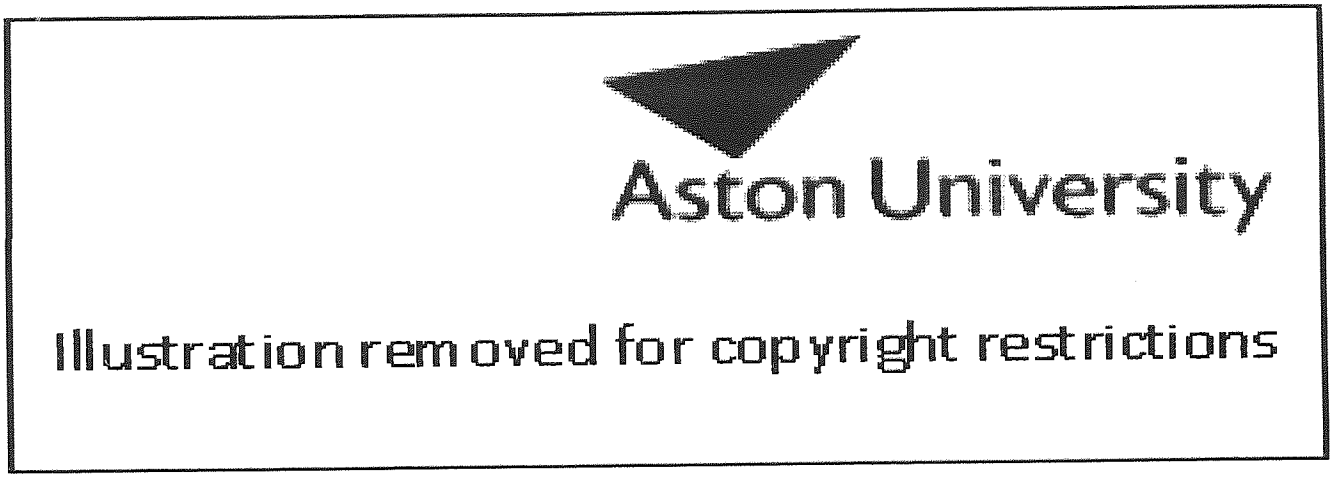

Figure 2-11. Schematic diagram of the cryogenics used in MEG. (a) The location of various MEG components within the cryogenic dewar. (b) The principles of the dewar operation. From Vrba and Robinson 2001b.

2.4.4 Shielding

Although modern day gradiometers are good enough at removing external noise to enable MEG recordings to take place without the need of specialised recording environments, it is common for the MEG system to be enclosed within a shielded room (see Figure 2-12 for a photograph of the Aston room). This reduces the fluctuating external magnetic field by being constructed of one or more layers of a high

permeability alloy such as μ-metal or aluminium. The Aston room contains two μ-metal layers that shields the room from static and low frequency noise by "funnelling" distorting fields away from the room interior, whilst an aluminium layer reduces high frequency noise by inducing eddy currents which create magnetic fields that are of opposite direction to the external field causing cancellation.(Cuffin and Cohen 1977).

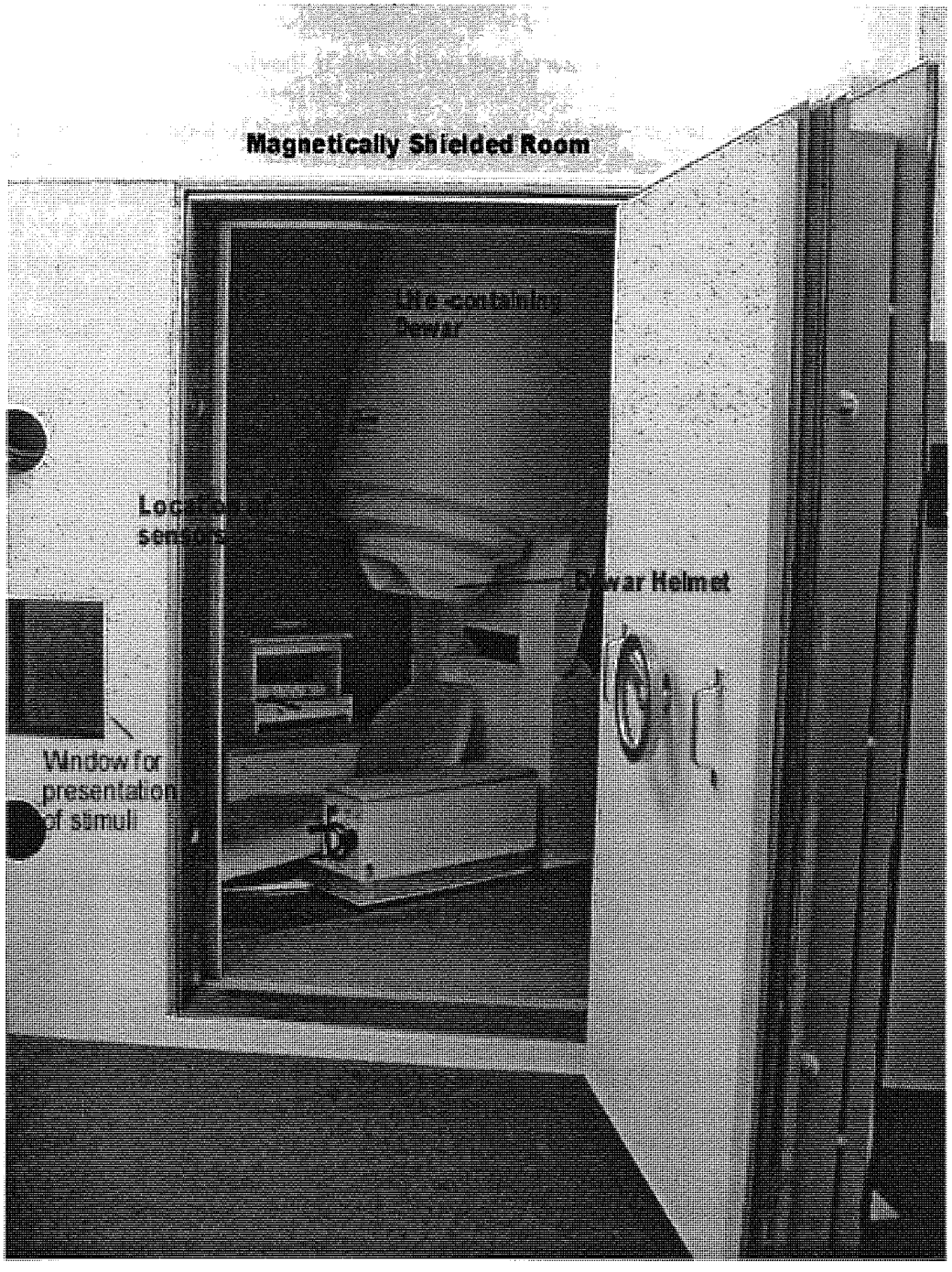

Figure 2-12. Overleaf. The Aston CTF Omega 151-channel Neuromagnetometer in a magnetically shielded room. The stimuli are projected from the outside through a window in the shielded room and onto a mirror inside the room.

2.5 MEG source reconstruction

Measured magnetic fields outside of the skull can be used to determine the electrical sources within the brain. To achieve this the bioelectromagnetic inverse problem needs to be solved although this has no unique solution (Helmholtz 1853). The inverse problem can only be 'solved' if one solves the forward problem, the practice of computing the output of the MEG sensors due to a given activation in the brain. Thus, one requires knowledge of both the predicted data (forward problem) and the measured data to produce a reconstructed source (inverse problem). In the following sections the inverse and forward problems are outlined in more detail and several different algorithms commonly used to solve the inverse problem are described.

2.5.1 Forward problem

As mentioned in section 2.2.3, when neurons fire both primary and volume currents are set up which contribute to the magnetic fields and electrical potentials recorded at the scalp using MEG and EEG respectively. MEG is most sensitive to primary currents (Okada 1982), with the forward problem involving the computation of the external magnetic field produced by these primary currents for a specific set of neural current sources.

2.5.1.1 Volume Conductor Models

In order to localise the sources of magnetic fields it is essential that accurate head models are used that incorporate the correct geometry and electrical properties of the head. There are many different layers between an electrical / magnetic source in the

brain and the scalp and the effect of these on the recorded signals has to be modelled. The head is traditionally modelled as a homogenous and isotropic volume conductor and in the simplest case is assumed to be a sphere. As the layers of the brain and skull affect the EEG signal more than the MEG signal, head models that consist of three concentric spheres, representing the different layers, are used for EEG. However, it has been shown that for MEG a head model that consists of a set of concentric spheres is equivalent to a homogeneous sphere (Grynszpan and Gesolowitz 1973) meaning that it is sufficient to use a single spherical model of the head which is achieved by using a segmented image of the subject's head from their MRI scan (de Munck 1992). In the case of the temporal cortex the single spherical model is less accurate, meaning that more realistic head modelling with the boundary element method or finite element method may be required (see Gesolowitz 1970 and Hamalainen and Sarvas 1989 for detailed descriptions of these methods). Synthetic Aperture Magnetometry (SAM) (see section 2.6.1) uses a multisphere approach (Huang *et al.* 1999) in which a separate sphere is fitted locally to the head near each sensor. This has been shown to be almost as accurate as realistic head modelling of the conductor geometry.

2.5.2 The inverse problem

To eliminate the non-uniqueness of the inverse problem, *a-priori* constraints have to be added to the mathematical calculations. These *a-priori* constraints may involve spatial information (Okada 1982), temporal information (Aine *et al.* 1989) or information about source strength (Scherg and Berg 1991). Several different algorithms incorporating these constraints are available and can be divided into two general categories: those for localisation of discrete sources and those for localisation of distributed sources. These

algorithms find a unique solution to the inverse problem in relation to the constraints and/or assumptions that are made by the model.

2.5.2.1 Discrete source algorithms

2.5.2.1.1 Equivalent current dipole (ECD) fitting

For post-synaptic primary currents, both spatial and temporal summation is possible when sufficient synapses (about 10^6) are activated in relative synchrony (Nunez 1986). This summed activity creates a change in the magnetic field that is strong enough for detection by MEG. At a typical measurement distance, which is at least 2 cm from the source, many current configurations seem dipolar (Hamalainen and Sarvas 1989) and can therefore be modelled as a single current source, the ECD. The dipole model is usually fitted to one or more peak latencies in the recorded waveform. The dipole parameters are calculated by taking a first guess, usually based on the location in the brain where the experimenter expects the activation to occur, and the forward problem is then computed for this initial guess. The difference between this computed field and the measured magnetic field is assessed using a least-squares measure and the dipole parameters are adjusted in an iterative fashion until the least-squares difference is minimised. The position, orientation and strength of this optimum ECD can be superimposed on the co-registered MRI of the subject.

The stability of the dipole solution can be assessed using Monte Carlo analysis (Medvick *et al.* 1989). This simulates repeating the experiment on many occasions with the assumption that due to differing recording parameters a slightly different localisation will be produced each time. The true parameters calculated for the original

dipole are mixed with random noise with a Gaussian distribution and this noisy data is then used to obtain another source localisation. This is repeated over many iterations with the variability of the solutions giving a measure of the robustness of the original solution. A 95% ellipsoid based on the distribution of the dipole locations can then be displayed on the subject's MRI (Singh *et al.* 1997) along with the original dipole solution.

The localisation of sources using the ECD is only accurate in situations where there exists a clear evoked response to time- and phase-locked stimuli in the recorded signal and thus a high signal to noise ratio. This methodology therefore lends itself to studies involving the major sensory cortices where the signals are large and can be easily evoked at the same latencies. However, there is an increasing interest in higher order cognitive functions such as memory and language, which cannot be adequately localised using this method. In the right situation a stable solution is often found when an equivalent single dipole can adequately explain the recorded data. However, there are problems in fitting more than one dipole (Liu *et al.* 1998). Similarly, the accuracy of multiple dipole fitting is determined by the initial guess although this is partially overcome by using multi-start techniques (Huang *et al.* 1998, Aine *et al.* 2000). Furthermore if the number of dipoles modelled is wrong, this leads to large localisation errors (Hillebrand and Barnes 2002).

2.5.2.1.2 Multiple Signal Classification (MUSIC and R-MUSIC)

In order to robustly estimate the number and parameters of multiple dipolar sources an algorithm called multiple signal classification (MUSIC) has been developed (Mosher *et al.* 1992). In this method the MEG (or EEG) signals are formulated in an abstract

geometrical space, which, assuming a noise model, can be partitioned into separated signal and noise subspaces. The MUSIC algorithm computes the correlation between the signal from a model dipole and the signal space. The areas where the correlations are at their peak are assumed to be the locations of the dipoles. The strength of the sources can subsequently be computed (Greenblatt 1993).

A limitation of MUSIC is that locating the largest dipole within the source space is easy but it gets harder for the additional weaker dipoles. In addition, the dipoles have to be linearly independent, as when the time courses of the sources are linearly dependent the signal subspace cannot be determined accurately. These problems are solved with the Recursive Music algorithm (Mosher and Leahy 1998). R-MUSIC locates multiple sources within the source space by locating each source in sequence. It locates the largest source first and then scans the grid for the next largest source and so on until all of the sources are located. Despite the modifications of R-MUSIC several limitations of this methodology exist. There is no clear separation between the signal and the noise subspaces meaning that it is not possible to extract the signal subspace accurately. Consequently, the calculated source location may not be the true one. Furthermore when true separate sources show some linear interaction a false peak can be produced in the source space producing spurious results.

2.5.2.2 Distributed source algorithms

The previous methods are based on the assumption that the magnetic fields being recorded outside of the skull were being produced by discrete localised sources of activity. Although algorithms used to detect discrete sources can be used to detect distributed sources, errors in localisation are introduced if the sources are located in

convoluted parts of the cortical surface. What follows is a description of algorithms developed to enable the reconstruction of the properties of distributed brain activity.

2.5.2.2.1 Minimum-Norm Least-Squares (MNLS)

MNLS assumes that the primary current distribution can be approximated by a discrete set of dipoles at fixed locations within a source region that is defined *a-priori*. The solution to the inverse problem is taken as that which best fits the data in the least squares sense and exhibits the minimum norm property, which is the current distribution with the smallest overall source power that is capable of explaining the measured signals (see Hamalainen 1991 for more detailed explanation). In other words, MNLS looks for an inverse estimation that minimises the residual error, such that the sum of squares of the differences between the measured field pattern and that from the predicted field has minimum power among all least-squares solutions (See Wang *et al.* 1992 and Wang 1993 for a detailed discussion of the use of MNLS in neuromagnetism).

There are limitations to this method. Due to the fact that a distributed current on the surface can give the same field pattern as a deep dipole, MNLS favours solutions that are closest to the sensors and as a consequence solutions are biased towards the surface of the brain. Additionally, the obtained solutions are spread out and blurred meaning that they are difficult to interpret, although these blurred images can be used to estimate the number of sources present. This can then be used as a constraint with the algorithms described earlier to produce more accurate solutions. Due to the fact that the distributed source solutions produced by MNLS are an exact fit to the data, any noise present is also modelled with the data meaning that the method fails when there is a large amount of external noise present (Sekihara *et al.* 1994).

2.5.2.2.2 Low Resolution Electromagnetic Tomography (LORETA)

LORETA (Pasqual-Marqui *et al.* 1994) uses more physiological based assumptions compared to MNLS. With this technique, a collection of voxels is used to model the cortex, and the solution is determined by imposing the constraint that neuronal activity at each voxel has maximum similarity (in terms of orientation and strength) with that of adjacent voxels. It is argued that this constraint is consistent with physiology, as a high degree of synchronization of neighbouring neurons is necessary for spatial summation to produce extracranially measurable fields (Pasqual-Marqui *et al.* 1994). The method assumes that the current distribution is spatially smooth but does not assume that there are a limited number of sources present. Due to the way the solution is calculated the method has a low spatial resolution meaning that two adjacent sources may appear as one blurred source.

2.5.2.2.3 Focal Underdetermined System Solver (FOCUSS)

FOCUSS (Gorodnitsky and Rao 1997) uses similar principles to MNLS but with an additional spatial weighting on the solution. The algorithm uses an iterative process to place the values of the previously obtained solution into a weighting matrix which enhances large elements and reduces small elements. This is repeated until the output of the computation is not significant, indicating that convergence to a solution has occurred. It is claimed that the FOCUSS algorithm can resolve both the depth and extent of cortical sources (Gorodnitsky *et al.* 1995). However, in order to converge to the correct solution, the initial solution has to be precise (Gorodnitsky and Rao 1997) otherwise subsequent iterations are also inaccurate. Therefore, although the algorithm

always finds a localised solution, it is not necessarily the correct one with the final solution being highly dependent on the initial estimate (Hillebrand 2000).

2.6 Beamforming

Until recently MEG experiments have mostly been performed using the averaged evoked response paradigm. This assumes that the activation of the brain area of interest is phase locked to a particular stimulus meaning that averaging across epochs increases the SNR. However this methodology is only useful when studying the primary sensory and motor cortices where tight phase-locking to the stimulus transient can be assumed. Areas of cortex serving more cognitive functions are likely to have a more variable latency distribution, such that the character of the events cannot easily be captured with averaging.

A beamformer performs spatial filtering on data from a sensor array thus enabling the discrimination of signals of interest from those originating in other areas. The idea was first developed for the processing of radar and sonar signals (Van Veen and Buckley 1988) but has, over recent years, been incorporated into the processing of biomedical signals (Van Veen *et al.* 1997, Robinson and Vrba 1999. In relation to functional imaging a beamformer can be thought of as a collection of spatial filters each tuned to a different brain region with the output of these spatial filters being used to produce a beamformer based statistical parametric map.

2.6.1 Synthetic Aperture Magnetometry (SAM)

SAM is a novel spatial filtering technique based on the constrained minimum-variance beamformer (Van Veen *et al.* 1997). Conventional linearly constrained beamformers

(Van Veen *et al.* 1997) compute a spatial filter, at each point in space (target voxel), for each orthogonal direction without regard to source orientation. Conversely non-linear constrained beamformers, such as SAM, choose a source orientation that maximises the total power output of the spatial filter at each target voxel and have been shown to have better spatial resolution than conventional beamformers (Vrba and Robinson 2001a). SAM exploits the fact that, assuming sources are dipolar and that the sources are uncorrelated, there is a unique solution to the inverse problem. SAM minimises the power, coming from a voxel (source) of interest, such that signals emitted from sources outside of each specified voxel are suppressed without attenuating power from the sources at the specified coordinates. As a consequence images derived from applying SAM to a range of voxels are unique in three dimensions if the assumptions being made are correct.

As SAM exploits the spatial and temporal correlation of MEG data the technique requires the simultaneous acquisition of signals from a large array of MEG sensors recording the constantly varying biomagnetic signals being produced by the brain and reaching the scalp. The beamformer is calculated by [1]:

$$W_\theta^{\mathrm{T}} = (H_\theta^{\mathrm{T}} C^{-1} H_\theta)^{-1} H_\theta^{\mathrm{T}} C^{-1} \qquad (1)$$

where W_θ^{T} is the weights vector for the target voxel θ, H_θ^{T} is the lead field (the solution to the forward problem at any particular sensor location) and C is the data covariance matrix. The source activity from any particular voxel can be calculated by producing a weighted linear combination of all measurements (see Figure 2-13). The weighting coefficients, which are optimised based on the statistics of the data (Van Veen and Buckley 1988), are selected so that they emphasise the activity from the voxel of interest and attenuate signals from other locations.

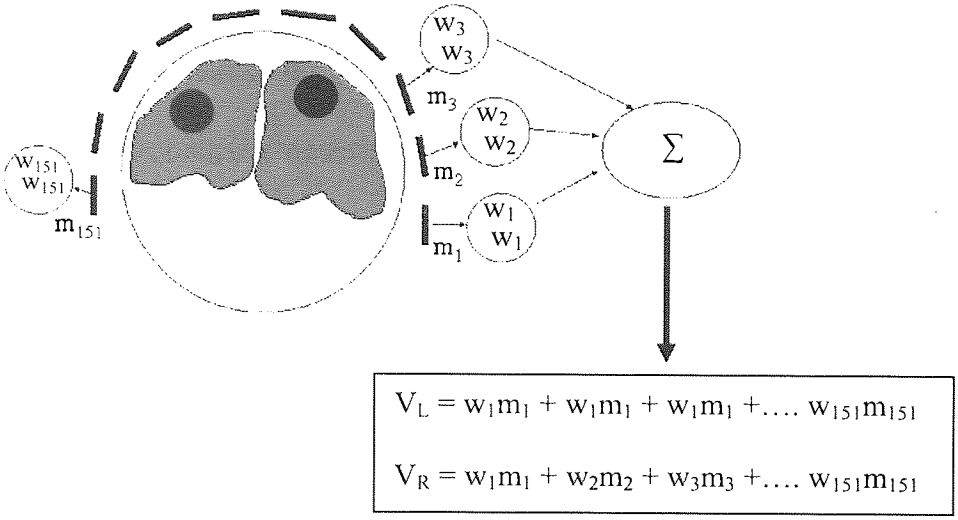

Figure 2-13. A diagrammatic representation of how SAM works. Two sources are shown in the brain, one in the right and one in the left hemisphere. The activity from these sources is recorded by each of the MEG sensors. Virtual electrodes of these areas can be calculated by means of a linear weighted combination of the activation of all of the MEG sensors. V_L is the estimated activity for the target location in the left hemisphere, V_R is the estimated activity for the target location in the right hemisphere, M refers to the sensor number and W is the weight vector calculated for the target locations in each hemisphere.

Thus spatial filters are designed that pass brain electrical activity from a specified location whilst attenuating activity originating at other locations. The MEG data is projected through these spatial filters to give a measure of current density as a function of time. As the time series of each voxel is calculated using a weighted sum of the MEG sensors they have the same millisecond time resolution as the original MEG signals. The output of this analysis is a synthetic depth electrode or *virtual electrode* (typically 5x5x5mm in size) at each location within the pre-defined source space (the subject's brain) and the power output of each virtual sensor can be displayed as a colour coded map on the subject's Magnetic Resonance Imaging scan (MRI). The entire time series can be divided into active and passive states and Fourier analysis can be performed to calculate the power in each frequency band of interest in each state; P_{active} and $P_{passive}$. In beamformer techniques such as SAM, the amount of differential

activation between the active and passive states is usually quantified using the neural-activity index (NAI, Van Veen *et al.* 1997) which is given by (P_{active} - $P_{passive}$) / noise. The spatial selectivity of the data can be further enhanced with the use of statistical probability mapping (SPM) (Friston *et al.* 1995, Singh *et al.* 2003).

An advantage of SAM is that no *a-priori* assumptions about the number of active sources are required as in dipole modelling. Similarly, there is no tendency for sources to drift to the surface as in MNLS (Grave de Peralta-Menendez and Gonzales-Andino 1998). As the solutions depend on data covariance they can therefore be used to image data that is not phase locked to a stimulus such as ERD and ERS (see section 2.6.2). Furthermore group statistical maps can be produced from the SPM analysis (see section 2.6.1.1).

One disadvantage of beamformer analyses, such as SAM, is that if two or more spatially separated sources temporally covary in synchrony then SAM will not detect them. However it has been shown that the temporal correlation must be greater than 0.7 before complete cancellation occurs (Van Veen *et al.* 1997). It is unlikely that two separate brain sources would correlate to such a high degree particularly over longer epoch lengths.

2.6.1.1 Group imaging of SAM data

The statistical analysis of group imaging data is well established in fMRI (Friston et al 1995) (see section 2.8 for a description of the fMRI technique). If one has an effect of interest (EOI) then the magnitude of this effect can be pooled across subjects and a T statistic map generated on a voxel by voxel basis. If the errors are assumed to be

normally distributed then the T values can be transformed into probabilities against the null hypothesis. This is commonly termed a fixed effects analysis and has the advantage of being sensitive for small numbers of subjects although, conversely, it has the disadvantage that the statistical significance is based purely on the intrasubject variance, meaning that the group images produced can be dominated by the responses of only one subject. It is therefore desirable to use a random-effects analysis which incorporates an appropriate mix of intra and inter subject variances and has been shown to be appropriate for the group imaging of functional data (Friston *et al.* 1999).

It is known that the spatial distribution of ERD/ERS as measured using SAM analysis can be highly variable between subjects and may not be normally distributed (Burgess and Gruzelier 1999) meaning that an assumption of a normal distribution as used in parametric statistics may be invalid (Singh *et al.* 2003). One approach to overcome this is to use a non-parametric permutation analysis (SnPM), which allows the statistical significance of voxel effects to be established without assuming a normal distribution (Nichols and Holmes 2002).

In the SnPM method the data itself produces the probability distribution against which the null hypothesis is tested so that no assumptions about the probability distribution have to be made. The method works as follows. Firstly the activation map of each subject is spatially normalised to a template brain, following which a voxel wise T statistic is calculated using the intersubject variances and a permutation test performed, measuring each voxel against the null hypothesis. The significance of the unpermuted T value is then tested against the distribution of the permutation analysis. It has been shown that the use of the pseudo-T statistic, incorporating variance smoothing,

increases the chance of detecting activations (Nichols and Holmes 2002) whilst the methodology can also correct for multiple comparisons. This is achieved by finding the largest T value in the whole volume from each permutation and producing a probability distribution of the largest T value across all permutations. If a probability threshold of 5% is set then the probability of any T value in the volume being greater than this threshold by chance is less than 5%.

The group imaging, as described here, does have some limitations which are not limited to SAM analysis but also to PET and fMRI. The spatial normalisation of each subject's structural MRI to a template image provides a good match of gross structure such as the outline of the brain. This may not be the case for the local structures such as sulci and gyri which can vary by several millimetres between subjects (Steinmetz *et al.* 1990). Group studies are further problematic in that they are open to a number of interpretations regarding areas of significant activation (Singh *et al.* 2003). An activated cortical area in a group study may represent a spatial location that is consistently activated in all subjects, but only weakly. This means there may be other areas with more significant activation but their locations may be so spatially variable in each individual that they are no longer significant after normalisation to template space.

2.6.1.2 Time-frequency analysis

In this thesis data is often presented in the form of time-frequency plots, which provide a time-frequency representation of the virtual electrode data. These are computed by means of Morlet wavelet decomposition of the neuronal power in the time and frequency domain. This analysis represents the data at different scales (frequencies) or resolutions using a scaled basis function known as a wavelet, which is localised both in

the frequency and the time domains. The wavelet function is obtained by taking a complex sine wave and localising it with a Gaussian envelope with the "scale" of the wavelet varied by changing a width parameter. With a moving FFT, as the frequency of interest changes, a different number of sinusoidal cycles fit within the temporal window. In contrast, the scaling properties of the wavelet transform mean that the same function is used at each frequency. This means that the optimum trade off is made between time and frequency resolution. The 2-D Gaussian profile of the wavelets means that the full-width half maximum (FWHM) of the response in the time and frequency domains are W_t and W_f respectively. In this thesis a wavelet width of 10 is used meaning that at each frequency f, $W_f = 0.235f$ and $W_t = 3.74/f$. Therefore as frequency increases, the frequency resolution decreases whilst the temporal resolution improves.

2.6.2 Cortical oscillations as measured with SAM

Cortical neurons can exhibit different responses to both sensory and cognitive processing. Time and phase-locked changes (see Figure 2-14), in the activation of a population of neurons, can be evoked by an external stimulus (e.g. visual evoked potential, auditory evoked potential). In order for these evoked potentials to be visualised the signal to noise ratio has to be improved by means of signal averaging. This technique assumes that the signal of interest has a consistent timing relationship with the stimulus whilst the background EEG or MEG activity is classed as noise. However, the evoked potential produced by this methodology cannot be considered a true reflection of the underlying cortical processes and at best is simply an approximation. In fact research suggests that some features of this evoked activity occurs due to 'phase resetting' of ongoing rhythms in the brain (e.g. alpha rhythms in

the visual cortex) towards a particular value in relation to the stimulus (Sayers *et al.* 1974, Makeig *et al.* 2002) meaning that information may be lost.

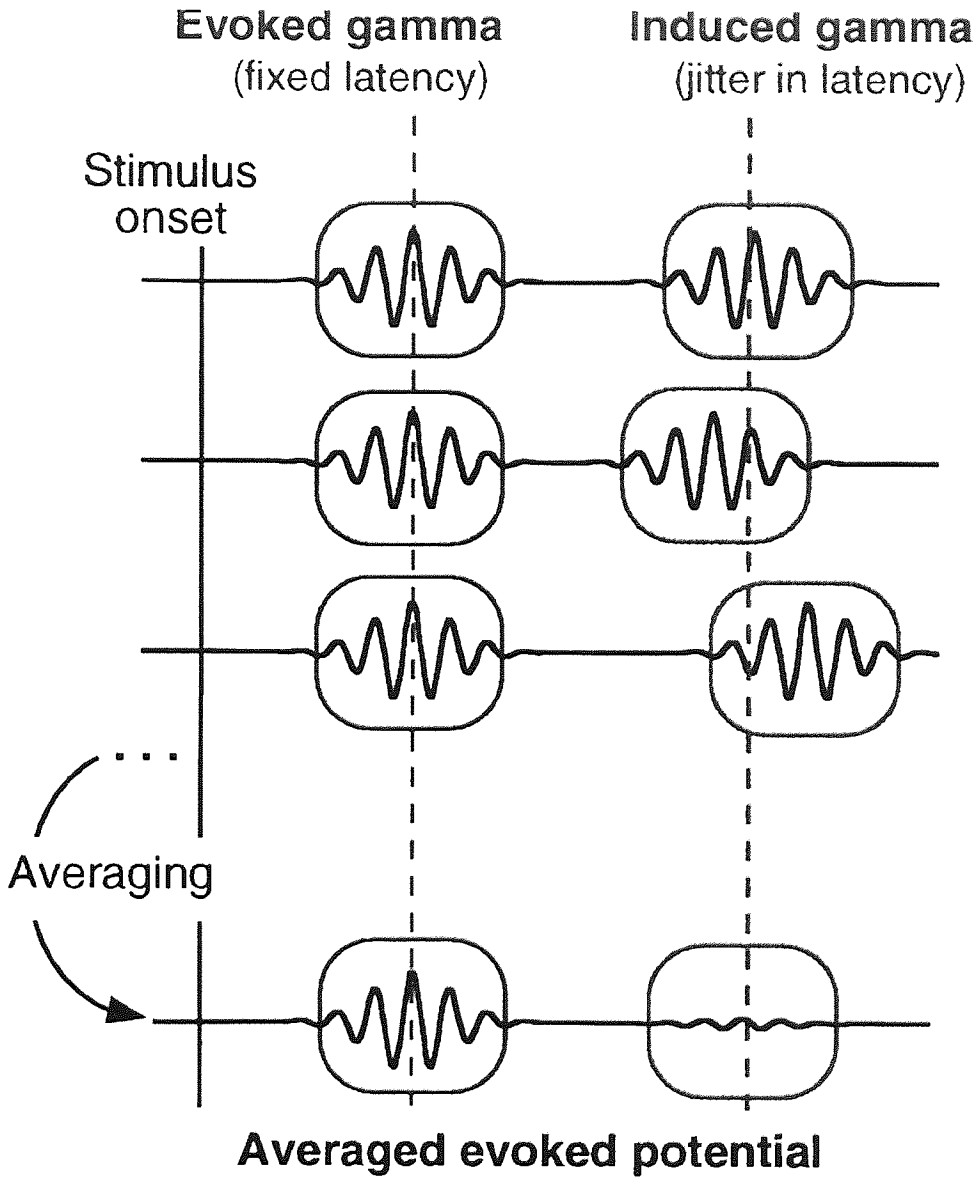

Figure 2-14. Schematic explanation of evoked and induced cortical activity (adapted from Tallon-Baudry and Bertrand 1999)

The second type of oscillatory response that cortical neurons exhibit is an *induced* change that is time-locked, but not phase-locked to a stimulus or processing activity. This type of response represents frequency specific changes in the ongoing EEG activity

such that increases or decreases in power can occur within given frequency bands. It has been shown that an increase in frequency specific cortical power is due to increased synchrony of the underlying neuronal populations and has been termed event-related synchronisation or ERS (Pfurtscheller 1992). Similarly it has been shown that a decrease in cortical power is due to a decrease in synchrony of the neural population and is termed event-related desynchronisation or ERD (Pfurtscheller and Aranibar 1977).

The evoked potential occurs due to transient post synaptic potentials triggered by a specific stimulus. ERD and ERS on the other hand occur due to the change in any one parameter that control oscillations in neuronal networks: (i) the intrinsic properties of the neuronal membrane, (ii) the structure of the interconnectivity between network elements and synaptic processes related to the function of feedback and feed-forward (thalamo-cortical and cortico-cortical) loops, and (iii) the modulating effects of the local or general neurotransmitters (Lopes da Silva and Pfurtscheller 1999, Singer 1993).

The frequency of brain oscillations is inversely proportional to the number of synchronously activated neurons underlying the activity with the higher the number of synchronised neurons the slower the oscillatory frequency (Singer 1993). Thus as the number of interconnecting neurons increases the frequency decreases and the amplitude increases (Lopes da Silva 1998).

The ERS and ERD phenomena can occur simultaneously at different locations on the scalp. Pfurtscheller *et al.* 1997 demonstrated the occurrence of simultaneous, and contralateral, mu rhythm ERD and occipital alpha rhythm ERS when subjects

performed a hand movement task. They also showed that voluntary hand movement could produce ERD in the cortical hand area while the foot area produced simultaneous ERS; the opposite pattern of activity occurred for foot movement. Furthermore, imagination of right hand movement produced contralateral beta ERD and an ipsilateral beta ERS. It has been shown that increased cellular excitability in thalamo-cortical systems results in a low amplitude desynchronised EEG (Steriade and Llinas 1988). Thus, at least for relatively low frequencies, the ERD shown above can be interpreted as an EEG correlate of activated cortical areas involved in the processing of cognitive or sensory information or the production of motor behaviour. Conversely a deactivated state, without information processing and decreased excitability of cortical neurons, is characterised by ERS (Pfurtscheller 1992).

2.7 Coregistration of MEG data with subject cortical anatomy

In order for the recorded MEG data to be of any use accurate coregistration with the subject's MRI scan is essential (the procedure used at Aston is described in detail in Adjamian *et al.* 2004). During the MEG recording, coils are placed on the subject's head such that when a small current is passed through them a magnetic field is produced which can be measured by the MEG system. As the SNR is high and the number of coils is known then the location of the coils can easily be determined by a least squares optimisation algorithm. In the Aston 151 channel system the mean localisation error of the coils is less than 1mm (CTF Systems Inc). The head coils serve two purposes: they enable the location of the MEG sensors with respect to the head and by localising the coils before and after the MEG recording the amount of movement that has taken place can be determined.

Co-registration is performed by aligning (using Align, Kozinska *et al.* 1997) two surfaces defined in the MRI and MEG co-ordinate system. The MRI 'head' points are obtained from the subject's MRI through segmentation and boundary extraction (see Pal and Pal 1993 and Clarke *et al.* 1995 for details of how this is performed). The MEG surface co-ordinates are measured using a 3D electromagnetic digitiser (Polhemus Isotrak). In order to minimise the error during this procedure a bite bar system is employed (Singh *et al.* 1997, Adjamian *et al.* 2004). The bite bar consists of a rigid plastic holder and dental thermoplastic into which the subjects make a dental impression. The plastic holder is placed onto a rigid wooden stand and the subject locates themselves within their dental impression so that movement is minimised.

The plastic holder contains four holes which are localised using the digitiser. Following this the location of each of the localisation coils on the head is obtained. The final procedure is to define the head surface with the digitiser. It is essential that no deformation of the skin surface occurs so the pen is not pressed too hard. During this procedure the digitising pen is moved back and forth across the whole surface of the scalp. However as the majority of the scalp is nearly spherical it is essential that points around the nose and eyes are included to produce better definition of the head shape (Wang *et al.* 1994). These digitised points are then surface matched to the MRI surface points (See Wang *et al.* 1994 for description of how this is done) so that the location of the sensors and the anatomical information are given in the same coordinate system. An example of this is shown in Figure 2-15.

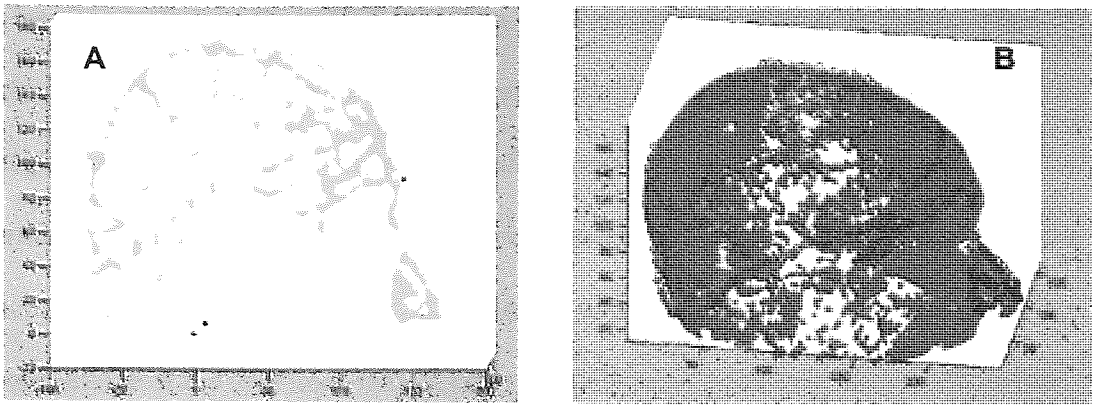

Figure 2-15. Overleaf. An example of the co-registration process. A. The points produced by using the digitising pen on the subject's head. B. The points co-registered with the subject's head shape (red) obtained from their MRI scan. The green points are the approximate alignment performed by the experimenter, the blue points represent the optimum co-registration (Using Align, www.ece.drexel.edu/ICVC/Align/align11.html)

There are several sources of possible co-registration error that can occur during the process. Errors can occur during the MRI scan itself with the subject movement possibly blurring the scalp boundary. Similarly, errors can occur during determination of the scalp itself. However, these MRI errors can usually be corrected by software tools. Errors in the MEG digitisation process occur as a result of user error and movement of the subject. If used correctly the error due to the 3D digitiser is approximately 0.1mm (Polhemus 1992). Deformation of the skin by the digitising pen can be approximately 1 to 3mm (Schwartz *et al.* 1996). Movement of the subject is negligible using the Aston system due to stabilising the subject with the bite bar.

2.8 Functional magnetic resonance imaging (fMRI)

2.8.1 Indirect measurements of neuronal activity

Whereas MEG is a direct measure of neuronal activation other imaging techniques exist that measure the activation of neurons indirectly by means of haemodynamic or metabolic effects. Positron Emission Tomography (PET) has been used successfully as

an imaging technique for many years (Fox and Raichle 1984, Fox *et al.* 1986). The technique relies on the administration of radioactive tracers and the acquisition of images that show the spatial distribution of the tracer within the brain during a particular task. Quantification of the regional cerebral blood flow (rCBF) that effect the tracer distribution results in a spatial map of the activated brain regions. The disadvantage of the technique is its relative invasiveness. Moreover the technique has very poor temporal resolution and relatively poor spatial resolution. Functional magnetic resonance imaging (fMRI) (Ogawa *et al.* 1992, Kwong *et al.* 1992) is capable of visualising the neuronal activations of the human brain in a non-invasive way by measuring the physiological changes in oxy- and deoxyhaemoglobin concentration in small cortical blood vessels following neuronal activation.

2.8.2 The Principles of MRI and fMRI

The magnetic resonance signal arises from the nuclei of atoms within the body which possess a property known as 'spin angular momentum', the most important of these being hydrogen nuclei which contain a single proton. The spin properties of the nucleus cause it to act as a small magnet and the strength of the magnetic moment depends on the type of nucleus. Due to this magnetic property a percentage of these nuclei will align themselves with a strong external magnetic field meaning that if a subject is placed into a very strong magnetic field (in the order of 1.5 – 7 Tesla) the spins of the atomic nuclei align themselves with the magnetic field such that their spins are orientated either 'parallel' or 'anti-parallel' with the field. The spins precess around the direction of the applied field at a characteristic frequency known as the Larmor frequency (equation 2) which is proportional to the strength of the magnetic field, with different nuclei precessing at different frequencies in the same magnetic field.

$$\nu = \gamma B_0 \tag{2}$$

where ν is the frequency in MHz, γ is the gyromagnetic ratio in MHz/Tesla for the nucleus under consideration and B_0 is the magnetic field strength in Tesla. This is an important equation in MRI as it relates the frequency of the resulting signal to the static magnetic field strength. The Larmor frequency for Hydrogen in a 3T scanner is approximately 128MHz.

To produce a measurable signal requires the application of a brief radio frequency (RF) electromagnetic pulse transverse to the applied magnetic field. This causes the spins of the atomic nuclei to precess in relative phase in the transverse direction. As the spins return to their original state (relax) they release RF energy which is detected by the receiver coil. Two types of relaxation occur; longitudinal (T1) and transverse (T2). Longitudinal relaxation occurs when the nuclear spins realign themselves with the original magnetic field. The time taken for 63% of the spins to return to their initial state is known as T1. Furthermore, the MR signal decays because the spins in the transverse direction start rotating out of phase. The time taken for 63% of the recorded signal strength to be lost is known as T2.

The RF pulse sequence is determined by two timing parameters, TE and TR, which affect the tissues highlighted by the scan. The interval between the excitatory RF pulse and the detection of the response of the tissues to this signal is defined as the echo time (TE) with the time between two RF pulses being known as TR. Biological tissues have different T1 and T2 relaxation times. The amount of signal lost at TE reflects the

relative tissue T2 values, so long TE values allow more T2 relaxation to occur and influence image contrast. Conversely tissues with a long T1 require a longer time for the longitudinal magnetisation to re-align meaning that re-exciting with an RF pulse, before the longitudinal relaxation is complete, can cause tissues with different T1 values to have different intensities within the image. A T1 or T2 weighted image can therefore be produced by an appropriate choice of TR and TE.

The precessional rate of protons depends on the local magnetic field, so by producing a spatially varying magnetic field it is possible to separate signals from different locations based on their frequency. To achieve this three mutually orthogonal sets of electromagnetic "gradient coils" are used to encode the spatial coordinates of the MR signal and reconstruct them into images (Harvey and Mansfield 1994).

2.8.3 Neuronal activation and BOLD response

The activation of a brain area produces an increase in the metabolism of its neuronal population which in turn causes an increase in the rCBF (see Figure 2-16). This is only to be expected as the area that is being activated requires increased oxygen and glucose supplies to feed the neuronal activity. Initially there is a drop in the oxygen level of the blood over the first fractions of a second following activation due to an increase in the local cerebral metabolic rate and this is sometimes termed the early response (Malonek and Grinvald 1996). However, following this there is a large increase in local oxygen concentration due to an over-supply of oxygenated blood which exceeds the transient need and this is sometimes termed the late response (Malonek *et al.* 1997). This local increase in blood oxygenation, occuring some 3 to 9 seconds after onset of the neuronal

activation, is the principle functional correlate measured using fMRI and is known as the blood oxygenation level dependent (BOLD) contrast.

2.8.4 BOLD theory

The theory behind BOLD is based on the observations of Thulborn 1982 who found that the transverse relaxation times of water protons could provide information about blood oxygenation. The magnetic state of the oxygen carrying molecule haemoglobin (Hb) is dependent on the amount of oxygen being carried by Hb. Hb is paramagnetic when deoxygenated (deoxyhaemoglobin) and diamagnetic when carrying oxygen (oxyhaemoglobin). Hb is found in the red blood cells, therefore the volume magnetic effect caused by the flow of red blood cells is dependent on the amount of dia- or paramagnetic Hb contained at any particular time. Thus, when the blood cells are fully oxygenated they have the same magnetic signature as the surrounding blood plasma in the vessels. Conversely, when the blood cells are deoxygenated they have an increased paramagnetism compared to the surrounding plasma so intravascular magnetic gradients occur. Similarly the paramagnetism of the deoxygenated blood differs from that of the tissues surrounding the blood vessels and so extravascular magnetic gradients are set up. These magnetic field inhomogeneities lead to a dephasing of the nuclear spins which has the effect of shortening the T2 relaxation time and so leads to a darker MR image.

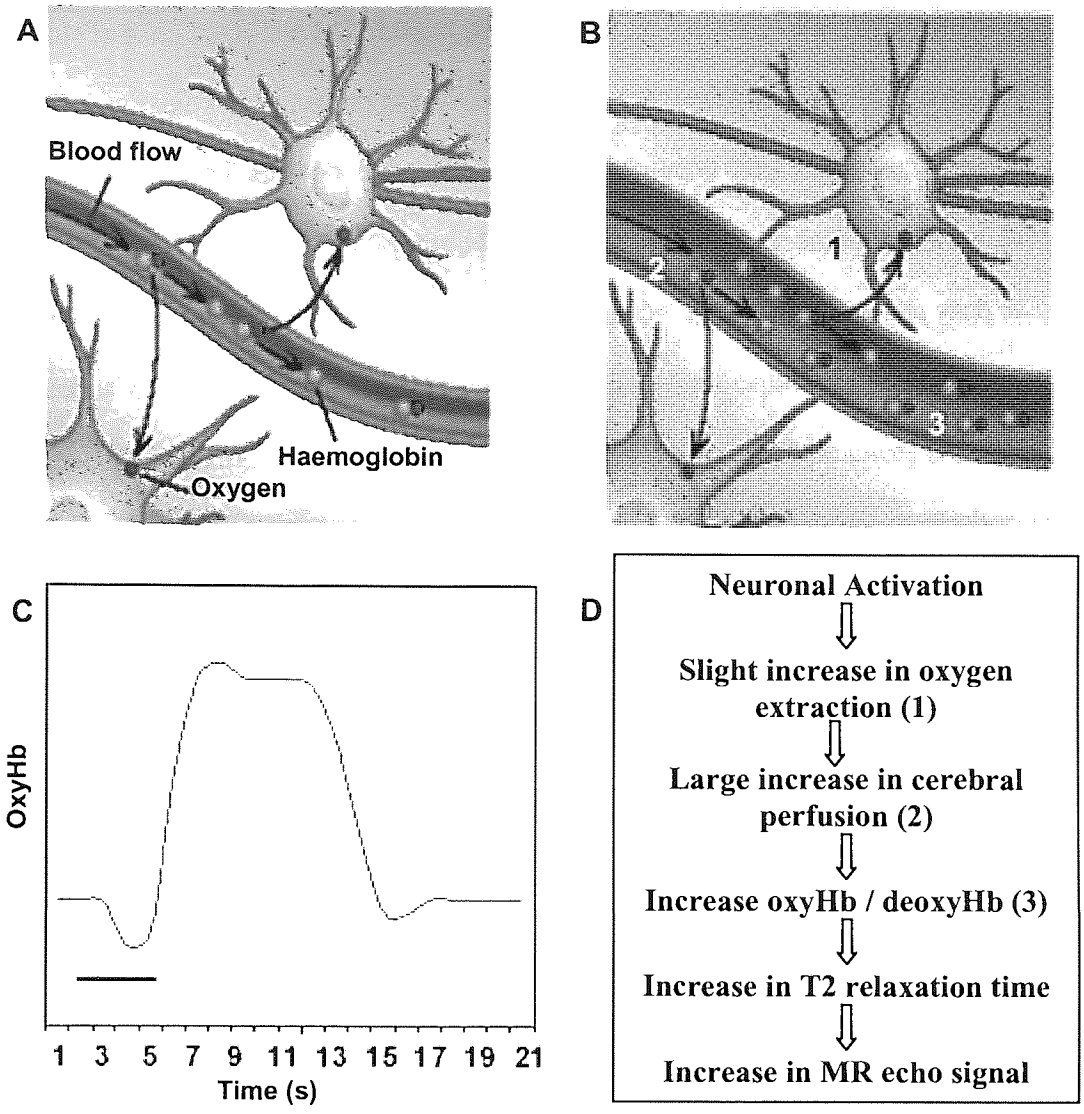

Figure 2-16. A diagrammatic explanation of the BOLD response. A. The situation at rest. B. The situation during neuronal activation with increase in oxygen perfusion being greater than the oxygen required by the neurons (Both A and B adapted from Raichle 1994). C. Timecourse of the change of oxyhaemoglobin concentration upon regional neuronal activation (horizontal bar). D. The sequence of cerebrovascular changes leading to increased T2 and increased MR signal.

2.8.5 Echo-planar imaging (EPI)

In choosing an MR scanning technique for fMRI, three related factors play an important role: spatial resolution, acquisition speed (i.e. temporal resolution) and signal-to-noise ratio (SNR), with the optimisation of one factor being at the cost of the other two. EP-fMRI requires the need for rapid acquisition techniques and this is achieved through echo-planar imaging (EPI) (Mansfield and Maudsley 1977). This technique makes it

possible to form complete MR images in as little as 40 ms since all encoding steps needed for image formation are achieved during the several tens of milliseconds that the MR signal is present after an RF excitation. Both spin-echo (SE) and gradient-echo (GE) EPI sequences have been proposed for use in fMRI (Bandettini *et al.* 1994). SE sequences tend to be more sensitive to oxygenation changes in small vessels such as capillaries whilst a GE sequence is equally sensitive to both capillaries and larger vessels (Ogawa *et al.* 1993, Boxerman *et al.* 1995). However SE sequences are seldom used in practice since neuronal activation induced signal changes are much smaller compared to GE sequences.

For a gradient-echo EPI sequence, at time zero a radiofrequency (RF) excitation 90° pulse with a narrow frequency range is transmitted to the subject in the presence of a spatial magnetic field gradient. As the magnetic resonance signal depends on the exact match between the RF excitation pulse frequency and the proton spin frequency, which depends, in turn, on the local magnetic field strength, this pulse will excite only the protons over a correspondingly narrow range of locations. In-plane spatial encoding is achieved by applying magnetic field gradients across this image slice and an echo train is generated by a rapidly alternating this gradient.

As the switching of the gradient is extremely rapid the amplitude of the gradient is small. Due to this phase encoding is achieved by gradient "blips", small phase encoding gradients that add up, in between the echoes. The phase gradient scheme is designed such that the echo with the highest amplitude occurs at time TE and this acquisition is sequentially repeated 100 to 120 times during the course of the fMRI experiment. The time between repetitions of the acquisition (TR) is typically at least

2000 ms which leaves a lot of time in between successive acquisitions of one slice through the brain to excite neighbouring slices, offering the possibility of multi-slice imaging without time penalty.

Disadvantages of the technique are the relatively low spatial resolution due to the small image matrix (typically 64x64 or 128x128, i.e. 3x3 mm^2 or 1.5x1.5 mm^2 pixel size). Similarly the large acquisition bandwidth needed for the rapid sampling results in a low SNR. This intrinsic low SNR of fMRI is compensated by the high temporal resolution that allows the acquisition of more images per fMRI experiment than other techniques.

2.8.6 fMRI experimental design

Traditionally fMRI experiments have employed designs using extended periods of ''on'' versus ''off'' activations, the so called block design, which have been the stalwart of functional imaging studies for many years (see Figure 2-17). However, although such block designs are necessary when imaging the haemodynamics of tasks that can be maintained for many seconds they are not ideal for measuring transient events where activity is detectable within seconds of stimulus onset.

Event-related experimental designs (ER-fMRI) have become increasingly popular in fMRI research in recent years. This design allows different trials or stimuli to be presented in arbitrary sequences, thus eliminating potential confounds, such as habituation, anticipation, set, or other strategy effects (Rosen *et al.* 1998)(See Figure 2-17). The technique was established by Dale and Buckner 1997 who showed that the lateralisation of the haemodynamic response following a visual stimuli was the same following both a block design and a rapidly presented random design.

The measurement of ER-fMRI is possible due to the nature of the BOLD-contrast haemodynamic response. For a brief sensory event the haemodynamic response is delayed in onset, occurring about 2 sec after neuronal activity, and is prolonged in duration (Blamire *et al.* 1992). For a neural event that lasts a second, the robust positive deflection of the BOLD contrast response will evolve over a 10–12-sec period while certain, more subtle, components of the response will have considerably longer recovery periods. However, these haemodynamic events do not need to be separated in time as ER-fMRI is able to measure the separate contributions of rapidly occurring neuronal events even when the haemodynamic responses they elicit overlap. The reason for this is that, on first approximation, the haemodynamic response summates in a linear fashion over time (Boynton *et al.* 1996, Dale and Buckner 1997). This means that separate sensory and higher level cognitive events can be elicited in rapid succession and their response contributions separated and analyzed.

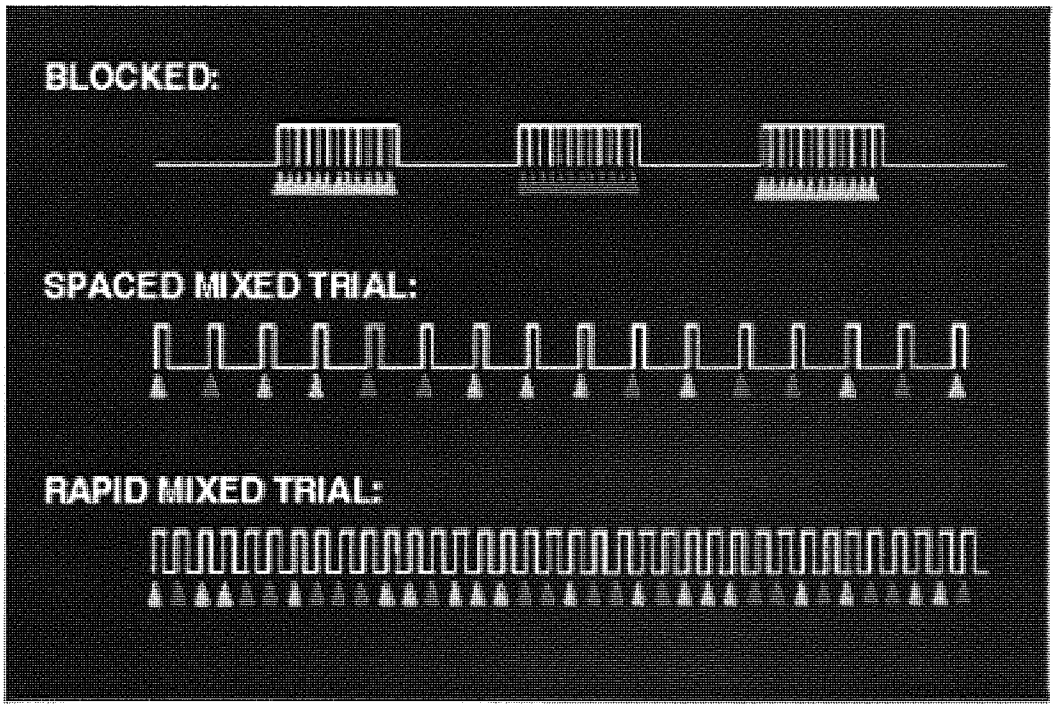

Figure 2-17. Overleaf. Schematic diagram illustrating the difference between two forms of ER-fMRI paradigms and a more traditional blocked trial paradigm. Each schematic shows two trial types indicated by either yellow or red arrows. In blocked trial paradigms (labeled blocked), the trial types are clustered together in succession so that the same trial type or condition occurs for an extended period of time. ER-fMRI, by contrast, allows paradigms that randomly intermix different trial types either by spacing them widely apart to allow the haemodynamic response from one trial to decay before the next trial occurs (spaced mixed trial), or by presenting them rapidly (rapid mixed trial) and using analysis methods to account for the overlap of the haemodynamic response across trials. Note that for successful separation of trial types in rapid mixed trial designs, randomisation or ISI jittering strategies must be used. (Adapted from Buckner 1998)

2.8.7 The processing of fMRI data

The processing of the fMRI data requires a number of analysis steps which, in the work presented in this thesis, are implemented using the software package SPM99.

2.8.7.1 Motion correction

The intensity changes measured during the BOLD response are extremely small (in the region of fractions of a percent). It is therefore vital that the data for analysis is not contaminated by sources of artefact. The major source of artefact is that of head motion during the acquisition process, which as well as reducing SNR can also introduce "false" activations. Similarly movement of a lesser degree can occur due to the pulsatile movement of cortical tissues. Large head movements are minimised by securing the subject's head during the recording. Post recording correction of head movement is achieved by the rigid realignment of the consecutively acquired images in the data series with the first image (Friston *et al.* 1995).

2.8.7.2 Slice Timing Correction

Event-related fMRI is a technique that is heavily dependent upon time-locking the stimulus to the data. To do so accurately requires one to account for the differential slice acquisition times, especially for longer TRs. Often slices are acquired in an interleaved manner, thus the first slice can differ in time from the second by as much as TR/2.

Correcting this phase shift requires one to interpolate the time series for each voxel, to a fixed reference time.

2.8.7.3 Spatial normalisation

This is the procedure by which individual brains are transformed so as to fit a "standard brain". During the procedure the variations in size, position and shape are corrected by warping the brain onto the template using 3 translations, 3 rotations, 3 scaling and 3 skewing factors (Worsley and Friston 1995). By performing this procedure the anatomical differences between individuals are reduced so allowing the production of group data. Secondly the location of activations can be expressed with respect to a fixed reference frame thus allowing the comparison of results between laboratories (Talairach and Tournoux 1988).

2.8.7.4 Spatial smoothing

The fMRI images are spatially smoothed or filtered prior to statistical analysis. This leads to an increased SNR provided that the width of the filter matches the spatial extent of the measured signal. Furthermore, smoothing the data after spatial normalisation removes any residual interindividual anatomical differences, thus improving the data for group analysis.

2.8.7.5 Temporal smoothing

Unlike spatial smoothing, which works on each volume separately, temporal smoothing (filtering) works on each voxel's time series separately. The main point of this filtering is to remove unwanted components of the BOLD signal without altering the signal of interest. Components of the time series that are varying more slowly than the signal of

interest are removed with high pass filtering whilst high frequency noise is reduced using low pass filtering.

2.8.7.6 Statistical analysis of fMRI data

In fMRI data the effect of a stimulus may be as little as 1% of the BOLD signal. The detection of this small signal, in a simple fMRI design, can be done by careful averaging of the data over time which differentiates the signal of interest from the large amount of background noise. However more complex designs require more complex analyses that depend on the construction of a model for the way in which BOLD response depends on the stimulus. Such a model must include a component of random error which explains how the observations vary even if the experiment is repeated on the same subject under exactly the same conditions. Statistical analysis of the data is used to best estimate the parameters in the model, including the variability of the errors. The mathematical background behind these statistics is beyond the scope of this thesis but the interested reader is referred to Friston *et al.* (1995) and Friston *et al.* (1998) for further details.

2.8.8 Comparison of SAM and fMRI

MEG and fMRI have complimentary strengths and weaknesses; MEG has excellent temporal resolution but variable spatial resolution whilst fMRI has excellent uniform spatial resolution but poor temporal resolution. The SAM technique (see section 2.6.1), as used in the analysis of MEG data in this thesis, allows the same experiments to be performed using both MEG and fMRI as identical block and event related experiments can be developed for the two modalities. The statistical analysis of the SAM data is formulated on a voxel by voxel basis meaning that statistically thresholded group

images can be produced similar to those produced in fMRI analysis (Singh *et al.* 2003). Similarly, it has been shown that there is an excellent spatial relationship between the haemodynamic response and ERD / ERS as measured by SAM (Singh *et al.* 2002). A major advantage of the SAM technique is that not only can the spatial localisation be determined but the temporal and oscillatory potential properties of the response to the stimulus can be analysed in detail.

2.9 Conclusion

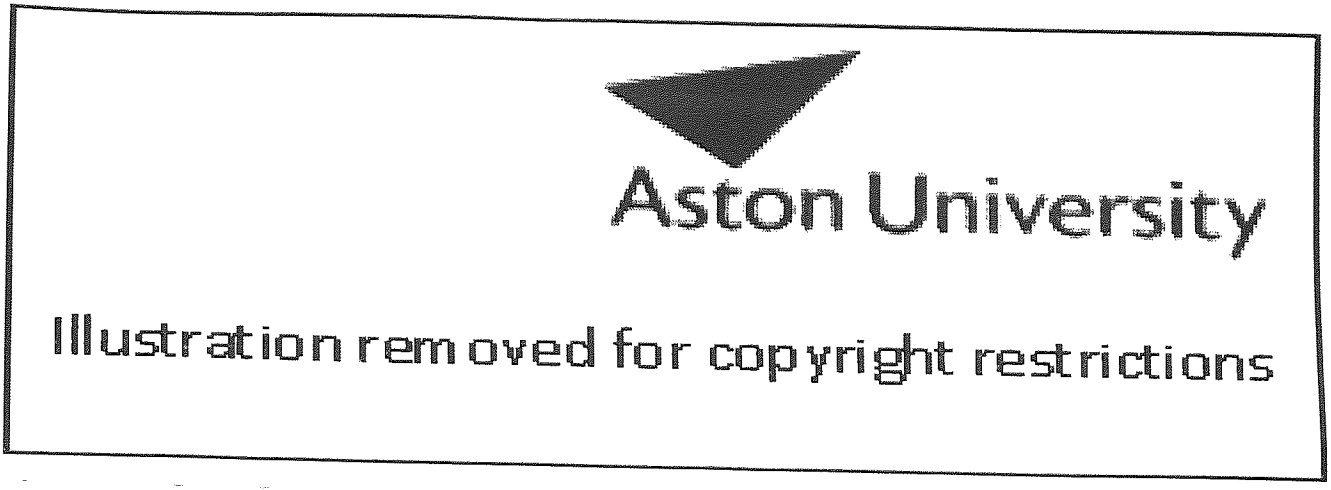

Figure 2-18. Comparison of temporal and spatial resolution between different functional imaging techniques. From CTF Systems Inc.

Magnetoencephalography has excellent temporal resolution (see Figure 2-18) and is a direct measurement of the ongoing electrical brain activity, unlike other functional imaging techniques such as PET, SPECT and fMRI which are based on indirect (metabolic) measures of neuronal activity. Historically, MEG studies have relied on dipole fitting techniques which are known to have a number of limitations (see section 2.5.2.1.1). The method chosen for the analysis of data in this thesis is SAM. The technique uses the data covariance to obtain solutions, meaning that task-related changes of spectral power can be obtained between active and passive states in terms of ERD and ERS. This allows information to be obtained about both the MEG source localisation and the frequency changes in underlying cortical activity that are taking place.

Recently, there have been increasing numbers of research papers using the functional imaging technique of synthetic aperture magnetometry (SAM), studying various cortical areas using a variety of experimental paradigms. However, our knowledge of the oscillatory changes that underpin these various cortical functions is still limited and, in particular, how these oscillatory changes link to changes in mean activity level and hence the BOLD response.

The visual cortex of the brain has been extensively studied for many years using a variety of methodologies such as psychophysics, single cell studies in animals and functional imaging studies in humans. As a result there is a huge knowledge base against which to compare the results of new methodologies. In the following experimental chapters SAM is used to study the oscillatory changes taking place in the visual cortex using a number of different experimental paradigms and comparing these results to previous fMRI studies. In two of the chapters the oscillatory changes in response to the parametric variation of a visual stimulus are studied and in one of these chapters (chapter 6) there is a direct comparison between cortical oscillatory changes and the BOLD response. Of the remaining experimental chapters, one studies the oscillatory changes in higher level cognitive functions (attention), whilst in the other the interesting phenomenon of implied motion is studied. Again these are both compared to previous studies using fMRI.

3. TEMPORAL FREQUENCY TUNING IN THE VISUAL CORTEX INVESTIGATED USING SYNTHETIC APERTURE MAGNETOMETRY (SAM)

3.1 Overview

This chapter uses Synthetic Aperture Magnetometry (SAM) analyses of Magnetoencephalographic (MEG) data to investigate how cortical response magnitude and frequency vary as a function of stimulus temporal frequency. The chapter begins by reviewing the literature on temporal frequency tuning and follows this by describing two separate experiments. The results highlight the variation in parametric response characteristics between medial visual cortex and extrastriate cortex.

The work in this chapter has been published previously:

Fawcett et al., Neuroimage 2004, 21(4), p. 1542-1553

3.1.1 Aims

To investigate if evoked and induced oscillatory responses in visual cortex vary parametrically with stimulus temporal frequency.

3.2 Introduction

How the visual cortex deals with the spatiotemporal aspects of our visual field is fundamental to how we view the world around us, and there is converging evidence from a variety of neuroscience research areas that temporal frequency is a fundamental visual attribute, and has a significant neural substrate dedicated to its analysis and representation (Krukowski *et al.* 2001).

3.2.1 Single cell studies of temporal frequency tuning

The temporal frequency sensitivity of V1 and a number of other visual areas have been investigated using single-cell studies (e.g. Foster *et al.* 1985; Gegenfurtner *et al.* 1997, Levitt *et al.* 1994; Tolhurst and Movshon 1975). These show that temporal frequency tuning is similar across areas V1, V2 and V3, with most cells having a fairly broadly tuned response that falls for frequencies greater than 8 Hz. This temporal frequency response within V1 appears to be a filtered version of the signal from the lateral geniculate nucleus (Hawken *et al.* 1996). Importantly, the cells in V1 and V2 show the same temporal frequency tuning for stimuli of different spatial frequencies, that is, spatial and temporal frequencies are separable parameters (Foster *et al.* 1985, Tolhurst and Movshon 1975). In contrast, cells within the motion complex V5/MT are commonly thought of as being optimally tuned for velocity, rather than temporal frequency (Perrone and Thiele 2001, Perrone and Thiele 2002, Rodman and Albright 1987) so that, by definition, the response properties of cells are not separable in terms of stimulus spatial and temporal frequency.

3.2.2 Psychophysical studies of temporal frequency tuning

Many psychophysical studies have also studied the temporal frequency sensitivity of human visual cortex. Presumably, psychophysical performance depends on the underlying temporal frequency sensitivities of all the visual areas, although how the neuronal response properties of V1 and V5/MT, for example, are combined in perceptual judgements is unclear. For example, there is some debate as to whether human psychophysical performance is temporal frequency- or velocity tuned. The optimal motion stimulus (Watson and Turano 1995) appears to be aligned along the spatial and temporal frequency axes, rather than along an isovelocity contour, with a

peak at 3 cycles/deg and 5 Hz, although other earlier studies suggested that temporal channels in the human motion system respond differently to low and high spatial frequencies (Tolhurst 1973). Several psychophysical studies have shown that the human motion system contains both low-pass and band-pass-tuned detectors of temporal frequency (Anderson and Burr 1985) and some models of speed perception postulate that velocity tuning in V5/MT occurs via a synthesis of these low-pass and band-pass channels in V1 (Perrone and Thiele 2002). In support of this, single-cell studies in primates have revealed neurons showing both low-pass- and band-pass-tuned responses to temporal frequency (Foster *et al.* 1985, Hawken *et al.* 1996).

3.2.3 Functional imaging studies of temporal frequency tuning

The temporal frequency tuning of human visual cortex has also been studied using functional imaging, which can potentially bridge the gap between single-cell studies in animals and human visual psychophysics. Using magnetoencephalography (MEG), the transient evoked response in area V5/MT has been shown to be broadly tuned from 1 to 30 Hz (Anderson *et al.* 1996), whilst in V1, it is band pass tuned to 8–10 Hz (Fylan *et al.* 1997). Electroencephalography studies (Morrone *et al.* 1996) also show that the amplitude of the visual-evoked potential (VEP) peaks at approximately 10 Hz in adults. Studies using positron emission tomography (PET) have shown that activation in the visual cortex peaks at a frequency of 8 Hz (Fox and Raichle 1984) and that this tuning characteristic is independent of the spatial characteristics of the stimulus (Fox and Raichle 1985). Similarly, fMRI studies of the blood oxygenation level-dependent (BOLD) response (Hagenbeek *et al.* 2001, Kwong *et al.* 1992, Kaufmann *et al.* 2001, Ozus *et al.* 2001, Singh *et al.* 2000, Thomas and Menon 1998) have shown activation peaking at 6–11 Hz. Rather surprisingly, it also seems that the temporal frequency

tuning curves obtained using fMRI are the same in all visual areas (Singh *et al.* 2000). These functional imaging studies used stimuli containing very different spatial frequency content, ranging from flickering LED stimuli to drifting sinusoidal gratings, yet all show very similar temporal frequency tuning curves.

3.2.4 Cortical oscillatory changes and temporal frequency tuning

In terms of EEG and MEG studies of cortical function, there has been much recent interest in the frequency specific oscillatory power changes that take place whenever a task is performed (see section 2.6.2). In the case of an ongoing visual stimulus containing temporal frequency structure (such as flicker), the evoked oscillatory power changes are equivalent to the well-known steady-state visual evoked potential (SSVEP, Herrmann 2001, Regan 2003, Silberstein 1995).

Using a combined fMRI and MEG paradigm it has been shown that the location of BOLD responses in cognitive studies closely match those cortical areas showing ERD and not ERS (Singh *et al.* 2002). In principle, therefore, the magnitude of ERS/ERD effects in response to visual stimuli could be a useful measure of temporal frequency tuning within visual cortex, and may help to clarify or confirm some of the results that have been found using indirect imaging techniques such as PET and fMRI. Although it is known that frequency specific changes do occur in the visual cortex to visual stimuli (Herrmann 2001, Lutzenberger *et al.* 1995, Sewards and Sewards 1999), the localisation and parametric variation of evoked oscillatory power changes and induced ERD/ERS has not been previously investigated. This study will therefore use synthetic aperture magnetometry (SAM) to investigate the response of the visual cortex to a low-level

stimulus by measuring the variations in cortical oscillatory power as a function of temporal frequency.

3.3 Methods

3.3.1 Experiment 1

Six normal right-handed subjects (2M, 4F, 31 ± 9yrs) gave their consent to participate in the study. MEG data was collected using a 151 channel CTF Omega system (CTF Systems Inc., Port Coquitlam, Canada) at a sampling rate of 312 Hz. Data was recorded in a single un-averaged 240 second run which was divided into sixteen 15 second long epochs (see Figure 3-1). The first, Passive, epoch consisted of 15 seconds of grey background with a central fixation spot. The second, Active, epoch consisted of 15 seconds of stimulus presentation. This Passive-Active design was repeated eight times to make a single 240 second run. The visual stimuli were generated by an Apple Powerbook and presented to the subject via an Eizo Flexscan T562-T monitor with a refresh rate of 85Hz, viewed through a window in the scanner room using a mirror.

A)

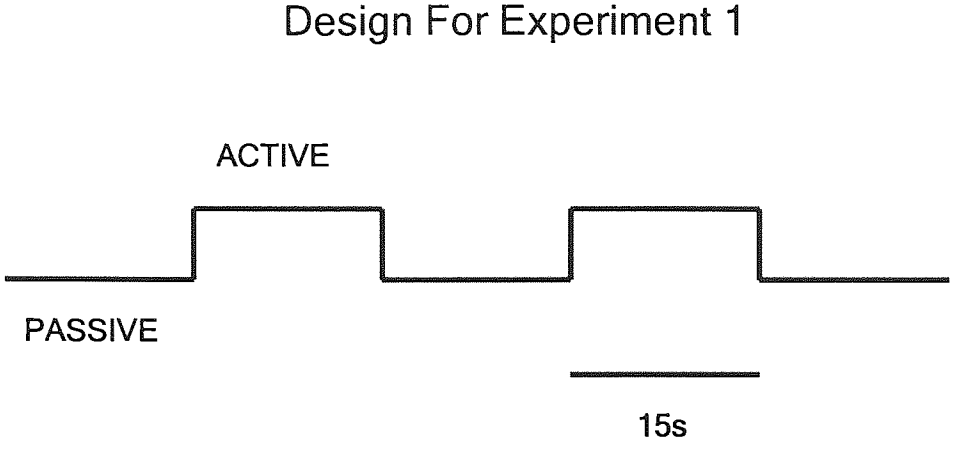

Temporal Frequencies 0, 2, 4, 8, 21Hz

8 Active phases for each stimulus frequency

B)

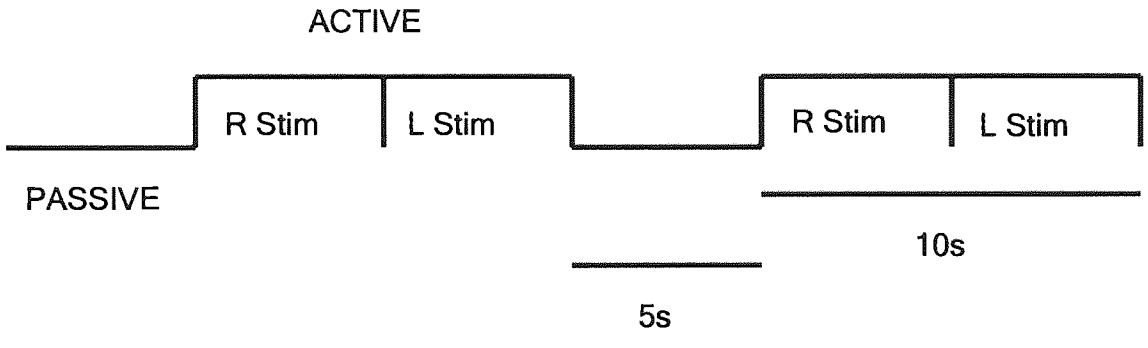

Temporal Frequencies 1, 2, 4, 8, 16Hz

20 Active phases for each stimulus frequency

Figure 3-1. Diagrammatic outline of the experimental paradigms used in this study. (A) Simple boxcar design used in experiment 1. A 15s passive period was followed by a 15s active period so that 8 active periods were recorded for each stimulus frequency. (B) Boxcar design used in experiment 2. The active and passive phases were reduced to 5s. During the active phase the stimulus appeared in the right lower visual field for 5s then moved to the left lower visual field for 5s. There were 20 active phases recorded for each stimulus frequency.

The stimulus consisted of a squarewave reversing checkerboard placed in the lower right visual quadrant, subtending 2° x 2° of visual angle with an eccentricity of 0.5° from both the horizontal and vertical meridians (see Figure 3-2) .

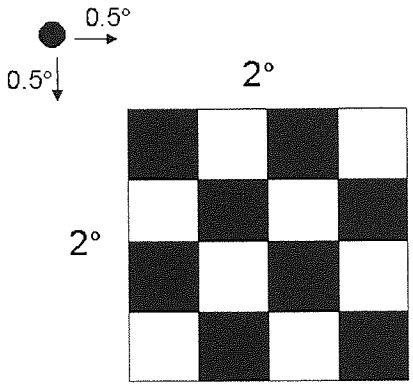

Figure 3-2. Diagramatic representation of the stimulus used in this study (not to scale). The stimulus was presented in the lower right visual quadrant to avoid cancellation effects that can occur with MEG due to opposing sources being present on either side of the calcarine fissure.

The use of a quadrant stimulus minimises the possibility of cancellation effects that can occur with MEG, due to current sources being present on two or more opposing banks of the calcarine sulci. Subjects were requested to fixate on a central fixation spot throughout the experiment. Stimuli with temporal frequencies of 0, 2, 4, 8 and 21Hz were randomly presented to each subject with only one temporal frequency presented in each run. The accuracy and stability of the stimulus frequency was verified using a photodiode placed on the presentation monitor. The subject rested for one minute after each 4 minute acquisition.

After the data was collected, a 3-D digitiser (Polhemus Isotrack) was used to digitise the shape of the subject's head in the MEG laboratory. Using Align

(www.ece.drexel.edu/ICVC/Align/align11.html) this surface was matched to a head surface extracted from the subject's own, previously acquired, anatomical MRI in order to coregister the MEG data with the subject's anatomy. Following this the MEG data was analysed using Synthetic Aperture Magnetometry (see section 2.6.1).

To produce the temporal frequency tuning curves, the peak SAM value within visual cortex for each of the stimulus frequencies and SAM analysis frequency bands was measured. The resultant values were normalised to a maximum of 100 for each subject, averaged across all subjects and plotted to produce the tuning curves. For those voxels showing the largest activation values, time–frequency representations were produced using Morlet wavelet analysis (see section 2.6.1.2).

3.3.2 Experiment 2

In the second experiment a sinusoidal, rather than square-wave, modulated reversing checkerboard stimulus was used. Six subjects (2M, 4F, 29.4 ± 6 yrs) were scanned in a single un-averaged 300 second long run which was divided into 5 second long epochs arranged in a Passive-Right-Left boxcar design (see Figure 3-1). The spatial form of the stimulus was the same as the first experiment and appeared first in the lower right visual field for five seconds before moving to the left lower visual field for five seconds. Temporal frequencies of 1, 2, 4, 8 and 17Hz were randomly presented to each subject. Only one temporal frequency was presented in each run. The peak voxel measurement was produced for both medial visual cortex and V5/MT and the resulting data was analysed using the same techniques as Experiment 1.

3.4 Results

3.4.1 Experiment 1

3.4.1.1 Occipital MEG responses

The first stage in a SAM analysis is to identify the oscillatory frequency ranges within which stimulus-related changes occur. In an initial analysis, this was done by examining the Fourier spectrum of the occipital MEG channels. Clear peaks were visible at the second harmonic of the stimulus frequency, f, that is, at 2f (see Figure 3-3).

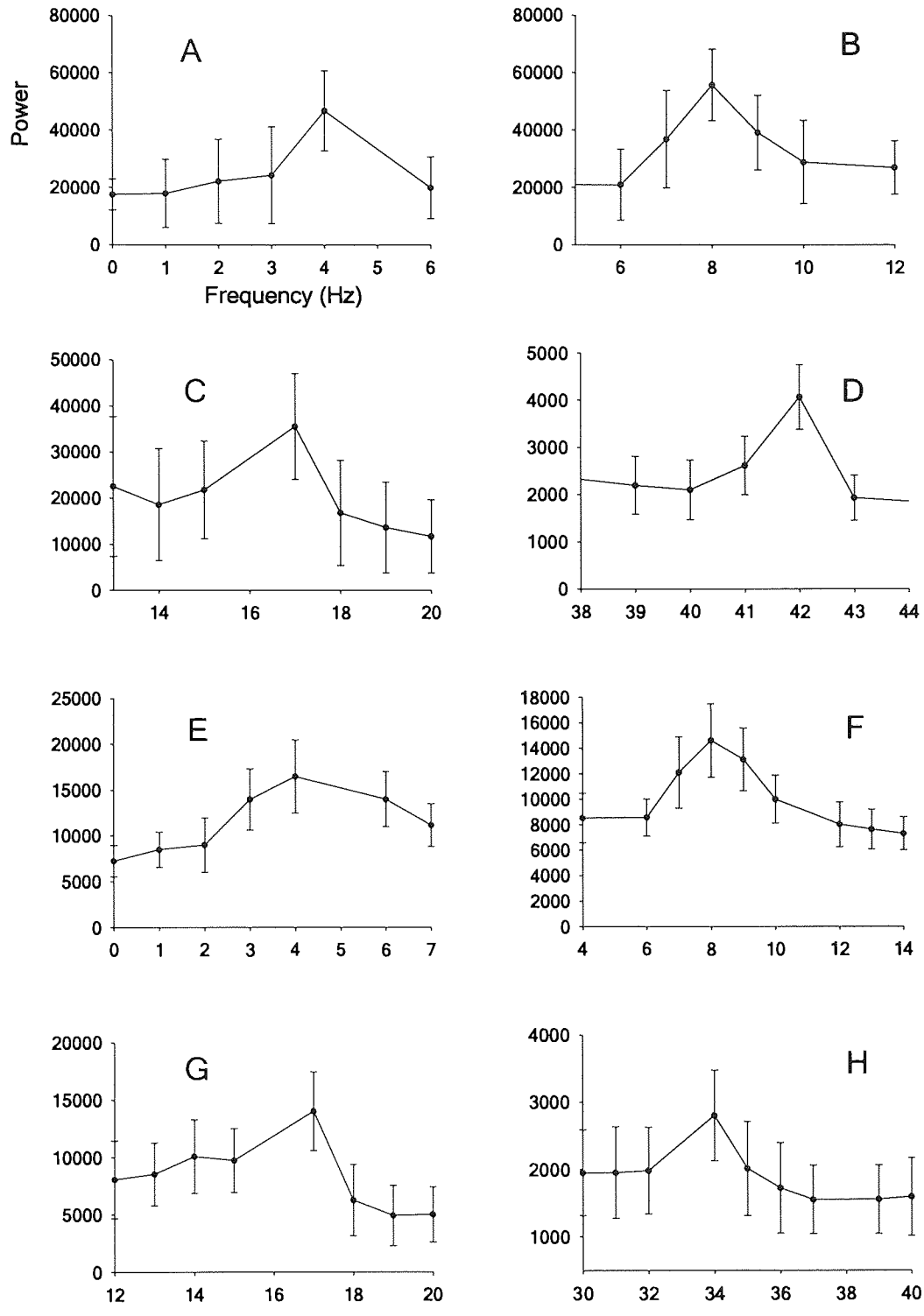

Figure 3-3. A plot of spectral power against frequency measured from the raw data, averaged across occipital gradiometers and across subjects. Data from experiment 1 is shown at stimulus frequencies of, A) 2Hz, B)4Hz, C)8Hz and D)21Hz. Data from experiment 2 is shown at stimulus frequencies of, E) 2Hz, F) 4Hz, G) 8Hz and H) 16Hz. Note that in each case only a small frequency window of the complete power spectrum is shown to highlight the 2f peak. The spectral power is scaled differently in each case to allow visualisation of the peaks. Error bars show the standard error of the mean.

3.4.1.2 SAM images

SAM images were then generated by calculating the difference in oscillatory power between the Active and Passive states, within narrow bands around the 2f frequencies, that is, 3–5 Hz, 7–9 Hz, 15–17 Hz and 41–43 Hz, as well as a broad-band analysis in the range 5–45 Hz. Figure 3-4 shows an example from a single subject of medial visual cortex activation within the 3–5 Hz band, produced by a checkerboard stimulus reversing at 2 Hz.

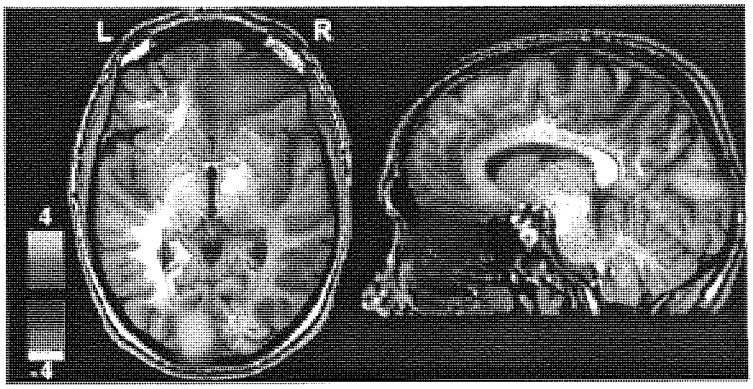

Figure 3-4. An example of a single-subject SAM image within the 3-5Hz response band, to a 2Hz stimulus. ERS (yellow/orange) is evident superior to the calcarine sulcus in the contralateral hemisphere.

Consistent with a right lower visual field stimulus, the activation appears in the left medial visual cortex above the calcarine sulcus, and is a stimulus-related power increase. Note that the activation is more superior than might be predicted for purely V1 activation. This can be explained either by the fact that the ERS is a summary of activation across multiple medial areas, or that it is a result of MRI–MEG coregistration errors, which can be several millimetres in the occipital lobe (Singh *et al.* 1997).

3.4.1.3 *Temporal frequency tuning curves*

Figure 3-5 shows the mean normalised temporal frequency tuning curves plotted from data recorded from the peak voxel value of each subject. It can be seen that the tuning curves peak at different stimulus frequencies depending on the SAM analysis band used, and that the broadband 5–45 Hz tuning curve peaks at a stimulus frequency of 4 Hz.

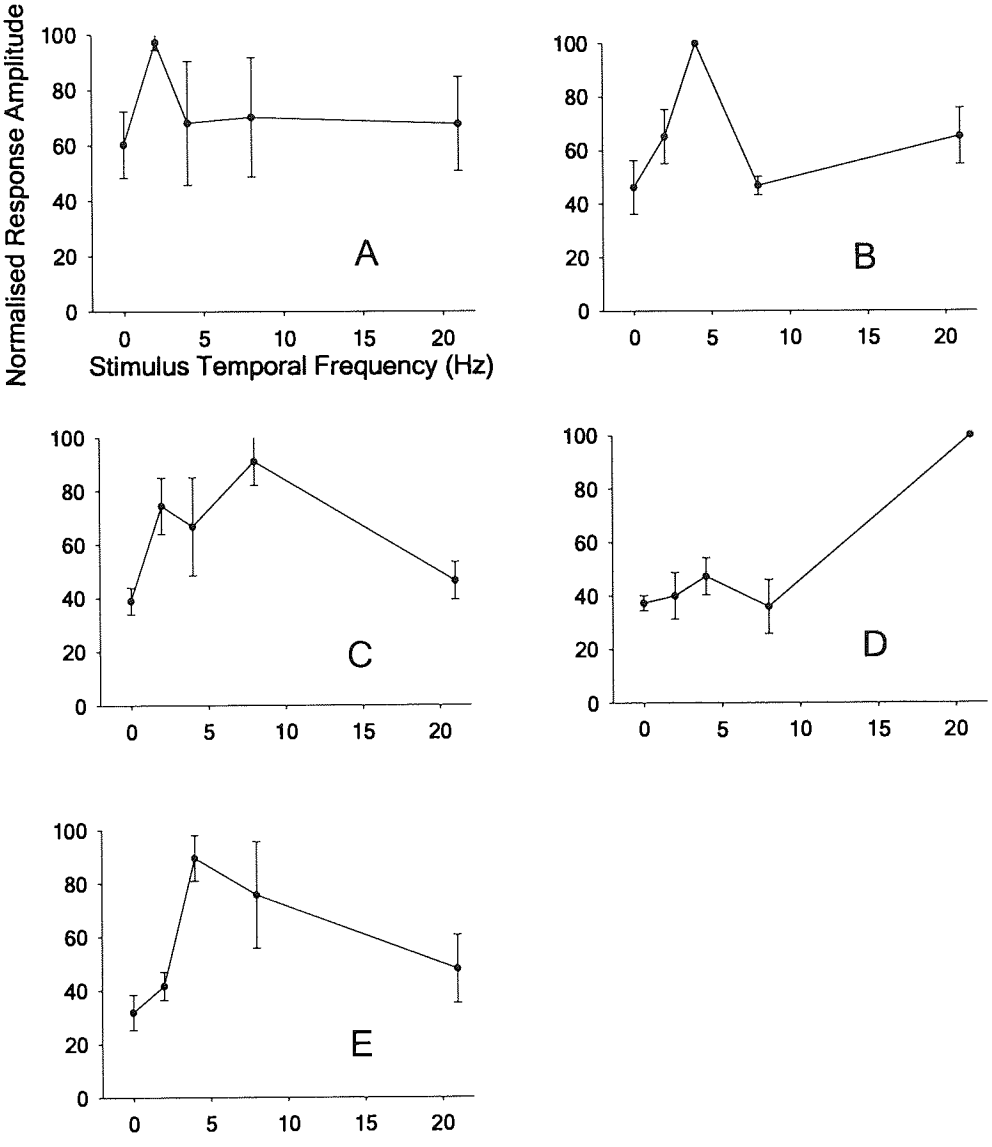

Figure 3-5. Normalised group-averaged SAM tuning curves for the response in contralateral medial visual cortex, elicited by a reversing checkerboard stimulus of various temporal frequencies (Experiment 1). Each separate panel shows the magnitude of the cortical response within a fixed frequency range; A. 3-5Hz, B. 7-9Hz, C. 15-17Hz, D. 41-43Hz, E. 5-45Hz as used in the SAM analysis. The error bars represent the standard error on the mean.

3.4.1.4 Time frequency analysis

With the SAM technique, we can isolate a voxel and analyse the activity within this voxel over the time course of the experimental paradigm. Figure 3-6 shows group-averaged time-frequency representations, using Morlet wavelet analysis, for voxels from the left medial visual cortex. The more sustained, steady-state, period of the response shows distinct bands of increased power within the cortex at harmonics which are multiples of double the stimulus frequency. The apparent modulation seen in the time dimension is caused by the wavelet analysis of white noise in the MEG recordings. It can be seen that this becomes less obvious at lower frequencies due to the lower temporal resolution at these frequencies.

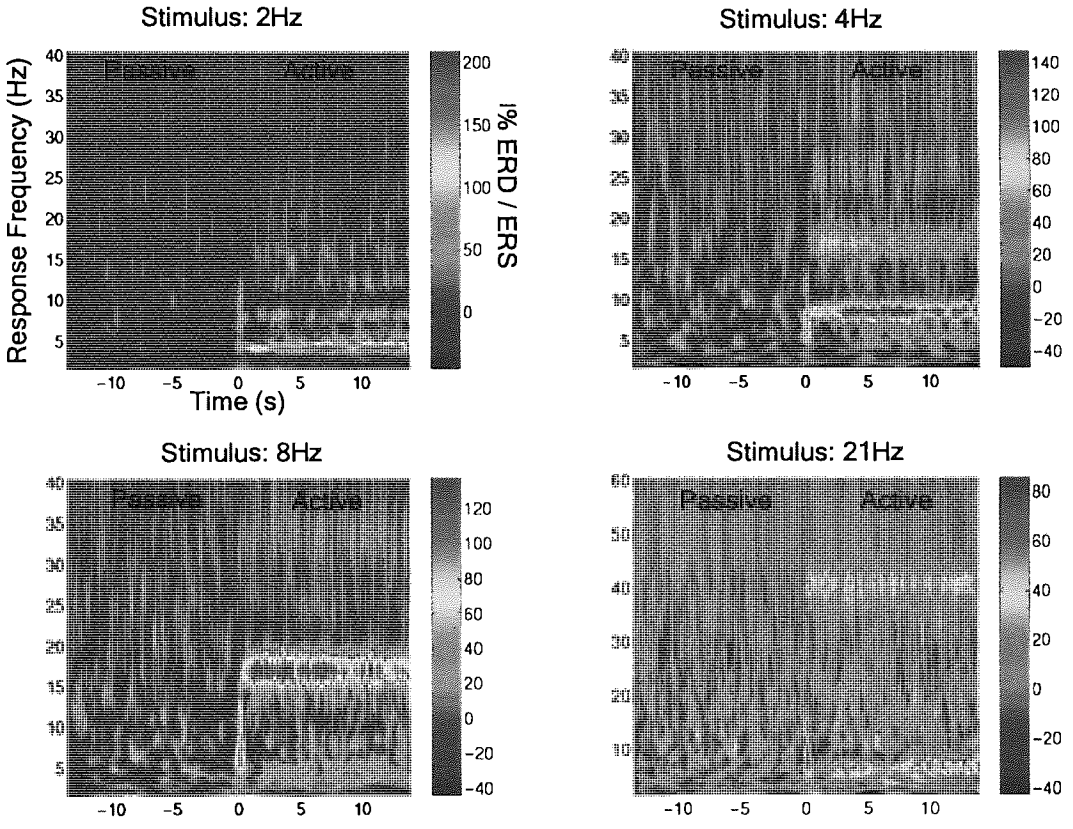

Figure 3-6. Time-frequency plots, averaged across all subjects, calculated using Morlet wavelet analysis from a voxel in the left (i.e. contralateral) medial visual cortex, to various stimulus frequencies. The time window used spanned an interval from 14s before the stimulus onset (passive phase) to 14s after the stimulus onset. The cortical harmonics of the stimulus frequency can be clearly seen in the active phase, together with an onset response shortly after the stimulus onset. The colour-bar to the right of each figure shows the ERS/ERD scale used, expressed as a percentage change from baseline.

This finding was consistent across all stimulus frequencies (see Figure 3-7 for how these cortical harmonics relate to the stimulus harmonics as recorded at the monitor).

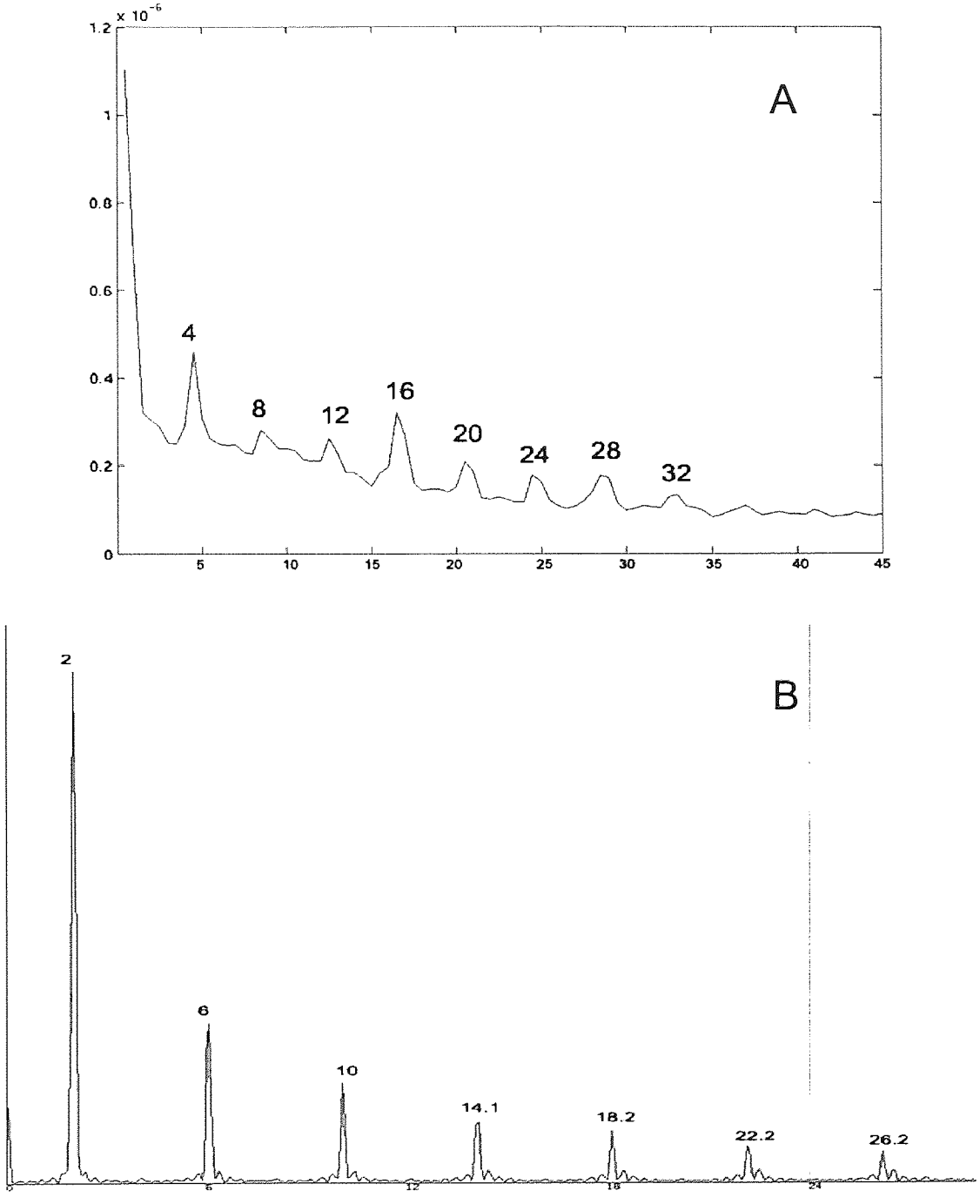

Figure 3-7. (A) A graphical representation, from a single subject in experiment 1,of the cortical harmonics seen in Figure 3-6 to a stimulus presentation at 2Hz. The graph shows the mean amplitude of the temporal components of the active phase of the experiment plotted as a function of frequency. (B) The FFT response of the stimulus monitor, measured using a photodiode placed onto the screen, during stimulus presentation at 2Hz.

3.4.1.5 Onset response

In addition to the steady-state response, there is a clear onset response at, or shortly after, the stimulus presentation (Figure 3-8 shows a more detailed spectrogram analysis of the onset response).

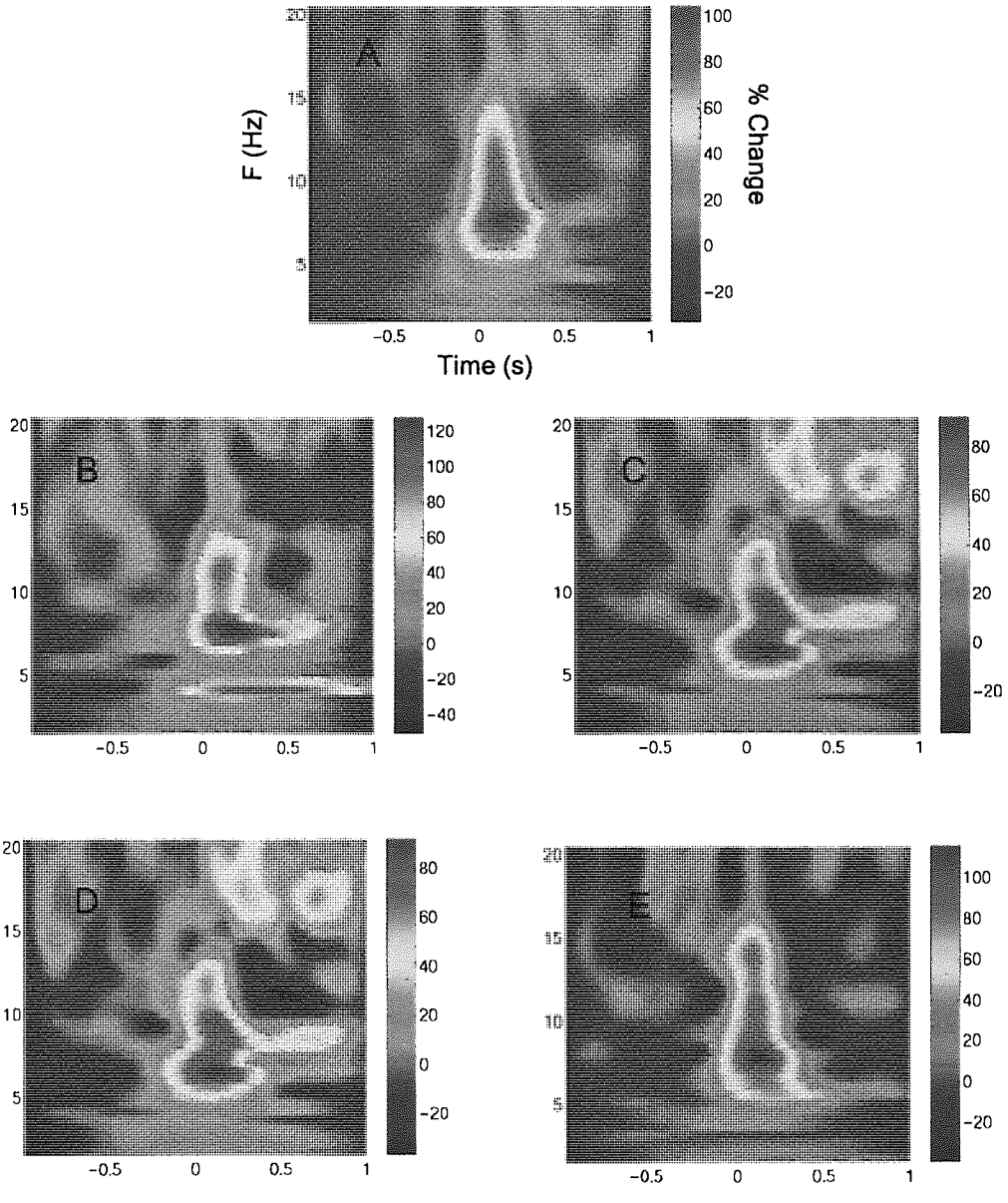

Figure 3-8. Group time-frequency representations showing the onset response produced by each stimulus frequency in experiment 1. A) Grand average representation produced from the group onset responses at all of the stimulus frequencies. B) Group onset response produced by 2Hz stimulus. C) Group onset response produced by 4Hz stimulus. D) Group onset response produced by 8Hz stimulus. E) Group onset response produced by 21Hz stimulus. The time window used spanned an interval from 1s before the onset of the active phase to 1s after the onset of the active phase.

There is evidence from both evoked potential studies (Kashikura *et al.* 2001) and single-cell studies (Muller *et al.* 2001) that on the sudden appearance of a stimulus there is an initial rapid increase in activation of neurons in V1 lasting up to 150 ms before activation reduces to a lower level. As shown in Figure 3-8 and Figure 3-9 the frequency content of this onset response seems to mostly consist of frequencies within the Alpha band (approximately 10 Hz).

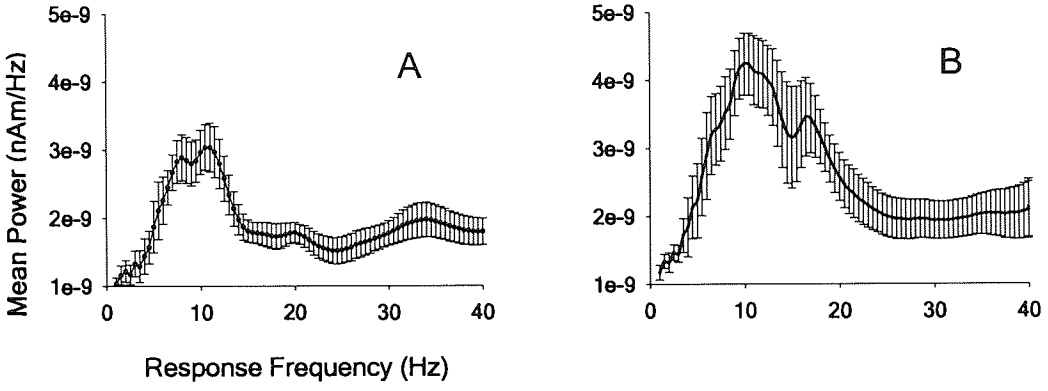

Figure 3-9. (A) Mean frequency content of the onset activation measured across all stimulus frequencies and subjects in experiment 1. (B) Mean frequency content of the onset activation measured across all stimulus frequencies and subjects in experiment 2. The error bars represent the standard error on the mean.

3.4.2 Experiment 2

3.4.2.1 Temporal frequency tuning curves

Figure 3-10 shows the normalised tuning curves obtained from medial visual cortex, using the sinusoidally modulating stimulus used in Experiment 2. The tuning curves are similar to those obtained in the first experiment.

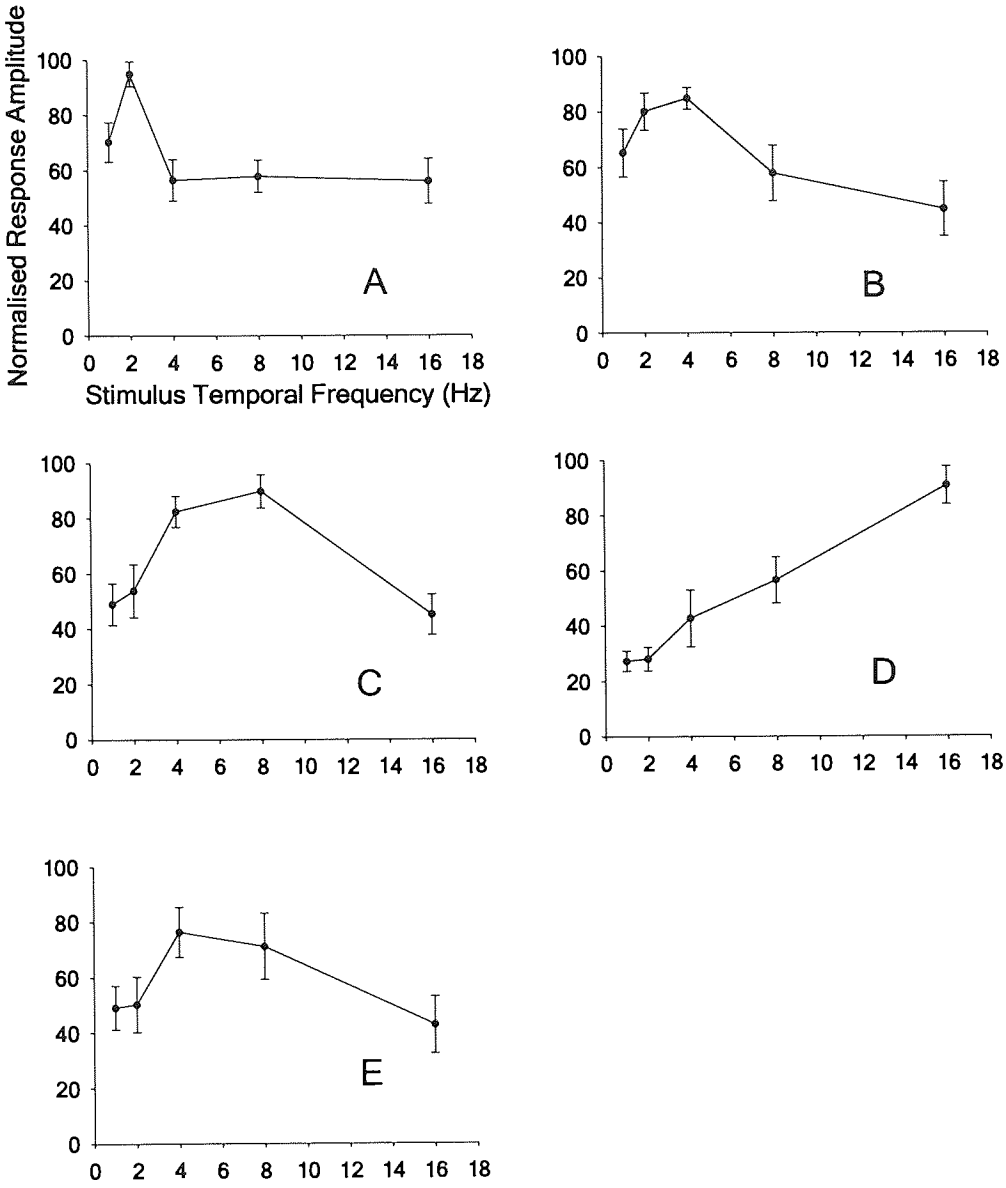

Figure 3-10. Normalised group-averaged SAM tuning curves for the response in contralateral medial visual cortex, elicited by a sinusoidally modulating checkerboard stimulus of various temporal frequencies (Experiment 2). Each separate panel shows the magnitude of the cortical response within a fixed frequency range; A. 3-5Hz, B. 7-9Hz, C. 15-17Hz, D. 33-35Hz, E. 5-45Hz as used in the SAM analysis. The error bars represent the standard error on the mean.

3.4.2.2 Time frequency analysis

Figure 3-11 shows the group-averaged time-frequency representations obtained from voxels in left and right medial visual cortex

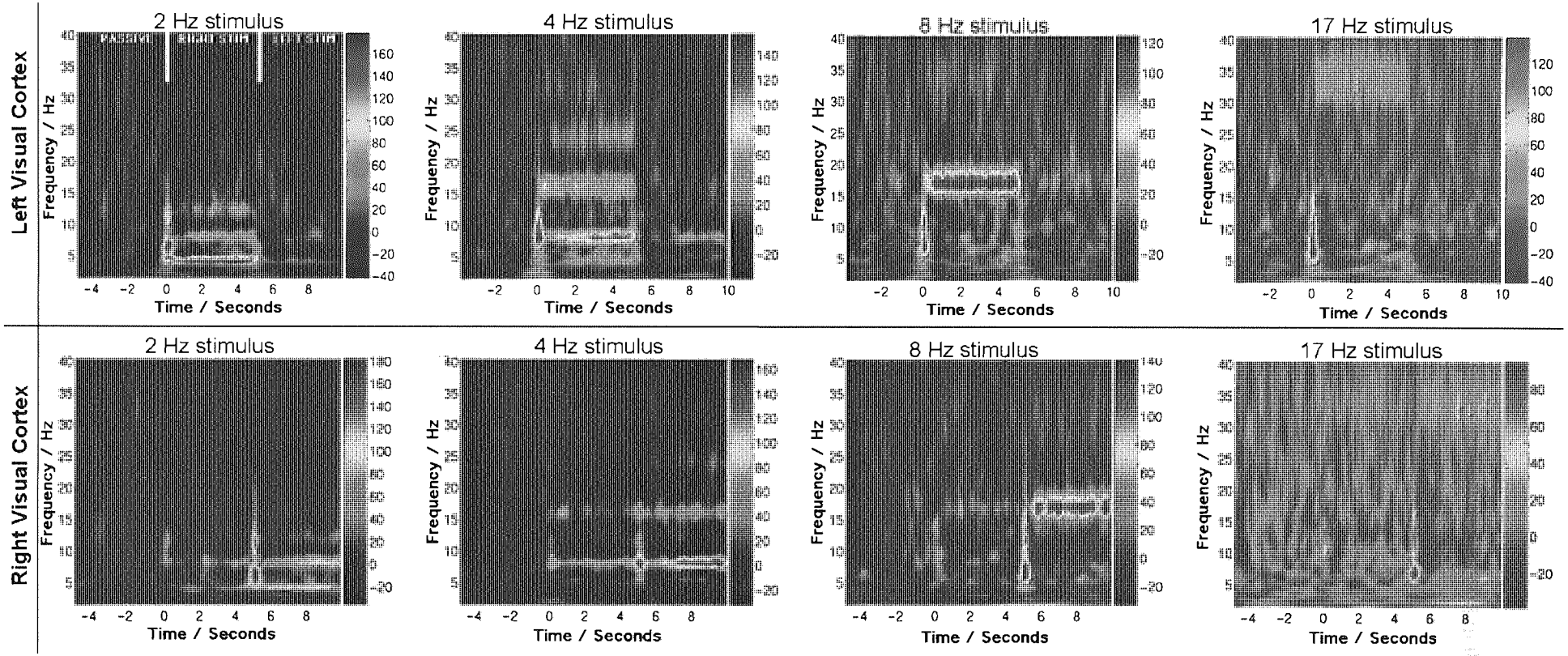

Figure 3-11. Group time-frequency representations calculated using Morlet wavelet analysis from a voxel in the left (top row) and right (bottom row) medial visual cortices in experiment 2. The time window spanned an interval from 5s before the onset of the Active phase of the experiment (Passive phase) to 10s after the onset of the Active phase. At the beginning of the Active phase (0 seconds), the stimulus appeared first in the right lower visual field for five seconds and then moved to the left lower visual field for five seconds. Moving left to right, the four columns show the response to a checkerboard which is sinusoidally reversing at 2Hz, 4Hz, 8 Hz and 17Hz. The colour-bar to the right of each figure shows the ERS/ERD scale used, expressed as a percentage change from baseline. Cortical harmonics of the stimulus frequency can be clearly seen when the stimulus is in the contralateral visual field, together with some weaker ipsilateral responses.

As with Experiment 1, there are clear onset responses recorded in the contralateral hemisphere and steady-state harmonics can again be clearly seen at all stimulus frequencies.

3.4.2.3 Contralateral / ipsilateral ratio

Responses ipsilateral to the stimulus are seen in both the left and right voxels (Figure 3-11). However, the magnitude of these ipsilateral responses is much weaker than the contralateral activation (Table 3-1)

Medial Visual Cortex

	Cortical Response Frequency					
Stimulus Frequency (Hz)	5-15Hz	15-25Hz	25-35Hz	35-45Hz	5-45Hz	Mean ± SE
1	5.35	5.08	7.48	9.10	4.61	6.3 ± 0.8
2	3.47	4.91	4.06	3.25	3.31	3.8 ± 0.7
4	4.31	4.98	6.58	6.89	3.77	5 ± 1
8	8.12	4.34	7.88	6.93	4.14	6.3 ± 0.5
17	10.92	11.94	9.40	8.12	6.02	9 ± 1

V5/MT

	Cortical Response Frequency					
Stimulus Frequency (Hz)	5-15Hz	15-25Hz	25-35Hz	35-45Hz	5-45Hz	Mean ± SE
1	1.54	2.27	1.84	2.50	1.42	1.9 ± 0.5
2	1.89	1.53	2.42	2.67	2.05	2.1 ± 0.2
4	1.88	3.10	3.60	2.46	2.95	2.8 ± 0.6
8	1.67	1.42	1.52	2.35	1.66	1.7 ± 0.1
17	2.44	3.05	2.66	2.09	1.66	2.4 ± 0.5

Table 3-1. Overleaf. A comparison of contralateral / ipsilateral response ratios in medial visual cortex and V5/MT. In all cases the ratio was greater than 1 i.e. more contralateral activation. The ratio between contralateral and ipsilateral activation is greater in medial visual cortex, compared to V5/MT. Note that broad frequency bands were used in medial visual cortex to allow direct comparison with the response in V5/MT. The medial visual cortex measurements were recorded from 6 hemispheres for the 1Hz stimulus and 12 hemispheres for other stimulus frequencies. The V5/MT measurements were taken from 9 hemispheres.

The contralateral-ipsilateral ratio information is shown graphically in Figure 3-12

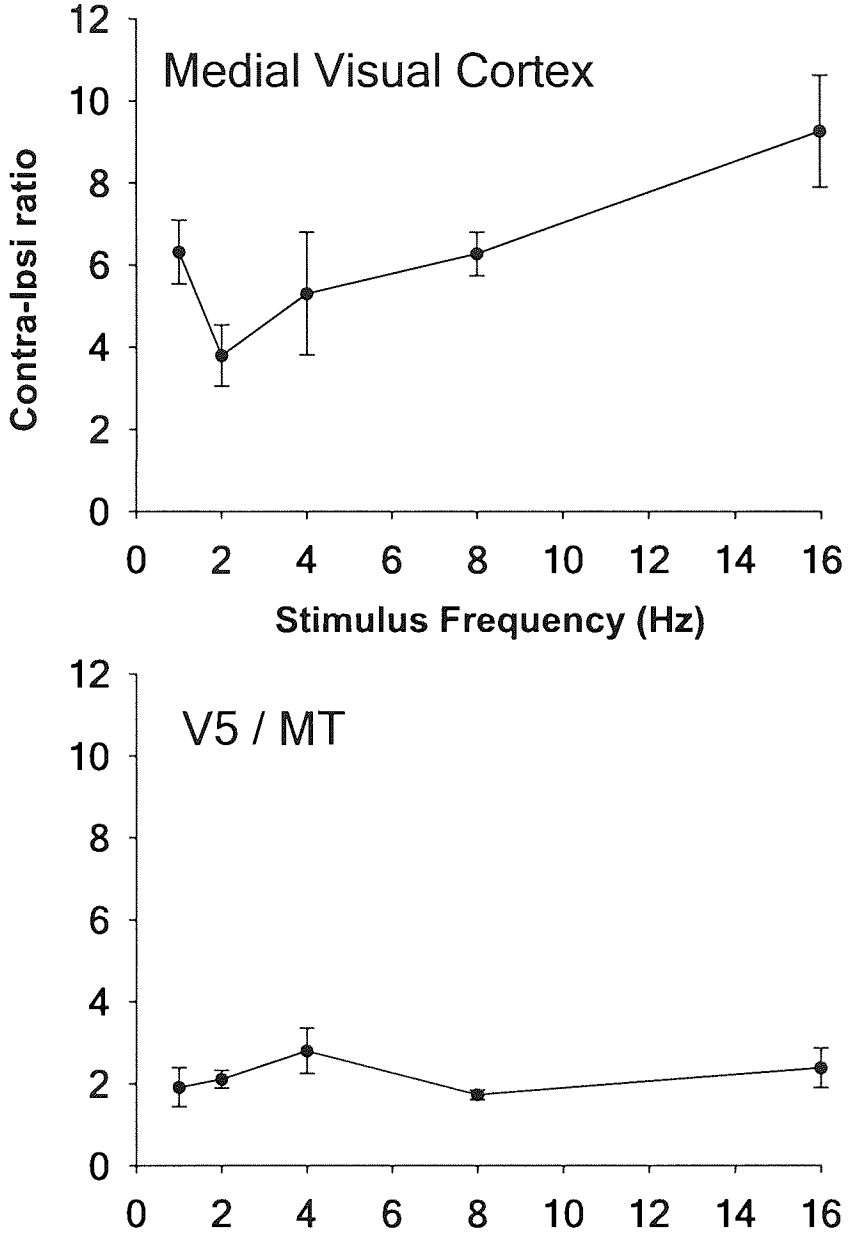

Figure 3-12. A graphical representation of the contralateral-ipsilateral response ratio between medial visual cortex and V5. A ratio nearer to 1 indicates greater similarity in response amplitude between contralateral and ipsilateral stimulation.

3.4.2.4 *Fundamental and onset responses*

The magnitude of the fundamental response (which always occurs at 2f, i.e., twice the stimulus frequency) was analysed in more detail, and Figure 3-13A shows the group tuning curve for this fundamental response. A clear peak at 8 Hz can be seen. In contrast, the amplitude of the onset response did not show any systematic variation in amplitude with stimulus frequency (Figure 3-13B).

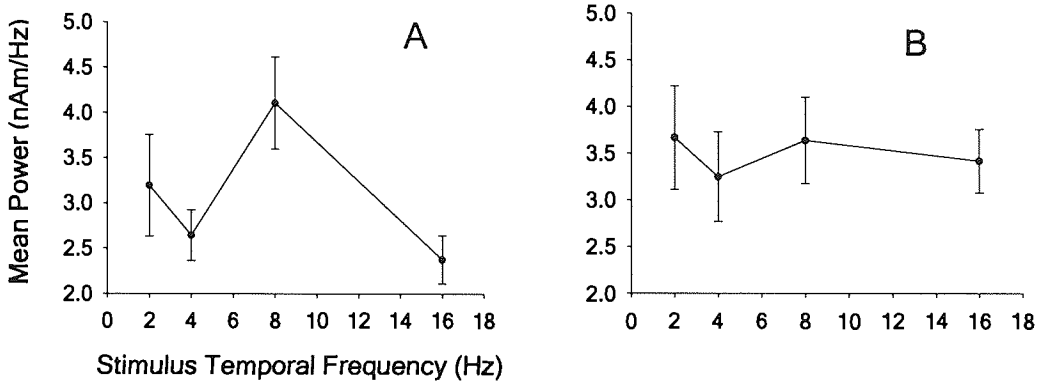

Figure 3-13. (A) Graph of mean strength of the fundamental harmonic versus stimulus frequency across all subjects in experiment 2. (B) Graph of mean strength of the onset magnitude versus stimulus frequency across all subjects in experiment 2. The error bars represent the standard error on the mean.

As with Experiment 1, and in contrast to the steady-state evoked responses, the frequency content of the onset response did not depend on the stimulus frequency. Figure 3-9B shows the frequency spectrum of the onset response, averaged across subjects and stimulus conditions, and clearly shows a peak at 10 Hz.

3.4.2.5 *Increasing width of tuning and time-frequency responses*

In both experiments, the spectral width of the oscillatory response functions increased with stimulus frequency. The width increases shown in Figure 3-5 and Figure 3-10 are probably due to the presence of higher harmonics (so that, e.g., the 2-Hz stimulus generates an 8 Hz harmonic, which will apparently widen the response in the 7–9 Hz

band). Note that an examination of the time-frequency spectrograms in Figure 3-6 and Figure 3-11 seem to clearly show that the spectral width of the fundamental response increases with stimulation frequency. However, this is an artefact of the wavelet reconstruction methods used—the apparent width shown in the spectrogram at any given frequency, f, is proportional to f. For the 17-Hz stimulus used in Experiment 2 and shown in Figure 3-11, the maximum response is at 34 Hz, and for this frequency the wavelet reconstruction has a FWHM of 8 Hz, compared to a FWHM of 0.9Hz for a response frequency of 4 Hz. The tuning curves shown in Figure 3-5 and Figure 3-10 do not involve a wavelet analysis and so are not subject to this effect.

3.4.2.6 V5/MT

In Experiment 1, no robust activation of area V5/MT was observed—only two of the six subjects showed V5/MT responses and these were to contralateral stimuli. Although the stimulus was certainly large enough to activate area V5/MT (Tootell *et al.* 1995), the low number of active phases used in the first experiment, and the fact that a flickering checkerboard stimulus rather than a moving stimulus was used may explain this lack of robust activation. With the increased number of active phases in the second experiment there was a marked increase in V5/MT activation, which allowed a comparison with medial visual cortex. Nine of twelve hemispheres showed a clear response. We located area V5/MT based on the nearest activation to known anatomical landmarks (Dumoulin *et al.* 2000). Figure 3-14(A) shows group V5/MT activation for the six subjects. The purple/white colours indicate that the response in extra-striate cortex is ERD, that is, oscillatory power in this frequency band decreases during stimulus presentation. The relative strength of the activation in the lateral occipital complex, LO, compared to V5/MT is probably because the stimulus is counterphasing, rather than moving.

Previous functional imaging studies have shown that activity in V5/MT is greater for moving stimuli, compared to an identical counterphasing stimulus (Heeger *et al.* 1999, Singh *et al.* 2000).

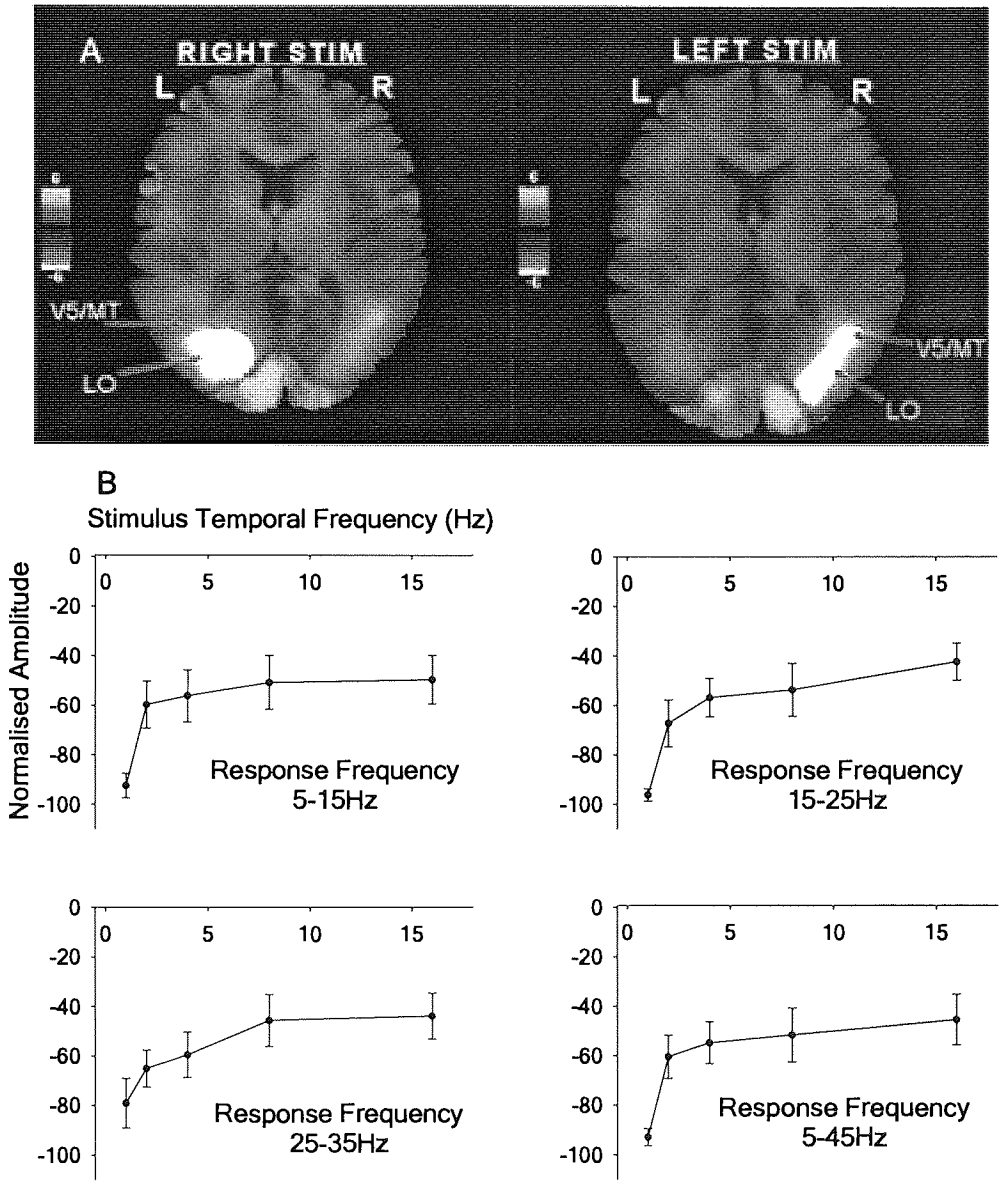

Figure 3-14. A. Group image of ERS/ERD effects in striate and extra striate cortex. This figure shows the peak ERS/ERD in each voxel, compiled across all stimulus frequencies and all cortical response frequencies, displayed on a template brain. Orange/yellow colours show strong group ERS effects, and are confined to medial visual cortex. Blue-white colours represent ERD and are most common in extra-striate visual areas such as the lateral occipital complex (LO) and the V5/MT complex. The axial template slice shown has a Z coordinate of +11. B. Normalised SAM activation levels in visual area V5/MT averaged over 9 hemispheres in 6 subjects, elicited by a sinusoidally modulated reversing checkerboard stimulus of various temporal frequencies. The error bars represent the standard error at each point.

Figure 3-14(B) shows the normalised temporal frequency tuning curves for area V5/MT. All response frequency bands exhibit the same, strongly low-pass, behaviour. A group time-frequency representation was produced for voxels isolated in both left and right V5/MT (see Figure 3-15). The pattern is very different to the sharply tuned ERS responses found in medial visual cortex. There is a broad desynchronisation of activity during the stimulus presentation period in the 5–20 Hz band. Interestingly, although there is a larger desynchronisation to a stimulus in the contralateral visual field, the response to the ipsilateral visual field is similar in amplitude (Table 3-1 and Figure 3-12). This is consistent with the larger receptive fields that V5/MT neurons possess and their known spread across the vertical meridian (Tootell *et al.* 1995, Tootell *et al.* 1998). It has been suggested in a recent fMRI study that this ipsilateral response is produced by the MST subregion of the V5/MT complex (Huk *et al.* 2002).

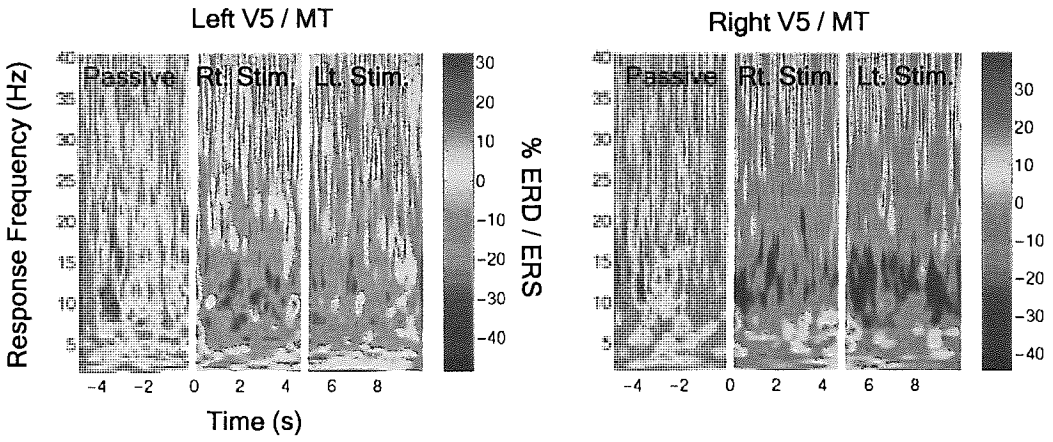

Figure 3-15. Group time-frequency representations calculated using Morlet wavelet analysis from a voxel in left and right V5/MT in experiment 2. At the beginning of the Active phase (0 seconds), the stimulus appeared first in the right lower visual field for five seconds and then moved to the left lower visual field for five seconds. The spectrograms show a broad desynchronisation in the 5-20Hz frequency band during the active phase as compared to the passive phase. No harmonic responses are present and no onset response is seen. There is greater desynchronisation to a stimulus in the contralateral hemisphere. The colour-bar to the right of each figure shows the ERS/ERD scale used, expressed as a percentage change from baseline.

3.5 Discussion

By measuring the difference in power between an active and a passive state it has been demonstrated that the amplitude of cortical oscillations within frequency-specific bands in medial visual cortex vary as a function of temporal frequency. Unlike a conventional EEG recording of the SSVEP, the higher spatial resolution of MEG, coupled with the SAM analysis technique, allows the localisation of stimulus-related changes in cortical oscillatory power. Within medial visual cortex, the fundamental response found in this study is at twice the stimulus frequency, which is different to the results of other SSVEP studies (e.g. Herrmann 2001), which obtain a fundamental response at the stimulus frequency. However, a patterned stimulus was used in this study, rather than the flashing LED of many other flicker studies, and the electroretinogram (ERG) is known to show a frequency doubling for patterned stimuli (Hess and Baker, Jr. 1984). This data therefore supports the interpretation that this frequency-doubled retinal response to patterned stimuli is preserved in primary visual cortex.

Although the mechanisms underlying frequency doubling for patterned stimuli are not clear, some plausible speculations can be made. Firstly, the absence of a response at the stimulus frequency, f, can be explained by spatial pooling of the response across adjacent checks (Spekreijse 1966). As these checks are oscillating in anti-phase, the effect is to ''average out'' the response at frequency f. The large response at 2f may then be explained by the existence of a pattern reversal specific response; at two points in each cycle, the checkerboard pattern transiently disappears, as all checks are briefly iso-luminant, before a reversed version of the pattern starts to appear. This may generate a transient pattern-reversal response, which will have a fundamental frequency of 2f (Spekreijse 1966). This could also explain why the square wave and sinusoidal stimuli

generate such similar results. If the pattern-reversal response occurs transiently at the two switchover points in the cycle, then it would have essentially the same morphology and frequency content, irrespective of whether the underlying stimulus is a square wave or a sinusoid. Whatever the precise details of the mechanism, this frequency doubling can only occur if nonlinear operations such as temporal edge detection and rectification are applied to the sinusoidal input.

3.5.1 Time-frequency analysis

The time-frequency spectrograms from both experiments show clear evidence of higher harmonic responses to the visual stimuli in medial visual cortex. In the case of Experiment 1, some higher harmonics are to be expected because of the square-wave nature of the visual stimulus, however, the strongest harmonic response appears to be at 4f , that is, twice the fundamental response found. This is not predicted as a square wave has its strongest harmonic at odd-multiples of the fundamental (see Figure 3-7). In Experiment 2, a 'purer' temporal frequency spectrum was created by using sinusoidal modulation. However, relatively strong harmonics at 4f and even 8f are still seen in the time-frequency spectrum (e.g. Figure 3-11, 4 Hz stimulation). These even-multiple harmonics have been previously seen in animal studies (Rager and Singer 1998) and EEG studies of the SSVEP (Herrmann 2001). These results again suggest the presence of a nonlinearity, possibly due to rectification, somewhere in the visual system, although whether this occurs in or before primary visual cortex is unclear. In addition, although it was attempted to generate a ''pure'' sinusoidal stimulus, artefacts will no doubt occur due to digitisation of the sinusoid, incomplete gamma correction of the monitor and possible nonlinearities in the early stages of the eye and retina.

3.5.2 Onset response

Although only relatively few epoch onsets were used in both experiments, the SAM technique was sensitive enough to show the onset transient produced in V1 at stimulus presentation. Analysis of this onset response in both experiments shows that most of the spectral power of the onset response is at approximately 10 Hz, supporting theories that suggest cortical-evoked potentials may be explained by phase locking of cortical oscillations in the alpha frequency band (Quian Quiroga *et al.* 2000). However, the magnitude and frequency content of the onset response did not vary parametrically with the temporal properties of the stimulus. The results therefore suggest that analyses of the steady-state oscillatory responses reveal more about the functional properties of the underlying neuronal population than the brief, phase-locked, transient evoked response that occurs at stimulus onset.

It is known that cortical neurons respond more strongly to some frequencies than to others, a characteristic sometimes described as a resonance phenomenon (Herrmann 2001). The findings support this theory in that it was found that the amplitude of the fundamental response in medial visual cortex, which occurs at 2f, is tuned for temporal frequency, with a maximum response occurring at a stimulus frequency of 8 Hz. The broadband, 5–45 Hz, analysis can be interpreted as a measure of the total integrated power evoked within a region, and for both experiments, medial visual cortex showed a peak response at a stimulus frequency of 4 Hz. This is in agreement with single-cell studies, which show most neurons to be optimally sensitive at 3–6 Hz (Foster *et al.* 1985) and psychophysical experiments describing the optimal motion stimulus at 4–5 Hz (Watson and Turano 1995, Watson *et al.* 1983), but differs from previous BOLD studies, which have uniformly found peaks at 8–10 Hz no matter what the spatial form

of the stimulus (Hagenbeek *et al.* 2001, Kaufmann *et al.* 2001, Kwong *et al.* 1992, Ozus *et al.* 2001, Singh *et al.* 2000, Thomas and Menon 1998). However, in a recent PET study of flicker sensitivity (Vafaee *et al.* 1999, Vafaee and Gjedde 2000), it was found that cerebral blood flow (CBF) peaked at 8 Hz, whilst the rate of cerebral oxygen consumption (CMR) peaked at 4 Hz. It is therefore possible that the disparity between the results found here (peaking at 4 Hz) and that of the BOLD studies (peaking at 8 Hz) is due to the measurement process and not the stimuli.

The magnetic fields measured externally with MEG are the net result of the summation of the currents due to thousands of post-synaptic potentials developing across similarly oriented neighbouring pyramidal neurons (Okada *et al.* 1997). That is, the virtual electrode estimates made here are most likely analogous to direct electrophysiological measures of local field potential (LFP) rather than spiking, or multi-unit activity (which is unlikely to sum constructively across the cortex, or over time). Recent work (Logothetis *et al.* 2001) has shown that the BOLD response is well characterised by a linear transformation of the magnitude change in the LFP across a 10–130 Hz frequency band. Given such findings, it is puzzling why the data (based on the change in the 5–45 Hz band) is not in closer agreement with previous BOLD imaging studies. In this study (Figure 3-10), the broadband response at 8 Hz is very similar to that at 4 Hz. Given that Logothetis *et al.* 2001 were able to account for only 50–60% of the variance of the BOLD signal using the LFP, it is possible that the key to the difference between the results lies in the unexplained variance, perhaps due to some nonlinear relationship between neuronal activity and oxygenation level.

3.5.3 Ipsilateral responses

During the second experiment, there was evidence of ipsilateral cortical responses at various stimulus frequencies in both the left and right visual medial cortex (see Figure 3-11). Although the weak nature of these responses precluded any in-depth analyses, the response frequencies appear to be the same as those generated in the contralateral response. An obvious question is whether this ipsilateral response is an artefact of the beamformer method, so that activity from the contralateral region is being erroneously represented in the ipsilateral source. This problem was checked by examining the correlation between the beamformer weights (Barnes and Hillebrand 2003). This analysis showed that there was no obvious cross-talk between the beamformers constructed for the two regions. An fMRI study of ipsilateral activation in visual cortex (Tootell *et al.* 1998) concluded that significant ipsilateral responses can be seen in visual cortex, although these are primarily confined to more lateral visual areas which have larger receptive fields. However, when a stimulus approaches the vertical meridian, such as our separation of only 0.5°, ''filling in'' to the ipsilateral hemisphere occurs (Tootell *et al.* 1998). This is the most likely explanation for the weak ipsilateral responses we see in this study.

3.5.4 Oscillatory power changes in medial visual cortex and V5/MT

One interesting implication of these results is that the relationship between oscillatory power changes and neuronal activation depends on the context and cortical region studied. In the case of primary visual cortex, the visual stimulus generates a phase-locked power increase, the magnitude of which varies parametrically with frequency. These power increases are equivalent to the well-studied SSVEP phenomenon and presumably represent direct ''driving'' of neurons within primary visual cortex. No

robust evidence of any induced oscillatory power changes, such as ERD effects, within the medial regions of visual cortex were found. However, in extra-striate areas such as V5/MT it was found that ERD was the primary response of cortical neurons to stimulation, confirming modelling studies which suggest that ERS is found in cortical areas that are at rest or in a deactivated state (Pfurtscheller 1992), whilst ERD is a correlate of activation. An alternative explanation is that the power reductions found in extra-striate cortex may represent inhibition or suppression by the stimuli used in these experiments. However, the checkerboard stimulus used here has been previously shown to activate extra-striate visual areas such as LO and V5 in fMRI and PET studies (e.g. Duann *et al.* 2002, Dumoulin *et al.* 2000, Vafaee *et al.* 1998, Watson *et al.* 1993). The finding of ERD within extra-striate areas also confirms previous SAM studies which have shown that the BOLD response is correlated with ERD activity in the cortex for cognitive tasks (Singh *et al.* 2002). This suggests a fundamental distinction between higher cortical areas, where increased mean neuronal activity correlates with ERD, and primary sensory cortices, which exhibit a direct stimulus- driven power increase.

3.5.5 Tuning differences between medial visual cortex and V5/MT

In addition, these results show fundamentally different tuning characteristics for medial visual cortex and V5/MT. There have been many studies looking at the velocity tuning of area V5/MT (e.g. Chawla *et al.* 1998, Rodman and Albright 1987). Indeed, many have argued that, unlike V1/V2 in which the response profile of individual neurons is separable in terms of spatial and temporal frequency (Foster *et al.* 1985, Levitt *et al.* 1994), V5/MT neurons are tuned for velocity, rather than temporal frequency (Perrone and Thiele 2001). The findings of this study suggest that the bulk neuronal response in V5/MT, for the spatially broadband stimulus used in this study, is low pass tuned for

temporal frequency. Note that no stationary stimulus was used as part of the paradigm in Experiment 2 so no comment can be made on whether this low-pass behaviour would persist down to the 0 Hz origin, although it seems likely that the response in V5/MT to a stationary stimulus would be reduced. The responses found in V5/MT were essentially bilateral with only a moderate preference for the contralateral visual field which can be interpreted as a direct consequence of the larger receptive fields found in this region. The ERD findings within V5/MT are different to a previously reported fMRI study, which found that V5/MT was band passed tuned, peaking at 9 Hz (Singh *et al.* 2000). As discussed above, this difference could be attributed to differing sensitivities to the bulk neuronal responses within V5/MT of the BOLD and ERD measures. However, the stimulus used in this study is very different to the fMRI study, in that it is broadband in spatial frequency and is counterphasing rather than drifting. If neurons within V5/MT are predominantly oriented along iso-velocity lines, as some single-cell studies have found (Perrone and Thiele 2001), then the spatial properties of the stimulus will fundamentally affect the temporal frequency response found. A natural extension of the work presented here would be to use SAM to examine the temporal frequency and velocity tuning characteristics of V5/MT (and striate visual cortex) using stimuli containing only one spatial frequency and direction, such as a drifting sinusoidal grating.

3.6 Conclusion

This study has provided a number of interesting and novel findings. It was shown that the evoked onset response has a maximal spectral power of approximately 10Hz, supporting work that suggests that cortical evoked potentials are the result of the phase locking of cortical oscillations in the alpha band. However the magnitude of this onset

response does not vary parametrically with temporal frequency, unlike the fundamental response which peaked in strength at a temporal frequency of 8Hz supporting evidence of a cortical resonance phenomenon. Similarly, some cortical harmonics seen in the time-frequency plots could not be explained simply on the basis of a direct response to the stimulus suggesting a nonlinearity in the visual system

Most interestingly, different tuning characteristics between medial visual cortex and V5/MT were found. Medial visual cortex showed sharply tuned ERS responses related to the SSVEP whilst V5/MT showed a low-pass tuned ERD response. Thus, important information has been provided about the relationship between ERD/ERS effects and neuronal activation in the cortex. It is clear that, within the visual cortex, fundamental aspects of the neuronal oscillatory response differ between striate and extra-striate visual areas.

4. EARLY AND LATE CORRELATES OF IMPLIED-MOTION PERCEPTION IN HUMAN MOTION AREA V5/MT

4.1 Overview

This chapter describes a series of experiments designed to investigate the cortical oscillatory changes in area V5/MT in response to an implied-motion stimulus. The chapter begins by introducing the concepts of representational momentum and implied-motion and reviews the literature on these topics. The chapter goes on to introduce the reader to extrastriate cortical areas known to be involved in motion perception and the response properties of these areas. The introduction ends by reviewing the current literature showing the cortical substrate underlying implied-motion.

The chapter continues by describing an initial psychophysical study designed to establish the ability of the functional imaging stimuli to produce a representational momentum effect. Following this, the main MEG experiment is described, together with further psychophysics experiments, and the results are discussed in terms of the role of V5/MT in the cognitive perception of implied-motion.

4.2 Representational Momentum and Implied-Motion

It has been proposed that movement cues are important in a number of perception processes (Cutting and Kozlowski 1977, Spelke 1982). The importance of such movement cues was first demonstrated by Freyd (1983) who showed that the mental representation of movement was a fundamental organising principle for human perception and cognition. Using a freeze frame paradigm (see section 4.6.2 for an explanation of the methodology) Freyd (1983) found that reaction times in a two alternative forced choice (same/ different) paradigm were increased in response to

pictures forward in time to the inducer picture as compared to pictures previous in time to the inducer. This was taken to mean that the implied-motion in the inducer image was being mentally represented and continued in the forward direction such that the 'forward pictures' were more difficult to differentiate from the original as they were mentally represented as being the same. This is often described as a forward distortion of recognition memory in the direction of implied-motion and has been termed representational momentum

It has been shown that representational momentum can be influenced by a number of different stimulus variables such as implied acceleration (Finke *et al.* 1986), velocity (Hubbard.T.L. 1990, Freyd and Finke 1985) and direction of motion (Halpern and Kelly 1993, Hubbard.T.L. 1990). Similarly the implied weight (Hubbard.T.L. 1997) and the implied friction acting upon an object (Hubbard.T.L. 1995, Hubbard.T.L. 1998b) also modulate the effect. Furthermore cognitive processes regarding information and expectations about target identity and behaviour appear to influence the representational momentum effect (Kelly and Freyd 1987, Reed and Vinson 1996, Freyd and Finke 1984, Hubbard.T.L. 1994, Nagai and Yagi 2001). Thus, unlike our response to illusions such as apparent motion (Liu *et al.* 2004, Watson *et al.* 1986, Braddick 1980, Anstis 1980) and the motion after effect (Anstis and Duncan 1983, Grunewald and Mingolla 1998, see Mather *et al.* 1998 for a comprehensive review) which are unrelated to knowledge and beliefs, representational momentum is evidence for the cognitive representation of motion. It has also been shown that the length of the retention interval between the target and the probing of the memory influences the extent of representational momentum (Freyd and Johnson 1987) as has the laterality of stimulus presentation (White *et al.* 1993) with greater effects being present in the right

hemisphere compared to the left. Furthermore dynamic effects have been noted using stimuli that imply motion but which themselves are static such as photographs (Bertamini 1993, Freyd 1983, Futterweit and Beilin 1994, Kourtzi and Kanwisher 2000a, Senior *et al.* 2000).

4.3 Motion areas of the brain

In section 1.8 the anatomy of the visual motion pathway was highlighted with reference to some of the major visual motion areas. Given the range of functions that motion processing serves it is not surprising that psychophysics, physiological and neuroimaging studies have revealed a number of brain areas which are responsive to different types of motion. In this section new areas are introduced and previously mentioned regions are described in more detail.

4.3.1 V5/MT

The most widely studied cortical area of motion is the V5/MT complex which contains a high percentage of directionally sensitive neurons (Dubner and Zeki 1971, Albright 1984, Lagae *et al.* 1994, Maunsell and Van Essen 1983) and is known to show a close correlation between psychophysical performance on a direction discrimination task and activity of motion selective cells in V5/MT (Newsome *et al.* 1989).

Zeki *et al.* (1991) using PET identified an area in the human temporo-parieto-occipital region which he proposed was the human homologue of monkey MT/V5 and this was subequently confirmed in a number of further studies (e.g. Watson *et al.* 1993, Tootell *et al.* 1995a, Dumoulin *et al.* 2000). Although there is variability in the location of V5/MT across individuals in relation to Talairach coordinates (Talairach and Tournoux

1988), there is broad agreement that the area is in the ascending branch of the inferior temporal sulcus (Dumoulin *et al.* 2000, Tootell *et al.* 1995a).

Using functional magnetic resonance imaging Tootell *et al.* (1995c) studied the functional properties of human V5/MT and showed a sensitivity to low contrast and a strongly reduced response for moving isoluminant gratings in agreement with monkey V5/MT neuronal responses (Gegenfurtner *et al.* 1994, Thiele *et al.* 1999). Subsequently, the visual area V5/MT has been implicated in a range of motion tasks including the motion after effect (Tootell *et al.* 1995b), apparent motion (Goebel *et al.* 1998) and biological motion (Bonda *et al.* 1996, Grossman *et al.* 2000)

4.3.2 V3 and V3A

It has been shown that motion responses occur in many cortical areas outside of MT/V5 and V1/V2, particularly in the cuneus, and other regions along the dorsal occipitoparietal stream (Dupont *et al.* 1994, Watson *et al.* 1993). It was initially thought that this activation may correspond to monkey V3 which contains a proportion of direction selective neurons (Gegenfurtner *et al.* 1997) although it has now been demonstrated that human area V3 shows little motion sensitivity (Tootell *et al.* 1995c). It was consequently shown that the activation focus in the cuneus corresponds to area V3A located near to the transverse occipital sulcus(Tootell *et al.* 1997, Ahlfors *et al.* 1999, Sunaert *et al.* 1999, Rees *et al.* 2000) an area, like MT/V5, that has a representation of the entire contralateral visual hemifield. Interestingly, human V3A is relatively motion selective compared to V3 in contrast to the macaque monkey area V3 which shows considerably more motion selectivity than V3A (Felleman and Van Essen 1987, Vanduffel *et al.* 2001) thus suggesting a reversal of the two areas between the

species. Spatial frequency tuning effects in V3 and V3A from both single cell (Gaska *et al.* 1988, Gegenfurtner *et al.* 1997) and functional imaging studies (Singh *et al.* 2000, Tootell *et al.* 1997) support this view.

4.3.3 KO and LO

Differences in motion direction produce the percept of kinetic boundaries, which are perceptually as sharp as luminance defined boundaries. However single cell, and lesion studies have shown that in the monkey, V5/MT plays a limited role in the processing of such kinetic boundaries (Marcar *et al.* 1995, Lauwers *et al.* 2000). Subsequent functional imaging studies using PET in humans have shown an area, separate to V5/MT responding best to stimuli of kinetic gratings rather than luminance defined gratings (Orban *et al.* 1995, Dupont *et al.* 1997) and this area has been named kinetic occipital (KO). Further studies comparing kinetic gratings to luminance gratings, uniform motion and transparent motion have confirmed that the KO region is involved in the processing of kinetic contours (Van Oostende *et al.* 1997, Tootell *et al.* 1998, Grossman and Blake 1999, Rees *et al.* 2000). The KO region is located posterior to area V5/MT and close to the lateral occipital sulcus between human V5/MT and human V3A (Van Oostende *et al.* 1997, Orban *et al.* 1995).

In a similar location, the lateral occipital (LO) region can be activated by comparing photographs of scenes and objects to uniform textures (Malach *et al.* 1995) and extends well beyond the KO region. Subsequent studies have shown that the LO area is activated by both luminance and motion defined objects (Grill-Spector *et al.* 1999). The exact location of LO is difficult to define as its activation is quite widespread, although Malach *et al.* (1995) defined the area as being located in the lateral fusiform gyrus and

branching anteriorly into ventral and dorsal branches. The dorsal or ascending branch is located just posterior to area MT/V5 thus locating it in the space between area V5/MT and the KO region.

4.3.4 Parietal Cortex

Many motion studies have shown a medial parietal activation when comparing moving with stationary stimuli (Watson *et al.* 1993, Dupont *et al.* 1994, Tootell *et al.* 1995c) and these were described in more detail by Sunaert *et al.* (1999). Using circular random textured patterns they described two regions in the occipital part of the intraparietal sulcus (IPS) one more ventral (VIPS) and one more dorsal at the junction of the parieto-occipital sulcus (POIPS). Similar regions of activation have been observed by Shulman *et al.* (1999) and Goebel *et al.* (1998). A further region of activation has been observed more dorsally along the parietal part of the IPS (Dupont *et al.* 1997, Braddick *et al.* 2001) which has been defined as a more anterior (DIPSA) and a pair of posterior regions (DIPSM/L) (Sunaert *et al.* 1999). Furthermore, activation of these parietal areas have been observed in attention paradigms(Culham *et al.* 1998) as well as tasks requiring cross-modal integration of information (Lewis *et al.* 2000, Bremmer *et al.* 2001).

4.4 Response to First- and second-order motion stimuli

When viewed on the retina objects are frequently lighter or darker than their backgrounds meaning that motion of the object can be detected by calculation of the change in position of luminance discontinuities at the object edge over time, which is known as first-order motion. It is also possible to detect object motion via the change in position of other characteristics such as colour, texture, contrast or flicker rate and this

is known as second-order motion (Smith 1994). Separate mechanisms have been demonstrated for the processing of first- and second-order motion in the electrophysiological and psychophysical literature (see Smith 1994 and Clifford and Vaina 1999 whilst Lu and Sperling 2001 provides a comprehensive review). Evidence from these as well as neurological studies (Greenlee and Smith 1997, Vaina *et al.* 2000) suggest the presence of parallel processing mechanisms with first-order information being extracted in early visual cortical areas and second order information being extracted in later visual cortical areas.

Using functional imaging, a number of different visual areas have been implicated in the analysis of first and second order motion stimuli (Smith *et al.* 1998, Dupont *et al.* 2003, Dumoulin *et al.* 2003, Seiffert *et al.* 2003, Wenderoth *et al.* 1999). Some studies have argued that second order motion activates V3 and VP more than first order motion whilst both types of motion produce equal activation in V5/MT (Smith *et al.* 1998, Wenderoth *et al.* 1999) whilst others have shown no difference between the two types of stimuli (Dupont *et al.* 2003, Seiffert *et al.* 2003). However, the results are difficult to interpret due to the different stimuli used both between studies and within studies for both first and second order motion. When the differences between the relative stimuli were controlled it was found that first order motion was computed in the precuneus region whilst second order motion activated regions such as LO and IPS (Dumoulin *et al.* 2003).

Although several visual areas respond well to flicker (Sunaert *et al.* 1999) both V3A and V5/MT respond more strongly to moving dots than to flicker (Tootell *et al.* 1995c, McCarthy *et al.* 1995, Braddick *et al.* 2001) with the response to flicker being

significantly reduced by the time signals reach the parietal cortex (Sunaert *et al.* 1999, Braddick *et al.* 2001). These functional imaging findings support those of single cell studies which have found decreased flicker response in V5/MT compared to V1 (Qian and Andersen 1994). The dot patterns and gratings to which V5/MT respond best are luminance defined stimuli. When the luminance of the stimulus is controlled it has been shown that, at equiluminance, moving gratings evoke only weak responses in V5/MT (Tootell *et al.* 1995c).

4.5 The neural substrate of implied-motion

There has been much exploration of the psychophysical parameters that effect representational momentum, but relatively little research into the cortical areas that underly this process. Different cortical areas have been implicated in the analysis of implied-motion though recent neuroimaging and single cell studies suggest that the visual motion area V5/MT plays an important role in the processing and cognitive representation of this information (Senior *et al.* 2000, Kourtzi and Kanwisher 2000a, Senior *et al.* 2002, Krekelberg *et al.* 2003). In functional imaging experiments of implied-motion using fMRI it has been shown that as well as activation of the V5 complex, areas ventral and posterior to this area have been activated including V3A, KO and LO (Senior *et al.* 2000, Kourtzi and Kanwisher 2000a) as well as anterior to V5/MT relating to STS (Jellama and Perrett 2003). Using MEG, and a complicated paradigm involving picture versus body rotation and perception v imagination to measure representational momentum, Amorim *et al.* (2000) described a fronto–parietal network of activation with no apparent activation of the posterior motion areas. However the results were analysed at the signal level rather than using source location modelling, thus making accurate assessment of the areas activated impossible.

However, there is the possibility that there is a differentiation between measures of pure implied-motion (Senior *et al.* 2000, Kourtzi and Kanwisher 2000a) and measures of representational momentum (Amorim *et al.* 2000) which require the use of working memory processes. This study will look at the role of V5/MT in the perception of implied-motion and review the results in the light of previous research on implied-motion and representational momentum.

4.6 Methods

4.6.1 Materials.

Scenes of irreversible, unambiguous motion were filmed using a Sony DCRVX2100 digital video camera using a fast shutter speed to allow clear capture of motion stills. Twelve different scenes depicting motion were filmed and from these three second video clips were captured (see Appendix I for an example of the stimuli used). The video sequences were filmed against a painted wall, in a bright room with additional illumination, during one session to control background luminance. From each video segment six still images were captured. The six captured stills showed a progression of object movement over the three second period. Similar stills were taken of the stimuli when they did not imply motion.

4.6.2 Procedure. Psychophysics (Freeze frame).

To confirm that the stimuli produced a representational momentum effect they were tested using the classical freeze frame methodology of Freyd (1983). 20 right handed psychology undergraduate students (10M, 10F, 19 ± 1.8 yrs) participated in the study. Stimuli consisted of 90 pairs of still photographic images made up of 30 pairs where the second image occurred after the initial image (forward condition), 30 pairs where

the second image occurred before the first image (backward condition) and 30 pairs were the second image was the same as the first image (see Figure 4-1). Images were presented on a computer monitor placed approximately 50cm away from the subject. The first image was shown for 250ms followed by a 250ms blank period after which the second picture of the pair was shown. The subjects took part in a two alternative (same / different) forced choice experiment, which they practiced beforehand, and were asked to respond quickly in deciding if the second image was the same or different to the first image using a button box placed on the lap. The stimuli were shown to the subjects using Presentation® (Version 0.70, www.neurobs.com) running under Windows 98 on a computer with a Pentium 4 Xeon processor and 1Gb of RAM and the reaction times were measured using the same software.

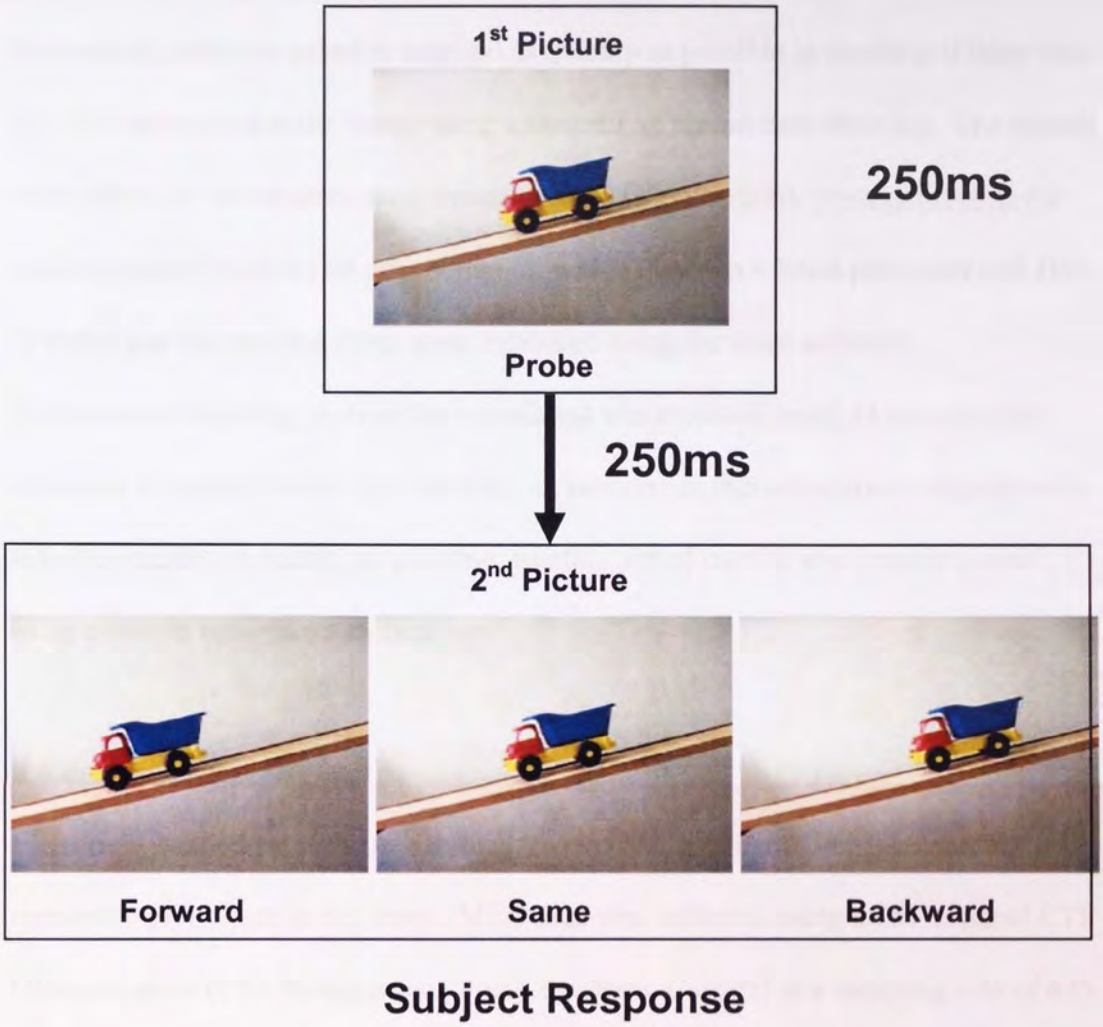

Figure 4-1. Diagramatic illustration of the freeze frame technique. An initial probe picture is shown for 250ms followed by a gap of 250ms after which a second picture is shown which may be forward in time to the probe, backward in time or the same as the probe. After presentation of the second picture the subject has to respond as quickly as possible as to whether the second picture is the same or different from the probe.

4.6.3 Procedure. Psychophysics (reaction time).

21 right handed subjects (11M, 10F, 33 ± 6.1yrs) participated in the study. The subjects sat 1 metre from a back projected screen onto which were shown 60 different photographic images (30 implied-motion, 30 control images showing no implied-motion). The stimulus subtended 25° horizontally and 18° vertically. The image presentation order was randomised across subjects and the ISI between images was

jittered between 500 – 4000ms to prevent expectation responses. The subjects took part in a two alternative (yes / no) forced choice experiment, which they practiced beforehand, and were asked to respond as quickly as possible in deciding if there was any motion implied in the image using a button box placed onto their lap. The stimuli were shown to the subjects using Presentation® (Version 0.70, www.neurobs.com) running under Windows 98 on a computer with a Pentium 4 Xeon processor and 1Gb of RAM and the reaction times were measured using the same software.

In a separate recording session the experiment was repeated using 32 actual video clips and 32 control video clips showing no motion. In this experiment subjects were asked to decide, as quickly as possible, whether actual motion was present or not using a button box placed on their lap.

4.6.4 Procedure: Imaging

Eight right handed subjects with normal vision (3M, 5F 30 ± 5.3yrs)) gave their consent to participate in the study. MEG data was collected using a 151-channel CTF Omega system (CTF Systems Inc., Port Coquitlam, Canada) at a sampling rate of 625 Hz. Data was recorded in 216 1.5s epochs between which an isoluminant grey background was shown for 250ms. The stimuli were shown to the subjects using Presentation® software (Version 0.70, www.neurobs.com) running under Windows 98 on a computer with a Pentium 4 Xeon processor and 1Gb of RAM. The stimuli were back projected onto a screen sitting one metre from the subjects' eyes in the shielded room via a Hitachi CP-S830E LCD projector. The stimulus subtended 25° horizontally and 18° vertically.

The 72 implied-motion stills (IM), 72 implied-static stills (C) and 72 blanks (B) were randomised by the Presentation® program. To control the stimulus presentation, ensuring that several images from the same category were not shown consecutively, the stimuli were shown as triplets. That is the pictures were shown one at a time but in sets of three, one from each of the picture groups. Thus 72 triplets were shown in each experimental run until all of the implied-motion stills had been presented. The same triplet order was used throughout an experimental run. To avoid order effects the structure of the triplets was changed for each experimental run as follows. There are six possible order combinations for the three picture types (1. IM, C, B 2. IM, B, C 3. C, IM, B 4. C, B, IM 5. B, IM, C 6. B, C, IM). The experiment was repeated x3 for each subject. There were 8 subjects which meant that each triplet combination was used x4 during the whole experiment. A fixation cross was in the centre of the viewing screen at all times

4.6.5 Procedure: Imaging, actual motion.

Data was recorded in 120, 2.5s epochs. 60 video clips of people or objects in motion were randomised with 60 video clips of people and objects showing no motion by the Presentation® program. There was an ISI of 0.5s between each video clip and the subjects were asked to maintain fixation on a cross in the centre of the screen, which was visible at all times.

4.6.6 Procedure: Eye Movement recording.

Eye movements were recorded in a separate session outside of the scanner using a Plusoptix Powerref II eye tracking system. The results showed that subjects were able to fixate adequately during the experimental paradigm (see Figure 4-10).

The subjects rested for 2 minutes after each stimulus run.

After the data were collected, a 3-D digitiser (Polhemus Isotrack) was used to digitise the shape of the subject's head in the MEG laboratory. Using Align (www.ece.drexel.edu/ICVC/Align/ align11.html), this surface was matched to a head surface extracted from the subject's own, previously acquired, anatomical MRI to coregister the MEG data with the subject's anatomy.

4.6.7 Data analysis.

Due to a problem with the triggering signal it was found that only one second of data was captured during each epoch of the implied-motion experiment. Initial viewing of the data showed that this was a sufficient epoch length to warrant continuing with the analysis. The data was split into 200ms segments and analysed using synthetic aperture magnetometry (SAM).

Statistical significance of group effects was assessed using nonparametric permutation testing (SnPM: http://www.fil.ion.ucl.ac.uk/spm/snpm) which has been shown previously to be effective in analysing SAM data (Singh *et al.* 2003).

4.7 Results

4.7.1 Freeze Frame Experiment

Before proceeding with the functional imaging experiment it was necessary to test whether the stimuli had the properties necessary to produce a representational momentum effect. The individual reaction times of the initial freeze frame

experiment are shown in Figure 4-2. Consistent with previous findings (e.g. Freyd 1983) there was a statistically significant difference in reaction time between the forward reaction time (973.6ms) and backward reaction time (924.2ms) conditions ($t = 2.934$, $df = 19$, $p<0.0045$) in the expected direction.

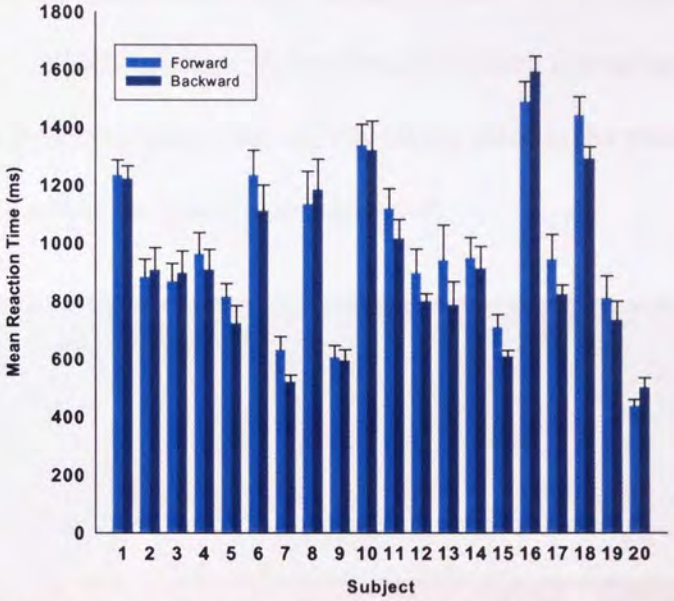

Figure 4-2. Individual mean reaction times for the forward and backward reaction time conditions of the freeze frame experiment. A t test showed the differences in reaction times to be significant. Error bars show the standard error of the mean.

These results confirm that although the magnitude of the representational momentum effect was not measured online during the functional imaging experiment, the stimuli are suitable for producing an implied-motion effect.

4.7.2 Implied-motion functional imaging

4.7.2.1 Actual motion condition

The location of the individual motion areas was first obtained by observing video images of the objects used in the implied-motion experiment.Given the broad frequency-band response of the V5/MT activation in the previous experiment, SAM images were generated across similar frequency bands, 5-15Hz, 10-20Hz, 15-25Hz

and 5-40Hz, for both the implied-motion and the video data. Figure 4-3 shows a group MEG/SAM image showing voxels in which the group mean effect, in the 10-20Hz band, is statistically significant ($p. < 0.05$) in the video-motion versus video-static condition, 0-2000ms following the presentation of the stimulus. Statistical significance was assessed using SnPM (see appendix II for the full output). The white colour indicates an ERD response, the evolution of which is seen more clearly by viewing a time frequency plot of the activity taking place in the voxels of V5/MT over the time course of the epoch (see Figure 4-4).

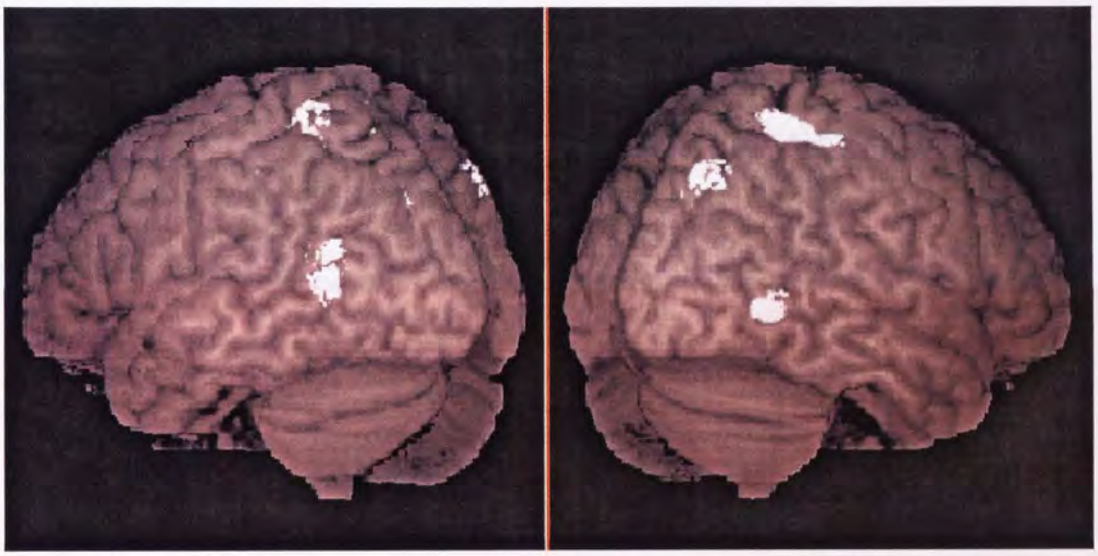

Figure 4-3. MEG/SAM image showing voxels in which the group mean effect is statistically significant (p. < 0.05) in the video motion versus video-static condition, 0-2000ms following the presentation of the stimulus in the 10-20Hz frequency band, calculated using nonparametric permutation testing (SnPM: http://www.fil.ion.ucl.ac.uk/spm/snpm). The white colour indicates an ERD response. There is clear bilateral activation of motion area V5/MT with significant clusters present on the right (54 -66 0) and on the left (-45 -66 12). Other areas known to be activated by motion stimuli were also seen such as DIPSA, VIPS and DIPSL (see section 4.3.4) (Sunaert et al. 1999, and Table 4-2 for Talairach coordinates).

The time frequency plot shows an initial brief evoked power increase over the first 200ms followed by a broad ERD response lasting for the duration of the stimulus. It is this ERD response over the measured time period that is shown in Figure 4-3.

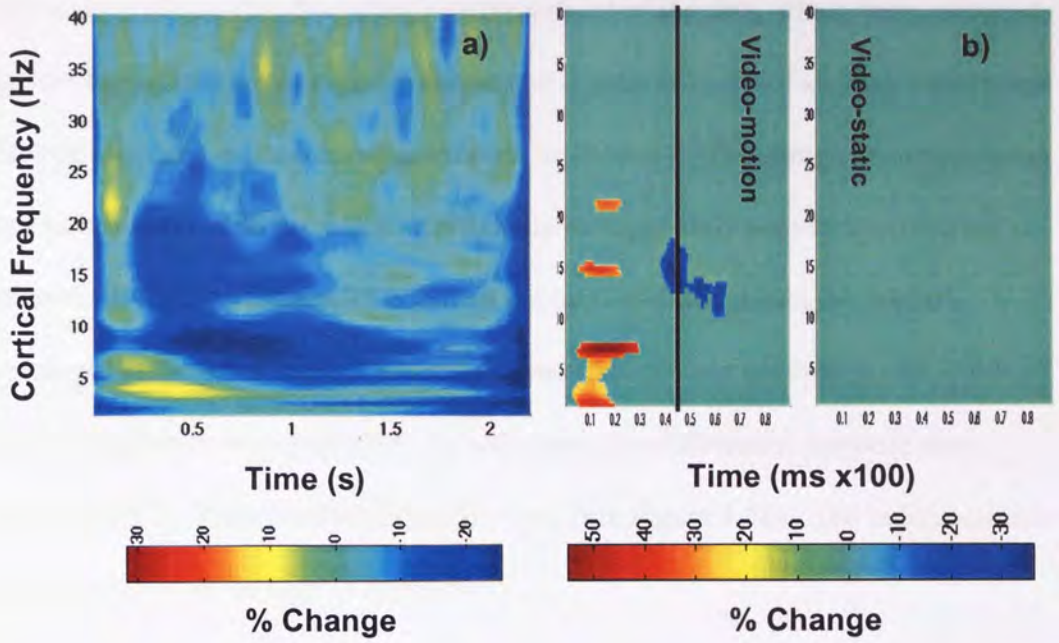

Figure 4-4. a) Time frequency plot, averaged across all subjects and calculated using Morlet wavelet analysis, from voxels in V5/MT showing the percentage change in activation between the video-motion and the video-static conditions. It can be seen that following a brief initial power increase there is a broad ERD response which lasts for the duration of the stimulus. A yellow / green colour indicates that activation in the video-motion condition was stronger than for the video-static condition whilst the blue purple colour indicates the converse. b) A non-parametric time-frequency analysis showing statistically significant voxels for the video-motion and video-static conditions ($p < 0.05$). The red / orange colour indicates a significant power increase when compared to the video-static baseline and the blue / purple colour indicates the converse. The timebase for this measurement has been shortened to allow direct comparison with the implied-motion data that follows. The black line indicates the reaction time for deciding that video motion is present (see Figure 4-12), although an active response was not required by the participant in the MEG recording.

4.7.2.2 Implied-motion experiment

Three experimental conditions were used. Following initial analysis of the data it was found that the implied-motion v implied-static and implied-motion v blank conditions produced similar results. The analysis shown in this section therefore will concentrate mainly on the implied-motion v implied-static condition (see appendix III and IV for details of the implied-motion v blank data).

The temporal evolution of oscillatory activity within the peak voxel in V5/MT, for the implied-motion and implied-static conditions, was examined using Morlet Wavelet

analysis to produce time-frequency representations of the data, which were averaged together to produce group representations (see Figure 4-5). The Talairach coordinates of the voxels used in the analysis are shown in Table 4-1. The results showed that the implied-motion stimuli produced significantly stronger early activations (peaking at between 100-200ms) in area V5/MT than the implied-static condition, whilst conversely the implied-static condition showed stronger late activations (600-900ms) than the implied-motion condition. In both cases this differential response was mainly in the 15-20Hz cortical frequency band (see Figure 4-5c). The individual time frequency plots can be seen in Appendix V.

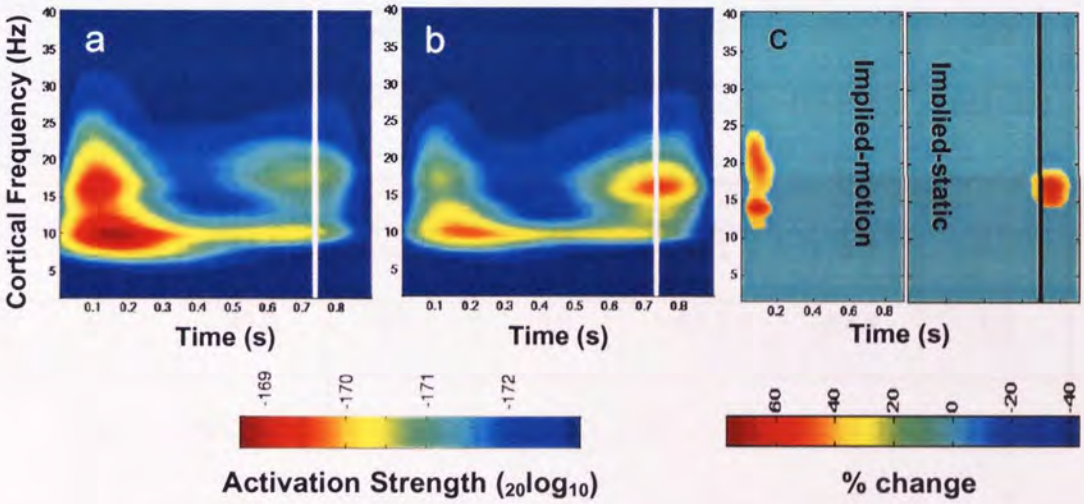

Figure 4-5. Time-frequency plots, averaged across all subjects (12 hemispheres) and calculated using Morlet wavelet analysis, from voxels showing the peak activation in left and right V5/MT (see Table 4-1 for Talairach coordinates of voxels used). The plots show activation following presentation of* a.. *implied-motion pictures and* b. *implied-static pictures. There is a clear difference in cortical activation between the two conditions, with stronger early activation in the implied-motion condition and stronger late activation in the implied-static condition.* c. *A non-parametric time-frequency analysis showing the statistically significant voxels for implied-motion and implied-static conditions ($p < 0.05$). In all cases the vertical line depicts the mean reaction time for deciding whether implicit-motion is present (see section 4.7.4).

The non-parametric time frequency plots for the actual video and implied-motion conditions (see Figure 4-4b and Figure 4-5c) show different patterns of activation.

Both conditions show an initial early response although the activation is more discrete for the implied-motion condition. The actual motion condition shows a desynchronisation occurring at approximately 400ms whereas the implied-motion condition shows a late response at approximately 700ms within the 15-20Hz frequency band.

SUBJECT	Right V5/MT (mm)			Left V5/MT (mm)		
	X	Y	Z	X	Y	Z
1	51.2	-74.3	2.0	NAI<2.0	NAI<2.0	NAI<2.0
2	48.2	-75.3	-2.0	-46.2	-73.3	0.0
3	55.2	-66.3	0.0	NAI<2.0	NAI<2.0	NAI<2.0
4	54.2	-66.3	3.0	-42.2	-72.3	5.0
5	52.2	-70.3	0.0	NAI<2.0	NAI<2.0	NAI<2.0
6	44.2	-65.3	2.0	NAI<2.0	NAI<2.0	NAI<2.0
7	50.2	-62.3	-1.0	-40.2	-70.3	3.0
8	47.2	-71.3	-3.0	-45.2	-69.3	3.0
Mean	50.3 ± 3.9	-68.9 ± 4.6	0.0 ± 2.1	-43.4 ± 2.8	-71.3 ± 1.8	2.8 ± 1.8

Table 4-1. Individual talairach coordinates of the V5/MT peak voxels used to create spectrogram images in Figure 4-5. Peak voxels used in the analysis exceeded NAI = 2.0.

Given the results of the non-parametric analysis (Figure 4-5c) the SAM images were recalculated in the 15-20Hz band. Figure 4-6 shows individual results that have been spatially normalised to a template brain and group-averaged. Statistically significant ($p. < 0.05$) bilateral activation clusters of the V5/MT complex, in the 15-20Hz frequency band, were identified in the group results both within the first 200ms and later at 700-900ms, calculated using nonparametric permutation testing (SnPM).

Additionally activation was seen to spread through areas LO/KO and V3A (see Table 4-2 for comparison with areas activated from other studies and see Appendix VI and VII for the full SnPM output). Individual responses can be seen in Appendix VIII.

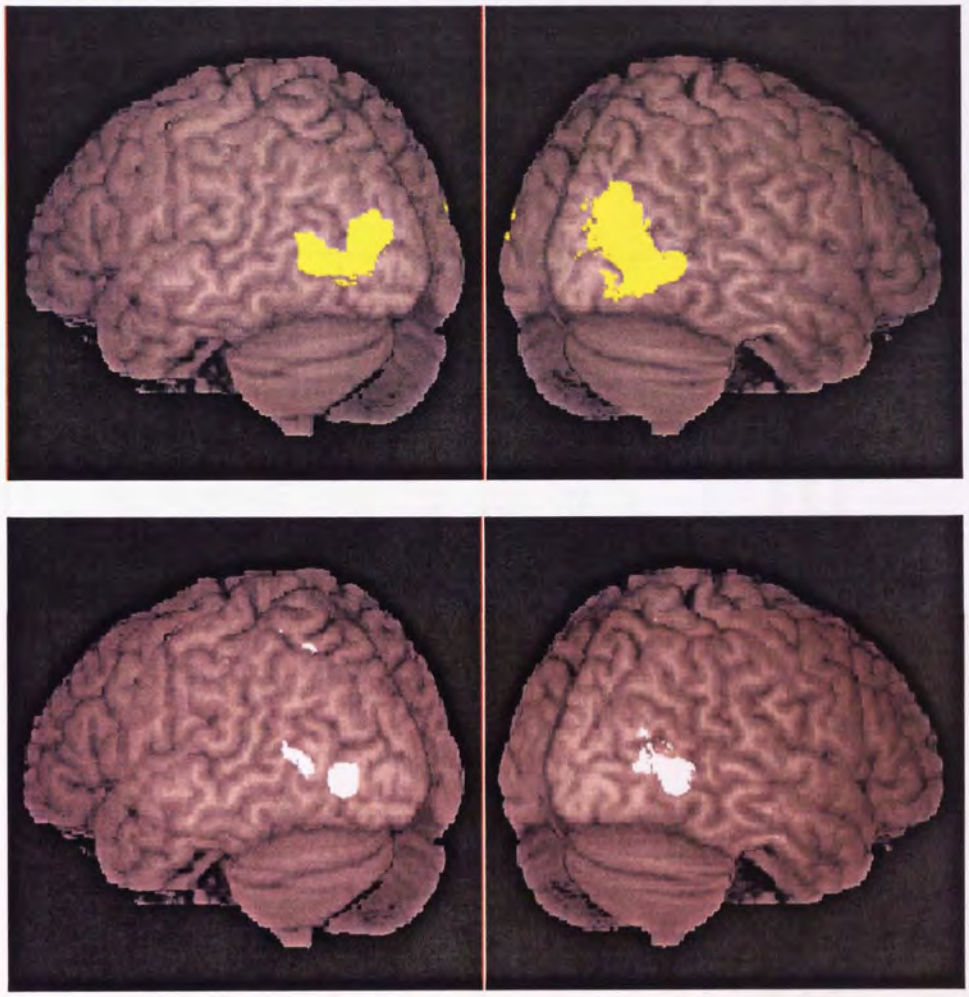

Figure 4-6. Top. Group MEG/SAM image showing voxels in which the group mean effect is statistically significant (p. <0.05) in the implied-motion v implied-static condition, 100-300ms following presentation of the stimulus in the 15-20Hz frequency band,calculated using nonparametric permutation testing (SnPM: http://www.fil.ion.ucl.ac.uk/spm/snpm). There is clear bilateral activation of motion area V5/MT as well as motion areas LO, KO and V3A (see Table 4-2 for clarification). Significant clusters were present in Right V5/MT (54 -66 3) and Left V5/MT (-45 -75 3). Bottom. The same measurements as above but 700-900ms following stimulus presentation. There is bilateral activation of the V5/MT complex with no spread to other motion areas and significant clusters present in Right V5/MT (54 -66 3) and Left V5/MT (-54 -72 12). The coordinates of the left-sided response, although different from the early response was consistent with the location of the actual motion response measured using video stimuli (see Figure 4-3).

	Video motion v video no motion	Implied motion v implied static 0.1 – 0.3	Implied motion v implied static 0.6 – 0.9	Sunaert et al (1999)	Watson et al (1993)	Dupont et al (1997)	Goebel et al (1998)	Dumoulin et al (2000)
V5/MT	-45 -66 12 54 -66 0	-45 -75 3 54 -66 3	-54 -72 12 54 -66 3	-42 -66 2 42 -62 6	**42 -68 0**	**40 -67 0**	**47 -58 4**	-47 -76 2 44 -67 0
LO/KO	-27 -78 3	-39 -84 0 39 -78 3	-36 -87 3	-34 -80 4 28 -86 2		**31 -91 -2**		
V3A		-27 -96 15 36 -78 15		-24 -84 10 22 -90 10	**22 -86 8**		**14 -91 13**	
VIPS	-18 -78 30 33 -75 42			**24 -76 28**	**22 -78 32**			
DIPSA	-24 -48 63 36 -51 60			**33 -44 61**		**34 -48 40**		
DIPSM				**18 -60 62**		**22 -60 40**		
DIPSL	-15 -54 60			**15 -54 62**			**22 -54 52**	
Other	-30 -51 57 51 -39 57							

Table 4-2. Comparison of Talairach coordinates obtained in the present study (p. < 0.05) with previous studies of actual motion stimuli. The table shows that the areas activated in both the actual motion and implied motion conditions are in broad agreement with previous motion areas activated in a number of previous studies. Coordinates in bold are the average of both the left and right hemispheres combined. Results from Sunaert et al, Watson et al, Dupont et al and Goebel et al adapted from Sunaert et al. 1999.

A comparison of the cortical areas activated in the video and implied-motion conditions was made. Figure 4-7 shows the activated cortical areas in the actual motion and early and late responses in the implied-motion condition.

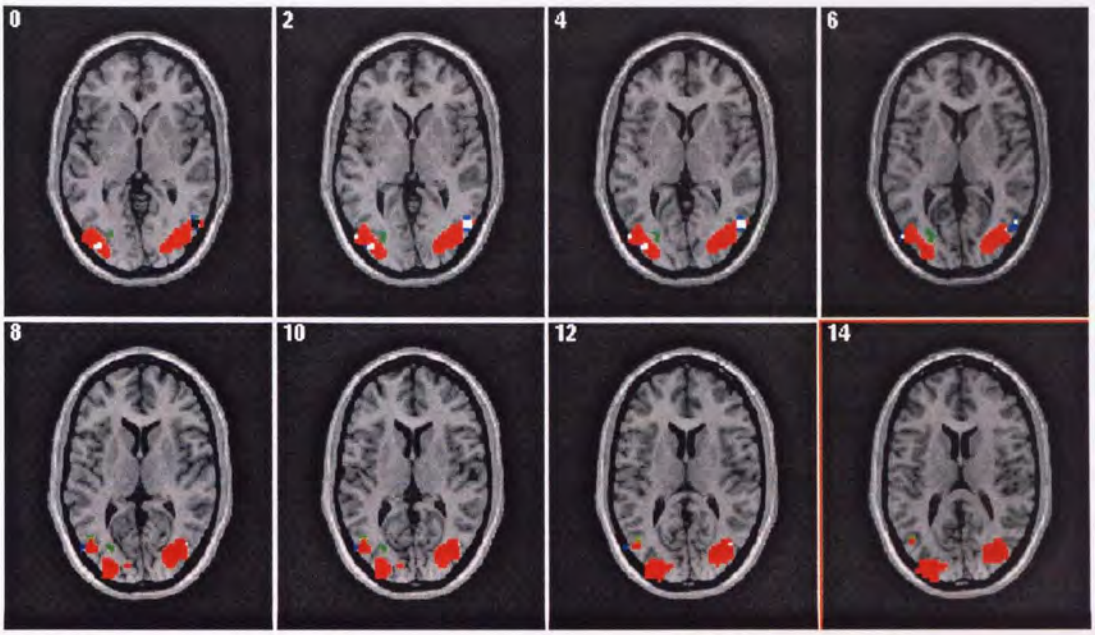

Figure 4-7. Statistically significant activated voxels (p. < 0.05) from group data in all three experimental conditions shown on the template brain. Eight axial slices at Talairach coordinates 0, +2, +4, +6, +8, +10, +12 and +14 are shown. Activity from the actual motion condition is coloured green, from the implied-motion 0.1-0.3sec condition is coloured red and from the implie- motion 0.6-0.9sec condition is coloured blue. Coincident voxels from all three conditions are coloured black and coincident voxels from the implied-motion 0.1-0.3 and 0.6-0.9 conditions are coloured white.

Coincident voxels from all three conditions were noted in right V5/MT. The response to the actual motion condition showed right and left V5/MT activity, with the left side located more ventrally than the right, as well as areas in the parietal cortex known to be associated with motion perception (see section 4.3.4). The early response of the implied-motion condition spread posteriorly to that of the actual motion condition to areas such as LO, KO and V3A (see sections 4.3.2 and 4.3.3). The late response from the implied-motion condition showed right V5/MT activation in agreement with the

early response and a left V5/MT response in agreement with the actual motion response.

It was necessary to know whether the response being produced by V5/MT (Figure 4-5) was limited to this area or was indicative of an overall response from the motion areas in general. Figure 4-8 shows the group time-frequency response from voxels approximating area V3A.

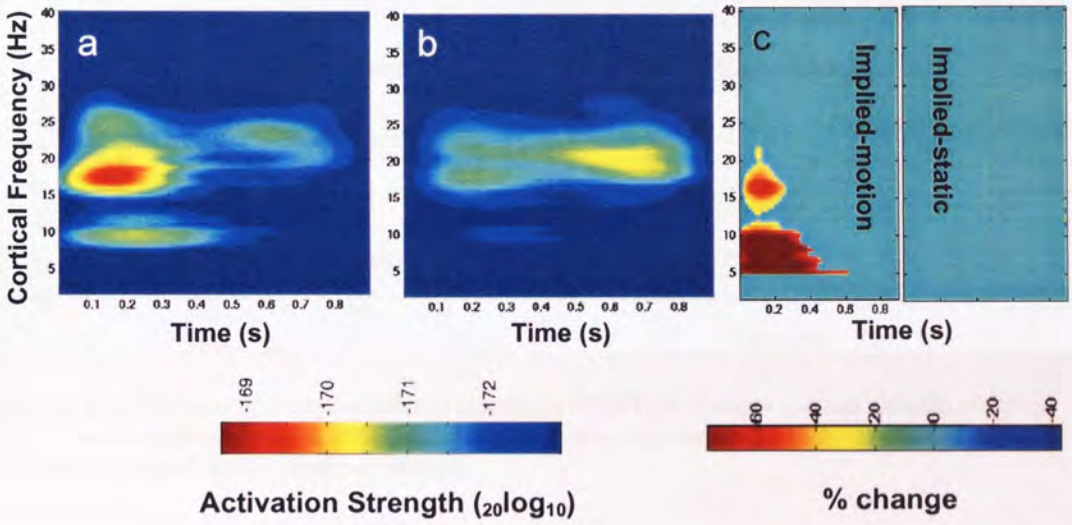

Figure 4-8. Time-frequency plots, averaged across all subjects and calculated using Morlet wavelet analysis, from voxels in left and right V3A. The plots show activation following presentation of* a. *implied-motion pictures and* b. *implied-static pictures. There is a clear difference in cortical activation between the two conditions, with stronger early activation in the implied-motion condition and stronger late activation in the implied-static condition.* c. *A non-parametric time-frequency analysis showing statistically significant voxels between implied-motion and implied-static conditions ($p < 0.05$).

The activation showed that the response of V3A was similar, though not identical, to that of V5/MT. There was again a stronger early response for implied-motion and a suggestion of a late response for the implied-static condition. A non-parametric time-frequency plot, measuring statistically significant differences between the implied-motion and implied-static conditions, showed a broader frequency range of early

activation than V5/MT although, unlike area V5/MT, the late activation difference was not statistically significant.

It was of interest to know whether the activations produced in the motion areas were induced or evoked activity (see section 2.6.2. for clarification of these terms). Figure 4-9 shows the measurements made from a single subject.

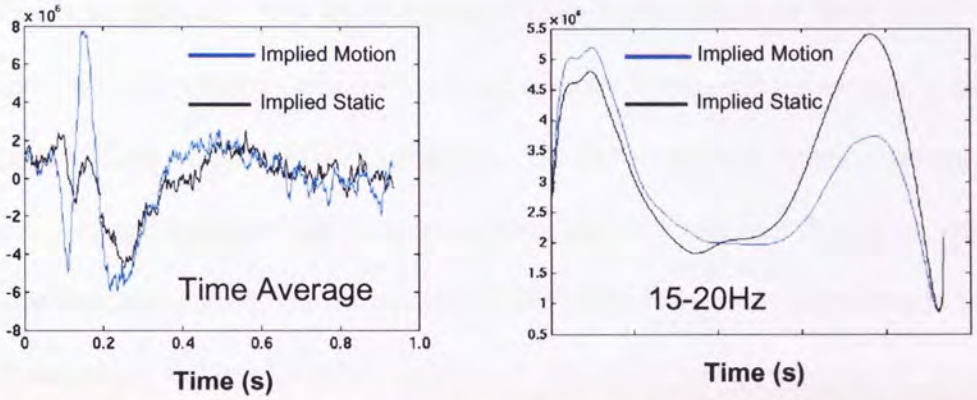

Figure 4-9. A measure of evoked v induced activity in V5/MT for a single subject. Graphs showing differences in response strength between the time averaged response and 15-20Hz bands of the implied-motion and implied-static conditions.

The time average response as seen in Figure 4-9 is a measure of the change in amplitude of activation across epochs as a function of time and is therefore a good measure of evoked cortical activity. The time averaged response shows a marked difference in early activation between the implied-motion and implied-static conditions, with implied-motion producing a larger response. However, between 600-900ms there is no difference in the time averaged response between the two conditions. Conversely, measurements in the 15-20Hz band shows a small difference between conditions for the early cortical response but show a marked difference for the later response where the implied-static condition shows a much stronger response.

This suggests that the early cortical response measured in this experiment is mainly an evoked response whilst the later response is purely induced cortical activity.

4.7.3 Eye Movements

It has been shown that eye movements can activate a network of cortical areas including V5/MT and the frontal eye fields (Corbetta *et al.* 1998). As it was not possible to monitor eye movements during the MEG recording session this possibility needed to be ruled out. In a separate session the eye movements of three of the subjects were monitored, using a Plusoptix Powerref II eye tracking system, under the same conditions as in the MEG experiment. The eye movement output is shown in Figure 4-10 and indicates that the subjects were able to fixate well during the implied-motion task, although it was not possible to differentiate the eye movements in the implied-motion and implied-static conditions. Eye movements in the actual motion condition showed slightly larger eye movements.

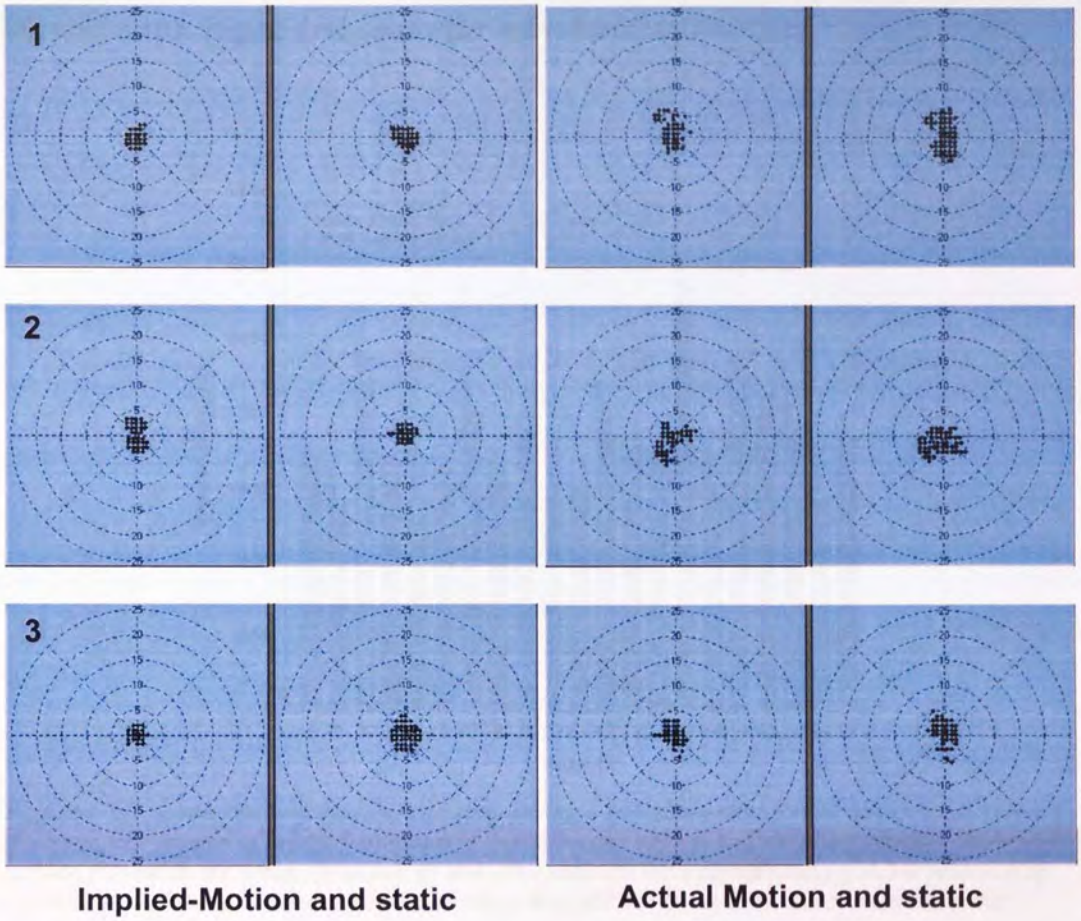

Figure 4-10. Eye tracking output from three subjects in the implied-motion and actual motion conditions

4.7.4 Implied-motion reaction time

In a separate experiment the subjects' reaction times to an implied-motion present / not present task was measured. Given the findings of a very early differential activation in V5/MT it was hypothesised that subjects would be able to identify whether implied-motion was present in a scene very quickly (within the first few hundred ms) and that this decision would occur faster when implied-motion was actually present. In fact subjects were much slower than predicted by the early response in V5/MT, although there was an advantage for the implied-motion

condition (implied-motion RT = 715ms, implied-static RT = 747ms, t = 2.315, df = 20, $p < 0.016$). Figure 4-11 shows the individual reaction times.

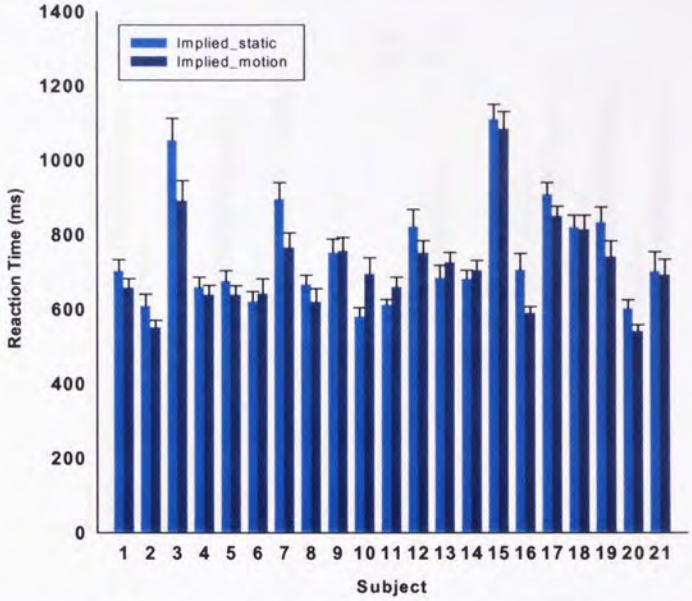

Figure 4-11. Mean reaction times of subjects, during a two alternative forced choice task, viewing photographic images of implied-motion and implied-static objects and deciding whether there was motion present in the image (implied) or not. The subjects were significantly quicker responding when images showed implied-motion than when they did not ($p < 0.016$). Error bars show the standard error of the mean.

The reaction times were slower than expected given the early response seen in the imaging data. To compare the implied-motion reaction times with those of actual motion the same subjects, in a separate session, took part in a two alternative forced choice actual motion present / not present condition. The subjects were significantly quicker responding when motion was present compared to when it was not present (Video actual motion RT = 483ms, Video no motion RT =516ms, t = 14.338, df = 20, $p<0.00025$). Figure 4-12 shows the individual reaction times. Again the reaction times were slower than suggested by the rapid early cortical response, although the reaction times for actual motion were faster than the reaction times for implied-

motion. Interestingly, the 483ms response time appears to coincide with the onset of statistically significant ERD appearing in V5/MT (see Figure 4-4).

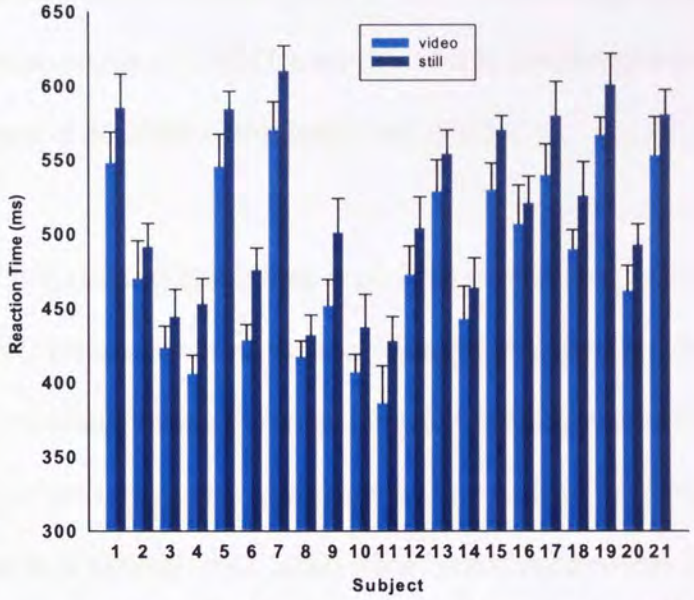

Figure 4-12. Mean reaction times of subjects, during a two alternative forced choice task, viewing video of actual motion and video of no motion and deciding whether motion was present or not. The subjects were significantly quicker responding when motion was present compared to when it was not present. Error bars show the standard error of the mean.

4.8 Discussion

The findings described here complement recent functional imaging studies (Kourtzi and Kanwisher 2000a, Senior *et al.* 2000) which suggest that motion area V5/MT is involved in the perception of implied-motion and this study shows, for the first time using functional imaging, the temporal evolution of this response. Consistent with previous findings (Kourtzi and Kanwisher 2000a, Senior *et al.* 2000) our early response (up to 300ms) extends beyond area V5/MT to incorporate motion areas LO, KO and V3A (see Figure 4-6) which are known to be activated by actual motion stimuli (Sunaert *et al.* 1999) suggesting that fMRI BOLD responses recorded previously (Kourtzi and Kanwisher 2000a, Senior *et al.* 2000) occur as a consequence

of this initial response. However, the late response recorded here (600-900ms) is confined to area V5/MT. This, and the results of the reaction time experiments, suggest the possibility that this area is involved in the perceptual process of extracting implied-motion information from the photographic stimuli. Evidence to support this comes from recent studies of V5/MT's involvement in the perception of motion stimuli (e.g. Antal *et al.* 2004, Krekelberg *et al.* 2003).

Using Glass (1969) patterns Krekelberg *et al.* 2003 showed that the perception of moving objects is computed during the analysis of their motion and that cells in the motion area have similar tuning to real and implied-motion, suggesting that the processing of the two is the same. Although the first stage of perception of global structure occurs in V1 (Smith *et al.* 2002) it has been suggested that further analysis by motion and orientation sensitive neurons in V5/MT mediate the early combination of motion signals and form that produce implied-motion (Kourtzi 2004).

The implied-motion using Glass patterns (Glass 1969) is derived from the form of the pattern itself rather than actual motion signals. Similarly implied-motion from photographic images is derived from the form of the objects in the photographs in relation to their surroundings with the addition of top-down knowledge of how the objects are going to act. It is therefore not surprising that areas such as LO, known to be involved in object recognition (Grill-Spector *et al.* 2001, Kourtzi *et al.* 2002, Kourtzi and Kanwisher 2000b) are activated by the implied-motion condition.

4.8.1 Alternative explanations of the cortical activation

The responses seen in this study, using implied-motion stimuli, could have been due to relatively low-level attributes such as luminance and contrast differences between

the implied-motion and implied-static images. However, this is unlikely as the images were all recorded in a single session with controlled lighting and the object content of the implied-motion and implied-static images was identical. Secondly it is also known that motion areas respond to temporal structure, such as pattern onset or offset in a stimulus (see section 4.4). It is unlikely that the responses recorded here are due to differing stimulus transients between the two conditions as both conditions were displayed for the same length of time and any flicker produced by the projection equipment was the same in both conditions. Thirdly, it is possible that the activations that were seen were due to subtle differences in content between the implied-motion and implied-static conditions. Although the gross content of the images in the two conditions was the same there were differences in the orientation of some of the object edges between the images. This is again an unlikely explanation of the strong activations that were recorded, as over the many runs both within and across subjects, the different orientation of edges will have averaged out across trials.

4.8.2 Reaction Time data

The measured reaction time responses to implied-motion occurred at a similar time with that of the late activation present in the functional imaging experiment, suggesting that this cortical activation is playing some part in the cognitive decision that implied-motion is present or not. Psychophysical studies of motion perception suggest that reaction times to motion onset are inversely proportional to motion velocity (Hohnsbein and Mateef 1992, Ball and Sekular 1980) with studies showing reaction times in the region of 180 – 300ms depending on the stimulus conditions (Smeets and Brenner 1994, Tynan and Sekular 1982, Ball and Sekular 1980). The reaction times to the actual motion stimuli (483ms) in this study are rather longer than

those reported previously although the stimuli used in studies are very different. The psychophysical studies reported here monitor the reaction time to the appearance of dot stimuli whereas this study uses actual video of object motion. Similarly subjects in this study are having to make a cognitive decision as to whether motion is present or not and press the appropriate button which adds to the reaction time. However the reaction time results from both the implied and actual motion tasks suggest that the initial early differential response in V5/MT cannot be used for a conscious decision as to whether actual or implied-motion is present.

4.8.3 The early response

Motion evoked responses have been studied for many years using both EEG (Ffytche *et al.* 1995, Bach and Ullrich 1997, Hollants-Gilhuijs *et al.* 2000) and MEG (Ahlfors *et al.* 1999, Bundo *et al.* 2000) Consistent with previous findings, as well as recent reports on magnetic motion-onset evoked responses (Schellart *et al.* 2004) and apparent motion evoked magnetic fields (Kaneoke *et al.* 1998, Kubota *et al.* 2004), the early response seen in the implied-motion condition at 100-200ms is consistent with the reports which show responses between 140-180ms in motion areas such as V5/MT and V3A. Similarly inspection of the time frequency plots from the actual motion condition in this study shows an early onset response at 100-200 ms (see Figure 4-4). Thus, when motion is perceived, either real or apparent, an evoked response occurs in the motion regions within the first 200ms. What is surprising about the response seen with the implied-motion data in this study is that no motion is actually present, suggesting a rapid analysis of objects and their implied momentum is taking place.

4.8.4 Comparison with other implied-motion studies

There was some overlap of activations between the actual motion and implied-motion conditions in bilateral V5/MT (see Figure 4-7). Consistent with previous studies (Kourtzi and Kanwisher 2000a, Senior *et al.* 2000) activations in the implied-motion condition spread posteriorly and ventrally from V5/MT into areas known to be involved with object recognition. However no Talairach coordinates were given in the Kourtzi and Kanwisher (2000a) data making direct comparison difficult although the areas of activation were similar to those seen in the present study. Data in the Senior *et al.* (2000) paper compared video of actual motion with photographic still images. There is a marked difference in image quality between video and photographic images which did not seem to be controlled for in this study. The present study compares video of actual motion with video of no motion thus controlling for any effects that differences in image quality may produce.

Although implied-motion and representational momentum are terms that are often interchangeable in the literature, in terms of functional imaging they would seem to be rather different phenomena. Representational momentum paradigms require the use of working memory to remember the last position of an object and allow comparison of this with the stimulus object. The processes involved in working memory, defined as a system for holding and manipulating information for a short period of time (Baddley 1986), have been shown to involve the pre frontal cortex (Fuster 2000, Goel and Grafman 1995, Ungerleider *et al.* 1998) and this has been supported by data from single cell recording (Funahashi *et al.* 1989) and lesion studies (Levy and Goldman-Rakic 1999, Goldman-Rakic 1987). The frontal activations, and lack of motion area activation, shown in some functional imaging studies (Amorim *et*

al. 2000) are likely to reflect this working memory effect and would also suggest that the V5/MT complex is not necessarily activated during cognitive processing of representational momentum.

Functional imaging studies that look simply at implied-motion whether using photographs (Senior *et al.* 2000, Kourtzi and Kanwisher 2000a) or Glass patterns (Krekelberg *et al.* 2003) require no such use of working memory and as with the current study show no significant frontal activations but do show activations of V5/MT and adjacent cortical areas. This raises the possibility that different cortical areas are activated by the two processes. It may well be that V5/MT is only activated when photographic images are shown, as these convey a more realistic view of the world, and may not be present with the other types of stimuli. Further functional imaging studies are therefore required to investigate the response of area V5/MT to other types of implied-motion inducing stimuli.

4.8.5 Eye movements

Although eye movements are known to activate a network of cortical areas including V5/MT (Corbetta *et al.* 1998, Petit and Haxby 1999, Kleiser *et al.* 2004) it is unlikely that eye movements could account for the activity seen in the implied-motion v implied-static condition. Measurement of eye movements outside of the scanner showed that subjects were able to maintain fixation adequately throughout the task. Although it was not possible to differentiate the eye movements in the implied-motion condition from the implied-static condition it seems unlikely that the two conditions would produce different eye movements. A fixation cross was present in the centre of the screen at all times and the only difference between the conditions was the content

of the photographic image which is unlikely to produce different eye movements. Larger eye movements were recorded in the actual motion condition so it cannot be ruled out that eye movements did contribute to the responses seen in this condition. However, the regions activated by the actual motion condition were in broad agreement with past studies (see Table 4-2).

4.9 Conclusion

The ecological function of this V5/MT response to implied-motion is debatable. Hubbard.T.L. (1998a) suggests that our cognitive system contains an implicit knowledge of physical principles which, even in a fleeting glance, gives us knowledge of how an object or thing will move in space and time and thus conveys a survival advantage. It may well be that the human motion system is so tuned to motion in everyday life that the mere implied presence of motion in a photographic image activates top-down processes which initially prime V5/MT to expect motion and also provides later feedback when motion is not present. Alternatively this process may occur in V5/MT itself. Whatever the mechanism, this priming would confer the advantage of a rapid response when real motion is present but would require a relatively long time to finally identify that motion is not present, which is consistent with the findings that are described here.

5. THE MEASUREMENT OF OSCILLATORY RESPONSES IN THE VISUAL CORTEX TO CHANGES IN VISUOSPATIAL ATTENTION AND STIMULUS CONTRAST USING SYNTHETIC APERTURE MAGNETOMETRY

5.1 Overview

This chapter describes an experiment to investigate the oscillatory changes occurring in the visual cortex in response to changes in stimulus contrast and covert spatial attention using Synthetic Aperture Magnetometry. The chapter begins by reviewing the literature on visuospatial attention and follows this by introducing how attention may effect the contrast response. The chapter continues by describing the experiment and discusses the results of both the modulation of alpha activity in visual cortex and the contrast response function as measured from the SAM data by relating them to past studies on attention.

5.2 Introduction

The human brain is receiving constant information from all the bodies senses. However, the brain's capacity for analysing this information is limited, requiring the need for attentional mechanisms that allocate brain resources to relevant and important information whilst filtering out irrelevant information. This is particularly true of the visual system (Broadbent 1958) where visuospatial attention refers to the allocation of cortical resources to a particular visual location and it is this form of attention that will be the focus of this chapter.

It is known that the detection of visual stimuli can be enhanced by the amount of attention that is directed towards them, with both accuracy and speed of response of subjects to target stimuli improving at an attended location (Posner 1980) whilst

attention also increases the perceptual sensitivity for the discrimination of target stimuli (Lu and Dosher 1998). However, whilst selectively giving priority to certain aspects of the visual field may simply involve shifting gaze from one location to another many situations, such as driving, involve attending to locations in the periphery of vision without actually shifting gaze to these locations. This shifting of visual attention without shifting gaze is known as covert attention and has been shown to influence performance in a range of perception tasks such as contrast sensitivity (Carrasco *et al.* 2000, Cameron *et al.* 2002, Lu and Dosher 1998, Lee *et al.* 1999), visual search (Carrasco and McElree 2001, Nackayama and Mackeben 1989) and spatial resolution (Yeshurun and Carrasco 2000).

5.2.1 Single cell studies of attention

When attention is directed towards a stimulus presented within the receptive field of a neuron, responses to the stimulus are enhanced compared to when attention is directed elsewhere. This effect has been shown at many levels of the visual processing system such as V1 (Motter 1993), V2 (Luck *et al.* 1997, Motter 1993), V4 (Connor *et al.* 1997, Luck *et al.* 1997, McAdams and Maunsell 1999) and V5/MT (Recanzone and Wurtz 2000, Treue and Maunsell 1996) although the effect is typically weakest in the early stages of visual processing and strongest in the later stages (see Figure 5-1).

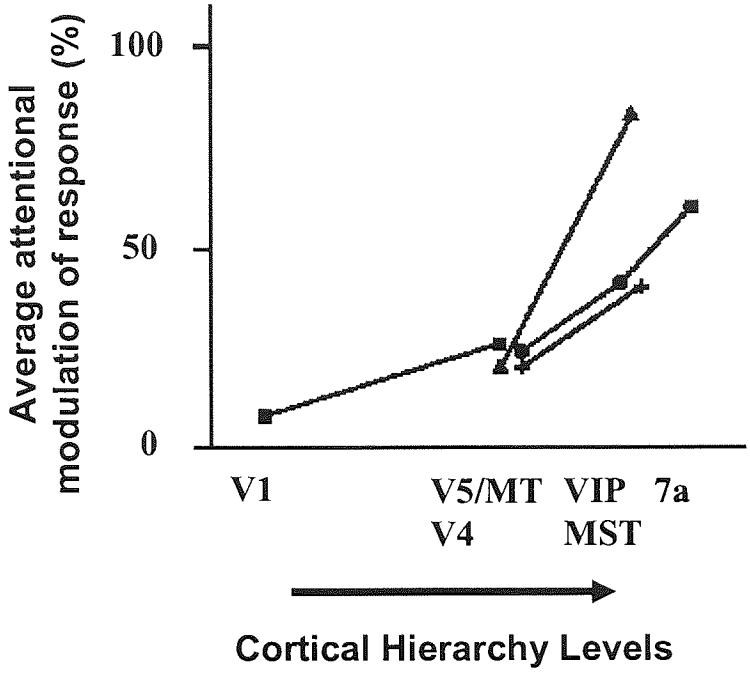

Figure 5-1. Average attentional modulation of response in various visual cortical areas (Adapted from Maunsell and Cook 2002).

This modulation of response is seen in both spatial and feature attention (Corbetta *et al.* 1991, McAdams and Maunsell 2000, Treue and Martinez-Trujillo 1999) and increases with task difficulty (Spitzer and Richmond 1991). However, whilst attention increases the neuronal response it does not change the variability of response (McAdams and Maunsell 1999) or the tuning characteristics of neurons (Reynolds *et al.* 2000).

5.2.2 Functional imaging studies of attention

Evidence from functional imaging studies of covert attention suggest that a network of cortical areas such as the posterior parietal lobe around the intraparietal cortex, superior parietal lobule and the frontal eye fields are activated by various visuospatial tasks (Corbetta *et al.* 1998, Nobre *et al.* 1997, Vandenberghe *et al.* 1997) whilst further studies have suggested that this activation is the result of a general spatial attention network that operates independently of the requirements of the visuospatial task (Hopfinger *et al.* 2000, Kastner *et al.* 1999).

Using fMRI and a stimulus consisting of two circular patches, which were present at all times on either side of a central fixation point, it was shown that subjects performing a speed discrimination task showed an increased BOLD response in primary visual cortex contralateral to the side of cued attention (Gandhi *et al.* 1999). This modulation of response in early visual processing has been seen across a number of functional imaging studies (Tootell *et al.* 1998, Brefczynski and DeYoe 1999, Martinez *et al.* 1999).

5.2.3 Effect of attention on contrast response

According to the biased competition model of attention (Desimone and Duncan 1995) there is competition for neural resources, within the visual cortex, between bottom up sensory processes responding to stimulus characteristics such as colour and contrast and top down processes whereby attention to a particular visual location improves the processing of stimuli presented at that location by activation of a cortical attention network (e.g. Corbetta *et al.* 1998, Corbetta and Shulman 2002, Nobre *et al.* 1997, Vandenberghe *et al.* 1997).

The bottom up hypothesis suggests that attention does not alter the nature of the stimulus but serves to increase the sensitivity of cortical neurons to that stimulus in a way that is similar to increasing the intensity of stimulus characteristics (Maunsell and Cook 2002). It is known that increasing stimulus contrast makes a neuron's response stronger without changing its selectivity for other stimulus characteristics (Dean 1981, Holub and Morton-Gibson 1981, Sclar and Freeman 1982, Albrecht and Hamilton 1982, Skottun *et al.* 1987, Geisler and Albrecht 1997). Consequently recent research has

concentrated on how attentional processes mimic the effects of increasing stimulus intensity.

In terms of neuronal reactions to contrast, two types of response are possible; contrast gain and response gain. According to the contrast gain response model (see Figure 5-2A), the sensitivity of neurons' contrast response is increased by attention thus shifting the contrast response function to the left, indicating that neurons at the attended location require less contrast to produce the same response than for neurons at an unattended location, although the shape of the tuning curve remains unchanged (Reynolds and Desimone 1999, Reynolds and Desimone 2003, Reynolds *et al.* 2000, Treue 2000, Martinez-Trujillo and Treue 2002). The response gain model (see Figure 5-2B) suggests that attention alters the response of the neuron by differentially increasing its firing rate for a given contrast, particularly at higher contrasts, thus steepening the slope of the contrast response function (Reynolds and Desimone 1999, Reynolds and Desimone 2003, Reynolds *et al.* 2000, Treue 2000, Martinez-Trujillo and Treue 2002).

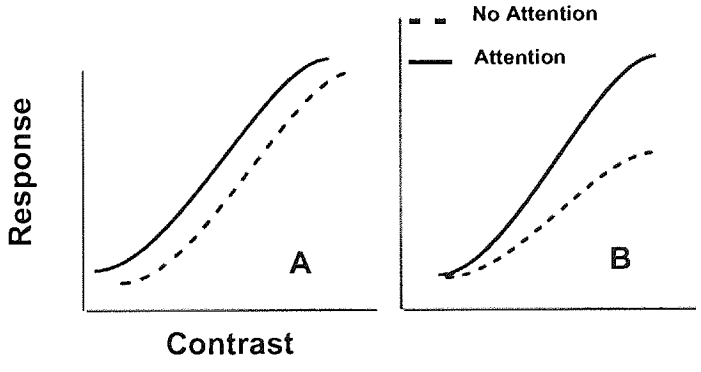

Figure 5-2. Schematic of neural contrast response functions and how they may be affected by attention. A. Contrast gain model. B. Response gain model. Adapted from Cameron et al. 2002.

A number of recent single cell and lesion studies have confirmed the role of attention on increasing the intensity of stimulus characteristics (Bisley and Goldberg 2003, De Weerd *et al.* 1999, Gottlieb *et al.* 1998, Martinez-Trujillo and Treue 2002, McAdams and Maunsell 1999, Reynolds and Desimone 1999, Reynolds *et al.* 2000, Reynolds and Desimone 2003, Treue 2003). Consistent with these findings it has been demonstrated that attention causes a reduction in neuronal contrast response thresholds within or below the normal dynamic range of the neurons whilst having very little effect on responses for stimuli at or above saturation contrast (Reynolds *et al.* 2000, Carrasco *et al.* 2004). This has been confirmed by further studies which have quantified spatial attention in terms of luminance contrast in visual areas V5/MT (Martinez-Trujillo and Treue 2002) and V4 (Reynolds and Desimone 2003) and estimated that attending to a stimulus increased luminance contrast by up to 56%.

There have been few functional imaging studies that have looked at the contrast response function, although it has been shown that the magnitude of the BOLD response varies with perceived contrast in primary visual cortex (Boynton *et al.* 1999, Goodyear *et al.* 2000) and across a range of visual areas (Boynton *et al.* 1999). Similarly it has been shown that the magnitude of the hemodynamic response saturates at a low image contrast (5%), as predicted by the magnocellular predominance in V5/MT (Tootell *et al.* 1995) a finding which has been confirmed using MEG (Anderson *et al.* 1996).

5.2.4 Oscillatory changes and attentional modulation in visual cortex

The physiology literature has reported attentional modulation of neuronal responses in many extrastriate cortical areas such as V2 (Luck *et al.* 1997, Motter 1993), V4 (Connor

et al. 1997, Luck *et al.* 1997, McAdams and Maunsell 1999) and V5/MT (Recanzone and Wurtz 2000, Treue and Maunsell 1996). However few reports (Motter 1993) provide evidence that attentional modulation occurs in the primary visual cortex (V1) and even then the response is very weak. Similar results are seen in the event related potential (ERP) and MEG literature (Heinze *et al.* 1994, Mangun *et al.* 1998, Martinez *et al.* 1999). In contrast, several recent fMRI studies have reported robust effects of attention on V1 responses (Watanabe *et al.* 1998, Brefczynski and DeYoe 1999, Gandhi *et al.* 1999, Martinez *et al.* 2001, Smith *et al.* 2000), demonstrating that attentional effects operate very early in the visual pathway. A combined ERP and fMRI study suggests that the attentional modulation measured in visual area V1 occurs later than that expected from initial activation of the area suggesting that the modulation being recorded is due to feedback processes from other visual areas rather than direct modulation by V1 itself (Martinez *et al.* 1999, Noesselt *et al.* 2002).

Previous research would suggest that cortical oscillations have a role to play in attentional processes (Ray and Cole 1985, Fries *et al.* 2001). When primary visual cortex receives no input it oscillates predominantly in the alpha frequency, which is considered to reflect cortical idling (Pfurtscheller *et al.* 1996). At the same time as alpha power decreases, the randomly distributed phase of the alpha activity during baseline is reset leading to an increase of phase-locked (evoked) activity (Brandt 1997). This simultaneous increase of phase locked alpha and decrease of alpha power (ERD) after a stimulus is described as the alpha paradox (Klimesch *et al.* 2000). The failure of previous ERP and MEG studies may well reflect their ability to measure this phase locked activity but not the none phase locked (induced) activity. A recent MEG study incorporating a combination of independent component analysis, dipole fitting and

scalogram analysis of the data has showed that directing attention to a stimulus location produces statistically significant changes in oscillatory activity in primary visual cortex with enhancement of alpha and beta activity (Yamagishi *et al.* 2003). The changes therefore seen with some fMRI studies may reflect these oscillatory changes and not reflect feedback mechanisms (Martinez *et al.* 1999, Noesselt *et al.* 2002). In this study both the modulation of cortical oscillatory activity with attention and how this varies with stimulus parameters are measured using Synthetic Aperture Magnetometry.

5.3 Methods

Six normal right-handed subjects (3M, 3F, 30 ± 4.2yrs) gave their consent to participate in the study. MEG data was collected using a 151 channel CTF Omega system (CTF Systems Inc., Port Coquitlam, Canada) at a sampling rate of 625 Hz. Data was recorded in a single un-averaged 240 second run which could be divided, for analysis purposes, into either sixteen 15 second long epochs (see Figure 5-3) or 80 individually triggered epochs, each 2.2 seconds long, consisting of 40 attend left and 40 attend right trials (see Figure 5-3). The first 15 second block consisted of 5 presentations of attend left stimuli, with a central fixation point indicating the side to attend and the second 15 second block consisted of 5 presentations of attend right stimuli (see Figure 5-3). This attend left and attend right design was repeated eight times to make a single 240 second run. The visual stimuli were generated by an Apple Powerbook and presented to the subject via an Eizo Flexscan T562-T monitor with a refresh rate of 85Hz, viewed through a window in the scanner room using a mirror.

The stimulus consisted of a drifting sinusoidal grating (~12 degrees/sec, 1.5 cycles/degree) presented in circular apertures positioned either to the left, the right or

left / right simultaneously of a central fixation point. The apertures were 3° in diameter and centred 7° from fixation (see Figure 5-4).

Subjects were requested to fixate on a central fixation spot at all times and a line on the fixation point indicated whether fixation should be focused to the left or the right. The task consisted of the presentation of a grating for 900ms followed by a grey background for 200ms followed by a second grating for 900ms with a gap of 1000ms before the next presentation. The orientation of the second grating was rotated either clockwise or anticlockwise to the first and the subject responded clockwise / anticlockwise using the index finger of their right hand and a button box placed on their lap. Subjects practiced the task on three separate occasions outside of the scanner and again in the scanner prior to the MEG recording. The degree of orientation of the second grating presentation was set on a per subject basis to achieve a correct response level of between 80 and 90% (see Figure 5-4).

Stimuli were presented in two location conditions and three contrast conditions. In the one-patch condition the stimuli were presented with only one patch present (left or right) with the subject being asked to attend to the side of presentation. At no time was the subject asked to attend to a location where no stimulus was present. In the two-patch condition stimuli were presented simultaneously to patches on the left and right of fixation with the subject being asked to attend to one side. During the two-patch task, the orientations of the patches on the attended and unattended sides were different so the subjects had to attend to the indicated side to correctly respond, thus indicating that the subject's attention was being allocated appropriately. Stimuli with contrasts of 100%, 25% and 6.25% were presented in each location condition, with only one contrast type

being used during any one run. Thus, each subject took part in six separate measurement conditions with a rest period of two minutes between each run. The stimulus presentation order was randomised across subjects.

After the data was collected, a 3-D digitiser (Polhemus Isotrack) was used to digitise the shape of the subject's head in the MEG laboratory. Using Align (www.ece.drexel.edu/ICVC/Align/align11.html) this surface was matched to a head surface extracted from the subject's own, previously acquired, anatomical MRI in order to coregister the MEG data with the subject's anatomy. The MEG data was analysed using Synthetic Aperture Magnetometry (SAM) in frequency bands 8-13Hz, 10-20Hz, 15-20Hz, 15-25Hz and 5-40Hz (see section 2.6.1 for further details).

5.3.1 Eye movements

During the attention task eye movements were monitored at all times. Electrodes were placed on the outer canthus of each eye to monitor horizontal eye movements and placed above and below the right eye to monitor vertical eye movements. Prior to the MEG recording the EOG of each subject was calibrated by asking them to follow horizontally and vertically moving white dots on the screen. The calibration was set at a horizontal eye movement of 1.5° meaning that any epoch containing an eye movement above this level was manually rejected from the analysis. The calibration level meant that at no time was the patch being attended visualised centrally.

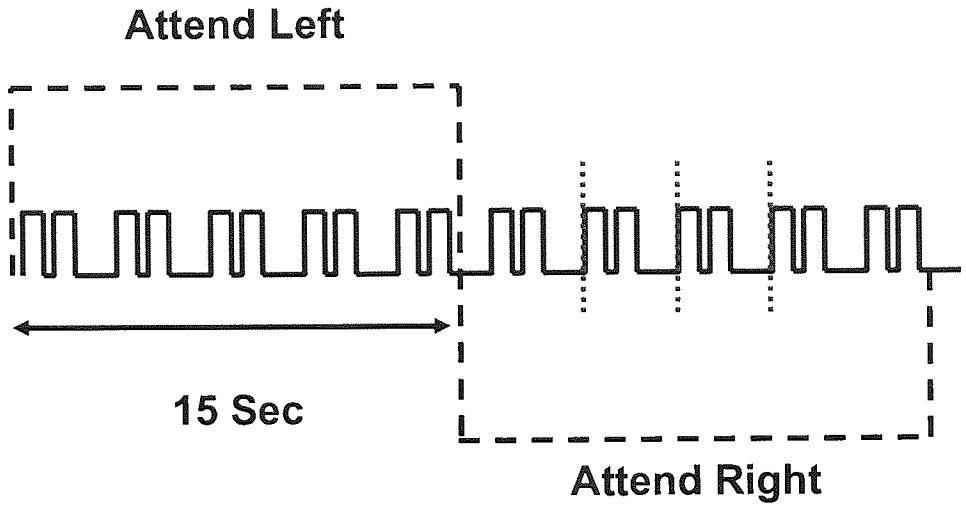

Figure 5-3. Diagrammatic outline of the experimental paradigms used in this study. The thick black dashed line indicates the boxcar design used in one of the analyses. Sixteen 15sec blocks were recorded, 8 attend left and 8 attend right. The dashed blue line indicates the individual triggers that were used in a separate analysis, 80 triggers in total (40 attend left and 40 attend right).

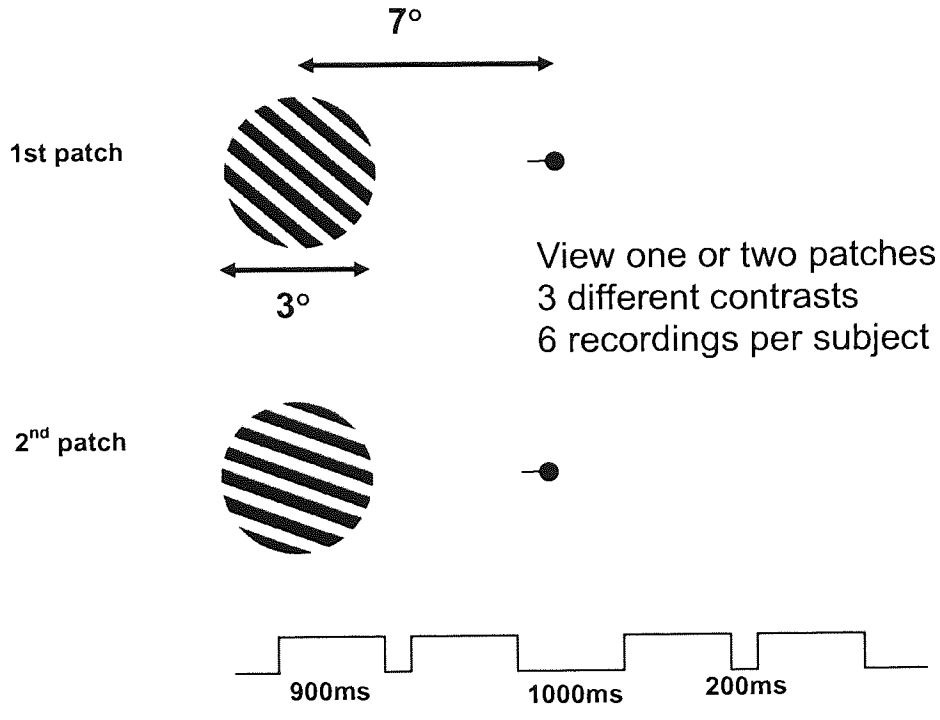

Figure 5-4. A diagrammatic representation of the stimulus used in the study. The diagram shows the set up in the 1 patch condition although it can be extrapolated for the 2 patch condition. The second patch is orientated differently to the first (in this case anticlockwise) and the subject has to indicate the direction of orientation change.

5.4 Results

5.4.1 Subject response data

In an attention paradigm it is vital to know if the subjects are attending correctly. Table 5-1 shows the percentage of correct responses of each subject across each stimulus condition.

Subject	100_1	100_2	25_1	25_2	6.25_1	6.25_2	Mean
1	83.5	82.5	86.2	81.2	87.5	78.5	83.2
2	82.1	77.2	80.0	81.8	86.2	85.0	82.1
3	90.0	83.8	83.8	82.5	95.0	87.5	87.1
4	93.8	84.6	87.5	81.0	80.8	75.6	83.9
5	83.8	80.0	88.8	86.2	78.8	86.2	84.0
6	79.6	76.9	81.6	81.0	83.4	82.5	80.8
Mean	85.5	80.8	84.7	82.3	85.3	82.6	

Table 5-1. Percentage of the correct responses per subject in the orientation task across stimulus conditions. The first number of the stimulus condition is the percentage contrast and the second is the number of patches. Note that contrast does not systematically affect performance on the task.

The difficulty of the orientation task paradigm was altered for each subject to achieve a correct response percentage between 80 and 90%. This was maintained across subjects indicating that subjects were attending appropriately throughout.

5.4.2 Spatial localisation of attentional response

The location of peak activation across a range of analysis frequencies was analysed to compare with previous attention studies (see Figure 5-5). Consistent with previous

functional imaging studies (Corbetta *et al.* 1998, Nobre *et al.* 1997, Vandenberghe *et al.* 1997) a network of posterior parietal and frontal activations is seen. Interestingly, the 2 patch data (Figure 5-5B), in which the attentional load is greatest, shows stronger posterior parietal activations than the 1 patch data . Further analysis showed that the occipital and parietal activations occurred mainly within the alpha (8-13Hz) band whilst the frontal activations occurred in the beta (15-25Hz) band.

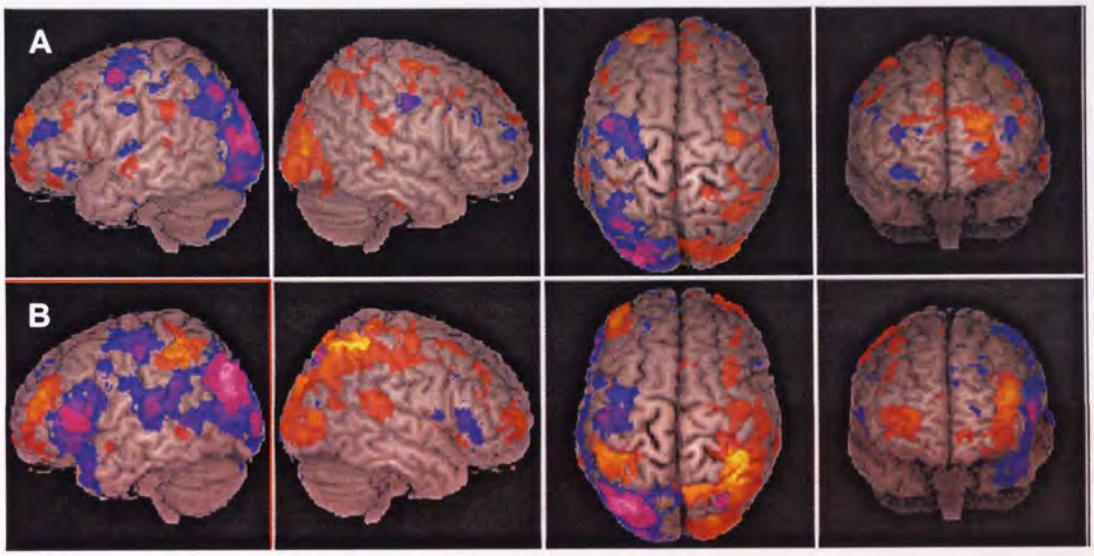

Figure 5-5. The peak group SAM image for the block analysis (attend right – attend left). This shows the peak power increase or decrease at each voxel in the brain (0-2.2sec), irrespective of which frequency band the power change occurred within, for A. 1 patch and B. 2 patch conditions (threshold NAI = 2.0). The blue/purple colour indicates that voxels in that location are most active in the attend-L compared to attend-R condition whilst the yellow/orange colour indicates the converse

The 1-patch condition was included for localisation purposes and the results of the block group analysis, in the 8-13Hz frequency band, are shown in Figure 5-6. Analysis of the individual data indicated that bilateral visual cortices (10 hemispheres in total, see appendix XIV) were stimulated by the attention paradigm although, surprisingly, no consistent activation of primary visual cortex was seen across subjects. This was probably due to the nature of the stimulus which was located centrally within each visual field so stimulating both upper and lower banks of the calcarine sulcus, leading to

cancellation of activation. The yellow colour indicates that voxels at that location are more active in the attend-R compared to the attend-L condition and conversely for the white colour. Thus, alpha power is reduced contralateral to the side of stimulation and attention.

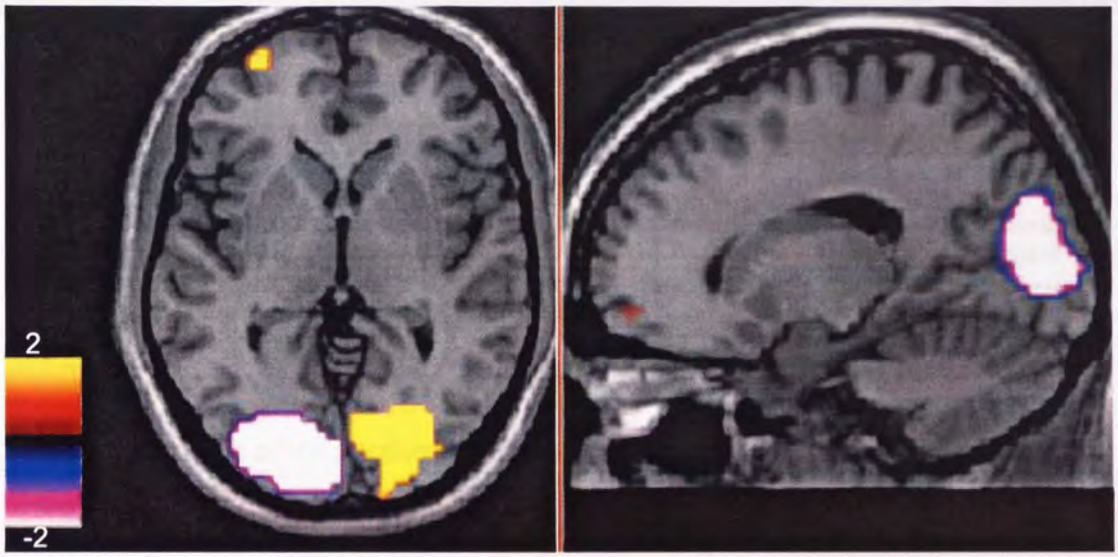

Figure 5-6. Group SAM activation from 6 subjects, superimposed onto a template brain, measured in the 8-13Hz frequency band, 0-2.2sec following stimulus appearance, in the 1-patch block analysis (attend R – attend L) thresholded at NAI = 2. The yellow colour indicates that voxels at that location are more active in the attend R compared to the attend L condition and conversely for the white colour.

The group SAM results from the 2-patch block condition are shown in Figure 5-7. The retinotopic location of the stimulus patches are identical meaning that, if eye movements are controlled, any change in activation is due to attention. Again it can be seen that bilateral visual cortices are activated in the stimulus condition indicating that an attentional effect is occurring in the visual cortex. The visual cortex activation is both more discrete and weaker, as indicated by the lower threshold set to view the activations (NAI = 1.5 as opposed to NAI = 2 in Figure 5-6), than for the one-patch condition.

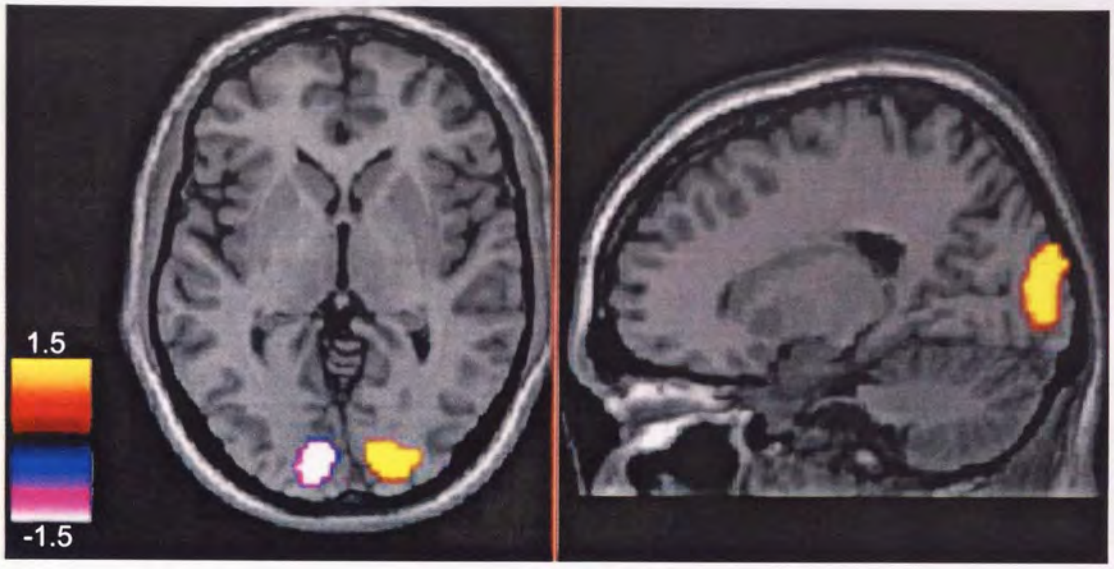

Figure 5-7. Group SAM activation from 6 subjects, superimposed onto a template brain, measured in the 8-13Hz frequency band, 0-2.2sec following stimulus appearance, in the 2 patch block condition (attend R – attend L) thresholded at NAI = 1.5. The yellow colour indicates that voxels at that location are more active in the attend R compared to the attend L condition and conversely for the white colour.

For further analysis of the attentional modulation the peak voxel, from the 1-patch analysis, was used for further time-frequency analysis of the 2-patch data (see section 5.4.3) and the Talairach coordinates of these are shown in Table 5-2. Analysis of the individual trigger data showed that similar activation (10 hemispheres) of visual cortex occurred, although slightly different peak voxels were activated and used in the analysis (Table 5-3). The peak coordinates from both analysis conditions indicated that these were from area V2 (Hasnain *et al.* 1998), although the identification of visual areas on the basis of Talairach coordinates is, at best, approximate.

Subject	Left (mm)	Right (mm)
1	-10 -92 4	9 -89 2
2	-13 -91 -2	10 -92 1
3	NCR	12 -94 3
4	-6 -94 1	NCR
5	-7 -88 -3	8 -86 -1
6	-12 -85 3	6 -88 1
Mean	-9.6 (± 3.1) -90 (± 3.5) 0.6 (±3.1)	9 (± 2.2) -90 (± 3.2) 1.2 (± 1.5)

Table 5-2. Individual Talairach coordinates of voxels used in the time frequency block analysis. Figures in brackets = SD. NCR = no clear response

Subject	Left (mm)	Right (mm)
1	NCR	8 -87 3
2	-11 -91 1	11 -89 4
3	-9 -93 3	11 -92 3
4	-8 -91 1	7 -92 2
5	-10 -89 0	NCR
6	-12 -87 4	7 -87 4
Mean	-10 (± 1.6) -90.2 (± 2.3) 1.8 (±1.6)	8.8 (± 2.0) -89.4 (± 2.5) 3.2 (± 0.8)

Table 5-3. Individual Talairach coordinates of voxels used in the time frequency individual trigger analysis. Figures in brackets = SD. NCR = no clear response

5.4.3 Time frequency analysis

The temporal evolution of the group cortical response in the left and right visual cortex, for the 2-patch condition, is shown for the block (Figure 5-8) and individual trigger analysis (Figure 5-9). It can be observed visually, from both analysis conditions, that

there is a reduction in power, within the alpha band, in the voxel contralateral to the side of attention (e.g. attend L, right voxel when compared to attend L, left voxel).

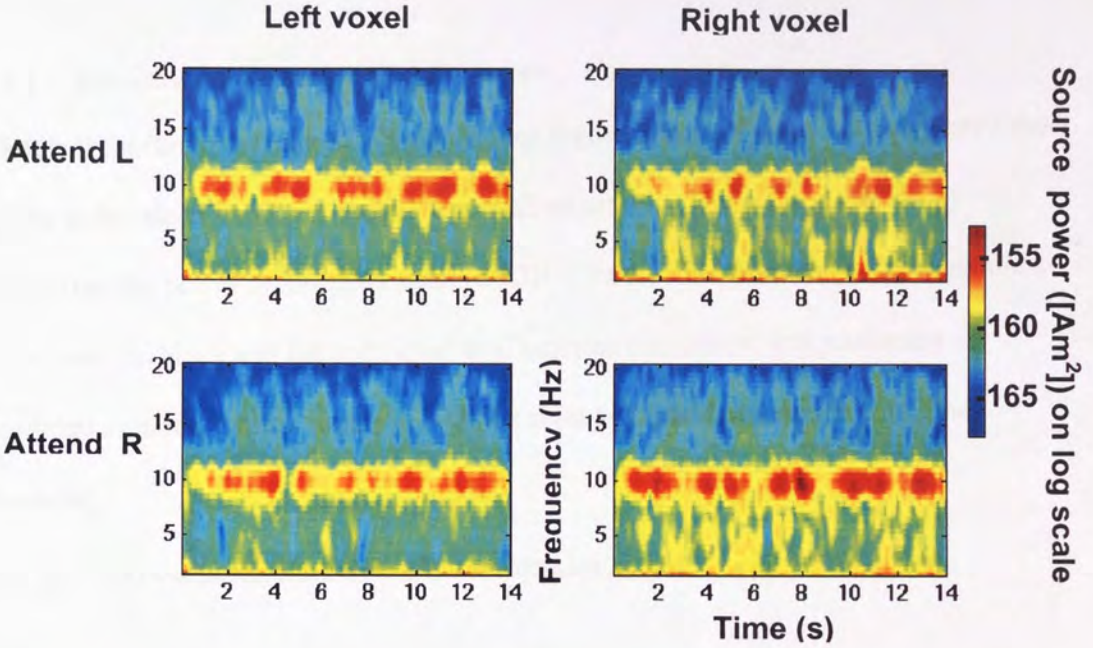

Figure 5-8. Time-frequency plots, from the block analysis, showing the activation power in left and right voxels positioned in visual cortex for the 2-patch condition when the subject attends to the right and to the left patch. Results averaged across subjects and contrast conditions. The results show that alpha power is reduced when attending to stimuli in the contralateral visual field.

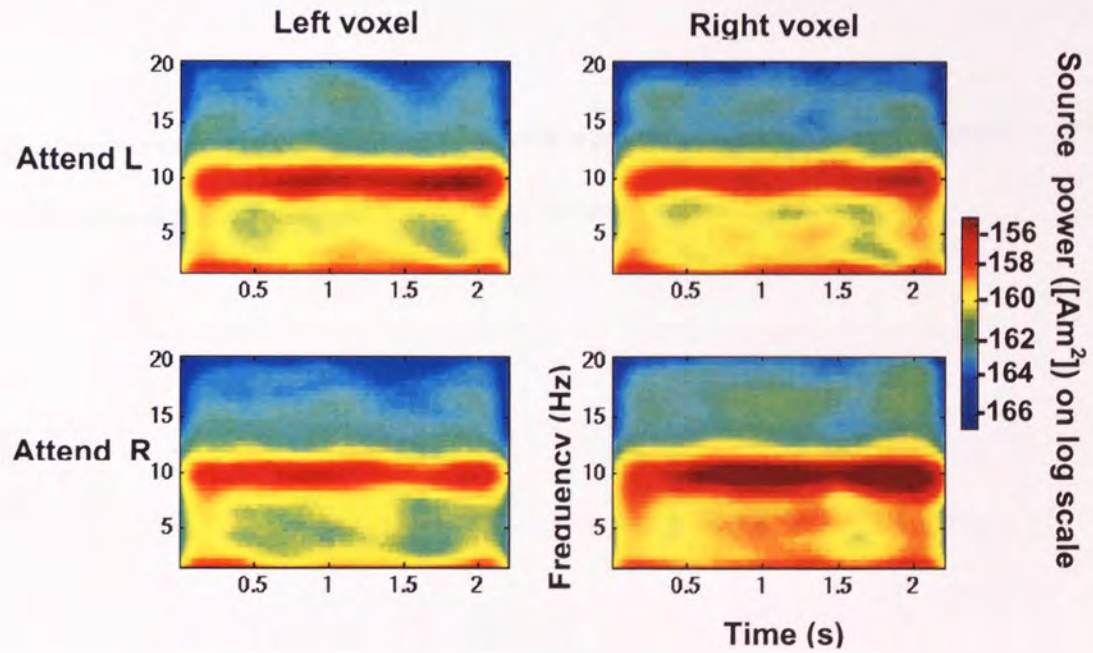

Figure 5-9. Overleaf. Time-frequency plots, in the individual trial analysis, showing the activation power in left and right voxels positioned in visual cortex for the 2-patch condition when the subject attends to the right and to the left patch. Results averaged across subjects and contrast conditions. The results show that alpha power is reduced in the voxels when attending to stimuli in the contralateral visual field.

5.4.4 Attentional modulation of alpha power

Results from the time-frequency analysis (see Figure 5-8 and Figure 5-9) suggested that power in the alpha band was modulating with attention. This was quantified by measuring the power in the alpha band (8-13Hz), in the time frequency representations from both the block and the individual trial analysis conditions, and producing a modulation index, M, for voxels in both the right and left visual cortex using the formula;

If p_c = power in the contralateral attend condition and

p_i = power in the ipsilateral attend condition

$$\mathbf{M} = \left(\frac{p_c - p_i}{p_c + p_i} \right) * \mathbf{100}$$

The results of the analysis from the two-patch stimulus condition are shown for the block (Figure 5-10) and the individual trial analysis (Figure 5-11)

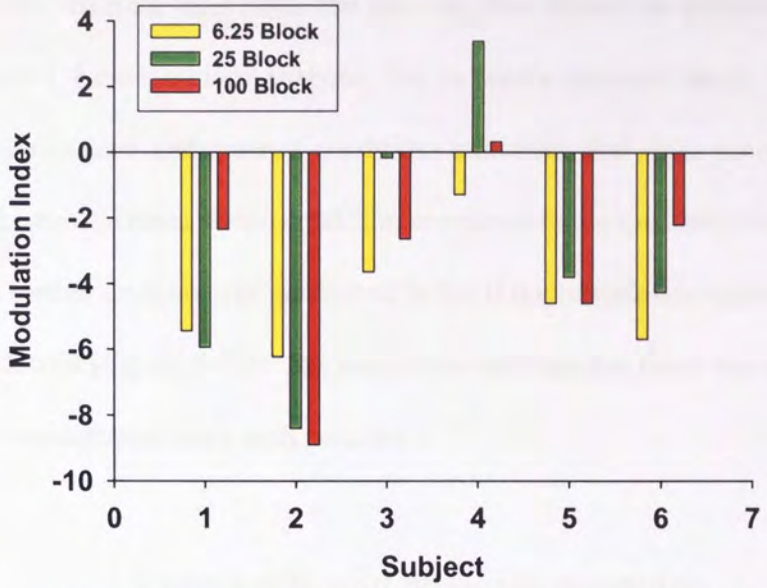

*Figure 5-10. Modulation index ((Contralateral attend – Ipsilateral attend / Contralateral attend + Ipsilateral attend)*100) of alpha power (8-13Hz) for voxels in left and right visual cortex in the 2 patch stimulus condition and shown for the block analysis. A negative number indicates that alpha power is reduced in the voxels when the attended stimulus is in the contralateral visual field (results from the left and right voxels are combined).*

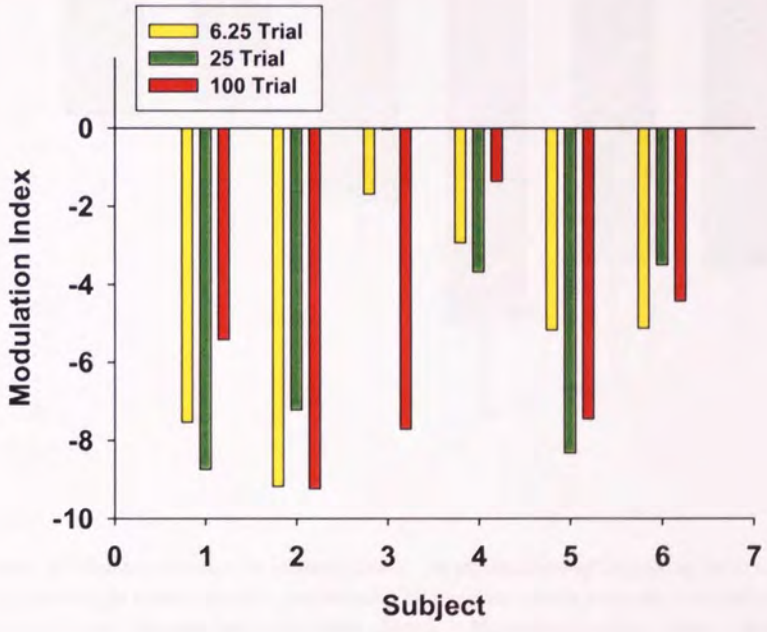

Figure 5-11. Modulation index for the individual trial analysis. Details of graph same as Figure 5-10.

The results showed that the modulation index was consistently negative apart from one run for subject 3, from the individual trial analysis, that showed no difference and two runs for subject 4, from the block analysis, that showed a converse result. This result was seen across subjects and contrast conditions indicating that alpha power was reduced for the contralateral attend condition compared to the ipsilateral attend condition. A further analysis was performed to see if the modulation index altered as a function of contrast (Figure 5-12). The results showed that that there was no consistent change of the modulation index with contrast.

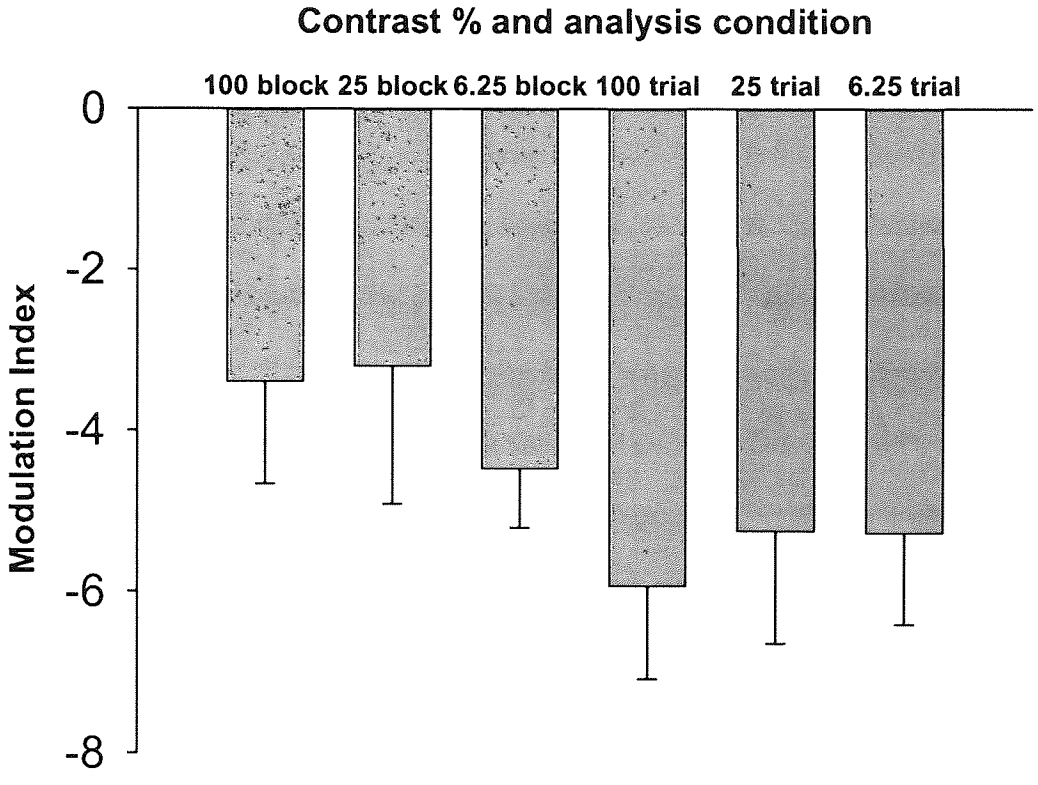

Figure 5-12. Mean modulation index in visual cortex, as a function of contrast, measured across 10 hemispheres (left and right hemispheres combined) for the two-patch stimulus condition. The labels refer to the contrast % and the analysis condition (block = block design data, trial = individual trial data). Error bars show SEM.

5.4.4.1 Alpha power in parietal cortex

Group analysis of the one-patch block data, using non-parametric permutation testing (SnPM), showed statistically significant ($p.<0.05$) activations in the right parietal and bilateral occipital cortices (see appendix XV and appendix XVI for the full SnPM outputs) for attend-right – attend-left and attend-left – attend-right, in the 8-13Hz frequency band (Figure 5-13). Surprisingly, although clusters were present in both left and right extrastriate cortex, no significant activation was present in area V2 where peak SAM voxels were located. This is probably due to the small number of subjects used in the study (6) and that only five subjects showed activations in left or right visual cortex for either the block or individual trigger analysis

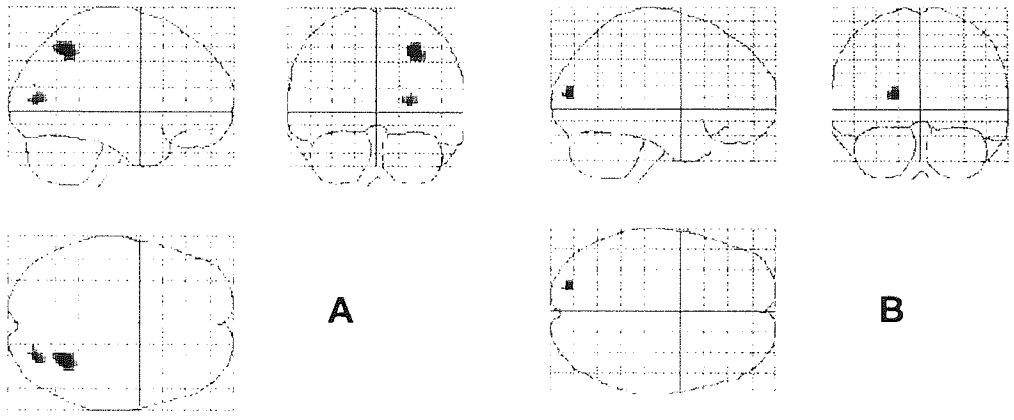

Figure 5-13. Statistically significant voxels (p. <0.05) from non-parametric permutation testing for A. attend-right – attend-left and B. attend-left – attend-right in the 8-13Hz band. This analysis shows areas where alpha power increases in the particular comparison made.

Time-frequency analysis from a voxel in the right parietal cortex is shown in Figure 5-14.

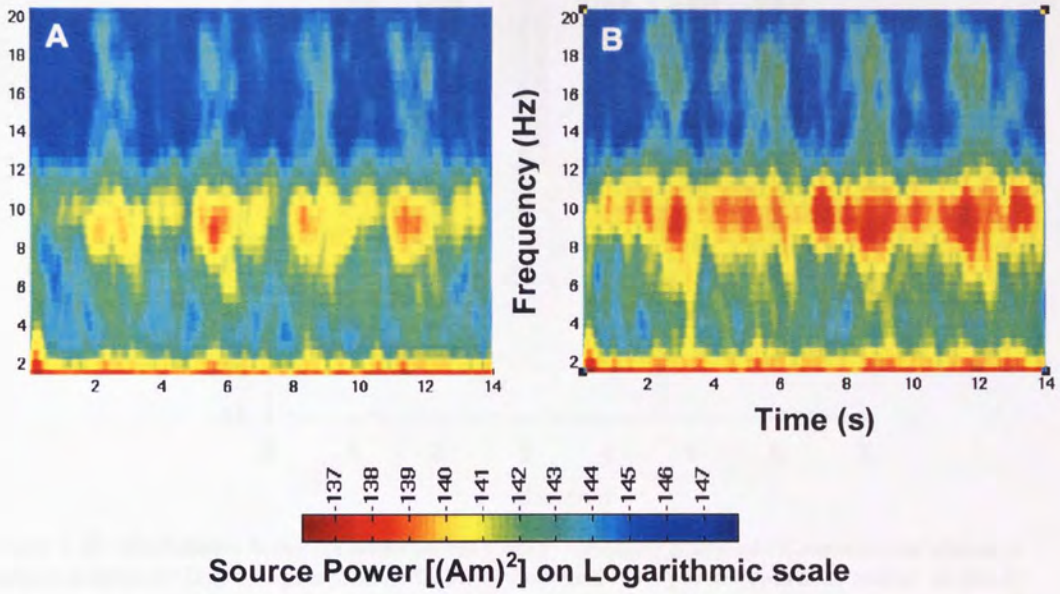

Figure 5-14. Time frequency plots from a voxel in the right intraparietal sulcus in A) contralateral-attend and B) ipsilateral-attend conditions. It can be seen that similar to visual cortex, activation occurs mainly in the alpha band and there is modulation of alpha power between ipsilateral- and contralateral-attend conditions

Similar to visual cortex, the parietal activation showed modulation of alpha power between the contralateral-attend and ipsilateral-attend. A modulation index (Figure 5-15) was calculated (see section 5.4.4 for the formula).

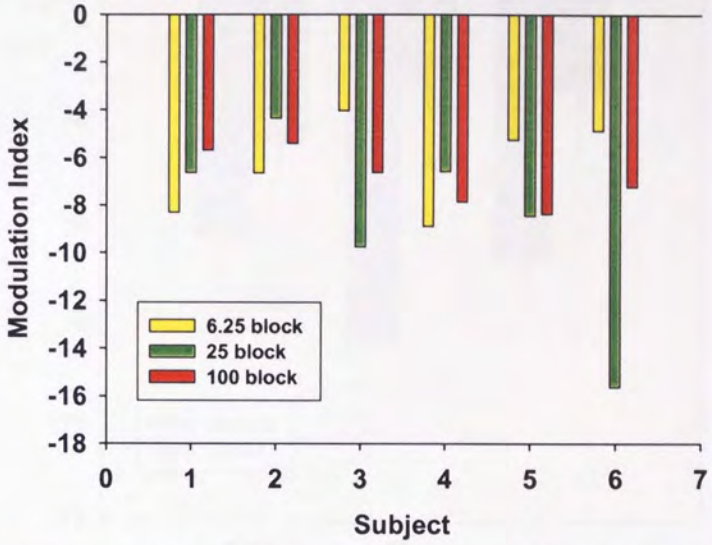

Figure 5-15. Modulation index ((Contralateral attend – Ipsilateral attend / Contralateral attend + Ipsilateral attend)*100) of alpha power (8-13Hz) for voxels in right intraparietal sulcus in the 2-patch stimulus condition and shown for the block analysis. A negative number indicates that alpha power is reduced in the voxels when the attended stimulus is in the contralateral visual field.

Comparing the visual cortex modulation index with that of the intraparietal sulcus it can be seen that modulations within the parietal area are both consistently negative across subjects (compare Figure 5-10 and Figure 5-15) and larger (see Figure 5-16) when compared to visual cortex.

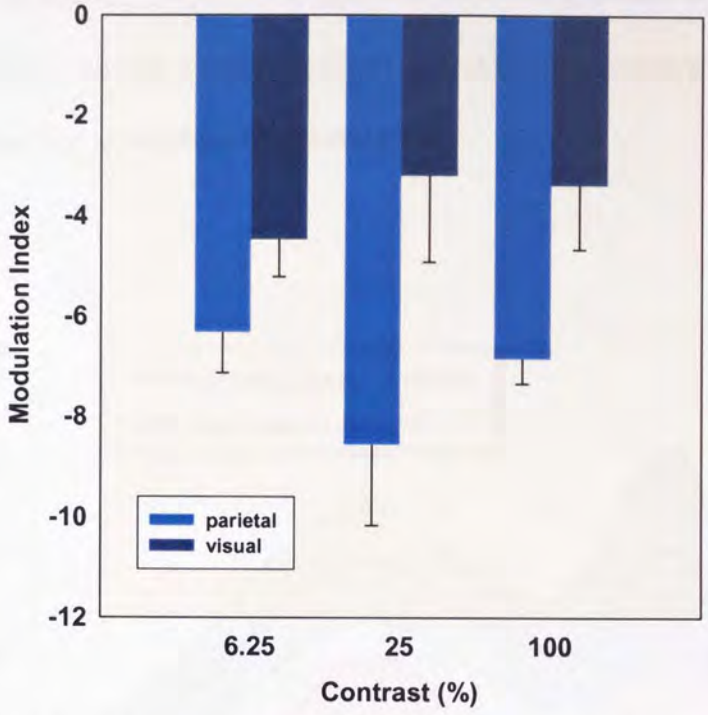

Figure 5-16. Comparison of mean modulation index across subjects for the 2-patch block condition from voxels in the intraparietal sulcus and visual cortex.

5.4.5 Evoked v induced activity

Further analysis was performed to differentiate whether the response being viewed was evoked or induced cortical activity. Induced activity, as before, can be quantified from the average time-frequency representations of the virtual-electrode data, whilst evoked activity is quantified by time-domain averaging to yield an evoked response. The results from the two-patch condition from the individual trigger analysis can be seen in Figure 5-17 and Figure 5-18. The measurement of the induced activity shows a clear difference between the contralateral-attention and ipsilateral-attention conditions. There is a baseline shift of alpha power, with lower alpha power recorded in the contralateral-attend condition. During the presentation of each stimulus patch, in the attention paradigm, there is a rise in alpha power at both contralateral and ipsilateral locations, which is occurring several hundred milliseconds after the patch appears. The rapid fall off of the response at the end of the analysis window is due to the Hanning filter used in

the analysis of the results. Inspection of the block data (see appendix XVII) showed that this modulating rise and fall of induced alpha power was occurring throughout the block trial in response to the stimulus presentation.

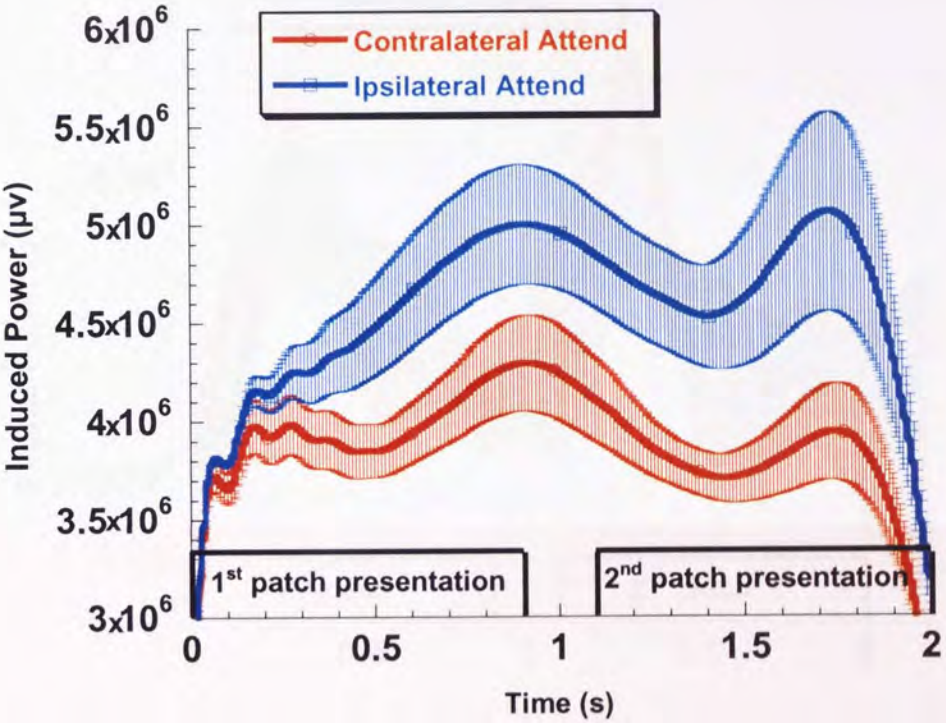

Figure 5-17. Measurement of mean induced cortical activity in the 8-13Hz frequency band, for the two-patch condition individual trigger analysis, averaged across contrast conditions, hemispheres and subjects. The rapid fall off at the end of the timing window is due to the Hanning filter used in the analysis. The timing of the attention stimulus presentation is shown by the black lines at the bottom of the graph. Error bars show the SEM.

The evoked response results (Figure 5-18), from the two-patch condition, show that there is clear activation occurring approximately 200-300ms after the presentation of both the first and second stimulus patches. Interestingly there is no evidence of an induced response occurring at the same time (Figure 5-17). However, the induced cortical response is several times larger than the evoked cortical response and may well be swamping any induced effect caused by the evoked activity in Figure 5-17.

Furthermore, there is a significant facilitation of contralateral evoked activity after the presentation of the second stimulus patch, when the attention task actually has to be performed.

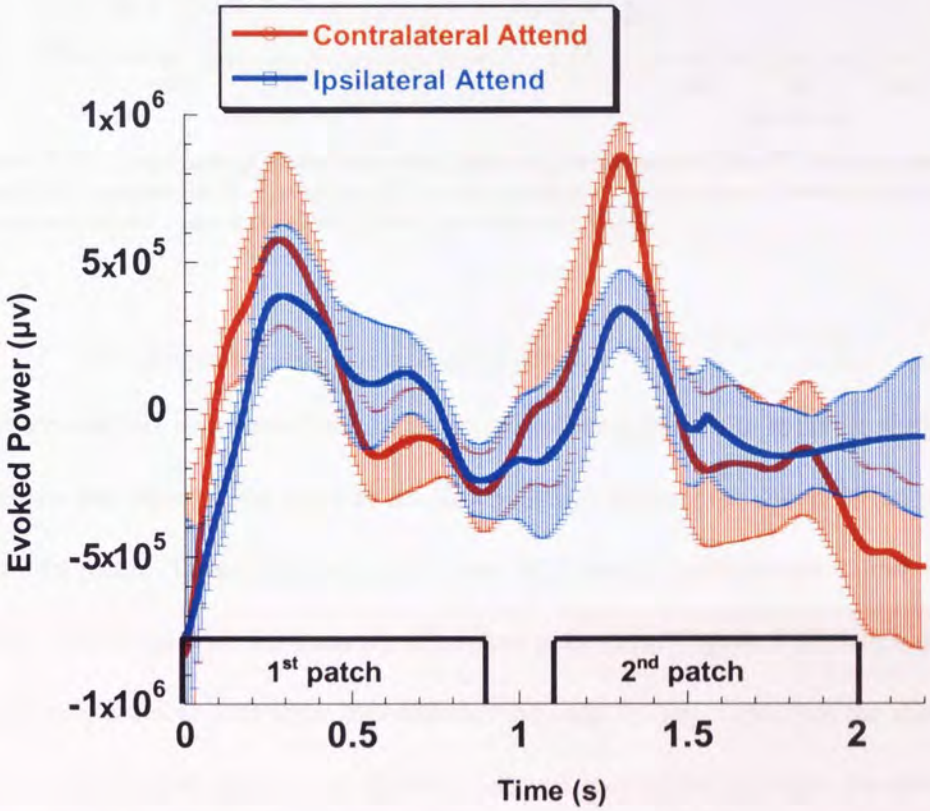

Figure 5-18. Measurement of mean evoked cortical activity averaged across contrast conditions, hemispheres and subjects for the two-patch condition. The presentation of the attend stimulus is indicated by the lines at the bottom of the graph. There is facilitation of the evoked response, contralateral to the attended location, after the presentation of the 2nd stimulus patch. Error bars show the SEM.

Further analysis showed that the amplitude of the evoked activity reduced with decreasing contrast (Figure 5-19). See appendix XVIII for how the amplitude was calculated.

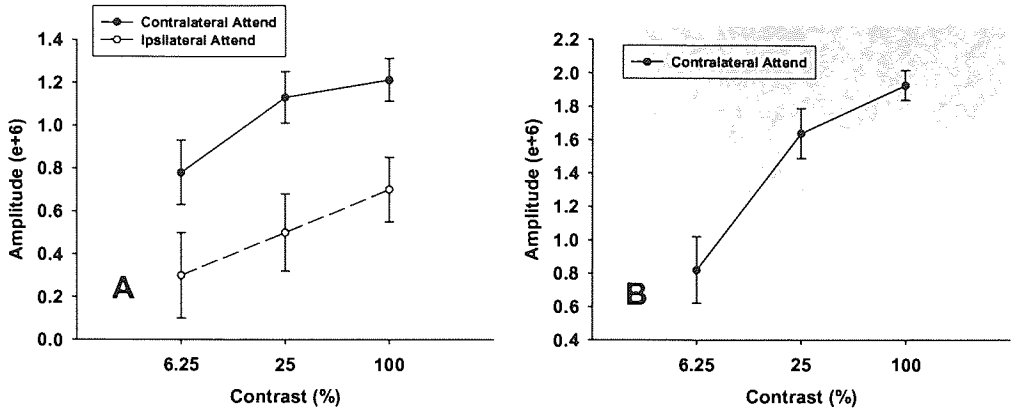

Figure 5-19. Amplitude of evoked response, following presentation of the 2nd stimulus patch, as a function of contrast for A. 2-patch and B. 1-patch conditions. No ipsilateral evoked response was measurable in the 1-patch condition. Error bars show the SEM.

5.4.5.1 Time frequency analysis of evoked activity

Further analysis was performed on the individual trigger data to measure the oscillatory changes that were taking place in the first 500ms following the presentation of the first stimulus patch. Time-frequency plots from the 2-patch condition are shown in Figure 5-20. Consistent with the measure of evoked activation (Figure 5-18) there is an increase in cortical activation 200-400ms following the appearance of the stimulus patch in both contralateral- and ipsilateral-attend conditions although the nature of this activation differs between the two conditions. In the contralateral-attend condition there is an increase in alpha power which is not evident in the ipsilateral-attend condition, whilst there is a bilateral increase in beta activations although this is greatest for the contralateral-attend condition. Finally, there is a hint of weak gamma activations for both conditions.

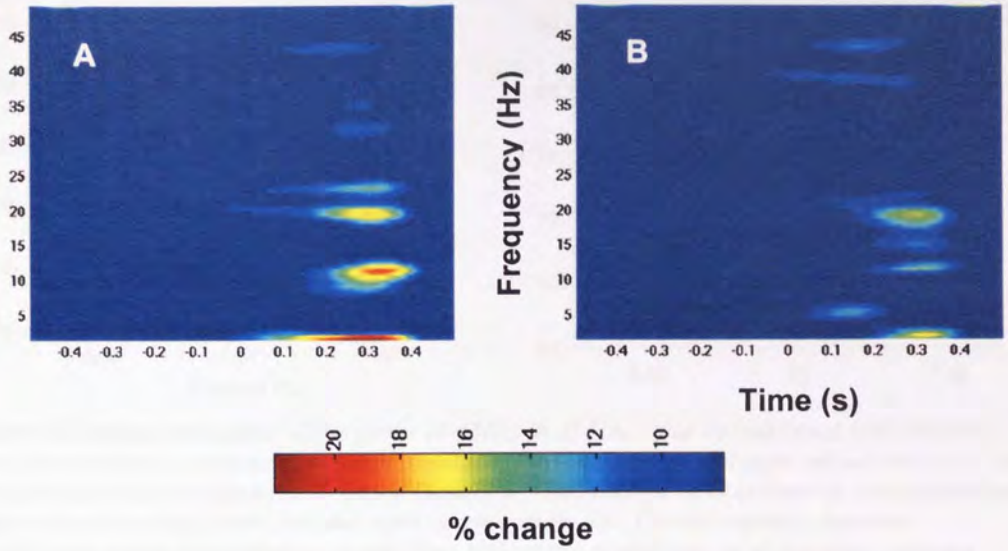

Figure 5-20. Time-frequency analysis of 2-patch individual trigger data for A) contralateral-attend and B) ipsilateral-attend conditions, showing the percentage change between an active condition (0 to 0.5s) and a passive condition (-0.5 to 0s). The stimulus appeared at 0s.

5.4.6 Contrast response of alpha activity

It was of interest to see whether the alpha power from the visual cortex changed as a function of contrast. The contrast response graphs from the 1-patch (Figure 5-21) and 2-patch (Figure 5-22) analysis are shown (see section 3.3 for an explanation of how the normalised amplitudes were created). The discrepancy between the contralateral and ipsilateral attend responses reflects the modulation of the alpha power between conditions. It can be seen that, from both analysis conditions, there is evidence of slight contrast tuning, within the alpha band, from both the one and two patch attention conditions.

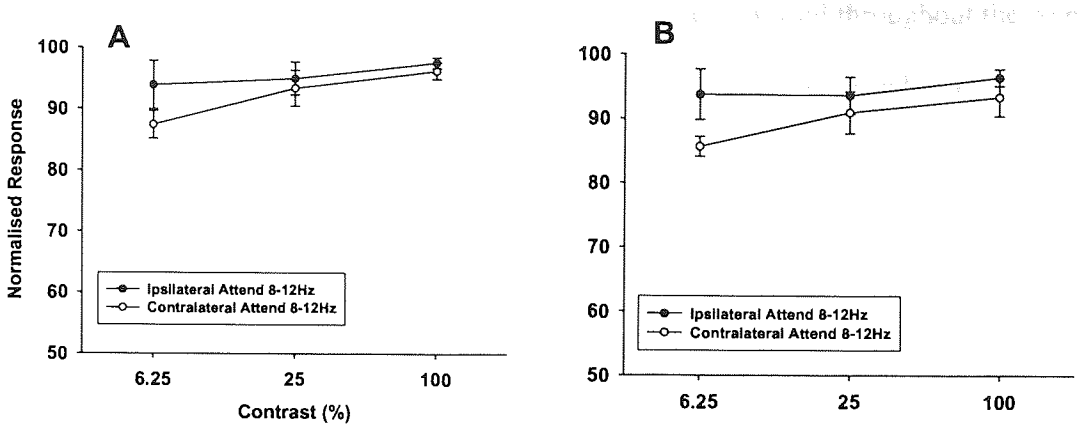

Figure 5-21. Mean normalised alpha power (8-13Hz) in A) block and B) individual trial analysis, measured at various contrasts in 1- patch condition, for voxels in left and right visual cortex for both contralateral-attend and ipsilateral- attend locations. Contralateral and ipsilateral data normalised using the same scaling factor (left and right voxels combined). The discrepancy between contralateral-attend and ipsilateral- attend data reflects the modulation of alpha power between conditions

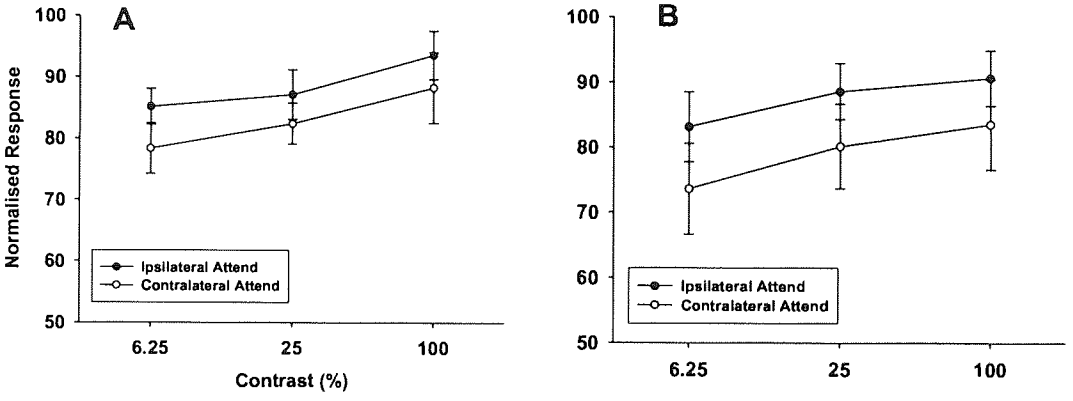

Figure 5-22. Mean normalised alpha power (8-13Hz) for A) block and B) individual trial analysis, measured at various contrasts in 2-patch condition, for voxels in left and right visual cortex at both contralateral attend and ipsilateral attend locations. Contralateral and ipsilateral data normalised using the same scaling factor (left and right voxels combined). The discrepancy between contralateral attend and ipsilateral attend data reflects the modulation of alpha power between conditions

5.4.7 Eye movements

It has been shown that eye movements can activate a network of cortical areas (Corbetta et al 1998). Similarly the control of eye movements is vital in an attention paradigm, for if the stimulus is viewed foveally then this will affect attentional responses as well as the cortical areas activated. The EOG recording from a single subject is shown in

Figure 5-23. It shows that the subject was able to fixate very well throughout the whole of the recording session. The points indicated with an * are the times when eye movements were greater than the calibration threshold and these epochs were not used in the analysis. The eye movements for all individuals can be seen in appendix IX to XIII. The data shows that the majority of subjects showed very few eye movements and fixated well throughout. The exception to this was subject 2 who demonstrated an exceptional amount of vertical eye movements in the form of blinks. However, in this paradigm it is not the vertical eye movements that are important but the horizontal ones. Subject 2 showed more horizontal eye movements above threshold than other subjects but was still included in the final analysis with these epochs removed.

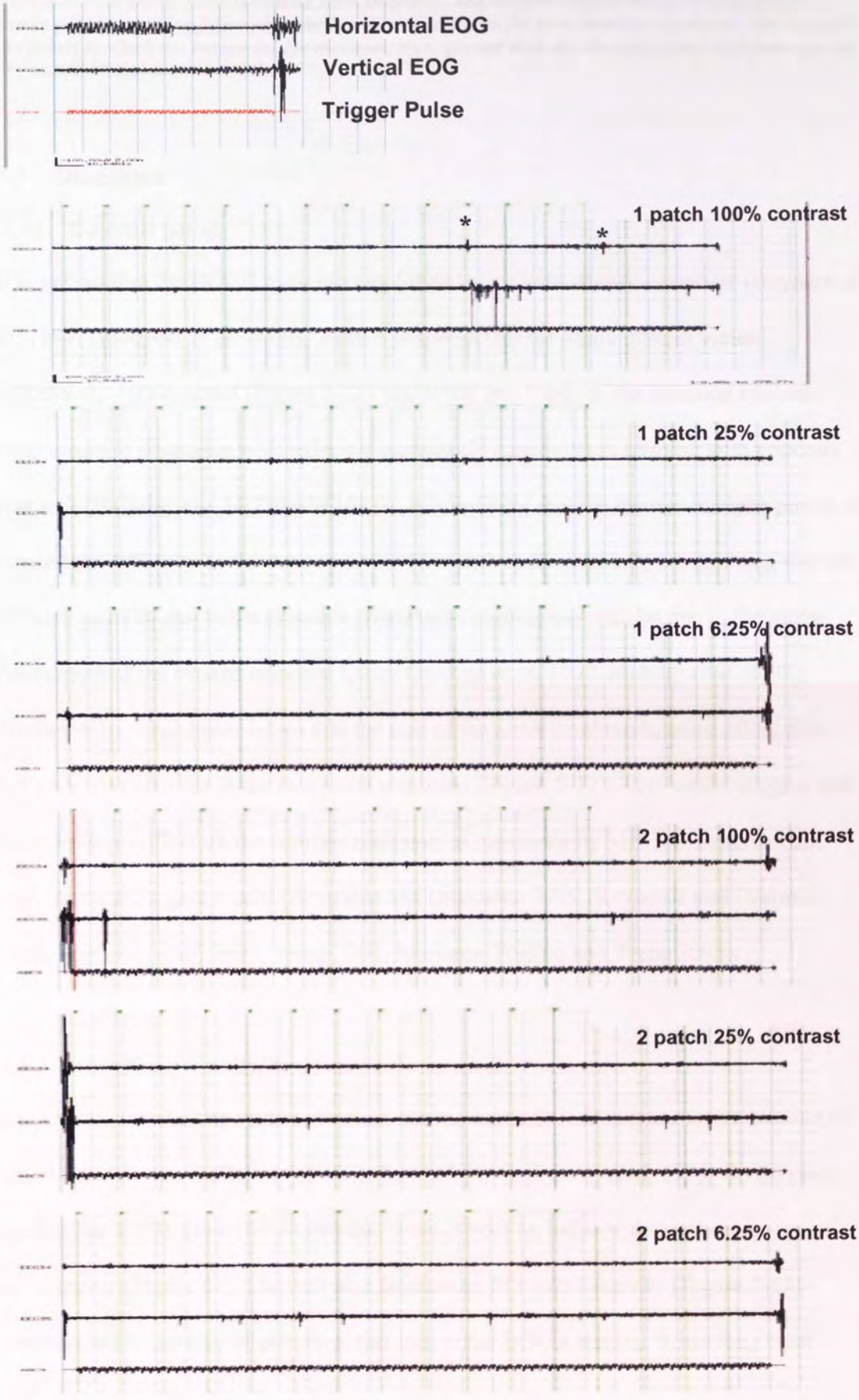
Horizontal EOG
Vertical EOG
Trigger Pulse
1 patch 100% contrast
1 patch 25% contrast
1 patch 6.25% contrast
2 patch 100% contrast
2 patch 25% contrast
2 patch 6.25% contrast

Figure 5-23. overleaf. EOG recording from subject 1. The baseline calibration for this subject is shown at the beginning followed by the eye movement traces for each stimulus condition. The * shows the points at which the horizontal eye movements are greater than the threshold level and these epochs were not included in the analysis.

5.5 Discussion

5.5.1 Contrast tuning

It is known that the BOLD response amplitude varies with stimulus contrast (Boynton *et al.* 1999, Goodyear *et al.* 2000). Here it is shown that the alpha rhythm varies moderately with contrast (Figure 5-22) whilst the amplitude of the attention evoked field response decreases with reducing contrast (Figure 5-19) in keeping with previous research (Halliday and McDonald 1981). It is unlikely that the change in alpha power is due to task difficulty as this was controlled for each individual subject, meaning that the changes must be due to the stimulus characteristics and may well be due to the alpha component of the evoked response Quian Quiroga *et al.* 2000, Makeig *et al.* 2002). Furthermore, it has been shown that the size of the attentional modulation effect does not vary with contrast in the two patch condition (Figure 5-12). This would suggest that the attentional effect on the contrast response, as measured by MEG, is in agreement with the contrast gain model (Reynolds and Desimone 1999, Reynolds and Desimone 2003, Reynolds *et al.* 2000, Treue 2000, Martinez-Trujillo and Treue 2002).

5.5.2 Attentional modulation of cortical responses

It is known that shifting spatial attention can modulate BOLD responses in a number of visual cortex areas, including V1 (Gandhi *et al.* 1999, Somers *et al.* 1999, Brefczynski and DeYoe 1999). Here it is shown that there is both an induced desynchronisation of alpha power (Figure 5-17) as well as a facilitation of evoked activity (Figure 5-18), contralateral to the side of attention, that mirror the BOLD results. It has long been

known that the posterior alpha rhythm is desynchronised by a visual stimulus (Adrian and Matthews 1934). In this study this desynchronisation is shown to modulate with changes in visual spatial attention and the use of the SAM technique allows the precise localisation of such changes.

It has previously been shown that induced alpha power decreases over a large portion of the scalp in response to an attended visual stimulus (Marrufo *et al.* 2001). The results shown here suggest that alpha changes are confined to the visual cortex. However, the images have been thresholded at such a level as to remove the weaker responses, in the alpha band, occurring in other cortical areas.

Unlike the two-patch condition, which has stimuli in both the attend and non-attend fields of view, the one-patch condition has a stimulus in only one visual field. Given this, a surprising finding from this study is how similar the alpha power is, from the one-patch condition, between the ipsilateral and contralateral attend conditions (Figure 5-21). However, there is increasing evidence that, rather than being simply an 'idling' rhythm of the cortex, increases in alpha power occur where cortical activity is being suppressed in relation to possible distractors, as part of the process of focusing attention on important targets (Jensen *et al.* 2002, Cooper *et al.* 2003). Consistent with this idea it has been shown that increases in alpha activity occur in areas ipsilateral to the side of cued attention where distractors in the visual field are likely to occur (Worden *et al.* 2000). In the present study, as part of the block design, the subjects are cued to attend to the same side for five epochs at a time. It is therefore possible that ipsilateral changes in alpha power are occurring as part of this cueing process. In the two-patch condition although the block design is the same it is likely that this cueing effect on the alpha rhythm is offset by the presence of an actual stimulus patch.

A recent MEG study (Yamagishi *et al.* 2003) has shown that alpha power modulates with attention in primary visual cortex. The group showed that, in contralateral visual cortex, alpha power increases, when attention is directed towards a visual stimulus compared to when it is directed away. These results are very different to those shown in this study, recorded from an area approximating to extrastriate visual area V2, where there is a sustained decrease in alpha power when attention is directed toward the stimulus compared to when attention is directed away. However, there are significant differences, other than location, between the studies. The attentional task in the present study involved shifting attention between gratings in the left and right visual field which were always present during a trial whilst the stimulus in the Yamagishi *et al.* 2003 study was always presented in the lower right visual field and was presented for only 300ms during each trial sequence. Secondly, the present study used a black / white drifting grating as the stimulus whilst the Yamagishi *et al.* 2003 study used red / green modulated gratings, known to evoke large responses from the visual cortex (Fylan *et al.* 1997)

It is known that there is a differentiation between evoked and induced alpha in relation to attentional tasks (Klimesch *et al.* 2000, Brandt 1997, Klimesch *et al.* 1998, Klimesch 1999) with tasks showing an increase in evoked alpha power and a decrease in induced alpha power. Furthermore, it has been shown that the alpha rhythm has a strong influence on the early evoked components of event related potentials (Basar 1999, Basar and Schurmann 1994) and it has also been proposed that some aspects of evoked potentials may be the result of phase resetting of cortical oscillations in the alpha band (Makeig *et al.* 2002, Quian Quiroga *et al.* 2000). Results from the present study (Figure

5-20) are in agreement with this, showing increased alpha power 200ms after the appearance of the stimulus patch, contralateral to the side of attention. This would suggest that it is evoked alpha power that is being seen in the Yamagishi *et al.* 2003 study in relation to primary visual cortex activation.

5.6 Conclusion

There are both induced and evoked modulation changes with visuo-spatial attention in cortical activations, consistent with previous changes observed in the BOLD response. There are small induced changes in alpha activation with contrast, but larger changes in evoked potential amplitudes. This suggests that the increases in BOLD amplitude with contrast, seen in previous studies, are most likely related to this evoked activity. However, the precise relationship between BOLD increases, evoked-response increases and induced desynchronisation is still debatable. The stability of the modulation effects with changing contrast supports contrast gain models of neuronal response.

6. CORTICAL OSCILLATORY CHANGES TO MOTION COHERENCE: COMPARISON WITH THE FMRI BOLD RESPONSE.

6.1 Overview

The work in this chapter involves a direct comparison of cortical oscillatory changes with those of the BOLD response in relation to the parametric variation of a motion coherence stimulus. The chapter begins with an introduction reviewing the literature. Following this the methodology and results of the two experimental threads are outlined. The chapter ends with a discussion about the link between the BOLD response and cortical oscillatory changes.

6.2 Introduction

The characteristics of the motion system have been covered across several sections in this thesis (see sections 1.9 and 4.3) and will not be revisited here.

It has been shown that there are two anatomically segregated populations of neurons in V5/MT, one with antagonistic receptive field surrounds and another with receptive field surrounds that augment the response from the centre and it has been proposed that these process local and global aspects of a visual scene (Born and Tootell 1992). Random dot kinetograms (RDKs) (see Figure 6-1) have proved to be a suitable stimulus pattern for studying the integration of this ambiguous local motion information into a global coherent perception that is thought to take place in V5/MT (Movshon *et al.* 1985, Newsome *et al.* 1990). These patterns have no net global direction when the dots move in random directions (Williams and Sekular 1984) and a global signal can be introduced, in a graded fashion, by increasing the percentage of coherently moving dots. Consequently, it has been shown that neuronal responses increase their firing rates with

increasing coherence (Britten *et al.* 1993) and that these neural responses correlate with the perceived motion direction (Newsome *et al.* 1989)

Neurophysiological studies have shown that V5/MT neurons are driven best by a stimulus that moves coherently in a single direction (Allman *et al.* 1990, Snowden *et al.* 1991), whilst neurons in V1 are poorly driven by such a stimulus (Allman *et al.* 1990). Conversely V5/MT neurons respond poorly to incoherent motion whilst V1 respond well (Snowden *et al.* 1991).

Several functional imaging studies using PET (Cheng *et al.* 1995, McKeefry *et al.* 1997) and MEG (Lam *et al.* 2000, Maruyama *et al.* 2002) have investigated the cortical response to coherent and incoherent random dot patterns by comparing 100% coherent with incoherent (0%) motion at varying speeds of dot motion but without measuring the response to varying coherence levels. Contrary to the single cell results, these have shown that the cortical responses to the two types of motion are similar (Cheng *et al.* 1995, Lam *et al.* 2000, Maruyama *et al.* 2002) or that area V5/MT responds better to incoherent than to coherent motion (McKeefry *et al.* 1997). A single MEG study has been reported which measured dipole responses to varying motion coherence levels (Nakamura *et al.* 2003). The study proposed that as coherence increased, latency of the response remained constant whilst the amplitude increased in an area that the authors reported to be V5/MT. However a close inspection of the data shows that the reported response was above and anterior to the recognised location of V5/MT as reported in many previous studies of motion stimuli (Watson *et al.* 1993, Tootell *et al.* 1995, Dumoulin *et al.* 2000). The responses were consistant between hemispheres in contrast

to results from electrophysiology which appear to show a right hemisphere emphasis to the results (Niedeggen and Wist 1999).

There is a complicated relationship between population neuronal responses and single neuron responses to a stimulus (Scannel and Young 1999). However a recent fMRI study has shown a strong linear relationship between the BOLD response and motion coherence with the results suggesting a close relationship between the bulk neuronal response as measured by the BOLD response and single cell responses (Rees *et al.* 2000).

It is common for functional imaging studies to compare a pair of experimental conditions (e.g. motion present, motion not present) which, although useful in differentiating visual areas responsible for motion processing, gives no information about the mechanisms underlying this activation (Wandell 1999). No previous studies have been reported on the oscillatory changes that underlie the cortical response to coherent motion. Therefore in this experiment we have attempted to characterise the oscillatory changes that take place in the human motion system to a parametric variation in the strength of a motion signal.

6.3 Methods

6.3.1 Stimuli

The stimulus was programmed on a Mac Powerbook. Each trial consisted of stochastic motion stimuli, presented to one of two square apertures (12°x 12°) located 2° below and 2° eccentric to the left and right of a central fixation point (see Figure 6-1). Each aperture contained 1000 evenly distributed dots, with each dot subtending ~4 arc min

and moving at a velocity of ~10 degrees per s. Dots were white, of 100% contrast on a black background, each having an infinite lifetime. The coherence of the stimulus was defined by the proportion of total dots moving horizontally (0, 12.5, 25, 50 100%) either to the left or right within an aperture, with the remaining dots moving randomly. The coherence level, direction of motion and side of presentation were randomised, with the dots in the other aperture remaining static. Stimuli were presented for 1000ms followed by a 1625ms period during which subjects indicated whether motion was to the left or right by pressing one of two buttons using the index finger of their right hand. During this response period both apertures remained present but with static dots. Subjects were required to maintain fixation on the central point of the screen at all times. In both the fMRI and MEG paradigms a proportion of the stimulus conditions consisted of null trials during which static dots were presented and the subjects were not required to respond.

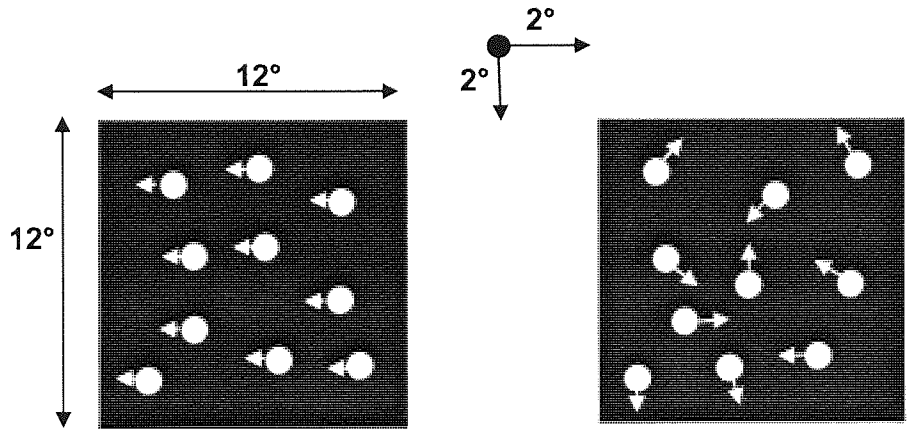

Figure 6-1. Schematic representation of the stimulus used in this experiment. The left aperture shows the 100% coherence condition and the right aperture shows the 0% coherence condition. Further stimulus conditions of 50%, 25% and 12.5% are not shown but consisted of varying percentages of coherently moving dots intermixed with random dots. The two stimulus conditions are shown together for explanation purposes although during the experiment only one stimulus condition was shown during any one trial with the other aperture showing static dots. A further static trial was also included as a baseline measure.

6.3.2 fMRI

6.3.2.1 Subjects

Eight right handed volunteers (6M, 2F, 33.9 ± 10.3yrs) with no neurological disorders gave their consent to take part in the study.

6.3.2.2 fMRI data acquisition

The functional fMRI data were acquired using a rapid-presentation event-related design (Burock *et al.* 1998). The recording session was separated into three runs, each 420 seconds long, with each run containing 20 trials (10 moving left, 10 moving right) at each of the 5 coherence levels and 60 null trials containing static dots. In each run there were therefore 160 trials, each randomly assigned from one of the 21 trial types, with a fixed inter-trial interval of 2.625 seconds. Images were acquired on a 3T Siemens Trio system using a receive-transmit head coil. Contiguous gradient echoplanar images (EPI) were acquired as 25 approximately axial slices with a TR/TE of 1500ms/30ms, flip angle 90°, matrix 64 x 64 voxels with a 3x3x3 mm isotropic resolution. This acquisition volume covered the whole of the occipital lobes, the temporal lobes and the inferior portion of the parietal and frontal lobes. To remove initial saturation effects, the first 20 seconds of each run were discarded, leaving 280 volumes for the analysis. Between runs a separate high-resolution anatomical scan (MP-RAGE, 1mm isotropic voxels) was obtained.

6.3.3 MEG

6.3.3.1 Subjects

Eight right handed volunteers (4M, 4F, 29.8 ± 5.1yrs) gave their consent to take part in the study.

6.3.3.2 MEG data acquisition

MEG data was collected using a 151 channel CTF Omega system (CTF Systems Inc., Port Coquitlam, Canada) at a sampling rate of 625Hz. Each subject took part in two runs, each containing 30 trials at each coherence condition (15 moving left and 15 moving right) and 15 null trials containing static dots, 165 trials in total. The number of trials for each coherence level was the same between experiments (60 fMRI and 60 MEG) although the MEG data was collected over 2 separate runs and the fMRI data collected over 3. In all other respects, the experiment was identical to the fMRI protocol. The stimuli were back projected onto a screen in the shielded room via a Hitachi CP-S830E lcd projector.

6.3.4 Data Analysis

6.3.4.1 fMRI

Images were prepared for analysis using SPM99 (http://www.fil.ion.ucl.ac.uk) by first correcting for head movement and the acquisition delay between slices. The EPI images were then normalised to the standard SPM99 EPI template and smoothed with a Gaussian kernel of 6 x 6 x 6 mm^3 FWHM. Within the GLM framework, a model was fitted which had a separate factor for each subject, coherence and side of presentation. The result of this analysis was a separate functional activation image for each trial type and for each subject. These activation images were then carried forward to the linear coherence analysis stage (see section 6.3.5).

6.3.4.2 MEG

After the data was collected, a 3-D digitiser (Polhemus Isotrack) was used to digitise the shape of the subject's head in the MEG laboratory. Using Align (www.ece.edu/ICVC/Align/align11.html) this surface was matched to a head surface

extracted from the subjects's own, previously acquired, anatomical MRI in order to coregister the MEG data with the subject's anatomy. The MEG data was analysed using Synthetic Aperture Magnetometry (SAM) (see section 2.6.1 for further details). A separate SAM image was generated for each frequency band trial type, for each subject. As with the fMRI data, these images were then carried forward to the second-level analysis stage (section 6.3.5).

6.3.5 Linear activation analysis

Analysis was performed on both the fMRI and MEG activation images to assess if any cortical voxels were varying linearly with motion coherence. Using in-house analysis software, voxels showing a linear response (increasing or decreasing) with increasing motion coherence were found. The linear response was calculated as follows. Each voxel has five numbers associated with it, reflecting the magnitude of activation for each coherence level. A linear fit was performed to this data and a correlation coefficient image produced, reflecting how well each voxel fits the linear model. This correlation coefficient image was then smoothed with a 6mm Gaussian kernel to maximise signal to noise and corrected significance levels ($p.<0.05$) were then assigned using permutation testing. ROIs were then extracted from the thresholded results and the individual data was quantified within these ROIs to produce response curves with error bars.

6.4 Results

6.4.1 Subject response data

The subject responses obtained from the scanning sessions for both the fMRI (Figure 6-2) and MEG (Figure 6-3) experiments were fit with Weibull functions. The mean

coherence threshold (75% correct two-alternative forced choice) was 38.9% (s.e.m., 5.1%) for the fMRI experiment and 20% (s.e.m., 2.2%) for the MEG experiment. The coherence threshold from the fMRI study is greater than that found in previous studies (Rees *et al.* 2000). There is a surprising difference between the coherence thresholds recorded between the MEG and fMRI studies. Eight subjects were used in each experiment and four of the subjects were common between both experiments. Although the tasks were the same the environments were different, one taking place in a noisy fMRI environment and the other in a quiet MEG environment. It may be that there was a learning effect with the task, as the MEG experiment followed the fMRI. However, training was given to each subject prior to each experiment It is also a possibility that the differing coherence thresholds may be the result of changes in concentration between the two experiments, with concentration in the fMRI experiment being affected by the noisier environment.

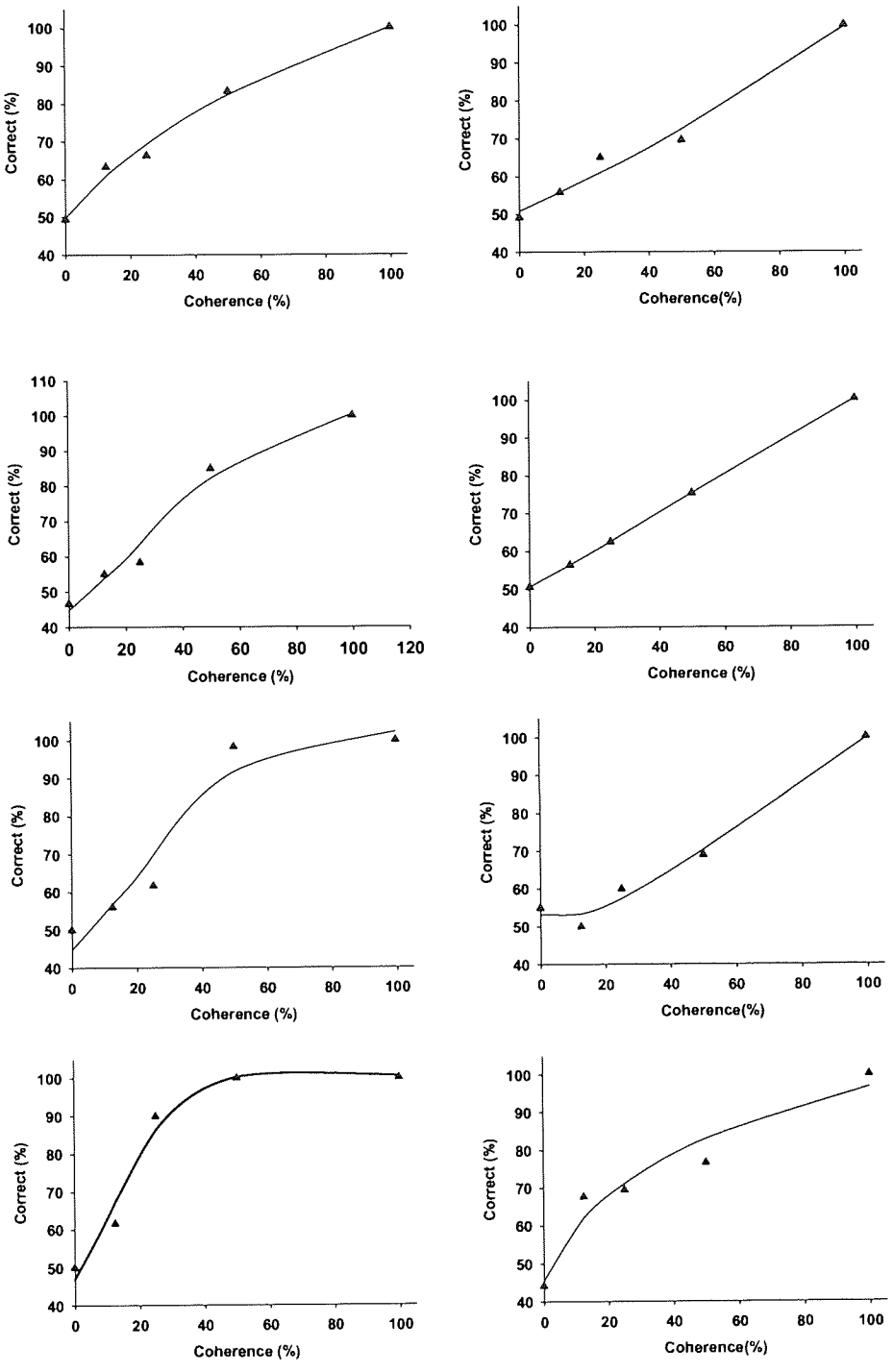

Figure 6-2. Psychopysical results for subjects in the fMRI experiment. Lines show the best-fitting Weibull function

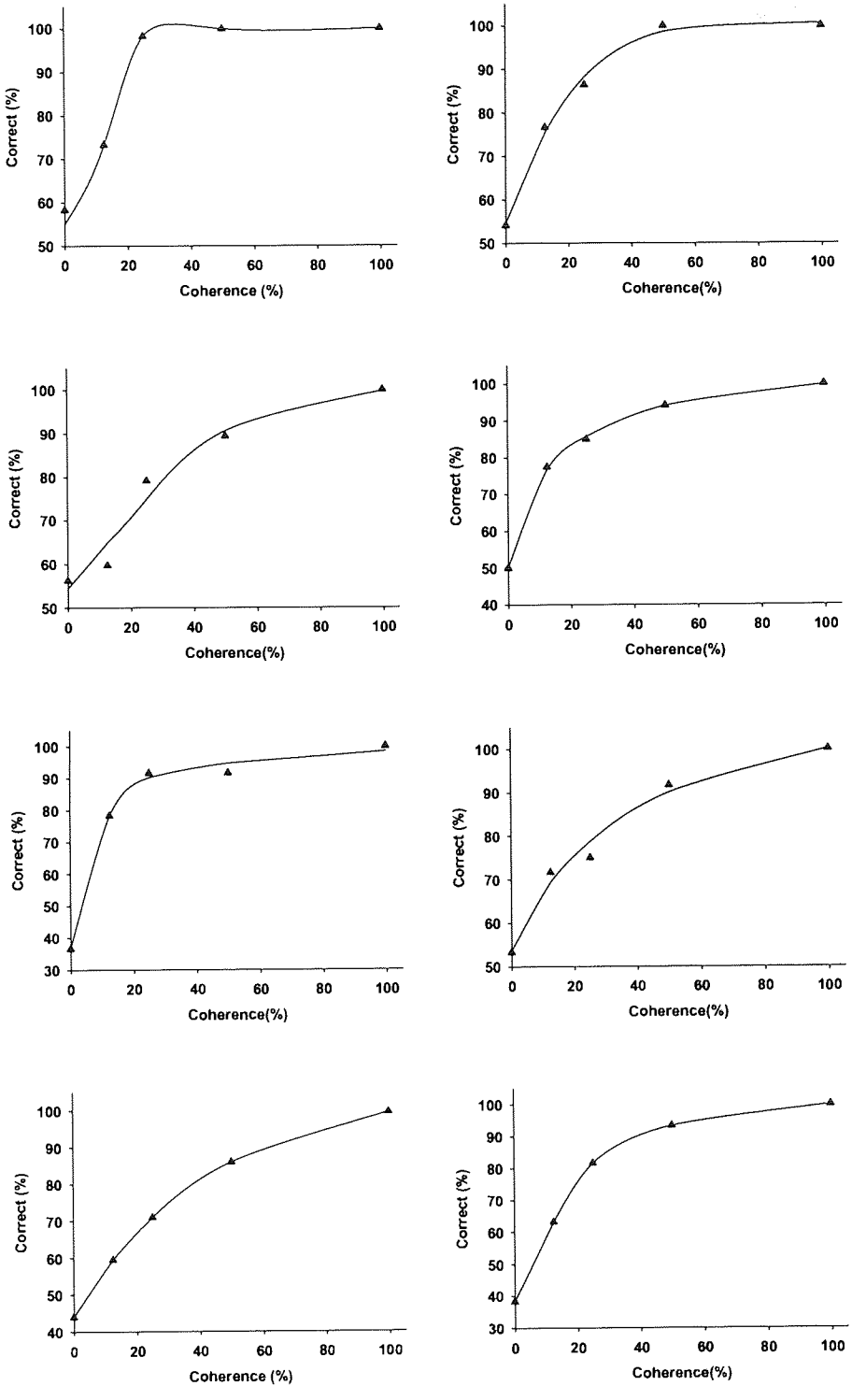

Figure 6-3. Psychopysical results for subjects in the MEG experiment. Lines show the best-fitting Weibull function

6.4.2 *Comparison of fMRI and MEG response*

The location of peak activation, across all coherence levels, was plotted on a template brain for both the fMRI (Figure 6-4 top) and MEG (Figure 6-4 bottom) experiments.

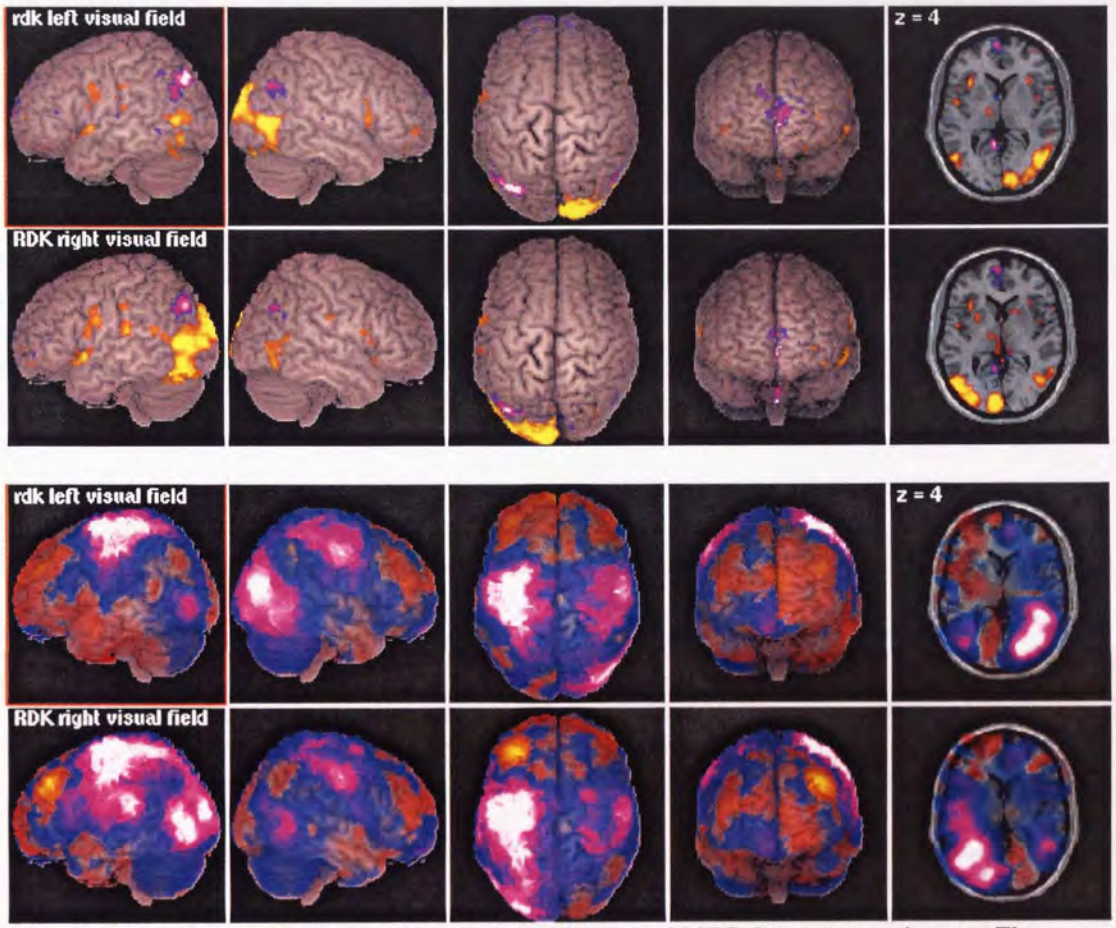

Figure 6-4. Peak activation images from both fMRI (top) and MEG (bottom) experiments. The MEG images are thresholded at NAI = 3.0. There is remarkably consistent activation across both modalities over a number of cortical areas. Activation over sensori-motor cortex is more pronounced in the MEG images as this area was not acquired in the fMRI experiment. In the fMRI analysis the yellow / orange colour indicates positive BOLD and the purple / white colour indicates a negative BOLD response. In the MEG responses a blue / white colour indicates ERD and orange / red indicates ERS.

There is a remarkable similarity of response between the fMRI and MEG experiments with retinotopically specific responses being present in both extrastriate cortices to coherent motion in both left and right visual fields. There are also differences in response. The fMRI response shows a primary visual cortex response which is not present in the MEG experiment. Conversely the MEG response shows a large

response in the left sensorimotor cortex which is not present in the fMRI data due to the fact that this area was not acquired in the fMRI experiment. The large response in the MEG data is due to subjects responding with their right index finger to the motion coherence stimuli. Further analysis of the MEG data showed that the extrastriate cortex activity occurred mainly in the 10-20Hz frequency band whilst the sensorimotor cortex activation occurred at 15-25Hz. The ERS activation in the left frontal cortex occurred in a broad 5-40Hz band. The finding of beta desynchronisation in areas such as V5 / MT confirm the findings seen in both the temporal frequency (chapter 3) and implied-motion (chapter 4) experiments.

6.4.3 Negative BOLD response

Analysis of the fMRI data showed that there were distinct areas of cortex that showed a negative BOLD response to the motion coherence stimuli. These areas include ventral medial-frontal cortex, angular gyrus and posterior cingulate cortex. The group negative BOLD response can be seen from both angular gyrus (Figure 6-5 top) and posterior cingulate (Figure 6-5 bottom) areas. There is a clear reduction in the negative BOLD response with increasing motion coherence of the stimulus (See section 6.4.4.2 for further analysis).

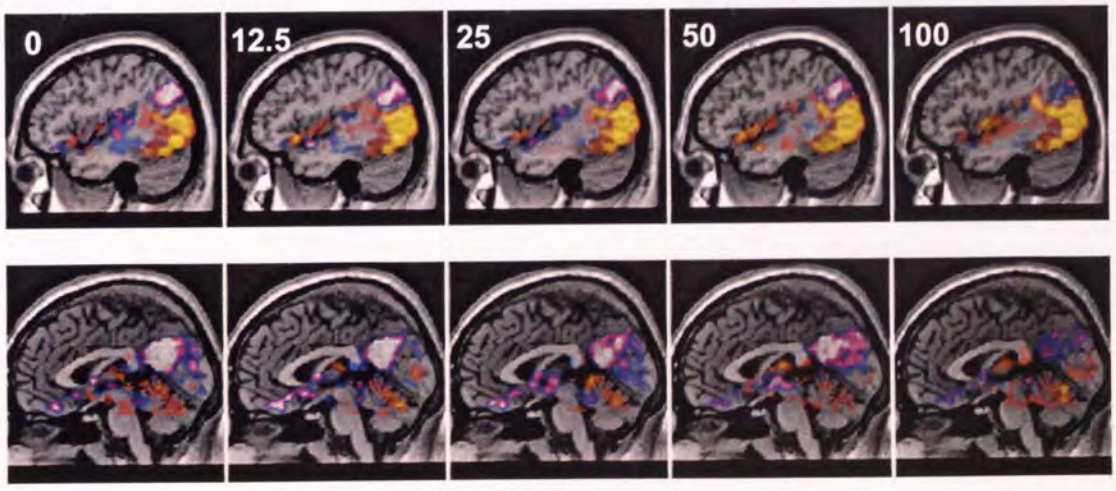

Figure 6-5. Overleaf. Evidence of negative BOLD response to motion coherence stimuli from angular gyrus (top) and posterior cingulate (bottom) areas. There is a clear reduction in the negative BOLD response with increasing motion coherence of the stimulus.

6.4.4 Linear response data

The Talairach coordinates of the areas showing a significant linear response to motion coherence are shown in Table 6-1.

Cortical area	Talairach coordinates (mm)
Positive BOLD	
Right V5	**45.2 -66.3 0.0**
Right LO	**45.2 -69.3 -10.0**
Right Fusiform	**23.0 -50.0 14.0**
Right Insula	**33.0 16.0 3.0**
Negative BOLD	
Medial frontal cortex	**-3.0 -57.0 -3.0**
Posterior cingulate / precuneus	**3.0 -54.0 33.0**
Left Angular Gyrus	**-39.2 -72.0 39.0**
MEG	
Right V5	**48.0 -70.0 3.0**
Right Fusiform	**27.0 -70.0 -16.0**
Medial Frontal cortex	**-9.0 63.0 -3.0**

Table 6-1. Talairach coordinates of the peak voxels (from the group analysis) in the ROIs used in the linear activation analysis.

6.4.4.1 *fMRI positive BOLD*

Analysis of the positive BOLD voxels showing a linear response with motion coherence revealed several areas, including V5 / LO, fusiform gyrus and insula (Figure 6-6).

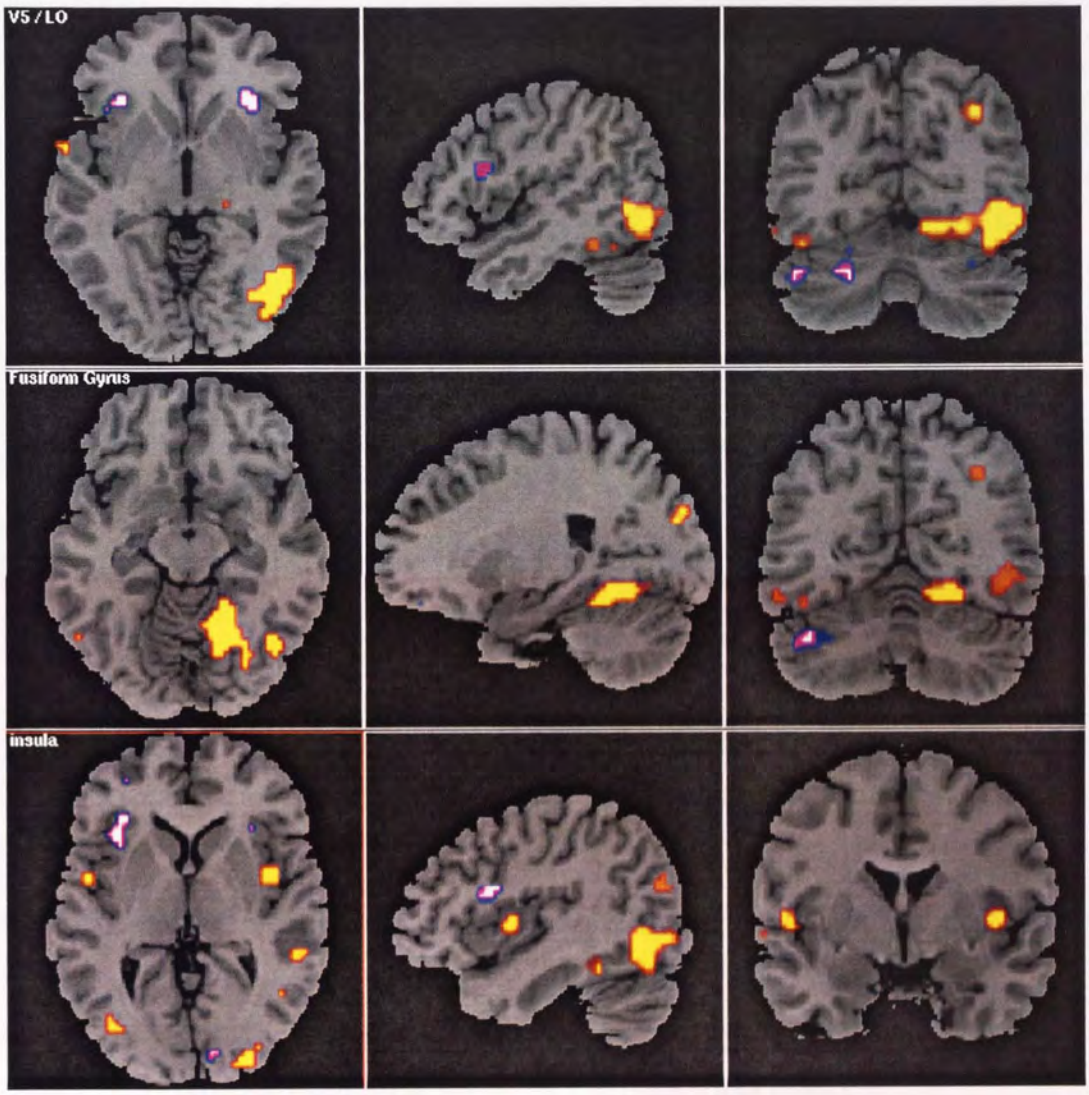

Figure 6-6. Analysis showing positive BOLD voxels varying linearly with motion coherence to a stimulus in the left visual field. The yellow colour indicates voxels in which activation increases with increasing coherence whilst the white/purple colour indicates voxels in which activation decreases with increasing coherence.

6.4.4.2 *fMRI negative BOLD*

Analysis of the negative BOLD voxels showing a linear response with motion coherence showed that areas such as medial frontal cortex, posterior cingulate cortex and the angular gyrus showed significant effects (Figure 6-7).

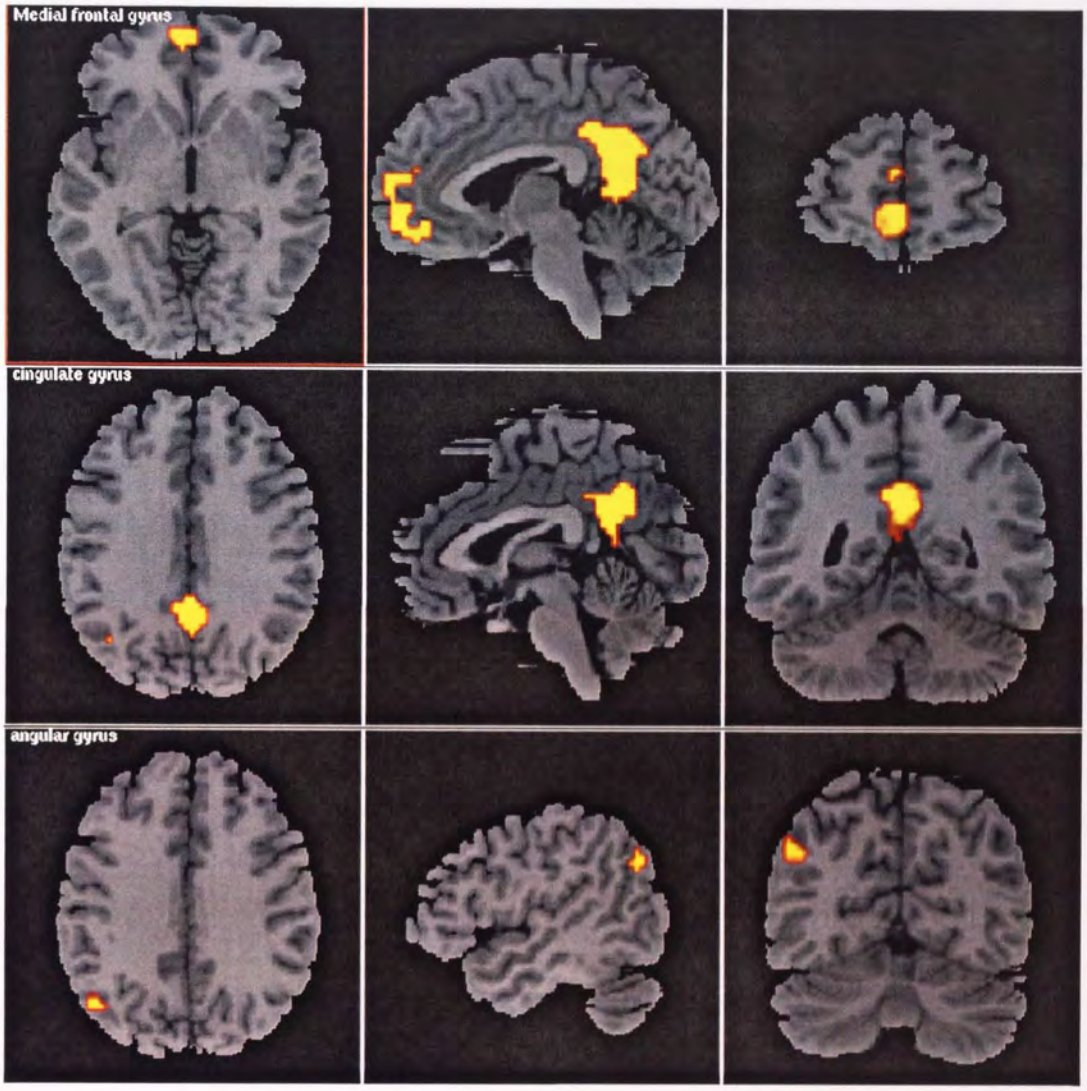

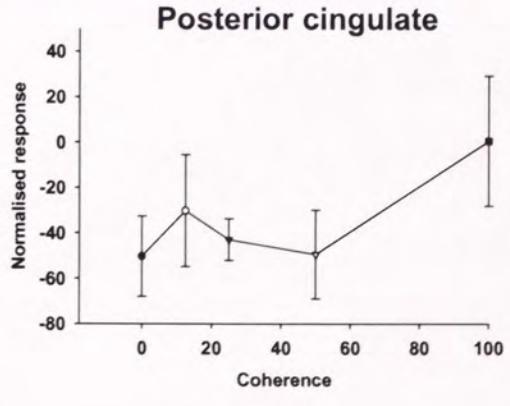

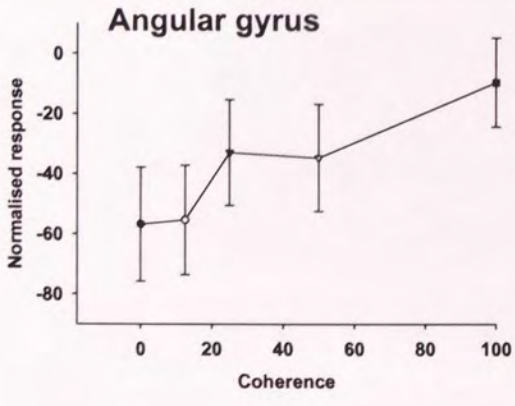

Figure 6-7. Overleaf. Analysis showing negative BOLD voxels varying linearly with motion coherence. The yellow colour indicates voxels in which activation increases with increasing coherence. Graphs show the normalised BOLD response from both the posterior cingulate cortex and angular gyrus. It can be seen that in both these areas the negative BOLD response decreases with increasing motion coherence although the response is more marked in the angular gyrus.

6.4.4.3 Linear MEG that is coincidental with fMRI response

Similar analysis was performed on the MEG data across a number of frequency bands although only the 10-20Hz band showed significant results. Figure 6-8 shows the cortical oscillatory activity, in the 10-20Hz band, varying linearly with motion coherence. Figure 6-8A and Figure 6-8B show areas where the ERD response varies linearly whilst Figure 6-8C shows areas where the ERS response varies linearly. Coincidental areas with the BOLD response were found in the fusiform gyrus, V5 / LO and medial frontal cortex.

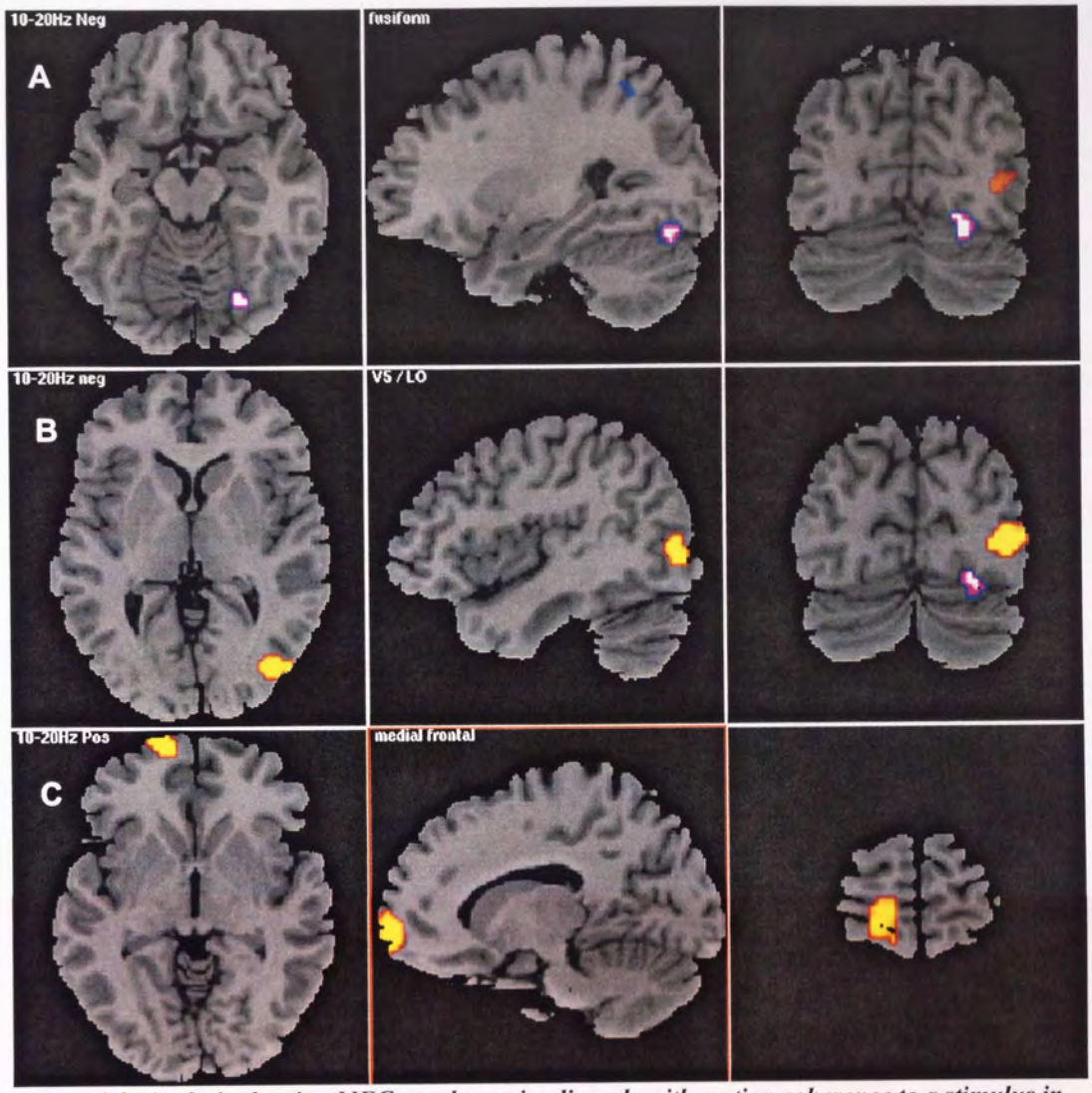

Figure 6-8. Analysis showing MEG voxels varying linearly with motion coherence to a stimulus in the left visual field. The yellow colour indicates voxels in which activation increases with increasing coherence and the white / purple colour indicates voxels in which activation decreases with increasing motion coherence. A and B show an ERD response whilst C shows an ERS response.

6.4.5 Linear response analysis (fMRI v MEG)

The response profiles from the areas coincidental between the fMRI and MEG experiments are shown in Figure 6-9. It can be seen that in area V5 / MT the contralateral BOLD response increases linearly with motion coherence. The contralateral MEG data shows an ERD response that reduces linearly with coherence. In the fusiform gyrus the BOLD response shows a slight linear increase with coherence whilst the MEG data shows an increasing ERD response. In medial frontal cortex there is a negative BOLD response which reduces with increasing coherence whilst the MEG data shows an ERS response which increases with increasing coherence.

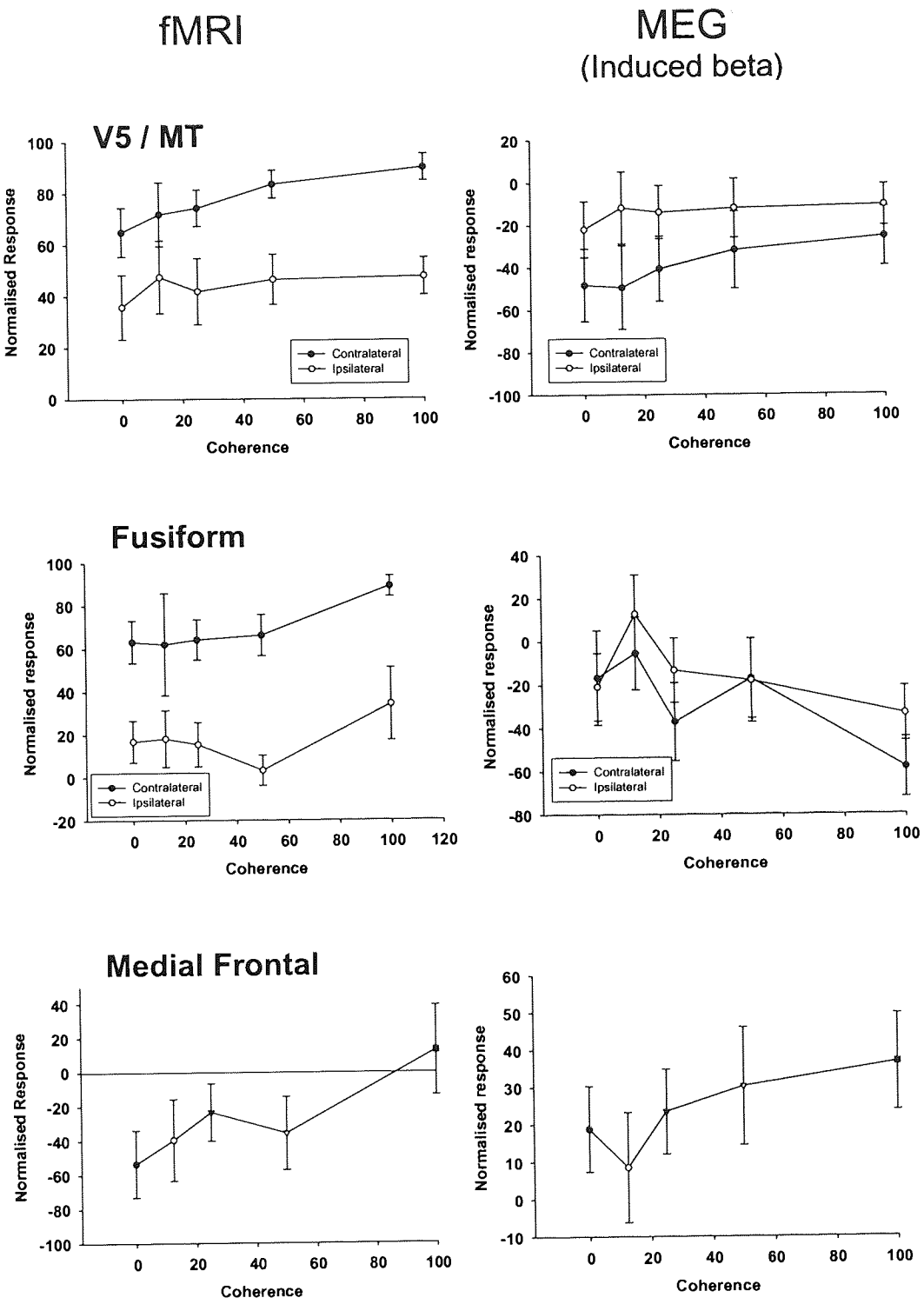

Figure 6-9. Normalised response curves showing responses in cortical areas activated in both the fMRI and MEG experiments. The results of the MEG experiment are from the 10-20Hz frequency band. For the fMRI data a negative value represents a negative BOLD response whilst for the MEG data a negative value represents a power decrease. The error bars show the SEM.

6.4.6 *BOLD responses in other cortical areas*

The study of Rees *et al.* (2000) showed that there was a differing BOLD response in area KO to that of V5 / MT. In the present study activation of areas posterior and inferior to V5 / MT were noted. Analysis of the response profile of this area (Figure 6-10A) showed that there was a linear increase in the BOLD response with increasing motion coherence similar to that of area V5 / MT. Analysis of the responses from the insula (Figure 6-10B) showed a decrease in the BOLD response with increasing coherence, consistent with previous findings (Rees *et al.* 2000)

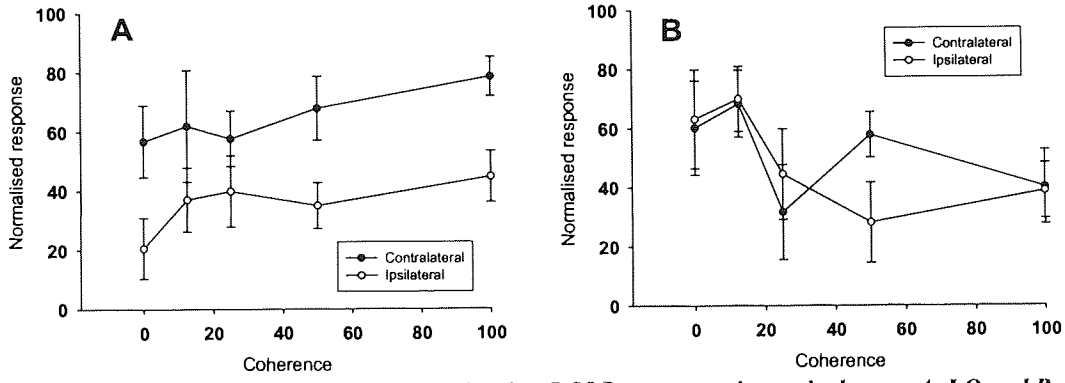

Figure 6-10. Normalised response curves showing BOLD responses in cortical areas A. LO and B. Insula. The error bars show the SEM.

6.4.7 *V5 MEG evoked data*

In this study, due to the use of a brief trial based design, it is possible to look not only at induced oscillatory effects but also at the phase-locked time-averaged evoked activity. The linear analysis showed that there was statistically significant activation in right V5 / MT. The individual data were reviewed and each subject's evoked response from the peak voxel in V5 / MT was calculated. The grand average evoked response in V5 / MT across subjects and coherence levels is shown in Figure 6-11. The evoked response showed a morphology (early P1 followed by N2 at approximately 200ms) that was

consistent with previous studies using coherent dots (Niedeggen and Wist 1999, Bach and Ullrich 1994, Wist *et al.* 1994)

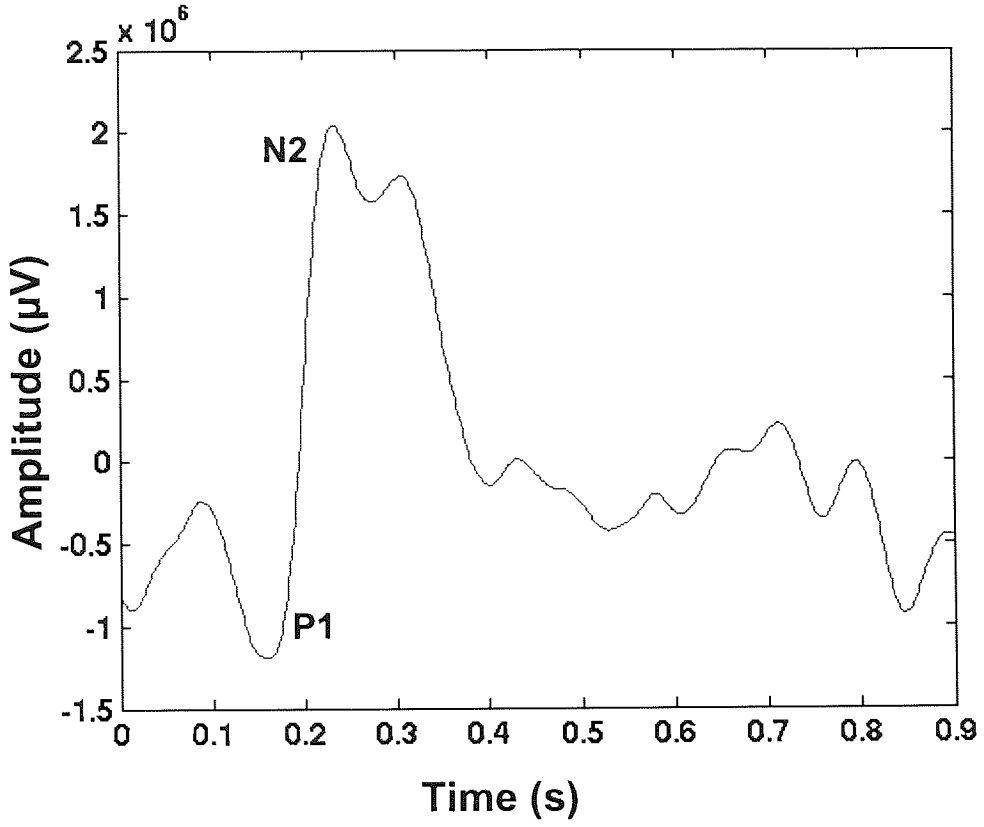

Figure 6-11. Grand average evoked response from all motion coherence levels and subjects from voxels in V5 /MT. P1 and N2 refer to the commonly seen peaks seen in the motion coherence evoked potential.

Analysis of the evoked potential amplitude (P1 to N2) showed that the amplitude increased linearly with coherence level (Figure 6-12).

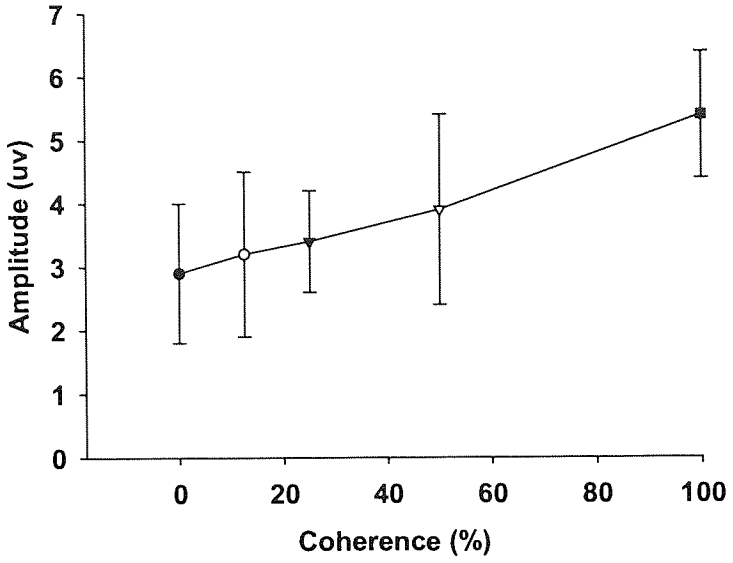

Figure 6-12. Evoked potential amplitude (P1-N2) as a function of motion coherence

A comparison of how the BOLD, induced and evoked responses compare with each other in V5 / MT is shown in Figure 6-13.

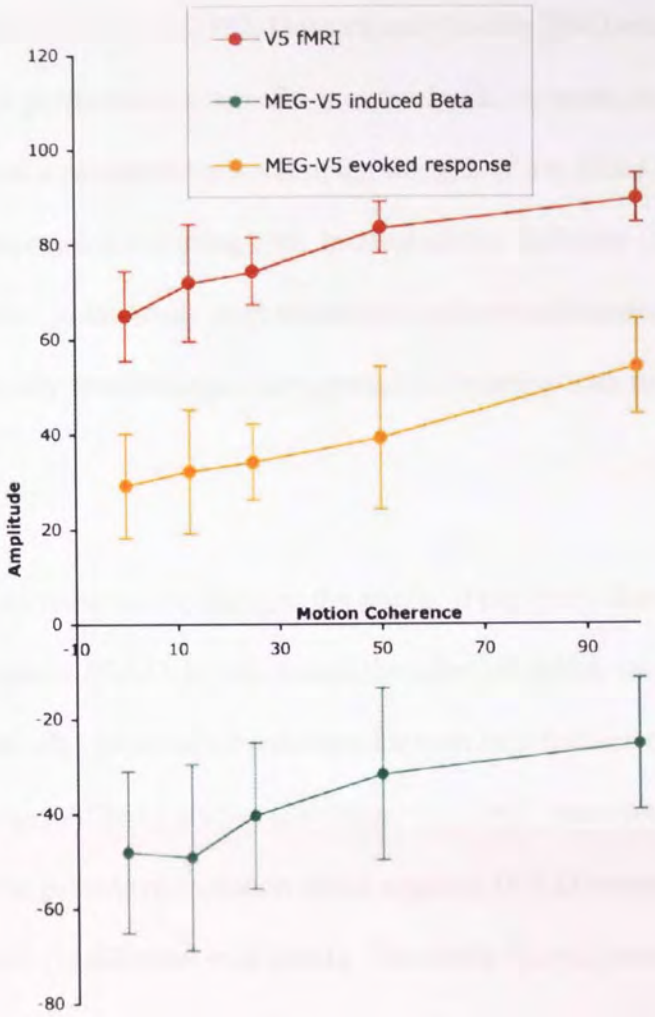

Figure 6-13. Graph comparing the response profiles of the BOLD, induced beta and evoked responses from area V5 / MT.

6.5 Discussion

6.5.1 Negative BOLD response

Common cortical areas consistently show reductions in the BOLD response across a range of different stimuli (Mazoyer *et al.* 2001, Binder *et al.* 1999, Shulman *et al.* 2001). These areas include the medial frontal cortex (both dorsal and ventral), anterior cingulate gyrus, posterior cingulate cortex and angular gyrus. These cortical areas consistently have the highest resting baseline metabolic rate (Raichle *et al.* 2001) and it has been proposed that they have an important role in tasks such as self-referential

mental activity (Castelli *et al.* 2000, Gusnard *et al.* 2001) and the monitoring of the world around us (Vogt *et al.* 1992, Gusnard and Raichle 2001) which are suppressed when the brain performs an externally generated task. A recent study, using auditory stimuli, showed a parmetric variation in the strength of this BOLD decrease, with increasing suppression occurring with increasing task difficulty (McKiernan *et al.* 2003). However, in this study even the easiest auditory task caused a large suppression to occur with only small changes in suppression occurring with further increases in task difficulty.

In keeping with these recent findings, the results of this study show areas of cortex exhibiting negative BOLD, in response to the stimulus, which varies parametrically with task demands. Much of the evidence for such an effect has come from meta-analyses of many different studies (Shulman *et al.* 2001, Mazoyer *et al.* 2001) and only recently has the parametric variation of the negative BOLD response been shown using auditory stimuli (McKiernan *et al.* 2003). This study shows parametric variation in the negative BOLD response to a visual direction-discrimination task (see Figure 6-5 and Figure 6-7). Contrary to the finding of this work, a recent study, of these negative BOLD areas, using visual stimuli showed no change in posterior cingulate cortex and anterior cingulate (Greicius *et al.* 2003). However, the visual task involved no cognitive input, a vital factor in producing such an effect, requiring simply the passive viewing of a moving and stationary checkerboard stimulus.

It has been suggested that brain areas in the prefrontal cortex such as the anterior cingulate are activated in conditions of response conflict (Carter *et al.* 1998, Devinsky *et al.* 1995) which Rees *et al.* (2000) point out is the probable reason for the decreasing

activation, in this area, with increasing coherence found in their study. Although the area activated in the Rees study is more dorsal than in the present study, their finding of a reduction in response amplitude with increasing coherence, is consistent with the finding in this study of decreasing negative BOLD with increasing coherence in ventral medial frontal cortex. Thus, a possible explanation of the activity seen in the dorsal prefrontal cortex, in the Rees study, is that this is a negative BOLD response which is varying parametrically with the stimulus coherence in an area known to show a negative BOLD response during goal directed behaviour (Gusnard *et al.* 2001).

Negative BOLD effects are often present in the visual cortex in response to a visual stimulus (Smith *et al.* 2000, Smith *et al.* 2004, Tootell *et al.* 1998). However, the interpretation of such effects is debated. Some argue that the effect is due to activated cortical areas 'blood stealing' from nearby areas (Shmuel *et al.* 2002), whilst others suggest that it is due to the suppression of neural activity (Smith *et al.* 2000, Smith *et al.* 2004). The effects in this study occur far from the visual cortex and are therefore unlikely to be due to 'blood stealing' but the result of the suppression of ongoing resting neural activation (Gusnard *et al.* 2001, Gusnard and Raichle 2001, Raichle *et al.* 2001). In the present study, as task difficulty increases (motion coherence reduces) the subjects find it more difficult to assess the direction of coherent motion. As a result of this the self-monitoring areas of the cortex (medial frontal cortex, posterior cingulate and angular gyrus) show increased negative BOLD activity as the normal resting neuronal levels of activation are suppressed to cope with the increased cognitive demands of the task.

6.5.2 Cortical areas showing a linear response

The results of the BOLD linear response data were in general agreement with those published previously (Rees *et al.* 2000), showing a linear response to motion coherence in area V5 / MT. Here, for the first time, it is shown that there are both induced oscillatory and evoked responses, coincidental with the BOLD response, which also vary linearly with motion coherence.

There are differences between the results found previously and the present study. A difference in response profile has previously been reported between V5 / MT and areas posterior, superior and medial to it corresponding to areas KO and V3A which show a non-linear U shaped response to motion coherence, although the non-linearity was quite modest (Rees *et al.* 2000). The responses in the present study are recorded more inferior to the previously reported results (approximating to area LO) and show a linear response to motion coherence consistent with that of V5 / MT. Thus, there are motion areas that show a difference in response profile, to coherence stimuli, with that of V5 / MT (Rees *et al.* 2000) and others that show a similar response as shown in this study.

6.5.2.1 MEG responses

A review of the response profiles from the areas that are coincidental between fMRI and MEG (Figure 6-9) show that there is a complex relationship between cortical oscillatory responses, as recorded by SAM, and the BOLD response. Area V5 / MT shows a linearly increasing BOLD response with a linearly reducing ERD response. The fusiform gyrus shows a linearly increasing BOLD response with an increasing ERD response whilst the medial frontal cortex shows a decreasing negative BOLD response with a linearly increasing ERS response.

The fusiform gyrus has been shown to be activated in a number of motion studies (Dupont *et al.* 1994, de Jong *et al.* 1994, Shipp *et al.* 1994). Similarly the area has been shown to be activated during both direction discrimination (Cornette *et al.* 1998) and orientation discrimination (Orban *et al.* 1997) tasks. In the present study the area shows both a linear BOLD response and a linearly increasing ERD response in the 10-20Hz frequency band. This is in keeping with previous studies showing that the BOLD response is spatially coincidental with ERD.

In area V5 / MT the BOLD response is seen to increase linearly with coherence whilst ERD activation is seen to decrease (Figure 6-9), contrary to the idea that ERD is found in cortical areas that are activate (Pfurtscheller and Lopes da Silva 1999b, Lopes da Silva and Pfurtscheller 1999, Pfurtscheller and Lopes da Silva 1999a). However, the linear response data as seen in Figure 6-9 is a measure of the overall, combined, effect from both the evoked and induced activations. The evoked-response from voxels in V5 / MT shows a linear increase in amplitude with increasing coherence (Figure 6-12), consistent with the BOLD response. Thus, the voxels in V5 / MT are showing both a reduction in synchronisation (ERD), in response to the stimulus, and also an evoked-response which is increasing in amplitude with coherence, leading to the combined effect of an apparent reduction in ERD activation. Other studies have shown increased evoked response amplitude with coherence using both EEG (Niedeggen and Wist 1999) and MEG (Nakamura *et al.* 2003) although none have been able to show a direct link to the BOLD response. The similarity of the evoked-potential amplitude response with that of the BOLD response, shown here, would suggest that the BOLD is well correlated with this initial evoked activity.

Similarly, it was found that there was increasing ERS activation in ventral medial-frontal cortex which also showed linear negative BOLD activation in response to the stimulus. Although it is known that increases in cortical power occur in primary sensory cortices in direct response to a given stimulus (see section 3.5.4), ERS is commonly associated with cortical areas at rest (Pfurtscheller 1992). Thus, in this experiment, when the negative BOLD response is at its largest, indicating maximal deactivation of that area, one would expect the ERS response to be at its largest and vicae versa. This is contrary to the findings reported here. However, much of the research on ERS has itself concentrated on the response of primary sensory cortices showing that when one part of the sensory system is activated another is deactivated (e.g. Plewnia *et al.* 2003, Alegre *et al.* 2004, Pfurtscheller and Lopes da Silva 1999a). Recent research suggests that the brain areas that show decreased BOLD activity during cognitive tasks also show significant functional connectivity during the resting state, providing evidence of a default mode network of tonically active cortical areas (Greicius *et al.* 2003). Given their complex role in the constant monitoring of the body and environment it is therefore possible that these areas do not respond in the conventional way one would expect to any given stimulus. Further research is required to confirm or deny this finding.

6.6 Conclusion

Here it is shown that relatively complex relationships between cortical responses and stimulus characteristics can be identified using SAM, in the same way as has previously been demonstrated using fMRI. It is debatable as to which aspect of the neuronal response relates to the BOLD response: the brief evoked potential that occurs when a

stimulus is presented or the induced, time-locked, activations that occur in specific frequency bands. Whilst it has been shown here that there is excellent spatial relationship between both the SAM and BOLD responses, of more significance is the fact that a number of cortical areas show a linear change in both induced and evoked activations coincidental with areas showing a linear change in the BOLD response. In an area known to be crucial in motion perception (V5 / MT) it has been shown that it is the evoked potential amplitude that varies with the same profile as the BOLD response (Figure 6-13) suggesting, at least in this particular cortical area, that this is the underlying neuronal activation causing the BOLD response. However, across several studies in this thesis, it has been shown that a baseline reduction in beta power (ERD) is a very robust and well localised finding in V5 / MT. It may be that in the presence of a driving phase-stable stimulus in brief events, as is the case in this study, that the evoked response shows a tight relationship with the stimulus parameters but this is colocalised with a generic reduction in beta power, which simply reflects the activation of V5 / MT.

It is shown here that there are specific cortical areas that show a negative BOLD response which varies parametrically with the coherence stimulus. Only recently has such a parametric variation of this response been demonstrated using auditory stimuli and this study may be the first to show such a parametric variation using a visual task.

The results shown here identify the complex relationship between underlying cortical activations and the BOLD response. The SAM technique has provided information that will help to explain this complex interaction and has shown itself to be an excellent and complementary technique to that of fMRI.

7. CONCLUSIONS AND FUTURE RESEARCH

7.1 Conclusions

This work has used Synthetic Aperture Magnetometry (SAM) to investigate the oscillatory changes taking place in the visual cortex, to a variety of visual paradigms, and how these relate to the BOLD response.

Investigation of the oscillatory changes taking place in response to a parametric variation of the stimulus temporal frequency (chapter 3) reveal fundamental differences in both tuning characteristics and oscillatory power changes occurring within striate and extrastriate cortex (Fawcett et al 2004).

SAM has been able to reveal the temporal evolution of the response to implied-motion in area V5 / MT (chapter 4). The results suggest that this area plays an important role in the perception of such stimuli. The early (evoked) SAM responses show a striking similarity in cortical activations with previously published investigations using BOLD and suggests an earlier and perhaps more central role for V5/MT in performing this complex visual scene analysis.

Investigation of the attentional modulation of cortical oscillatory activity reveals that both induced and evoked activity modulates with shifting visuo-spatial attention in areas consistent with known changes in the BOLD response (chapter 5). There is no change in the modulation effect with contrast although there are changes in evoked response

amplitude that suggest that known BOLD changes with contrast are most likely related to this evoked activity.

A direct comparison of SAM and the BOLD response reveals that a number of cortical areas show a linear change in both induced and evoked activations coincidental with areas showing a linear change in the BOLD response (chapter 6). In an area known to be crucial in motion perception (V5 / MT) it has been shown that it is the evoked potential amplitude that varies with the same profile as the BOLD response suggesting, at least in this particular cortical area, that this is the underlying neuronal activation causing the BOLD response.

7.2 Future work

This thesis has raised some interesting questions and provides the basis for further work:

The results in chapter 3 were obtained using a stimulus of broad spatial frequency, SAM could be used to examine the temporal frequency and velocity tuning characteristics of V5/MT (and striate visual cortex) using stimuli containing only one spatial frequency and direction, such as a drifting sinusoidal grating.

A further thesis could be produced from the results of chapter 4. What are the functional imaging differences between representational momentum and implied-motion stimuli? Is V5 / MT activated simply by photographs of movement or is it activated by stimuli such as words or abstract drawings that imply motion?

By using an increased number of subjects, to improve SNR and a quadrant stimulus, to reduce cancellation effects across the calcarine, more robust primary cortex activation may be produced in the attention paradigm (chapter 5). It would of interest to compare this with the BOLD response to see if the modulation of activation between two modalities covaries in primary visual cortex.

Further work is required to examine the complex responses, of the various cortical motion areas, to motion coherence stimuli (chapter 6). How important is the size of the stimulus to the results obtained? Previous research suggests that with small patches the response in V5/MT is larger for coherent motion (Rees *et al.* 2000), whilst for full-field stimulation the response is larger for incoherent motion (McKeefry *et al.* 1997). This effect could be systematically investigated by using patches of different sizes.

A new variant on SAM, recently developed in our laboratory (Brookes *et al.* 2004) allows the localisation of evoked, rather than induced, activity within the cortex. For both the attention and motion-coherence experiments, this technique could prove useful in comparing the location of evoked and induced activity, and may help to reveal activity in the primary visual cortex. In the context of the results described in this thesis, this could be an important future research area, as the precise contribution of evoked and induced oscillatory power changes to activity measured using BOLD appears to be task and context dependent.

REFERENCES

Adjamian, P., Barnes, G. R., Hillebrand, A., Holliday, I. E., Singh, K. D., Furlong, P. L., Harrington, E., Barclay, C. W., and Route, P. J. G. (2004). Co-registration of magnetoencephalography with magnetic resonance imaging using bite-bar-based fiducials and surface-matching. *Clinical Neurophysiology* **115**, 691-698.

Adrian, E. and Matthews, B. (1934). The Berger rhythm: potential changes from the occipital lobe in man. *Brain* **57**, 355-385.

Ahlfors, S. P., Simpson, G. V., Dale, A. M., Belliveau, J. W., Liu, A. K., Korvenoja, A., Virtanen, J., Huotilainen, M., Tootell, R. B. H., Aronen, H. J., and Ilmoniemi, R. J. (1999). Spatiotemporal Activity of a Cortical Network for Processing Visual Motion Revealed by MEG and fMRI. *Journal of Neurophysiology* **82**, 2545-2555.

Aine, C., Georgre, J., Medvick, P., Supek, S., Flynn, E., and Bodis-Wollner, I. (1989). Identification of multiple sources in transient visual evoked neuromagnetic responses. In 'Advances in Biomagnetism.' (Eds S. J. Williamson, M. Hoke, G. Stroink, and M. Kotani.) (Plenum Press: New York.)

Aine, C., Huang, M., Stephen, J., and Christner, R. (2000). Multistart algorithms for MEG empirical data analysis reliably characterise locations and time courses of multiple sources. *Neuroimage* **12**, 159-172.

Albrecht, D. G. and Hamilton, D. B. (1982). Striate cortex of monkey and cat: contrast response function. *Journal of Neurophysiology* **48**, 217-237.

Albright, T. D. (1984). Direction and Orientation Selectivity of Neurons in Visual Area MT of the Macaque. *Journal of Neurophysiology* **52**, 1106-1130.

Albright, T. D. and Desimone, R. (1987). Local precision of visuotopic organisation in the middle temporal area (MT) of the macaque. *Experimental Brain Research* **65**, 582-592.

Alegre, M., de Gurtubay, I. G., Labarga, A., Iriarte, J., Malanda, A., and Artieda, J. (2004). Alpha and beta oscillatory activity during a sequence of two movements. *Clinical Neurophysiology* **115**, 124-130.

Allman, J. M., Miezin, F. M., and McGuiness, E. (1990). Direction and velocity specific responses from beyond the receptive field in the middle temporal visual area. *Perception* **14**, 105-126.

Amorim, M., Lang, W., Lindinger, G., Mayer, D., Deecke, L., and Berthoz, A. (2000). Modulation of spatial orientation processing by mental imagery instructions: A MEG study of representational momentum. *Journal of Cognitive Neuroscience* **12**, 569-582.

Anderson, S. J. and Burr, D. C. (1985). Spatial and temporal selectivity of the human motion detection system. *Vision Research* **25**, 1147-1154.

Anderson, S. J., Holliday, I. E., Singh, K. D., and Harding, G. F. A. (1996). Localization and functional analysis of human cortical area V5 using magneto-encephalography. *Proceedings of the Royal Society of London Series B-Biological Sciences* **263**, 423-431.

Anstis, S. M. (1980). The perception of apparent movement. *Philosophical Transactions of the Royal Society London, Series B* **290**, 153-168.

Anstis, S. M. and Duncan, K. (1983). Separate motion aftereffects from each eye and from both eyes. *Vision Research* **23**, 161-169.

Antal, A., Nitsche, M. A., Kruse, W., Kincses, T. Z., Hoffmann, K. P., and Paulus, W. (2004). Direct current stimulation over V5 enhances visuomotor coordination by improving motion perception in humans. *Journal of Cognitive Neuroscience* **16**, 521-527.

Bach, M. and Ullrich, D. (1994). Motion adaptation governs the shape of motion-evoked cortical potentials. *Vision Research* **34**, 1541-1547.

Bach, M. and Ullrich, D. (1997). Contrast dependency of motion-onset and pattern-reversal VEPs: interaction of stimulus type, recording site and response component. *Vision Research* **37**, 1845-1849.

Baddley, A. (1986). 'Working memory.' (Oxford University Press: New York.)

Ball, K. and Sekular, R. (1980). Models of stimulus uncertainty in motion perception. *Vision Research* **29**, 1261-1266.

Bandettini, P. A., Wong, E. C., Jesmanowicz, A., Hinks, R. S., and Hyde, J. S. (1994). Spin-echo and gradient-echo EPI of human brain activation using BOLD contrast: a comparative study at 1.5T. *NMR Biomedicine* **7**, 12-20.

Barnes, G. R. and Hillebrand, A. (2003). Statistical flattening of MEG beamformer images. *Human Brain Mapping* **18**, 1-12.

Basar, E. (1999). 'Brain function and oscillation, II: integrative brain function, neurophysiology and cognitive processes.' (Springer: Berlin.)

Basar, E. and Schurmann, M. (1994). Functional aspects of evoked alpha and theta responses in humans and cats. *Biological Cybernetics* **72**, 175-183.

Beneveto, L. A. and Standage, G. P. (1983). The organisation of projections of the retinorecipient and nonretinorecipient nuclei of the pretectal complex and layers of the superior colliculus to the lateral pulvinar and medial pulvinar in the macaque monkey. *Journal of Comparative Neurology* **271**, 307-336.

Bertamini, M. (1993). Memory for position and dynamic representations. *Memory and Cognition* **21**, 449-457.

Binder, J. R., Frost, J. A., Hammeke, T. A., Bellgowan, P. S. F., Rao, S. M., and Cox, R. W. (1999). Conceptual processing during the concious resting state: A functional MRI study. *Journal of Cognitive Neuroscience* **11**, 80-93.

Bisley, J. W. and Goldberg, M. E. (2003). Neuronal activity in the lateral intraparietal area and spatial attention. *Science* **299**, 81-86.

Blamire, A. M., Ogawa, S., Ugurbil, K., Rothman, D., McCarthy, G., Ellermann, J. M., Hyder, F., Rattner, Z., and Shulman, R. G. (1992). Dynamic mapping of the human visual cortex using by high-speed magnetic resonance imaging. *Proceedings of the National Academy of Science USA* **89**, 11069-11073.

Bonda, E., Petrides, M., Ostry, D., and Evans, A. (1996). Specific involvment of human parietal systems and the amygdala in the perception of biological motion. *Journal of Neuroscience* **16**, 3737-3744.

Born, R. T. and Tootell, R. B. H. (1992). Segregation of global and local motion processing in primate middle temporal visual area. *Nature* **357**, 497-499.

Boxerman, J. L., Bandettini, P. A., Kwong, K. K., Baker, J. R., Davis, T. L., Rosen, B. R., and Weisskoff, R. M. (1995). The intravascular contribution to fMRI signal change: Monte Carlo modelling and diffusion-weighted studies in vivo. *Magnetic Resonance in Medicine* **34**, 4-10.

Boycott, B. B. and Dowling J.E. (1969). Organisation of the primate retina: light microscopy. *Philosophical Transactions of the Royal Society London* **255**, 109-176.

Boycott, B. B. and Kolb, H. (1973). The horizontal cells of the rhesus monkey retina. *The Journal of Comparative Neurology* **148**, 115-139.

Boynton, G. M., Demb, J. B., Glover, G. H., and Heeger, D. J. (1999). Neuronal Basis of Contrast Discrimination. *Vision Research* **39**, 257-269.

Boynton, G. M., Engel, S. A., Glover, G. H., and Heeger, D. J. (1996). Linear systems analysis of functional magnetic resonance imaging in human V1. *Journal of Neuroscience* **16**, 4207-4221.

Braddick, O. J. (1980). Low-level and high-level processes in apparent motion. *Philosophical Transactions of the Royal Society London, Series B* **209**, 137-151.

Braddick, O. J., O'Brien, J. M., Wattam-Bell, J., Atkinsin, J., Hartley, T., and Turner, R. (2001). Brain areas sensitive to coherent visual motion. *Perception* **30**, 61-72.

Brandt, M. E. (1997). Visual and auditory evoked phase resetting of the alpha EEG. *International Journal of Psychophysiology* **26**, 285-298.

Brefczynski, J. A. and DeYoe, E. A. (1999). A physiological correlate of the 'spotlight' of visual attention. *Nature Neuroscience* **2**, 370-374.

Bremmer, F., Schlack, A., Shah, N. J., Zafiris, O., Kubischik, M., Hoffman, K., Zilles, K., and Fink, G. R. (2001). Polymodal motion processing in posterior parietal and premotor cortex: a human fMRI study strongly implies equivalencies between humans and monkeys. *Neuron* **29**, 287-296.

Brookes, M. J., Hall, S. D., Furlong, P. L., Barnes, G. R., Hillebrand, A., Singh, K. D., Holliday, I. E., Francis, S. T., Morris, P. G. (2004). A general linear model for MEG beamformer imaging. *Neuroimage In press.*

Britten, K. H., Shadlen, M. N., Newsome, W. T., and Movshon, J. A. (1993). Responses of neurons in macaque MT to stochastic motion signals. *Visual Neuroscience* **10**, 1157-1169.

Broadbent, D. E. (1958). 'Perception and Communication.' (Pergamon Press: London.)

Bruce, V., Green, P. R., and Georgeson, M. A. (2003). 'Visual perception; physiology, psychology and ecology.' (Psychology Press: Hove and New York.)

Buckner, R. L. (1998). Event-related fMRI and the haemodynamic response. *Human Brain Mapping* **6**, 373-377.

Bullier, J., Girard, P., and Salin, P. A. (1994). The role of area 17 in the transfer of information to extrastriate visual cortex. In 'Primary visual cortex in primates.' (Eds A. Peters and K. S. Rockland.) pp. 301-330. (Plenum Press: New York.)

Bundo, M., Kaneoke, Y., Inao, S., Yoshida, J., Nakamura, A., and Kakigi, R. (2000). Human visual motion areas determined individually by magnetoencephalography and 3D magnetic resonance imaging. *Human Brain Mapping* **11**, 33-45.

Burgess, A. P. and Gruzelier, J. H. (1999). Methodological advances in the analysis of event-related desynchronisation data: reliability and robust analysis. In 'Event-Related Desynchronisation: Handbook of Electroencephalography and Clinical Neurophysiology, Revised Series, Vol. 6.' (Eds G.Pfurtscheller and F.H.Lopes da Silva.) (Elsevier:

BurkHalter, A. and Bernardo, K. L. (1989). Organisation of corticocortical connections in human visual cortex. *Proceedings of the National Academy of Sciences of the United States of America* **86**, 1071-1075.

Burock, M. A., Buckner, R. L., Woldorff, M. G., Rosen, B. R., and Dale, A. M. (1998). randomized event-related experimental designs allow for extremely rapid presentation rates using functional MRI. *Neuroreport* **9**, 3735-3739.

Callaway, E. M. (1998). Local circuits in primary visual cortex of the macaque monkey. *Annual Review Neuroscience* **21**, 47-74.

Cameron, E. L., Tai, J. C., and Carrasco, M. (2002). Covert attention affects the psychometric function of contrast sensitivity. *Vision Research* **42**, 949-967.

Cantley, L. (1986). Ion transport systems sequenced. *Trends in Neurosciences* **9**, 1-3.

Carrasco, M., Ling, S., and Read, S. (2004). Attention alters appearance. *Nature Neuroscience* **7**, 308-313.

Carrasco, M. and McElree, B. (2001). Covert attention accelerates the rate of visual information processing. *Proceedings of the National Academy of Science USA* **98**, 5363-5367.

Carrasco, M., Penpaci-Talgar, and Eckstein, M. (2000). Spatial covert attention increases contrast sensitivity along the CSF: support for signal enhancement. *Vision Research* **40**, 1203-1215.

Carter, C. S., Braver, T. S., Barch, D. M., Botvinick, M. M., Noll, D., and Cohen, J. D. (1998). Anterior cingulate cortex, error detection, and the online monitoring of performance. *Science* **280**, 747-749.

Casagrande, V. A. and Kaas, J. H. (1994). The afferent, intrinsic and efferent connections of primary visual cortex in primates. In 'Cerebral Cortex, Vol.10, Primary visual cortex in primates.' (Eds A. Peters and K. S. Rockland.) pp. 201-259. (Plenum Press: New York.)

Castelli, F., Happe, F., Frith, U., and Frith, C. (2000). Movement and mind: a functional imaging study of perception and interpretation of complex intentional movement patterns. *Neuroimage* **12**, -314.

Cavanagh, P. and Mather, G. (1989). Motion: The long and the short of it. *Spatial Vision* **4**, 103-129.

Chawla, D., Phillips, J., Buechel, C., Edwards, R., and Friston, K. J. (1998). Speed-Dependant Motion-Sensitive Responses in V5: An fMRI Study. *Neuroimage* **7**, 86-96.

Cheng, K., Fujita, H., Kanno, I., Miura, S., and Tanaka, K. (1995). Human cortical regions activated by wide-field visual motion: an H2(15)O PET study. *Journal of Neurophysiology* **74**, 413-427.

Clare, M. H. and Bishop, G. H. (1954). Responses from an association area secondarily activated from optic cortex. *Journal of Neurophysiology* **17**, 271-277.

Clarke, L. P., Velthuizen, R. P., Camacho, M. A., Heine, J. J., Vaidyanathan, M., Hall, L. O., Thatcher, R. W., and Silbiger, M. L. (1995). Review of MRI segmentation: methods and applications. *Magnetic Resonance Imaging* **13**, 343-368.

Clifford, C. W. G. and Vaina, L. M. (1999). A computational model of selective deficits in first and second order motion processing. *Vision Research* **39**, 113-130.

Cohen, D. and Cuffin, B. N. (1983). Demonstration of useful differences between magnetoencephalogram and electroencephalogram. *Electroencephalograhy and Clinical Neurophysiology* **56**, 38-51.

Cohen, D. and Halgren, E. (2003). Magnetoencephalography (Neuromagnetism). In 'Encyclopaedia of Neuroscience.' (Eds G. Adelman and B. H. Smith.) pp. 1-7. (Elsevier Science Ltd: New York.)

Connor, C. E., Preddie, D. C., Gallant, J. L., and Van Essen, D. C. (1997). Spatial attention effects in macaque area V4. *Journal of Neuroscience* **17**, 3201-3214.

Cooper, N. R., Croft, R. J., Dominey, S. J. J., Burgess, A. P., and Gruzelier, J. H. (2003). Paradox lost? Exploring the role of alpha oscillations during externally vs. internally directed attention and the implications for idling and inhibition hypotheses. *International Journal of Psychophysiology* **47**, 65-74.

Corbetta, M., Akbudak, E., Conturo, T. E., Snyder, A. Z., Ollinger, J. M., and Drury, H. (1998). A common network of functional areas for for attention and eye movements. *Neuron* **21**, 761-773.

Corbetta, M., Miezin, F. M., Dobmeyer, S., Shulman, G. L., and Petersen, S. E. (1991). Selective and divided attention during visual discriminations of shape, colour and speed: functional anatomy by positron emission tomography. *Journal of Neuroscience* **11**, 2383-2402.

Corbetta, M. and Shulman, G. L. (2002). Control of goal directed and stimulus driven attention in the brain. *Nature Reviews Neuroscience* **3**, 201-215.

Cornette, L., Dupont, P. G., Rosier, A. M., Sunaert, S., Van Hecke, P., Michiels, J., Mortelmans, L., and Orban, G. A. (1998). Human brain regions involved in direction discrimination. *Journal of Neurophysiology* **79**, 2749-2765.

Cowey, A. (1979). Cortical maps and visual perception: the Grindley Memorial Lecture. *The Quarterly Journal of Experimental Psychology* **31**, 1-17.

Cowey, A. and Perry, V. H. (1980). The projection of the fovea to the superior colliculus in rhesus monkeys. *Neuroscience* **5**, 53-61.

Cragg, B. G. (1969). The topography of the afferent projections in the circumstriate visual cortex of the monkey studied by the Nauta method. *Vision Research* **9**, 733-747.

Crook, J. M., Lange-Malecki, B., Lee, B. B., and Valberg, A. (1988). Visual resolution of macaque retinal ganglion cells. *Journal of Physiology* **396**, 205-224.

Cuffin, B. N. and Cohen, D. (1977). Magnetic fields of a dipole in special volume conductor shapes. *IEEE Transactions in Biomedical Engineering* **24**, 372-381.

Culham, J. C., Brandt, S. A., Cavanagh, P., Kanwisher, N., Dale, A. M., and Tootell, R. B. H. (1998). Cortical fMRI activation produced by attentive tracking of moving targets. *Journal of Neurophysiology* **80**, 2657-2670.

Cutting, J. E. and Kozlowski, L. T. (1977). Recognising friends by their walk: Gait perception without familiarity. *Bulletin of the Psychonomic Society* **9**, 353-356.

Dale, A. M. and Buckner, R. L. (1997). Selective averaging of rapidly presented individual trials using fMRI. *Human Brain Mapping* **5**, 329-340.

de Jong, B. M., Shipp, S., Skidmore, B., and Frackowiak, R. S. (1994). The cerebral activity related to the visual perception of forward motion. *Brain* **117**, 1039-1054.

de Munck, J. C. (1992). A linear discretization of the volume conductor boundary integral equation using analytically integrated elements. *IEEE Transactions in Biomedical Engineering* **39**, 986-990.

De Weerd, P., Peralta, M. R. 3., Desimone, R., and Ungerleider, L. G. (1999). Loss of attentional stimulus selection after extrastriate cortical lesions in macaques. *Nature Neuroscience* **2**, 753-758.

De Yoe, E. A. and Van Essen, D. C. (1985). Segregation of efferent connections and receptive field properties in visual area V2 of the macaque. *Nature* **317**, 58-61.

De Yoe, E. A. and Van Essen, D. C. (1988). Concurrent processing streams in monkey visual cortex. *Trends in Neurosciences* **11**, 219-226.

Dean, A. F. (1981). The variability of discharge of simple cells in the cat striate cortex. *Experimental Brain Research* **44**, 437-440.

Derrington, A. M. and Lennie, P. (1984). Spatial and temporal contrast sensitivities of neurones in lateral geniculate nucleus of macaque. *Journal of Physiology* **357**, 219-240.

Desimone, R. and Duncan, J. (1995). Neural mechanisms of selective attention. *Annual Review Neuroscience* **18**, 193-222.

Desimone, R. and Schein, S. J. (1987). Visual Properties of Neurons in Area V4 of the Macaque: Sensitivity to Stimulus Form. *Journal of Neurophysiology* **57**, 835-868.

Devinsky, O., Morrell, M. J., and Vogt, B. A. (1995). Contributions of anterior cingulate cortex to behaviour. *Brain* **118**, 279-306.

DeVries, S. H. (2000). Bipolar cells use kainate and AMPA receptors to filter visual information into seperate channels. *Neuron* **28**, 847-856.

Dowling J.E. and Boycott, B. B. (1966). Organisation of the primate retina: electron microscopy. *Proceedings of the Royal Society of London, B,* **166**, 80-111.

Dowling, J. E. (1987). 'The Retina: An Approachable Part of the Brain.' (Harvard University Press: Cambridge, MA.)

Duann, J. R., Jung, T. P., Kuo, W. J., Yeh, T. C., Makeig, S., Hsieh, J. C., and Sejnowski, T. J. (2002). Single-trial variability in event-related BOLD signals. *Neuroimage* **15**, 823-835.

Dubner, R. and Zeki, S. M. (1971). Response Properties and Receptive Fields of Cells in an Anatomically Defined Region of the Superior Temporal Sulcus in the Monkey. *Brain Research* **35**, 528-532.

Dumoulin, S. O., Baker, C. L., Hess, R. F., and Evans, A. C. (2003). Cortical specialisation for processing first and second order motion. *Cerebral Cortex* **13**, 1375-1385.

Dumoulin, S. O., Bittar, R. G., Kabani, N. J., Baker, C. L., Le Goualher, G., Pike, G. B., and Evans, A. C. (2000). A new anatomical landmark for reliable identification of human area V5/MT: a quantitative analysis of sulcal patterning. *Cerebral Cortex* **10**, 454-463.

Dupont, P. G., De Bruyn, B., Vandenberghe, R., Rosier, A. M., Michiels, J., Marchal, G., Mortelmans, L., and Orban, G. A. (1997). The kinetic occipital region in human visual cortex. *Cerebral Cortex* **7**, 292.

Dupont, P. G., Orban, A., De Bruyn, B., Verbruggen, A., and Mortelmans, L. (1994). Many areas in the human brain respond to visual motion. *Journal of Neurophysiology* **72**, 1420-1424.

Dupont, P. G., Sary, G., Peuskens, H., and Orban, G. A. (2003). Cerebral regions processing first- and higher order motion in an opposed-direction discrimination task. *European Journal of Neuroscience* **17**, 1509-1517.

Felleman, D. J. and Van Essen, D. C. (1987). Receptive Field Properties of Neurons in Area V3 of Macaque Monkey Extrastriate Cortex. *Journal of Neurophysiology* **57**, 889-920.

Felleman, D. J. and Van Essen, D. C. (1991). Distributed hierarchical processing in the primate cerebral cortex. *Cerebral Cortex* **1**, 1-47.

Ffytche, D. H., Guy, C. N., and Zeki, S. (1995). The parallel visual motion inputs into areas V1 and V5 of human cerebral cortex. *Brain* **118**, 1375-1394.

Finke, R. A., Freyd, J. J., and Shyi, G. C. W. (1986). Implied velocity and acceleration induce transformations of visual memory. *Journal of Experimental Psychology: General* **115**, 175-188.

Foster, K. H., Gaska, J. P., Nagler, M., and Pollen, D. A. (1985). Spatial and Temporal Frequency Selectivity of Neurones in Visual Areas V1 and V2 of the Macaque Monkey. *Journal of Physiology* **365**, 331-363.

Fox, P. T., Mintun, M. A., Raichle, M. E., Miezin, F. M., Allman, J. M., and Van Essen, D. C. (1986). Mapping human visual cortex with positron emission tomography. *Nature* **323**, 806-809.

Fox, P. T. and Raichle, M. E. (1984). Stimulus rate dependence of regional cerebral blood flow in human striate cortex, demonstrated by positron emission tomography. *Journal of Neurophysiology* **51**, 1109-1120.

Fox, P. T. and Raichle, M. E. (1985). Stimulus Rate Determines Regional Blood Flow in Striate Cortex. *Annals of Neurology* **17**, 303-305.

Freeman, R. D. and Ohzawa, I. (1990). On the neurophysiological organisation of binocular vision. *Vision Research* **30**, 1661-1676.

Freyd, J. J. (1983). The mental representation of movement when static stimuli are viewed. *Perception & Psychophysics* **33**, 575-581.

Freyd, J. J. and Finke, R. A. (1984). Representational momentum. *Journal of Experimental Psychology-Learning Memory and Cognition* **10**, 126-132.

Freyd, J. J. and Finke, R. A. (1985). A velocity effect for representational momentum. *Bulletin of the Psychonomic Society* **23**, 443-446.

Freyd, J. J. and Johnson, J. Q. (1987). Probing the time course of representational momentum. *Journal of Experimental Psychology-Learning Memory and Cognition* **13**, 259-269.

Fries, P., Reynolds, J. H., Rorie, A. E., and Desimone, R. (2001). Modulation of oscillatory neuronal synchronisation by selective visual attention. *Science* **291**, 1560-1563.

Friston, K. J., Holmes, A. P., and Worsley, K. J. (1999). How many subjects constitute a study? *Neuroimage* **10**, 1-5.

Friston, K. J., Holmes, A. P., Worsley, K. J., Poline, J. B., Frith, C. D., and Frackowiak, R. S. J. (1995). Statistical parametric maps in functional imaging: a general linear approach. *Human Brain Mapping* **2**, 189-210.

Friston, K. J., Josephs, O., Rees, G., and Turner, R. (1998). Non-linear event-related responses in fMRI. *Magnetic Resonance in Medicine* **39**, 41-52.

Funahashi, S., Bruce, C., and Goldman-Rakic, P. (1989). Mnemonic coding of visual space in the monkey's dorsolateral prefrontal cortex. *Journal of Neurophysiology* **61**, 331-349.

Fuster, J. (2000). Executive frontal functions. *Experimental Brain Research* **133**, 66-70.

Futterweit, L. R. and Beilin, H. (1994). Recognition memory for movement in photographs: A developmental study. *Journal of Experimental Child Psychology* **57**, 163-179.

Fylan, F., Holliday, I. E., Singh, K. D., Anderson, S. J., and Harding, G. F. A. (1997). Magnetoencephalographic investigation of human cortical area V1 using color stimuli. *Neuroimage* **6**, 47-57.

Gandhi, S. P., Heeger, D. J., and Boynton, G. M. (1999). Spatial Attention Affects Brain Activity in Human Primary Visual Cortex. *Proceedings of the National Academy of Science USA* **96**, 3314-3319.

Gaska, J. P., Jacobson, L. D., and Pollen, D. A. (1988). Spatial and Temporal Frequency Selectivity of Neurons in Visual Cortical Area V3A of the Macaque Monkey. *Vision Research* **28**, 1179-1191.

Gegenfurtner, K. R., Kiper, D. C., Beusmans, J. M., Carandini, M., Zaidi, Q., and Movshon, J. A. (1994). Chromatic properties of neurons in macque MT. *Visual Neuroscience* **11**, 455-466.

Gegenfurtner, K. R., Kiper, D. C., and Levitt, J. B. (1997). Functional Properties of Neurons in Macaque Area V3. *Journal of Neurophysiology* **77**, 1906-1923.

Geisler, W. S. and Albrecht, D. G. (1997). Visual cortex neurons in monkeys and cats: detection, discrimination and identification. *Visual Neuroscience* **14**, 897-919.

Gesolowitz, D. B. (1970). On the magnetic field generated outside an inhomogeneous volume conductor by internal current sources. *IEEE Transactions in Magnetism* **6**, 247-346.

Ghosh, K. K., Goodchild, A. K., Sefton, A. E., and Martin, P. R. (1996). Morphology of retinal ganglion cells in a new world monkey, the marmoset Callithrix jacchus. *Journal of Comparative Neurology* **366**, 76-92.

Girard, P. and Bullier, J. (1989). Visual activity in area V2 during reversible inactivation of area 17 in the macaque monkey. *Journal of Neurophysiology* **62**, 1287-1302.

Girard, P., Salin, P. A., and Bullier, J. (1991a). Visual activity in Areas V3a and V3 During Reversible Inactivation of area V1 in the Macaque Monkey. *Journal of Neurophysiology* **66**, 1493-1503.

Girard, P., Salin, P. A., and Bullier, J. (1991b). Visual activity in macaque area V4 depends on area 17 input. *Neuroreport* **2**, 81-84.

Glass, L. (1969). Moire effect from random dots. *Nature* **223**, 578-580.

Goebel, R., Khorram-Sefat, D., Muckli, L., Hacker, H., and Singer, W. (1998). The constructive nature of vision: direct evidence from functional magnetic resonance imaging studies of apparent motion and motion imagery. *European Journal of Neuroscience* **10** , 1563-1573.

Goel, V. and Grafman, J. (1995). Are the frontal lobes implicated in "planning" functions? Interpreting data from the Tower of Hanoi. *Neuropsychologia* **33**, 632-642.

Goldman-Rakic, P. (1987). Circuitry of primate prefrontal cortex and regulation of behaviour by representational memory. In 'Handbook of physiology-The nervous system.' (Eds F. Plum and V. Mountcastle.) pp. 373-417. (American Physiological Society: Bethesda, MD.)

Goodyear, B. G., Nicolle, D. A., Humphrey, G. K., and Menon, R. S. (2000). BOLD fMRI response of early visual areas to perceived contrast in human amblyopia. *Journal of Neurophysiology* **84**, 1907-1913.

Gorodnitsky, I. F., George, J. S., and Rao, B. D. (1995). Neuromagnetic source imaging with FOCUSS: a recursive weighted minimum norm algorithm. *Electroencephalograhy and Clinical Neurophysiology* **95**, 231-251.

Gorodnitsky, I. F. and Rao, B. D. (1997). Sparse signal reconstruction from limited data using FOCUSS: a re-weighted minimum norm algorithm. *IEEE Transactions in Signal Processing* **45**, 600-616.

Gottlieb, J. P., Kusunoki, M., and Goldberg, M. E. (1998). The representation of visual salience in monkey parietal cortex. *Nature* **391**, 481-484.

Gouras, P. (1968). Identification of cone mechanisms in monkey ganglion cells. *Journal of Physiology* **199**, 533-547.

Grave de Peralta-Menendez, R. and Gonzales-Andino, S. L. (1998). A critical analysis of linear inverse solutions to the neuroelectromagnetic inverse problem. *IEEE Transactions in Biomedical Engineering* **45**, 440-448.

Greenblatt, R. E. (1993). Probablistic reconstruction of multiple sources in the bioelectromagnetic inverse problem. *Inverse Problem* **9**, 271-284.

Greenlee, M. W. and Smith, A. T. (1997). Detection and discrimination of first and second order motion in patients with unilateral brain damage. *Journal of Neuroscience* **17**, 804-818.

Greicius, M. D., Krasnow, B., Reiss, A. L., and Menon, V. (2003). Functional connectivity in the resting brain: a network analysis of the default mode hypothesis. *Proceedings of the National Academy of Science USA* **100**, 253-258.

Grill-Spector, K., Kourtzi, Z., and Kanwisher, N. (2001). The lateral occipital complex and its role in object recognition. *Vision Research* **41**, 1409-1422.

Grill-Spector, K., Kushnir, T., Edelman, S., Avidan-Carmel, G., Itzchak, Y., and Malach, R. (1999). Differential processing of objects under various viewing conditions in the human lateral occipital complex. *Neuron* **24**, 187-203.

Grossman, E. and Blake, R. (1999). Perception of coherent motion, biological motion and form-from-motion under dim light conditions. *Vision Research* **34**, 3721-3727.

Grossman, E., Donnelly, M., Price, R., Pickens, D., Morgan, V., and Neighbor, G. (2000). Brain areas involved in perception of biological motion. *Journal of Cognitive Neuroscience* **12**, 711-720.

Grunewald, A. and Mingolla, E. (1998). Motion aftereffect due to binocular sum of adaptation to linear motion. *Vision Research* **38**, 2963-2971.

Grynszpan, F. and Gesolowitz, D. B. (1973). Model studies of the magnetocardiogram. *Biophysical Journal* **13**, 911-925.

Gusnard, D. A., Akbudak, E., Shulman, G. L., and Raichle, M. E. (2001). Medial prefrontal cortex and sel-referential mental activity: Relation to a default mode of brain function. *Proceedings of the National Academy of Science USA* **98**, 4259-4264.

Gusnard, D. A. and Raichle, M. E. (2001). Searching for a baseline: Functional imaging and the resting human brain. *Nature Reviews Neuroscience* **2**, 685-694.

Hagenbeek, R. D., Rombouts, S. A. R. B., and Barkhof, F. (2001). Interindividual Differences in Stimulus Resonse Curve in the Striate Cortex as a Function of Flicker Frequency: An fMRI Study. *Neuroimage* **13**, S981.

Halliday, A. M. and McDonald, W. I. (1981). Visual evoked potentials. In 'Neurology I: Clinical neurophysiology.' (Eds E. Stolberg and R. R. Young.) pp. 228-258. (Butterworths: London.)

Halpern, A. R. and Kelly, M. H. (1993). Memory biases in left versus right implied motion. *Journal of Experimental Psychology-Learning Memory and Cognition* **19**, 471-484.

Hamalainen, M. (1991). Anatomical correlates for magnetoencephalography: integration with magnetic resonance images. *Clinical Physiology and Physiological Measurement* **12**, 29-32.

Hamalainen, M., Hari, R., Ilmoniemi, R. J., Knuutila, J., and Lounasmaa, O. V. (1993). Magnetoencephalography: Theory, instrumentation and applicationsto noninvasive studies of the working human brain. *Reviews of Modern Physics* **65**, 413-497.

Hamalainen, M. and Sarvas, J. (1989). Realistic conductivity geometry model of the human head for interpolation of neuromagnetic data. *IEEE Transactions in Biomedical Engineering* **36**, 165-171.

Hartline, H. K. (1938). The response of single optic nerve fibres of the vertebrate eye to illumination of the retina. *American Journal of Physiology* **121**, 400-415.

Harvey, P. R. and Mansfield, P. (1994). Avoiding peripheral nerve stimulation: gradient waveform criteria for optimum resolution in echo-planar imaging. *Magnetic Resonance in Medicine* **32**, 236-241.

Hasnain, M. K., Fox, P. T., and Woldorff, M. G. (1998). Intersubject variability of functional areas in the human visual cortex. *Human Brain Mapping* **6**, 301-315.

Hawken, M. J., Shapley, R. M., and Grosof, D. H. (1996). Temporal-Frequency Selectivity in Monkey Visual Cortex. *Visual Neuroscience* **13**, 477-492.

Heeger, D. J., Boynton, G. M., Demb, J. B., Seidemann, E., and Newsome, W. T. (1999). Motion opponency in visual cortex. *Journal of Neuroscience* **19**, 7162-7174.

Heinze, H. J., Mangun, G. R., Burchert, W., Hinrichs, H., Scholz, M., Munte, T. F., Gos, A., Scherg, M., Johannes, S., and Hundeshagen, H. (1994). Combined spatial and temporal imaging of brain activity during visual selective attention in humans. *Nature* **372** , 543-546.

Helmholtz, H. V. (1853). Ober einige Gesetze der Vertheilung elektrischer Str(5me in korperliche Leitem met Anwendung auf die tierisch-elektrischen Versuche. *Annals of physics and Chemistry* **89**, 211-233.

Hendrickson, A. E., Wilson, J. R., and Ogren, M. P. (1978). The neuroanatomical organisation of pathways between the dorsal lateral geniculate nucleus and visual cortex in Old World and New World primates. *Journal of Comparative Neurology* **182**, 123-136.

Hendry, S. H. and Yoshioka, T. (1994). A neurochemically distinct third channel in the macaque dorsal lateral geniculate nucleus. *Science* **264**, 575-577.

Hendry, S. H. C. and Reid, R. C. (2000). The koniocellular pathway in primate vision. *Annual Review of Neuroscience* **23**, 127-153.

Herrmann, C. S. (2001). Human EEG responses to 1-100 Hz flicker: resonance phenomena in visual cortex and their potential correlation to cognitive phenomena. *Experimental Brain Research* **137**, 346-353.

Hess, R. F. and Baker, C. L., Jr. (1984). Assessment of retinal function in severely amblyopic individuals. *Vision Research* **24**, 1367-1376.

Hillebrand, A. The development of constrained source localization algorithms for human imaging. 2000. Aston University, United Kingdom.
Ref Type: Thesis/Dissertation

Hillebrand, A. and Barnes, G. R. (2002). A quantitative assessment of the sensitivity of whole-head MEG to activity in the adult human cortex. *Neuroimage* **16**, 638-650.

Hohnsbein, J. and Mateef, S. (1992). The relation between the velocity of visual motion and the reaction time to motion onset and offset. *Vision Research* **32**, 1789-1791.

Hollants-Gilhuijs, M. A. M., Munck de, J. C., Kubova, Z., Royan van, E., and Spekreijse, H. (2000). The development of hemispheric asymmetry in human motion VEPs. *Vision Research* **40**, 1-11.

Holub, R. A. and Morton-Gibson, M. (1981). Response of visual cortical neurons of the cat to moving sinusoidal gratings: response contrast functions and spatiotemporal interactions. *Journal of Neurophysiology* **46**, 1244-1259.

Hopfinger, J. B., Buonocore, M. H., and Mangun, G. R. (2000). The neural mechanisms of top-down attentional control. *Nature Neuroscience* **3**, 284-291.

Horton, J. C. (1984). Cytochrome oxidase patches: a new cytoarchitectonic feature of monkey visual cortex. *Philosophical Transactions of the Royal Society London* **304**, 199-253.

Horton, J. C. and Hedley-Whyte, E. T. (1984). Mapping of cytochrome oxidase patches and ocular dominance columns in human visual cortex. *Philosophical Transactions of the Royal Society London* **304**, 255-272.

Huang, J. C., Mosher, J. C., and Leahy, R. M. (1999). A sensor weighted overlapping sphere head model and exhaustive head model comparison for MEG. *Physics in Medicine and Biology* **44**, 423-440.

Huang, M., Aine, C. J., Supek, S., Best, E., Ranken, D., and Flynn, E. R. (1998). Multi-start downhill simplex method for spatio-temporal source localisation in magnetoencephalography. *Electroencephalograhy and Clinical Neurophysiology* **108**, 32-44.

Hubbard.T.L. (1990). Cognitive representation of linear motion: Possible direction and gravity effects in judged displacement. *Memory and Cognition* **18**, 299-309.

Hubbard.T.L. (1994). Judged displacement: A modular process. *American Journal of Psychology* **107**, 359-373.

Hubbard.T.L. (1995). Cognitive representation of motion: Evidence for representational friction and gravity analogues. *Journal of Experimental Psychology-Learning Memory and Cognition* **21**, 241-254.

Hubbard.T.L. (1997). Target size and displacement along the axis of implied gravitational attraction: Effects of implied weight and evidence of representational gravity. *Journal of Experimental Psychology-Learning Memory and Cognition* **23**, 1484-1493.

Hubbard.T.L. (1998a). Representational momentum and other displacements in memory as evidence for nonconcious knowledge of physical principles. In 'Towards a science of conciousness: II. The second Tucson discussions and debates.' (Eds S. Hameroff, A. Kaszniak, and A. Scott.) pp. 505-512. (MIT Press: Cambridge, MA.)

Hubbard.T.L. (1998b). Some effects of representational friction, target size and memory averaging on memory for vertically moving objects. *Canadian Journal of Experimental Psychology* **52**, 44-49.

Hubel, D. H. (1988). 'Eye, Brain and Vision.' (Scientific American Library: New york.)

Hubel, D. H. and Wiesel, T. N. (1959). Receptive fields of single neurons in the cat's striate cortex. *Journal of Physiology* **148**, 574-591.

Hubel, D. H. and Wiesel, T. N. (1962). Receptive fields, binocular interaction and functional architecture in the cat's visual cortex. *Journal of Physiology* **160**, 106-154.

Hubel, D. H. and Wiesel, T. N. (1972). Laminar and columnar distribution of geniculocortical fibres in macaque monkey. *Journal of Comparative Neurology* **146**, 421-450.

Hubel, D. H. and Wiesel, T. N. (1977). Functional architecture of macaque visual cortex. *Proceedings of the Royal Society of London* **198**, 1-59.

Huk, A. C., Dougherty, R. F., and Heeger, D. J. (2002). Retinotopy and functional subdivision of human areas MT and MST. *Journal of Neuroscience* **22**, 7195-7205.

Jellama, T. and Perrett, D. I. (2003). Cells in monkey STS responsive to articulated body motions and consequent static posture: a case of implied motion. *Neuropsychologia* **41**, 1728-1737.

Jensen, O., Gelfand, J., Kounios, J., and Lisman, J. E. (2002). Oscillations in the alpha band (9-12Hz) increase with memory load during retention in a short-term memory task. *Cerebral Cortex* **12**, 877-882.

Kaneoke, Y., Bundou, M., and Kakigi, R. (1998). Timing of motion representation in the human visual system. *Brain Research* 201.

Kashikura, K., Kershaw, J., Yamamoto, S., Zhang, X., Matsuura, T., and Kanno, I. (2001). Temporal Characteristics of Event-Related BOLD Response and Visual-Evoked Potentials From Checkerboard Stimulation of Human V1: A Comparison Between Different Control Features. *Magnetic Resonance in Medicine* **45**, 212-216.

Kastner, S., Pinsk, M. A., De Weerd, P., Desimone, R., and Ungerleider, L. G. (1999). Increased activity in human visual cortex during directed attention in the absence of visual stimulation. *Neuron* **22**, 751-761.

Kaufmann, C., Gregor-Konstantin, E., Gossl, C., Putz, B., and Auer, D. P. (2001). Frequency Dependence and Gender Effects in Visual Cortical Regions Involved in Temporal Frequency Dependent Pattern Processing. *Human Brain Mapping* **14**, 28-38.

Kelly, M. H. and Freyd, J. J. (1987). Explorations of Representational Momentum. *Cognitive Psychology* **19**, 369-401.

Kleiser, R., Seitz, R. J., and Krekelberg, B. (2004). Neural correlates of saccadic suppression in humans. *Current Biology* **14**, 386-390.

Klimesch, W. (1999). EEG alpha and theta oscillations reflect cognitive and memory performance: a review and analysis. *Brain Research Reviews* **29**, 169-195.

Klimesch, W., Doppelmayr, M., Rohm, D., Pollhuber, D., and Stadler, W. (2000). Simultaneous desynchronisation and synchronisation of different alpha responses in the human electroencephalograph: a neglected paradox? *Neuroscience Letters* **284**, 97-100.

Klimesch, W., Doppelmayr, M., Russegger, H., Pachinger, T., and Schwaiger, J. (1998). Induced alpha band power changes in the human EEG and attention. *Neuroscience Letters* **244**, 73-76.

Kolb, H., Linberg, K. A., and Fisher, S. K. (1992). Neurons of the human retina: a Golgi study. *Journal of Comparative Neurology* **318**, 147-187.

Kourtzi, Z. (2004). But still it moves. *Trends in Cognitive Sciences* **8**, 47-49.

Kourtzi, Z., Bulthoff, H. H., Erb, M., and Grodd, W. (2002). Object selective responses in the human motion area MT/MST. *Nature Neuroscience* **5**, 17-18.

Kourtzi, Z. and Kanwisher, N. (2000a). Activation in human MT/MST by static images with implied motion. *Journal of Cognitive Neuroscience* **12**, 48-55.

Kourtzi, Z. and Kanwisher, N. (2000b). Cortical regions involved in perceiving object shape. *Journal of Neuroscience* **20**, 3310-3318.

Kozinska, D., Tretiak, O. J., Nissanov, J., and Ozturk, C. (1997). Multidimensional alignment using the euclidiean distance transform. *Graphical Models and Image Processing* **59**, 373-387.

Krekelberg, B., Dannenberg, S., Hoffmann, K. P., Bremmer, F., and Ross, J. (2003). Neural correlates of implied motion. *Nature* **424**, 674-677.

Krukowski, A. E., Troyer, T. W., and Miller, K. D. (2001). A Model of Visual Cortical Temporal Frequency Tuning. *Neurocomputing* **38-40**, 1379-1383.

Kubota, T., Kaneoke, Y., Maruyama, K., Watanabe, Z., and Kakigi, R. (2004). Temporal structure of the apparent motion perception: a magnetoencephalographic study. *Neuroscience Research* **48**, 111-118.

Kwong, K. K., Belliveau, J. W., Chesler, D. A., Goldberg, I. E., Weisskoff, R. M., Poncelet, B. P., Kennedy, D. N., Hoppel, B. E., Cohen, M. S., Turner, R., and . (1992). Dynamic magnetic resonance imaging of human brain activity during primary sensory stimulation. *Proceedings of the National Academy of Science USA* **89**, 5675-5679.

Lagae, L., Maes, H., Raiguel, S., Xiao, D. K., and Orban, G. A. (1994). Responses of macaque STS neurons to optic flow components - a comparison of areas MT and MST. *Journal of Neurophysiology* **71**, 1597-1626.

Lam, K., Kaneoke, Y., Gunji, A., Yamasaki, H., Matsumoto, E., Naito, T., and Kakigi, R. (2000). Magnetic response of human extrastriate cortex in the detection of coherent and incoherent motion. *Neuroscience* **97**, 1-10.

Lauwers, K., Saunders, R., Vogels, R., Vandenbussche, E., and Orban, G. A. (2000). Impairmaent in motion discrimination tasks is unrelated to amount of damage to superior temporal sulcus motion areas. *Journal of Comparative Neurology* **420**, 539-557.

Lee, D. K., Itti, L., Koch, C., and Braun, J. (1999). Attention activates winner-take-all competition among visual filters. *Nature Neuroscience* **2**, 375-381.

Levitt, J. B., Kiper, D. C., and Movshon, J. A. (1994). Receptive Fields and Functional Architecture of Macaque V2. *Journal of Neurophysiology* **71**, 2517-2541.

Levy, R. and Goldman-Rakic, P. (1999). Executive frontal functions. *Journal of Neuroscience* **19**, 5149-5158.

Lewine, J. D. and Orrison, W. W. J. (1995). Magnetic source imaging: basic principles and applications in neuroradiology. *Academic Radiology* **2**, 436-440.

Lewis, J. W., Beauchamp, M. S., and DeYoe, E. A. (2000). A comparison of visual and auditory motion processing in human cerebral cortex. *Cerebral Cortex* **10**, 873-888.

Liu, A. K., Belliveau, J. W., and Dale, A. M. (1998). Spatiotemporal imaging of human brain activity using functional MRI constrained magnetoencephalography data: Monte Carlo simulations. *Proceedings of the National Academy of Science USA* **95**, 8945-8950.

Liu, T., Slotnick, S. D., and Yantis, S. (2004). Human MT+ mediates perceptual filling-in during apparent motion. *Neuroimage* **4**, 1772-1780.

Livingstone, M. S. and Hubel, D. H. (1984). Anatomy and physiology of a color system in the primate visual cortex. *Journal of Neuroscience* **4**, 309-356.

Livingstone, M. S. and Hubel, D. H. (1987a). Connections between layer 4B of area 17 and the thick cytochrome oxidase stripes of area 18 in the squirrel monkey. *Journal of Neuroscience* **7**, 3371-3377.

Livingstone, M. S. and Hubel, D. H. (1987b). Psychophysical evidence for separate channels for the perception of form, colour, movement and depth. *Journal of Neuroscience* **7**, 3416-3468.

Livingstone, M. S. and Hubel, D. H. (1988). Segregation of form, color, movement, and depth: anatomy, physiology, and perception. *Science* **240**, 740-749.

Logothetis, N. K., Pauls, J., Augath, M., Trinath, T., and Oeltermann, A. (2001). Neurophysiological Investigation of the Basis of the fMRI Signal. *Nature* **412**, 150-157.

Lopes da Silva, F. H. (1998). Dynamics of EEGs as signals of neuronal populations: models and theoretical considerations. In 'Electroencephalography: Basic Principles, Clinical Applications and Related Fields.' (Eds E. Niedermeyer and F. H. Lopes da Silva.) pp. 76-92. (Williams and Wilkins: Baltimore.)

Lopes da Silva, F. H. and Pfurtscheller, G. (1999). Basic concepts on EEG synchronisation and desynchronisation. In 'Event-Related Desynchronisation. Vol. 6.' (Eds G.Pfurtscheller and F.H.Lopes da Silva.) pp. 3-11. (Elsevier Science:

Lu, Z. L. and Dosher, B. A. (1998). External noise distinguishes attention mechanisms. *Vision Research* **38**, 1183-1198.

Lu, Z. L. and Sperling, G. (2001). Three-systems theory of human visual motion perception: review and update. *Journal of the Optical Society of America* **A18**, 2331-2370.

Luck, S. J., Chelazzi, L., Hillyard, S. A., and Desimone, R. (1997). Neural mechamisms of spatial selective attention in areas V1, V2 and V4 of macaque visual cortex. *Journal of Neurophysiology* **77**, 24-42.

Lund, J. S. (1988). Anatomical organization of macaque monkey striate visual cortex. *Annual Review of Neuroscience* **11**, 253-288.

Lutzenberger, W., Pulvermuller, F., Elbert, T., and Birbaumer, N. (1995). Visual-stimulation alters local 40-hz responses in humans - an EEG study. *Neuroscience Letters* **183**, 39-42.

Makeig, S., Westerfield, M., Jung, T. P., Enghoff, S., Townsend, J., Courchesne, E., and Sejnowski, T. J. (2002). Dynamic brain sources of visual evoked responses. *Science* **295**, 690-694.

Malach, R., Reppas, J. B., Benson, R. R., Kwong, K. K., Jiang, J., Kennedy, W. A., Ledden, P. J., Brady, T. J., Rosen, B. R., and Tootell, R. B. H. (1995). Object-related activity revealed by functional magnetic imaging in human occipital cortex. *Proceedings of the National Academy of Science USA* **92**, 8135-8139.

Malonek, D., Dimagl, U., Lindauer, U., Yamada, K., Kanno, I., and Grinvald, A. (1997). Vascular imprints of neuronal activity: relationships between the dynamics of cortical blood flow, oxygenation and volume changes following sensory stimulation. *Proceedings of the National Academy of Science USA* **94**, 14826-14831.

Malonek, D. and Grinvald, A. (1996). Interactions between electrical activity and cortical microcirculation revealed by imaging spectroscopy: implications for functional brain mapping. *Science* **272**, 551-554.

Mangun, G. R., Buonocore, M. H., Girelli, M., and Jha, H. P. (1998). ERP and fMRI measures of visual spatial selective attention. *Human Brain Mapping* **6**, 383-389.

Mansfield, P. and Maudsley, A. A. (1977). Medical imaging by NMR. *British Journal of Radiology* **50** , 188-194.

Marcar, V. L., Xiao, D. K., Raiguel, S. E., Maes, H., and Orban, G. A. (1995). Processing of kinetically defined boundaries in the cortical motion area MT of the macaque monkey. *Journal of Neurophysiology* **74**, 1258-1270.

Marrufo, M. V., Vaquero, E., Cardoso, M. J., and Gomez, C. M. (2001). Temporal evolution of alpha and beta bands during visual spatial attention. *Cognitive Brain Research* **12**, 315-320.

Martin, J. H. (2000). 'Neuroanatomy: text and atlas.'

Martinez-Trujillo, J. C. and Treue, S. (2002). Attentional modulation strength in cortical area MT depends on stimulus contrast. *Neuron* **35**, 365-370.

Martinez, A., Anllo-Vento, L., Sereno, M. I., Frank, L. R., Buxton, R. B., Dubowitz, D. J., Wong, E. C., Hinrichs, H., Heinze, H. J., and Hillyard, S. A. (1999). Involvement of striate and extrastriate visual cortical areas in spatial attention. *Nature Neuroscience* **2**, 364-369.

Martinez, A., DiRusso, F., Anllo-Vento, L., Sereno, M. I., Buxton, R. B., and Hillyard, S. A. (2001). Putting Spatial Attention on the Map: Timing and Localisation of Stimulus Selection Processes in Striate and Extrastriate Visual Areas. *Vision Research* **41**, 1437-1457.

Maruyama, K., Kaneoke, Y., Watanabe, K., and Kakigi, R. (2002). Human cortical responses to coherent and incoherent motion as measured by magnetoencephalography. *Neuroscience Research* **44**, 195-205.

Mather, G., Verstraten, F., and Anstis, S. M. (1998). 'The motion aftereffect - a modern perspective.' (MIT Press: Cambridge, MA.)

Maunsell, J. H. R. and Cook, E. P. (2002). The role of attention in visual processing. *Philosophical Transactions of the Royal Society London, Series B* **357**, 1063-1072.

Maunsell, J. H. R. and Newsome, W. T. (1987). Visual processing in monkey extrastriate cortex. *Annual Review of Neuroscience* **10**, 776-783.

Maunsell, J. H. R. and Van Essen, D. C. (1983). Functional Properties of Neurons in Middle Temporal Visual Area of the Macaque Monkey. I. Selectivity for Stimulus Direction, Speed, and Orientation. *Journal of Neurophysiology* **49**, 1127-1147.

Mazoyer, B., Zago, L., Mellet, E., Bricogne, S., Etard, O., Houde, O., Crivello, F., Joliot, M., Petit, L., and Tzourio-Mazoyer (2001). Cortical networks for working memory and executive functions sustain the concious resting state in man. *Brain Research Bulletin* **54**, 287-298.

McAdams, C. J. and Maunsell, J. H. R. (1999). Effects of Attention on Orientation-Tuning Functions of Single Neurons in Macaque Cortical Area V4. *Journal of Neuroscience* **19**, 431-441.

McAdams, C. J. and Maunsell, J. H. R. (2000). Attention to both space and feature modulates neuronal responses in macaque area V4. *Journal of Neurophysiology* **83**, 1751-1755.

McCarthy, G., Spicer, M., Adrignolo, A., Luby, M., Gore, J., and Allison, T. (1995). Brain activation associated with visual motion studied by functional magnetic resonance imaging in humans. *Human Brain Mapping* **2**, 234-243.

McKeefry, D. J., Watson, J. D., Frackowiak, R. S., Fong, K., and Zeki, S. (1997). The activity in human areas V1/V2, V3, and V5 during the perception of coherent and incoherent motion. *Neuroimage* **5**, 1-12.

McKiernan, K. A., Kaufman, J. N., Kucera-Thompson, J., and Binder, J. R. (2003). A parametric manipulation of factors affecting task-induced deactivation in functional imaging. *Journal of Cognitive Neuroscience* **15**, 394-408.

Medvick, P. A., Lewis, P. S., Aine, C., and Flynn, E. R. (1989). Monte Carlo analysis of localisation errors in magnetoencephalography. In 'Advances in Biomagnetism.' (Eds S. J. Williamson, M. Hoke, G. Stroink, and M. Kotani.) (Plenum Press: New York.)

Merigan, W. H. and Maunsell, J. H. R. (1990). Macaque vision after magnocellular lateral geniculate lesion. *Visual Neuroscience* **5**, 347-352.

Morrone, M. C., Fiorentini, A., and Burr, D. C. (1996). Development of the temporal properties of visual evoked potentials to luminance and colour contrast in infants. *Vision Research* **36**, 3141-3155.

Mosher, J. C. and Leahy, R. M. (1998). Recursive MUSIC: A framework for EEG and MEG source localisation. *IEEE Transactions in Biomedical Engineering* **45**, 1342-1354.

Mosher, J. C., Lewis, P. S., and Leahy, R. M. (1992). Multiple dipole modelling and localisation from spatio-temporal MEG data. *IEEE Transactions in Biomedical Engineering* **39**, 541-557.

Motter, B. C. (1993). Focal attention produces spatially selective processing in visual cortical areas V1, V2 and V4 in the presence of competing stimuli. *Journal of Neurophysiology* **70**, 909-919.

Movshon, J. A., Adelson, E. H., Gizzi, M. S., and Newsome, W. T. (1985). The analysis of moving visual patterns. In 'Pattern recognition mechanisms.' (Springer: Berlin.)

Muller, J. R., Metha, A. B., Krauskopf, J., and Lennie, P. (2001). Information conveyed by onset transients in responses of striate cortical neurons. *Journal of Neuroscience* **21**, 6978-6990.

Nackayama, K. and Mackeben, M. (1989). Sustained and transient components of focal visual attention. *Vision Research* **29**, 1631-1646.

Nagai, M. and Yagi, A. (2001). The pointedness effect on representational momentum. *Memory and Cognition* **29**, 91-99.

Nakamura, H., Kashii, S., Nagamine, T., Matsui, Y., Hashimoto, T., Honda, Y., and Shibasaki, H. (2003). Human V5 demonstrated by magnetoencephalography using random dot kinematograms of different coherence levels. *Neurosci.Res.* **46**, 423-433.

Newsome, W. T., Britten, K. H., and Movshon, J. A. (1989). Neuronal correlates of perceptual decision. *Nature* **341**, 52-54.

Newsome, W. T., Britten, K. H., Salzman, C. D., and Movshon, J. A. (1990). 'Neuronal mechanisms of motion perception, Cold Spring Harbour symposia on quantitative biology, vol LV.' (Cold Spring Harbour Laboratories press:

Nichols, T. E. and Holmes, A. P. (2002). Nonparametric permutation tests for functional neuroimaging: a primer with examples. *Human Brain Mapping* **15**, 1-25.

Niedeggen, M. and Wist, E. R. (1999). Characteristics of visual evoked potentials generated by motion coherence onset. *Cognitive Brain Research* **8**, 95-105.

Nobre, A. C., Sebestyen, G. N., Gitelman, D. R., Mesulam, M. M., Frackowiak, R. S., and Frith, C. (1997). Functional localisation of the system for visuospatial attention using positron emission tomography. *Brain* **120**, 515-533.

Noesselt, T., Hillyard, S. A., Woldorff, M. G., Schoenfeld, A., Hagner, T., Jancke, L., Tempelmann, C., Hinrichs, H., and Heinze, H. J. (2002). Delayed striate cortical activation during spatial attention. *Neuron* **35**, 575-587.

Nunez, P. L. (1986). The brain's magnetic field: some effects of multiple sources on localization methods. *Electroencephalograhy and Clinical Neurophysiology* **63**, 75-82.

Ogawa, S., Menon, R. S., Tank, D. W., Kim, S. G., Merkle, H., Ellermann, J. M., and Ugurbil, K. (1993). Functional brain mapping by blood oxygenation level-dependent contrast magnetic resonance imaging: a comparison of signal characteristics with a biophysical model. *Biophysics journal* **64**, 803-812.

Ogawa, S., Tank, D. W., Menon, R., Ellermann, J. M., Kim, S. G., Merkle, H., and Ugurbil, K. (1992). Intrinsic signal changes accompanying sensory stimulation: functional brain mapping with magnetic resonance imaging. *Proceedings of the National Academy of Science USA* **89**, 5951-5955.

Okada, Y. (1982). Neurogenesis of evoked magnetic fields. In 'Biomagnetism: An interdisciplinary approach.' (Eds S. Williamson, G. L. Romani, L. Kaufman, and I. Modena.) (Pergamon Press: New York.)

Okada, Y. C., Wu, J., and Kyuhou, S. (1997). Genesis of MEG signals in a mammalian CNS structure. *Electroencephalograhy and Clinical Neurophysiology* **103**, 474-485.

Olveczky, B. P., Baccus, S. A., and Meister, M. (2003). Segregation of object and background motion in the retina. *Nature* **423**, 401-408.

Orban, G. A. (1997). Visual processing in macaque area MT/V5 and its satellites (MSTd and MSTv). In 'Cerebral Cortex.' (Eds K. S. Rockland, J. H. Kaas, and A. Peters.) pp. 359-379. (Plenum Press: New York.)

Orban, G. A., Saunders, R. C., and Vandenbussche, E. (1995). Lesions of the superior temporal cortical motion areas impair speed discrimination in the macaque monkey. *European Journal of Neuroscience* **7**, 2261-2276.

Orban, G. A., Vanduffel, W., and Tootell, R. B. H. (1997). Macaque visual areas involved in motion processing: a functional imaging study. *Society of Neuroscience Abstracts* **23**.

Ozus, B., Liu, H., Chen, L., Iyer, M. B., Fox, P. T., and Gao, J. (2001). Rate Dependence of Human Visual Cortical Response Due to Brief Stimulation: An Event-Related fMRI Study. *Magnetic Resonance Imaging* **19**, 21-25.

Pal, N. P. and Pal, S. K. (1993). A review on image segmentation techniques. *Pattern Recognition* **26**, 1277-1294.

Pasqual-Marqui, R. D., Michel, C. M., and Lehmann, D. (1994). Low resolution electromagnetic tomography: a new method for localising electrical activity in the brain. *International Journal of Psychophysiology* **18**, 49-65.

Pasternak, T. and Merigan, W. H. (1994). Motion perception following lesions of the superior temporal sulcus in the monkey. *Cerebral Cortex* **4**, 247-259.

Perrone, J. A. and Thiele, A. (2001). Speed skills: measuring the visual speed analyzing properties of primate MT neurons. *Nature Neuroscience* **4**, 526-532.

Perrone, J. A. and Thiele, A. (2002). A model of speed tuning in MT neurons. *Vision Research* **42**, 1035-1051.

Petit, L. and Haxby, J. V. (1999). Functional anatomy of pursuit eye movements as revealed by fMRI. *Journal of Neurophysiology* **82**, 463-471.

Pfurtscheller, G. (1992). Event-related synchronisation (ERS): and electrophysiological correlate of cortical areas at rest. *Electroencephalography and clinical Neurophysiology* **83**, 62-69.

Pfurtscheller, G. and Aranibar, A. (1977). Event-related cortical desynchroisation detected by power measurements of scalp EEG. *Electroencephalograhy and Clinical Neurophysiology* **42**, 817-826.

Pfurtscheller, G. and Lopes da Silva, F. H. (1999a). Event-Related EEG/MEG Synchronisationand Desynchronisation: Basic Principles. *Clinical Neurophysiology* **110**, 1842-1857.

Pfurtscheller, G. and Lopes da Silva, F. H. (1999b). Functional meaning of event-related desynchronisation (ERD) and synchronisation (ERS). In 'Event-Related Desynchronisation: Handbook of Electroencephalography and Clinical Neurophysiology, Revised Series, Vol. 6.' (Eds G.Pfurtscheller and F.H.Lopes da Silva.) (Elsevier:

Pfurtscheller, G., Stancak Jr, A., and Edlinger, G. (1997). On the existance of different types of central beta rhythms below 30Hz. *Electroencephalograhy and Clinical Neurophysiology* **102**, 316-325.

Pfurtscheller, G., Stancak, A., and Neuper, C. (1996). Event related synchronisation (ERS) in the alpha band-an electrophysiological correlate of cortical idling: a review. *International Journal of Psychophysiology* **24**, 39-46.

Plewnia, R. C., Hummel, F., and Gerloff, C. (2003). Event-related desynchronisation and excitability of the ipsilateral motor cortex during simple self-paced finger movements. *Clinical Neurophysiology* **114**, 1819-1826.

Polhemus. 3Space, ISOTRAK. User's Manual. 1992.
Ref Type: Pamphlet

Polyak, S. L. (1941). 'The Retina.' (University of Chicago Press: Chicago.)

Posner, M. (1980). Orienting of attention. *Quarterly Journal of Experimental Psychology* **32**, 25.

Qian, N. and Andersen, R. A. (1994). Transparent motion perception as detection of unbalanced motion signals. *Journal of Neuroscience* **14**, 7367-7380.

Quian Quiroga, R., Basar, E., and Schurmann, M. (2000). Phase locking of event related alpha oscillations. In 'Chaos in brain?' (Eds K.Lehnertz, C.E.Elger, J.Arnhold, and P.Grassberger.) pp. 301-304. (World Scientific:

Rager, G. and Singer, W. (1998). The response of cat visual cortex to flicker stimuli of variable frequency. *European Journal of Neuroscience* **10**, 1856-1877.

Raichle, M. E. (1994). Visualising the mind. *Scientific American* **270**, 58-64.

Raichle, M. E., Macleod, A. M., Snyder, A. Z., Powers, W. J., Gusnard, D. A., and Shulman, G. L. (2001). A default mode of brain function. *Proceedings of the National Academy of Science USA* **98**, 676-682.

Ray, W. J. and Cole, H. W. (1985). EEG alpha activity reflects attentional demands and beta activity reflects emotional and cognitive processes. *Science* **228**, 750-752.

Recanzone, G. H. and Wurtz, R. H. (2000). Effects of attention on MT and MST neuronal activity during pursuit initiation. *Journal of Neurophysiology* **83**, 777-790.

Reed, C. and Vinson, N. (1996). Conceptual effects on representational momentum. *Journal of Experimental Psychology-human perceptual performance* **22**, 839-850.

Rees, G., Friston, K., and Koch, C. (2000). A direct quantitative relationship between the functional properties of human and macaque V5. *Nature Neuroscience* **3**, 716-723.

Regan, D. (2003). 'Human Brain Electrophysiology: Evoked Potentials and Evoked Magnetic Fields in Science and Medicine.' (Elsevier: New York.)

Reynolds, J. H. and Desimone, R. (1999). The role of neural mechanisms of attention in solving the binding problem. *Neuron* **24**, 19-29.

Reynolds, J. H. and Desimone, R. (2003). Interacting roles of attention and visual salience in V4. *Neuron* **37**, 853-863.

Reynolds, J. H., Pasternak, T., and Desimone, R. (2000). Attention increases sensitivity of V4 neurons. *Neuron* **26**, 703-714.

Robinson, S. E. and Vrba, J. (1999). Functional Neuroimaging by Synthetic Aperture Magnetometry (SAM).' pp. 302-305. (Tohoku Univ. Press, Sendai:

Rodman, H. R. and Albright, T. D. (1987). Coding of Visual Stimulus Velocity in Area MT of the Macaque. *Vision Research* **27**, 2035-2048.

Rodman, H. R., Gross, C. G., and Albright, T. D. (1989). Afferent basis of visual responses in area MT of the macaque. I. Effects of striate removal. *Journal of Neuroscience* **9**, 2033-2050.

Rodman, H. R., Gross, C. G., and Albright, T. D. (1990). Afferent basis of visual responses in area MT of the macaque. II. Effects of superior colliculus removal. *Journal of Neuroscience* **10**, 1154-1164.

Romani, G. L. (1989). Fundamentals on neuromagnetism. In 'Advances in Biomagnetism.' (Eds S. J. Williamson, M. Hoke, G. Stroink, and M. Kotani.) (Plenum Press: New York.)

Rosen, B. R., Buckner, R. L., and Dale, A. M. (1998). Event-related fMRI: past, present and future. *Proceedings of the National Academy of Science USA* **95**, 773-780.

Rudolph, K. and Pasternak, T. (1999). Transient and permanent deficits in motion perception after lesions of cortical areas MT and MST in the macaque monkey. *Cerebral Cortex* **9**, 90-100.

Sandell, J. H. and Schiller, P. H. (1982). Effect of cooling area 18 on striate cortex cells in the squirrel monkey. *Journal of Neurophysiology* **48**, 38-48.

Sarvas, J. (1987). Basic mathematical and electromagnetic concepts of the biomagnetic inverse problem. *Physics in Medicine and Biology* **32**, 11-22.

Sayers, B., Mc, A., Beayley, H. A., and Henshall, W. R. (1974). The mechanism of auditory evoked EEG responses. *Nature* **247**, 481-483.

Scannel, J. W. and Young, M. P. (1999). Neuronal population activity and functional imaging. *Proceedings of the Royal Society of London, Biological Sciences* **266**, 875-881.

Schellart, N. A. M., Trindade, M. J. G., Reits, D., Verbunt, J. P. A., and Spekreijse, H. (2004). Temporal and spatial congruence of components of motion-onset evoked responses investigated by whole-head magneto-electroencephalography. *Vision Research* **44**, 119-134.

Scherg, M. and Berg, P. (1991). Use of prior knowledge in brain electromagnetic source analysis. *Brain Topography* **4**, 143-150.

Schiller, P. H. and Logothetis, N. K. (1990). The color-opponent and broad-band channels of the primate visual system. *Trends in Neurosciences* **13**, 392-398.

Schiller, P. H., Logothetis, N. K., and Charles, E. R. (1990a). Functions of the colour-opponent and broad-band channels of the visual system. *Nature* **343**, 68-70.

Schiller, P. H., Logothetis, N. K., and Charles, E. R. (1990b). Role of the color-opponent and broad-band channels in vision. *Visual Neuroscience* **5**, 321-346.

Schiller, P. H. and Malpeli, J. G. (1977). Properties and tectal projections of the monkey retinal ganglion cells. *Journal of Neurophysiology* **40**, 428-445.

Schiller, P. H., Sandell, J. H., and Maunsell, J. H. (1986). Functions of the ON and OFF channels of the visual system. *Nature* **322**, 824-825.

Schneider, G. E. (1969). Two visual systems. *Science* **163**, 595-602.

Schofield, A. J. (2000). What does second-order vision see in an image? *Perception* **29**, 1071-1086.

Schwartz, D., Lemoine, D., Poiseau, E., and Barillot, C. (1996). Registration of MEG/EEG data with 3D MRI: methodology and precision issues. *Brain Topography* **9**, 101-116.

Sclar, G. and Freeman, R. D. (1982). Orientation selectivity in the cats striate cortex is invariant with stimulus contrast. *Experimental Brain Research* **46**, 457-461.

Seiffert, A. E., Somers, D. C., Dale, A. M., and Tootell, R. B. H. (2003). Functional MRI studies of human visual motion perception: texture, luminance, attention and after-effects. *Cerebral Cortex* **13**, 340-349.

Sekihara, K., Scholtz, B., Bruder, H., and Graumann, R. (1994). Reconstructing current distributions from biomagnetic measurements under large external noise disturbances. *IEEE Transactions in Medical Imaging* **13**, 144-151.

Senior, C., Barnes, J., Giampietro, V., Simmons, A., Bullmore, E. T., Brammer, M., and David, A. S. (2000). The functional neuroanatomy of implicit-motion perception or 'representational momentum'. *Current Biology* **10**, 16-22.

Senior, C., Ward, J., and David, A. S. (2002). Representational momentum and the brain: An investigation into the functional necessity of V5/MT. *Visual Cognition* **9**, 81-92.

Sewards, T. V. and Sewards, M. A. (1999). Alpha-band oscillations in visual cortex: part of the neural correlate of visual awareness? *International Journal of Psychophysiology* **32** , 35-45.

Shipp, S., de Jong, B. M., Zihl, J., Frackowiak, R. S., and Zeki, S. (1994). The brain activity related to the to residual motion vision in a patient with bilateral lesions of V5. *Brain* **117**, 1023-1038.

Shipp, S. and Zeki, S. (1985a). Segregated output to area V5 from layer 4B of macaque monkey striate cortex. *Journal of Physiology* **369**, 32P.

Shipp, S. and Zeki, S. M. (1985b). Segregation of pathways leading from area V2 to areas V4 and V5 of macaque monkey visual cortex. *Nature* **315**, 322-325.

Shipp, S. and Zeki, S. M. (1989a). The organisation of connections between areas V5 and V1 in the macaque monkey visual cortex. *European Journal of Neuroscience* **1**, 309-332.

Shipp, S. and Zeki, S. M. (1989b). The organisation of connections between areas V5 and V2 in the macaque monkey visual cortex. *European Journal of Neuroscience* **1**, 333-354.

Shmuel, A., Yacoub, E., Pfeuffer, J., Van De Moortele, P. F., Adriany, G., Hu, X., and Ugurbil, K. (2002). Sustained negative BOLD, blood flow and oxygen consumption response and its coupling to the positive response in the human brain. *Neuron* **36**, 1195-1210.

Shulman, G. L., Fiez, J. A., Corbetta, M., Buckner, R. L., Miezin, F. M., Raichle, M. E., and Pertersen, S. E. (2001). Common blood flow changes across visual tasks: II. Decreases in cerebral cortex. *Journal of Cognitive Neuroscience* **9**, 648-663.

Shulman, G. L., Ollinger, J. M., Akbudak, E., Conturo, T. E., Snyder, A. Z., Petersen, S. E., and Corbetta, M. (1999). Areas involved in encoding and applying directional expectations to moving objects. *Journal of Neuroscience* **19**, 9480-9496.

Silberstein, R. B. (1995). Steady-state visual evoked potentials, brain resources and cognitive processes. In 'Neocortical dynamics and human EEG rhythms.' (Ed P. L. Nunez.) pp. 272-303. (Oxford University Press: Oxford.)

Sillito, A. M., Jones, H. E., Gerstein, G. L., and West, D. C. (1994). Feature-linked synchronisation of thalamic relay cell firing induced by feedback from the visual cortex. *Nature* **369**, 479-482.

Singer, W. (1993). Synchronisation of cortical activity and its putative role in information processing and learning. *Annual Review of Physiology* **55**, 349-374.

Singh, K. D., Barnes, G. R., and Hillebrand, A. (2003). Group imaging of task-related changes in cortical synchronisation using nonparametric permutation testing. *Neuroimage* **19**, 1589-1601.

Singh, K. D., Barnes, G. R., Hillebrand, A., Forde, E. m. E., and Williams, A. L. (2002). Task-Related Changes in Cortical Synchronisation are Spatially Coincident with the Haemodynamic Response. *Neuroimage*.

Singh, K. D., Holliday, I. E., Furlong, P. L., and Harding, G. F. A. (1997). Evaluation of MRI - MEG/EEG co-registration strategies using Monte Carlo simulation. *Electroencephalograhy and Clinical Neurophysiology* **102**, 81-85.

Singh, K. D., Smith, A. T., and Greenlee, M. W. (2000). Spatiotemporal frequency and direction sensitivities of human visual areas measured using fMRI. *Neuroimage* **12**, 550-564.

Skottun, B. C., Bradley, A., Sclar, G., Ohzawa, I., and Freeman, R. D. (1987). The effects of contrast on visual orientation and spatial frequency discrimination: a comparison of single cells and behaviour. *Journal of Neurophysiology* **57**, 773-786.

Smeets, J. B. J. and Brenner, E. (1994). The difference between the perception of absolute and relative motion: a reaction time study. *Vision Research* **34**, 191-195.

Smith, A. T. (1994). The detection of second-order motion. In 'Visual detection of motion.' pp. 145-176. (Academic press: London.)

Smith, A. T., Greenlee, M. W., Singh, K. D., Kraemer, F. M., and Hennig, J. (1998). The processing of first- and second-order motion in human visual cortex assessed by functional magnetic resonance imaging (fMRI). *The Journal of Neuroscience* **18**, 3816-3830.

Smith, A. T., Singh, K. D., and Greenlee, M. W. (2000). Attentional Suppression of Activity in the Human Visual Cortex. *Neuroreport* **11**, 271-277.

Smith, A. T., Williams, A. L., and Singh, K. D. (2004). Negative BOLD in the visual cortex: Evidence against blood stealing. *Human Brain Mapping* **21**, 213-220.

Smith, M. A., Bair, W., and Movshon, J. A. (2002). Signals in macaque striate cortical neurons that support the perception of Glass patterns. *The Journal of Neuroscience* **22**, 8334-8345.

Snowden, R. J., Treue, S., and Andersen, R. A. (1992). The response of area MT and V1 of the alert rhesus monkey to moving random dot patterns. *Experimental Brain Research* **88**, 389-400.

Snowden, R. J., Treue, S., Erickson, R. G., and Andersen, R. A. (1991). The response of area MT and V1neurons to transparent motion. *Journal of Neuroscience* **11**, 2766-2785.

Somers, D. C., Dale, A. M., Seiffert, A. E., and Tootell, R. B. H. (1999). Functional MRI Reveals Spatially Specific Attentional Modulation in Human Primary Visual Cortex. *Proceedings of the National Academy of Science USA* **96**, 1663-1668.

Spekreijse, H. Analysis of EEG responses in man evoked by sine wave modulated light. 1966. University of Amsterdam.
Ref Type: Thesis/Dissertation

Spelke, E. S. (1982). Perceptual knowledge of objects in infancy. In 'Perspectives in mental representation.' (Eds J. Mehler, M. Garrett, and E. Walker.) (Erlbaum: Hillsdale, N.J.)

Spitzer, H. and Richmond, B. J. (1991). Task difficulty: ignoring, attending to and discriminating a visual stimulus yield progressively more activity in inferior temporal neurons. *Experimental Brain Research* **83**, 340-348.

Steinmetz, H., Furst, G., and Freund, H. J. (1990). Variation of perisylvian and calcarine anatomical landmarks with stereotaxic proportional coordinates. *American Journal of Neuroradiology* **11**, 1123-1130.

Steriade, M. and Llinas, R. (1988). The functional states of the thalamus and the associated neuronal interplay. *Physics Review* **68**, 649-742.

Sunaert, S., Van Hecke, P., Marchal, G., and Orban, G. A. (1999). Motion responsive areas of the human brain. *Experimental Brain Research* **127**, 355-370.

Swinney, K. R. and Wikswo Jr, J. P. (1980). A calculation of the magnetic field of a nerve action potential. *Biophysical Journal* **32**, 719-732.

Talairach, J. and Tournoux, P. (1988). 'Co-planar stereotaxic atlas of the human brain.' (Thieme Medical Publishers Inc: New York.)

Thiele, A., Dobkins, K. R., and Albright, T. D. (1999). The contribution of colour to motion processing in macaque middle temporal area. *Journal of Neuroscience* **19**, 6571-6587.

Thomas, C. G. and Menon, R. S. (1998). Amplitude Response and Stimulus presentation Frequency response of Human primary Viual Cortex using BOLD EPI at 4T. *Magnetic Resonance in Medicine* **40**, 203-209.

Thulborn, K. R. (1982). Oxygenation dependence of the transverse relaxation time of water protons in whole blood at high field. *Biochemica et Biophysica Acta* **714**, 265-270.

Tolhurst, D. J. (1973). Seperate channels for the analysis of the shape and movement of a moving stimulus. *Journal of Physiology* **231**, 385-402.

Tolhurst, D. J. and Movshon, J. A. (1975). Spatial and temporal contrast sensitivity of striate cortical neurones. *Nature* **257**, 674-675.

Tootell, R. B., Mendola, J. D., Hadjikhani, N. K., Liu, A. K., and Dale, A. M. (1998a). The representation of the ipsilateral visual field in human cerebral cortex. *Proceedings of the National Academy of Science USA* **95**, 818-824.

Tootell, R. B., Reppas, J. B., Kwong, K. K., Malach, R., Born, R. T., Brady, T. J., Rosen, B. R., and Belliveau, J. W. (1995a). Functional analysis of of human MT and related visual cortical areas using magnetic resonance imaging. *Journal of Neuroscience* **15**, 3215-3230.

Tootell, R. B. H., Hadjikhani, N., Hall, E. K., Marrett, S., Vanduffel, W., Vaughan, J. T., and Dale, A. M. (1998b). The retinotopy of visual spatial attention. *Neuron* **21**, 1409-1422.

Tootell, R. B. H., Hadjikhani, N., Vanduffel, W., Liu, A. K., Mendola, J. D., Serano, M. I., and Dale, A. M. (1998c). Functional analysis of primary visual cortex (V1) in humans. *Proceedings of the National Academy of Science USA* **95**, 811-817.

Tootell, R. B. H., Mendola, J. D., Hadjikhani, N. K., Ledden, P. J., Liu, A. K., Reppas, J. B., Serano, M. I., and Dale, A. M. (1997). Functional Analysis of V3A and Related Areas in Human Visual Cortex. *Journal of Neuroscience* **17**, 7060-7078.

Tootell, R. B. H., Reppas, J. B., Dale, A. M., Look, R. B., Serano, M. I., and Malach, R. (1995b). Visual motion aftereffect in human cortical area MT revealed by functional magnetic resonance imaging. *Nature* **375**, 139-141.

Tootell, R. B. H., Reppas, J. B., Kwong, K. K., Malach, R., Born, R. T., Brady, T. J., Rosen, B. R., and Belliveau, J. W. (1995c). Functional Analysis of Human MT and Related Visual Cortical Areas Using Magnetic Resonance Imaging. *Journal of Neuroscience* **15**, 3215-3230.

Treue, S. (2000). Neural correlates of attention in primate visual cortex. *Trends in Neurosciences* **24**, 295-300.

Treue, S. (2003). Visual attention: the where, what, how and why of saliency. *Current Opinion in Neurobiology* **13**, 428-432.

Treue, S. and Martinez-Trujillo, J. C. (1999). Feature based attention influences motion processing gain in macaque visual cortex. *Nature* **399**, 575-579.

Treue, S. and Maunsell, J. H. (1996). Attentional modulation of visual motion processing in cortical areas MT and MST. *Nature* **382**, 539-541.

Tynan, P. D. and Sekular, R. (1982). Motion processing in peripheral vision: reaction time and perceived velocity. *Vision Research* **22**, 61-68.

Ungerleider, L. G., Courtney, S. M., and Haxby, J. V. (1998). A neural system for human visual working memory. *Proceedings of the National Academy of Science USA* **95**, 883-890.

Ungerleider, L. G. and Mishkin, M. (1979). The striate projection in the superior temporal sulcus of Macaca mulatta: location and topographic organisation. *Journal of Comparative Neurology* **188**, 347-366.

Ungerleider, L. G. and Mishkin, M. (1982). Two cortical visual systems. In 'Analysis of Visual Behavior.' (Eds D. J. Ingle, M. A. Goodale, and R. J. W. Mansfield.) pp. 549-586. (MIT Press: Cambridge, MA.)

Vafaee, M. S. and Gjedde, A. (2000). Model of blood-brain transfer of oxygen explains nonlinear flow-metabolism coupling during stimulation of visual cortex. *Journal of Cerebral Blood Flow and Metabolism* **20**, 747-754.

Vafaee, M. S., Marrett, S., Meyer, E., Evans, A. C., and Gjedde, A. (1998). Increased oxygen consumption in human visual cortex: response to visual stimulation. *Acta Neurol.Scand.* **98**, 85-89.

Vafaee, M. S., Meyer, E., Marrett, S., Paus, T., Evans, A. C., and Gjedde, A. (1999). Frequency-Dependent Changes in Cerebral Metabolic Rate of Oxygen During Activation of Human Visual Cortex. *Journal of Cerebral Blood Flow and Metabolism* **19**, 272-277.

Vaina, L. M., Soloviev, S., Bienfang, D. C., and Cowey, A. (2000). A lesion of cortical area V2 selectively impairs the perception of the direction of first-order visual motion. *Neuroreport* **11**, 1039-1044.

Van Essen, D. C. (1985). Functional organization of primate visual cortex. In 'Cerebral Cortex.' (Eds A. Peters and E. G. Jones.) (Plenum Publishing Company: New York.)

Van Essen, D. C., Anderson, C. H., and Felleman, D. J. (1992). Information processing in the primate visual system: an integrated systems perspective. *Science* **255**, 419-423.

Van Essen, D. C., Felleman, D. J., De Yoe, E. A., and Knierim, J. J. (1993). Probing the Primate Visual Cortex: Pathways and Perspectives. In 'Functional organization of the human visual cortex.' (Eds B. Gulyas, D. Ottoson, and P. E. Roland.) (Pergamon Press: Oxford.)

Van Essen, D. C., Felleman, D. J., DeYoe, E. A., Olvarria, J., and Knierim, J. J. (1990). Modular and hierarchichal organization of extrastriate visual cortex in the macaque monkey. *Quantitative Biology* **55**, 679.

Van Essen, D. C., Maunsell, J. H. R., and Bixby, J. L. (1981). The middle temporal visual area in the macaque: myeloarchitecture, connections, functional properties and topographic representation. *Journal of Comparative Neurology* **199**, 293-326.

Van Essen, D. C. and Zeki, S. (1978). The topographic organisation of rhesus monkey prestriate cortex. *Journal of Physiology* **277**, 193-226.

Van Oostende, S., Sunaert, S., Van Hecke, P., Marchal, G., and Orban, G. A. (1997). The kinetic occipital (KO) region in man: an fMRI study. *Cerebral Cortex* **7**, 690-701.

Van Veen, B. D. and Buckley, K. M. (1988). Beamforming: a versatile approach to spatial filtering. *IEEE ASSP Magazine* **4**, 4-24.

Van Veen, B. D., Van Drongelan, W., Yuchtman, M., and Sukuki, A. (1997). Localization of brain electrical activity via linearly constrained minimum variance spatial filtering. *IEEE Transactions of Biomedical Engineering* **44**, 867-880.

Vandenberghe, R., Duncan, J., Dupont, P. G., Ward, R., Poline, J. B., Bormans, S., Michiels, J., Mortelmans, L., and Orban, G. A. (1997). Attention to one or two features in left or right visual field: a positron emission tomography study. *Journal of Neuroscience* **17**, 3739-3750.

Vanduffel, W., Fize, D., Mandeville, J. B., Nelissen, K., Van Hecke, P., Rosen, B. R., Tootell, R. B. H., and Orban, G. A. (2001). Visual motion processing investigated using contrast-agent enhanced fMRI in awake behaving monkeys. *Neuron* **32**, 565-577.

Vogt, B. A., Finch, D. M., and Olson, D. R. (1992). Functional heterogeneity in cingulate cortex: the anterior executive and posterior evaluative regions. *Cerebral Cortex* **2**, 435-443.

Vrba, J. (1997). Baseline opimisation for noise cancellation systems. *IEEE-EMBS*.

Vrba, J. and Robinson, S. E. Differences between Synthetic Aperture Magnetometry (SAM) and linear beamformers. Neonen, J., Ilmoniemi, T., and Katilia, T. 12th International Conference on Biomagnetism, 681-684. 2001a. Espoo, Finland, Helsinki university of Technology.
Ref Type: Conference Proceeding

Vrba, J. and Robinson, S. E. (2001b). Signal processing in magnetoencephalography. *Methods* **25**, 249-271.

Wandell, B. A. (1999). Computational neuroimaging of human visual cortex. *Annual Review Neuroscience* **22**, 145-173.

Wandell, B. A., Engel, S. A., and Hel-Or, H. Z. (1996). Creating images of the flattened cortical sheet. *Investigative Opthamology and Vision Science* **37**, 81.

Wang, B., Toro, C., Zeffiro, T. A., and Hallett, M. (1994). Head surface digitisation and registration: a method for mapping positions on the head onto magnetic resonance images. *Brain Topography* **6**, 185-192.

Wang, J.-Z. (1993). Minimum-norm least squares estimation: magnetic source images for a spherical model head. *IEEE Transactions in Biomedical Engineering* **40**, 387-396.

Wang, J.-Z., Williamson, S. J., and Kaufman, L. (1992). Magnetic source images determined by a lead-field analysis: The unique minimum-norm least squares estimation. *IEEE Transactions in Biomedical Engineering* **39**, 665-675.

Wassle, H., Grunert, U., Rohrenbeck, J., and Boycott, B. B. (1989). Cortical magnification factor and the ganglion cell density of the primate retina. *Nature* **341**, 643-646.

Watanabe, M. and Rodieck, R. W. (1989). Parasol and midget ganglion cells of the primate retina. *The Journal of Comparative Neurology* **289**, 434-454.

Watanabe, T., Harner, A. M., Miyauchi, S., Sasaki, Y., Nielsen, M., Palomo, D., and Mukai, I. (1998). Task-Dependent Influences of Attention on the Activation of Human Primary Visual Cortex. *Proceedings of the National Academy of Science USA* **95**, 11489-11492.

Watson, A. B., Ahumada, A. J., and Farrell, J. E. (1986). Window of visibility: A psychophysical theory of fidelity in time-sampled visual motion displays. *Journal of the Optical Society of America* **3**, 300-307.

Watson, A. B., Barlow, H. B., and Robson, J. G. (1983). What does the eye see best. *Nature* **302**, 419-422.

Watson, A. B. and Turano, K. (1995). The optimal motion stimulus. *Vision Research* **35**, 325-336.

Watson, J. D., Myers, R., Frackowiak, R. S., Hajnal, J. V., Woods, R. P., Mazziotta, J. C., Shipp, S., and Zeki, S. (1993). Area V5 of the human brain: evidence from a combined study using positron emission tomography and magnetic resonance imaging. *Cerebral Cortex* **3**, 79-94.

Wenderoth, P., Watson, J. D. G., Egan, G. F., Tochon-Danguy, H. J., and O'Keefe, G. J. (1999). Second order components of moving plaids activate extrastriate cortex: a positron emission tomography study. *Neuroimage* **9**, 227-234.

White, A. J. R., Soloman, S. G., and Martin, P. R. (2001). Spatial properties of koniocellular cells in the lateral geniculate nucleus of the marmoset. *Journal of Physiology* **533**, 519-535.

White, H., Minor, S. W., Merrell, J., and Smith, T. (1993). Representational momentum effects in the cerebral hemispheres. *Brain and Cognition* **22**, 161-170.

Wiesel, T. N. and Hubel, D. H. (1966). Spatial and chromatic interactions in the lateral geniculate body of the rhesus monkey. *Journal of Neurophysiology* **29**, 1115-1156.

Wikswo, J. P. (1989). Biomagnetic sources and their models. In 'Advances in Biomagnetism.' (Eds S. J. Williamson, M. Hoke, G. Stroink, and M. Kotani.) (Plenum Press: New York.)

Williams, D. and Sekular, R. (1984). Coherent global motion percepts from stochastic local motions. *Vision Research* **24**, 55-62.

Wist, E. R., Gross, J. D., and Niedeggen, M. (1994). Motion aftereffects with random-dot checkerboard kinetograms: relation between psychophysical and VEP measures. *Perception* **23** , 1155-1162.

Worden, M. S., Foxe, J. J., Wang, N., and Simpson, G. V. (2000). Anticipatory biasing of visuospatial attention indexed by retinotopically specific alpha-band electroencephalography increases over occipital cortex. *Journal of Neuroscience* **20**, art-RC63.

Worsley, K. J. and Friston, K. J. (1995). Analysis of fMRI time-series revisited again. *Neuroimage* **2**, 173-181.

Wu, S. M. (1991). Input-output relations of the feedback synapse between horizontal cells and cones in the tiger salamander retina. *Journal of Neurophysiology* **65**, 1197-1206.

Wu, S. M. (1994). Synaptic transmission in the outer retina. *Annual Review of Physiology* **56**, 141-168.

Xu, X., Ichida, M. J., Allison, J. D., Boyd, J. D., Bonds, A. B., and Casagrande, V. A. (2001). A comparison of koniocellular, magnocellular and parvocellular receptive field properties in the lateral geniculate nucleus of the owl monkey. *Journal of Physiology* **531**, 203-218.

Yamagishi, N., Callan, D. E., Goda, N., Anderson, S. J., Yoshida, Y., and Kawato, M. (2003). Attentional modulation of oscillatory activity in human visual cortex. *Neuroimage* **20**, 98-113.

Yeshurun, Y. and Carrasco, M. (2000). The locus of attentional effects in texture segmentation. *Nature Neuroscience* **3**, 627.

Zeki, S., Watson, J. D. G., Lueck, C. J., Friston, K. J., Kennard, C., and Frackowiak, R. S. J. (1991). A Direct Demonstration of Functional Specialisation in Human Visual Cortex. *Journal of Neuroscience* **11**, 641-649.

Zeki, S. M. (1969). Representation of Central Visual Fields in Prestiate Cortex of Monkey. *Brain Research* **14**, 271-291.

Zeki, S. M. (1973). Colour coding in the rhesus monkey prestriate cortex. *Brain Research, Amsterdam* **53**, 422-427.

Zeki, S. M. (1974). Functional Organisation of a Visual area in the Posterior Bank of the Superior Temporal Sulcus of the Rhesus Monkey. *Journal of Physiology* **236**, 549-573.

Zeki, S. M. (1977). Colour coding in the superior temporal sulcus of rhesus moneky visual cortex. *Proceedings of the royal society of London, B* **197**, 195-223.

Zeki, S. M. (1978a). Functional specialisation in the visual cortex of the rhesus monkey. *Nature* **274**, 423-428.

Zeki, S. M. (1978b). The cortical projections of foveal striate cortex in the rhesus monkey. *Journal of Physiology* **277**, 227-244.

Zeki, S. M. (1978c). The third visual complex of rhesus monkey prestriate cortex. *Journal of Physiology* **277**, 245-272.

Zeki, S. M. (1978d). Uniformity and diversity of structure and function in rhesus monkey prestriate visual cortex. *Journal of Physiology* **277**, 273-290.

Zeki, S. M. (1983a). Colour coding in the cerebral cortex: the reaction of cells in monkey visual cortex to wavelength and colours. *Neuroscience* **9**, 741-765.

Zeki, S. M. (1983b). The distribution of wavelength and orientation cells in different areas of monkey visual cortex. *Proceedings of the Royal Society of London, B,* **217**, 449-470.

Zeki, S. M. (1993). 'A vision of the brain.' (Blackwell: Oxford.)

Zeki, S. M. and Shipp, S. (1988). The functional logic of cortical connections. *Nature* **335**, 311-317.

APPENDICES

Appendix I.

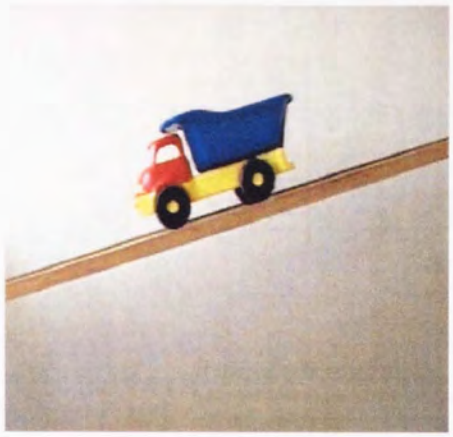

Implied Motion Pictures

Implied Static Pictures

Examples of stimuli used in the implied motion condition

Appendix II.

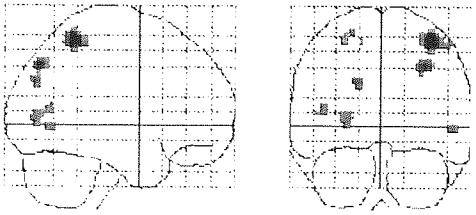

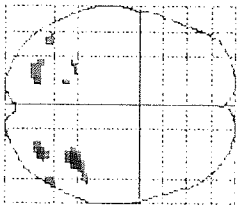

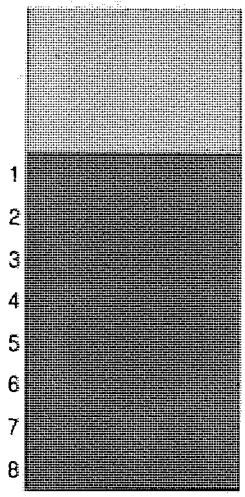

Design Matrix

P values & statistics: /mnt/scratch28/fawcett/hold

region	size {k}	Pseudo-t(T_{max} >= u)		{x,y,z} mm
1	83	3.53	0.004	36 -51 60
		2.90	0.039	51 -39 57
2	31	3.22	0.008	33 -75 42
3	19	3.02	0.027	-18 -78 30
4	12	2.92	0.035	54 -66 0
5	28	2.91	0.035	-27 -78 3
6	10	2.87	0.043	-24 -48 63
		2.79	0.047	-30 -51 57
7	10	2.85	0.043	-45 -66 12
8	2	2.72	0.047	-15 -54 60

alpha = 0.0500, df = 7 Critical threshold = 2.7070
Volume = 141448 3.00x 3.00x 3.00 mm voxels
Design: Multisubject, 1 scan per subj: 8(subj)
Perms: 256 permutations of conditions, bhPerms=1
Pseudo-t: Variance smoothed with FWHM [1000x1000x1000] mm

SnPM output for the video-motion v video-static condition for the 10-20Hz frequency band, 0-2000ms following stimulus presentation.

Appendix III.

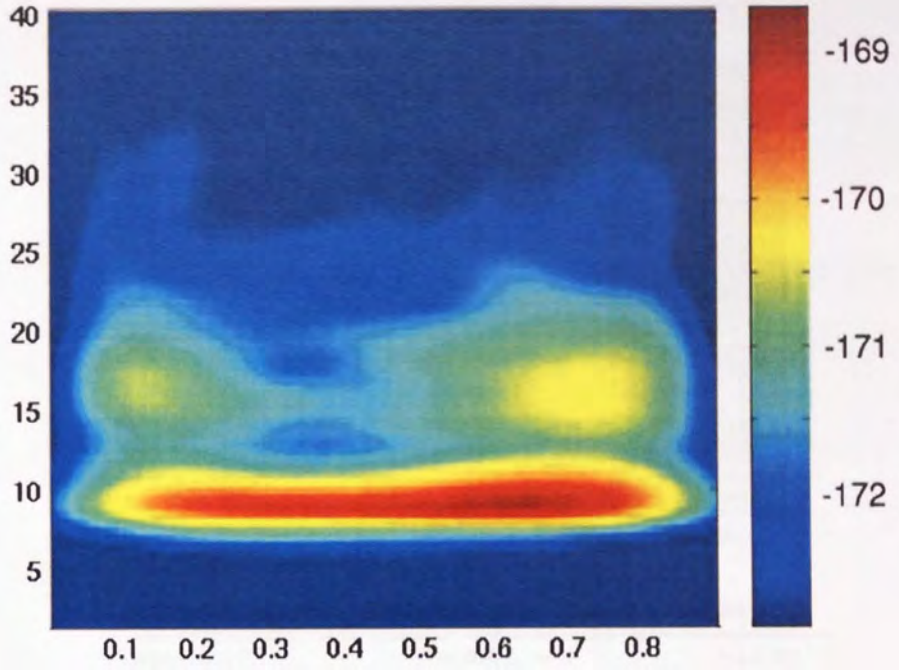

Time-frequency plot, averaged across all subjects (12 hemispheres) and calculated using Morlet wavelet analysis, from voxels showing the peak activation in left and right V5/MT . The plots show activation following presentation of blank pictures.

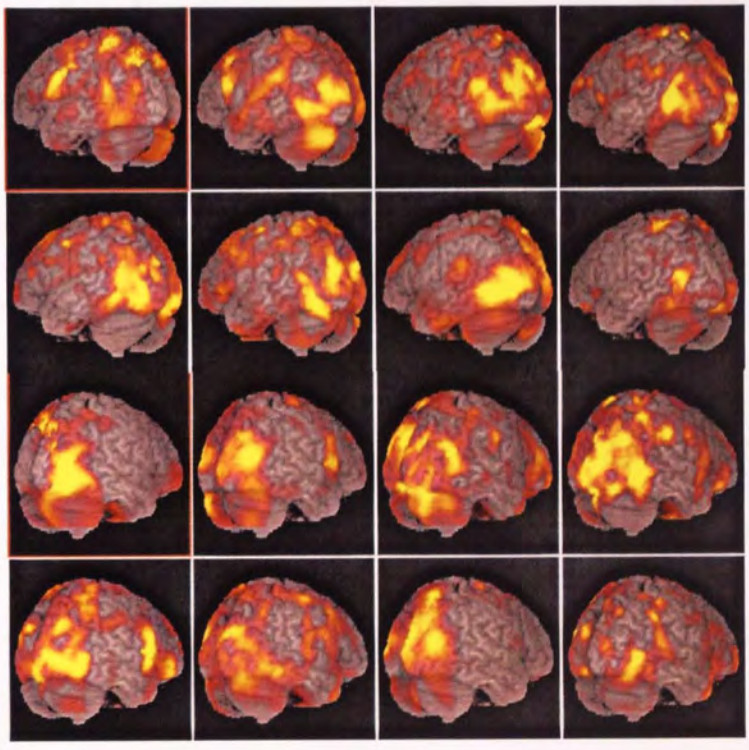

Individual responses from the left and right hemispheres for the implied-motion v blank condition in the 15-20Hz frequency band 100-300ms after stimulus presentation (threshold NAI = 2.0).

Appendix. IV.

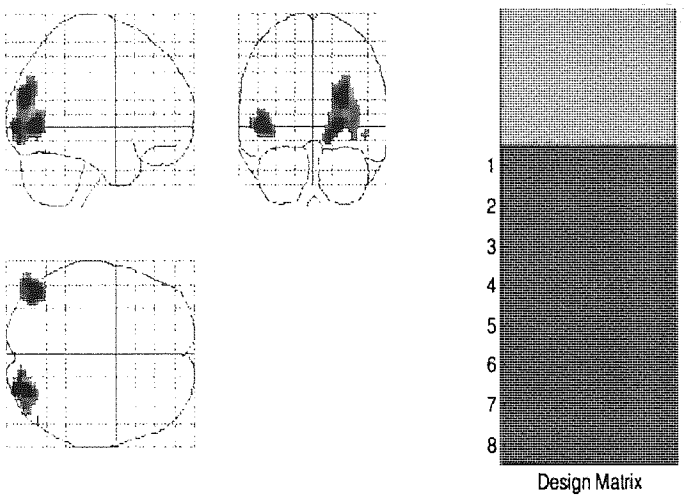

P values & statistics: ./impliedmotionvblank_0.1-0.3_15-20hz_1000

region	size {k}	PseudoP(T_{max} >= u)		{x,y,z} mm
1	**425**	**2.01**	**0.004**	**27 -81 21**
		2.00	0.004	21 -90 0
		1.87	0.004	15 -87 -6
2	**195**	**1.94**	**0.004**	**-48 -75 3**
3	**6**	**1.61**	**0.020**	**48 -72 -6**

SnPM output for the implied-motion v blank condition for the 15-20Hz frequency band, 100-300ms following stimulus presentation.

Appendix V

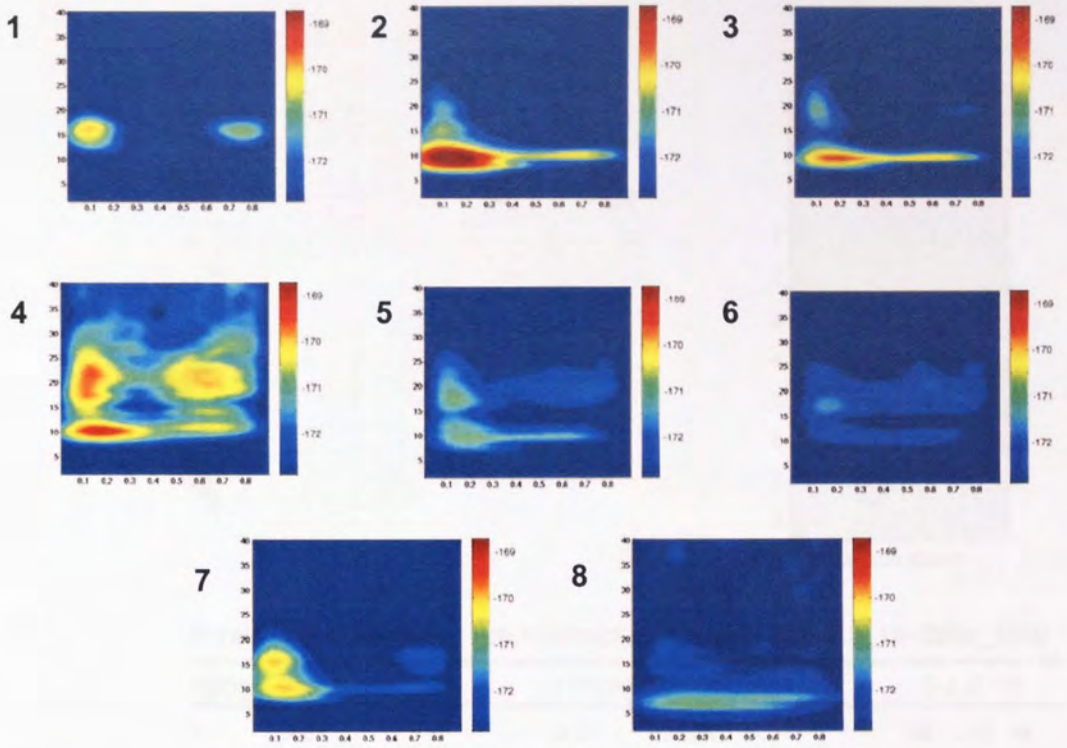

Individual time frequency plots for the implied-motion data in figure 4.5

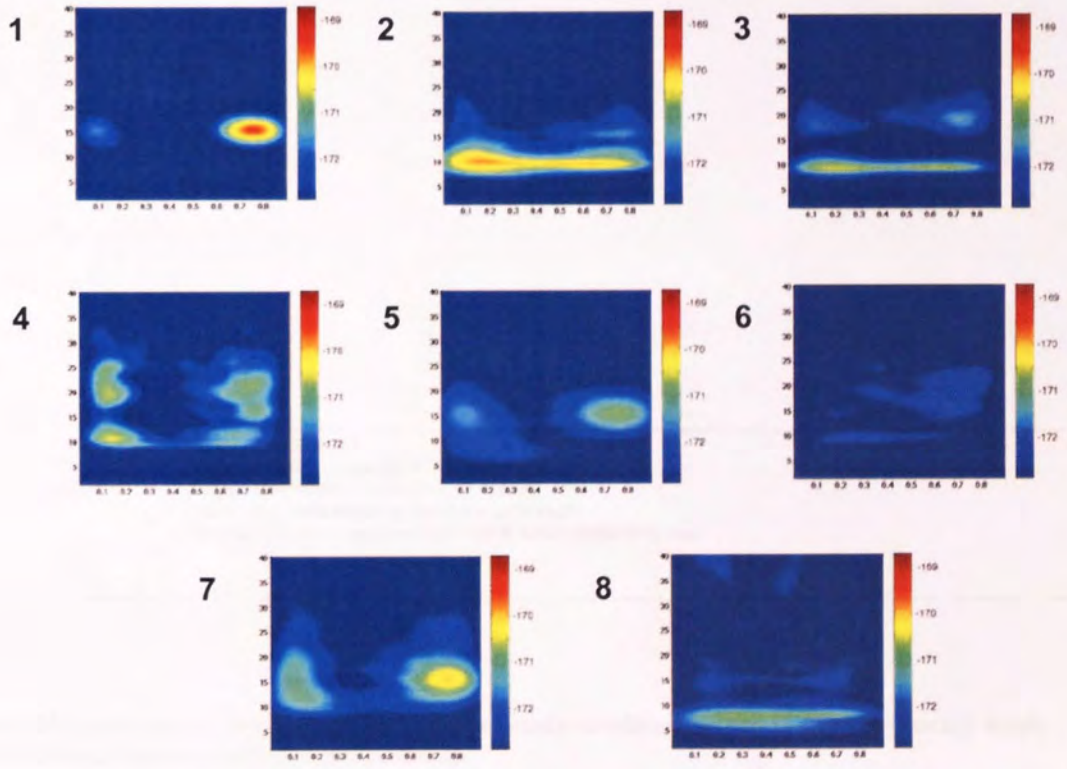

Individual time frequency plots for the implied-static condition in figure 4.5

Appendix VI.

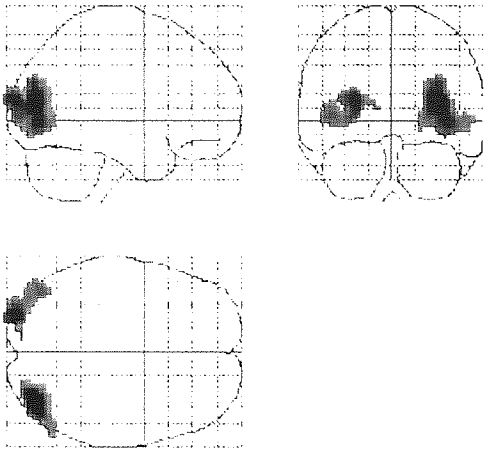

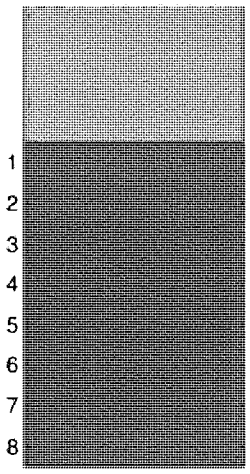

Design Matrix

P values & statistics: ./impliedmotionvcontrol_0.1-0.3_15-20hz_1000

region	size {k}	Pseudo-t (T_{max} >= u)		{x,y,z} mm
1	**566**	**2.21**	**0.004**	**36 -78 15**
		2.09	0.008	39 -78 3
		1.80	0.031	54 -66 3
2	**325**	**2.08**	**0.008**	**-27 -96 15**
		1.90	0.020	-45 -75 3
		1.82	0.031	-39 -84 0

alpha = 0.0500, df = 7 Critical threshold = 1.6619
Volume = 140757 3.00x 3.00x 3.00 mm voxels
Design: Multisubject, 1 scan per subj: 8(subj)
Perms: 256 permutations of conditions, bhPerms=1
Pseudo-t. Variance smoothed with FWHM [1000x1000x1000] mm

SnPM output for the implied-motion v implied-static condition for the 15-20Hz frequency band, 100-300ms following stimulus presentation.

Appendix VII

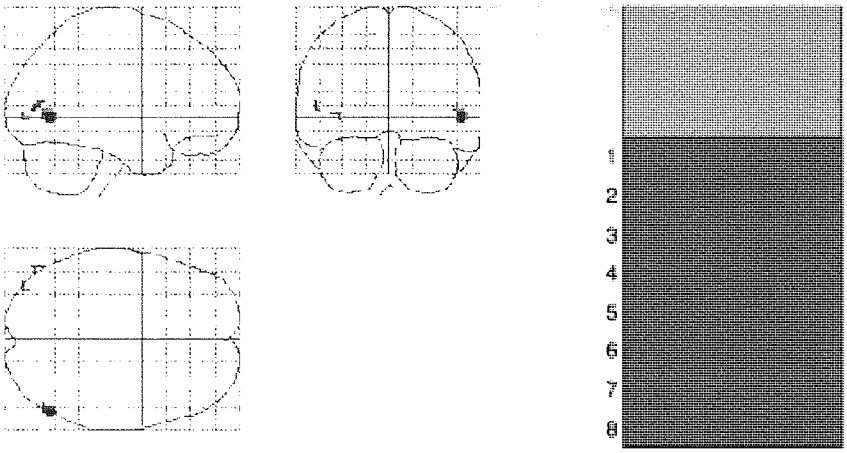

Design Matrix

P values & statistics: ./impliedmotionvcontrol_0.6-0.9_15-20hz_1000

region	size (k)	Pseudo-t (T_{max} >= u)	P(T_{max} >= u)	{x,y,z} mm
1	23	1.46	0.016	54 -66 3
2	7	1.39	0.031	-54 -72 12
3	5	1.38	0.031	-36 -87 3

alpha = 0.0500, df = 7 Critical threshold = 1.3511
Volume = 140733 3.00x 3.00x 3.00 mm voxels
Design: Multisubject, 1 scan per subj: 8(subj)
Perms: 256 permutations of conditions, bhPerms=1
Pseudo-t: Variance smoothed with FWHM [1000x1000x1000] mm

SnPM output for the implied-motion v implied-static condition for the 15-20Hz frequency band, 700-900ms following stimulus presentation.

Appendix VIII.

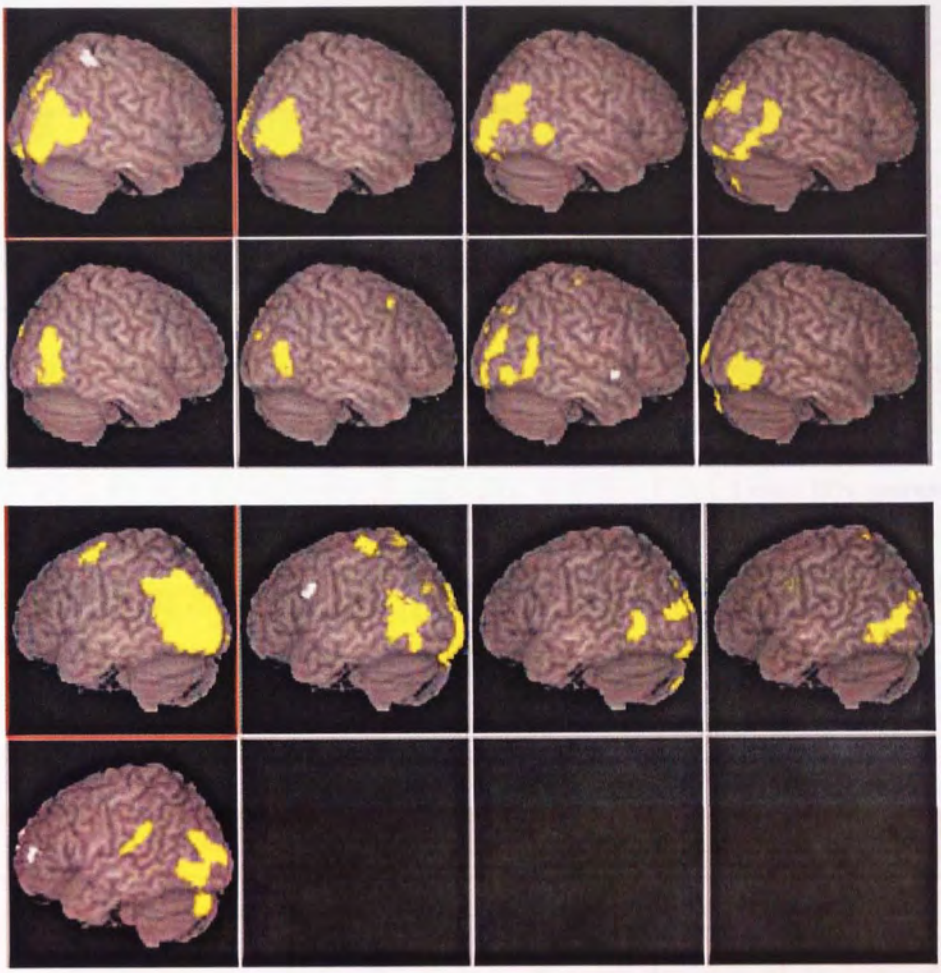

Individual responses from the left and right hemispheres for the implied-motion v implied static condition in the 15-20Hz frequency band, 100-300ms after stimulus presentation (threshold NAI = 2.0)

Appendix IX

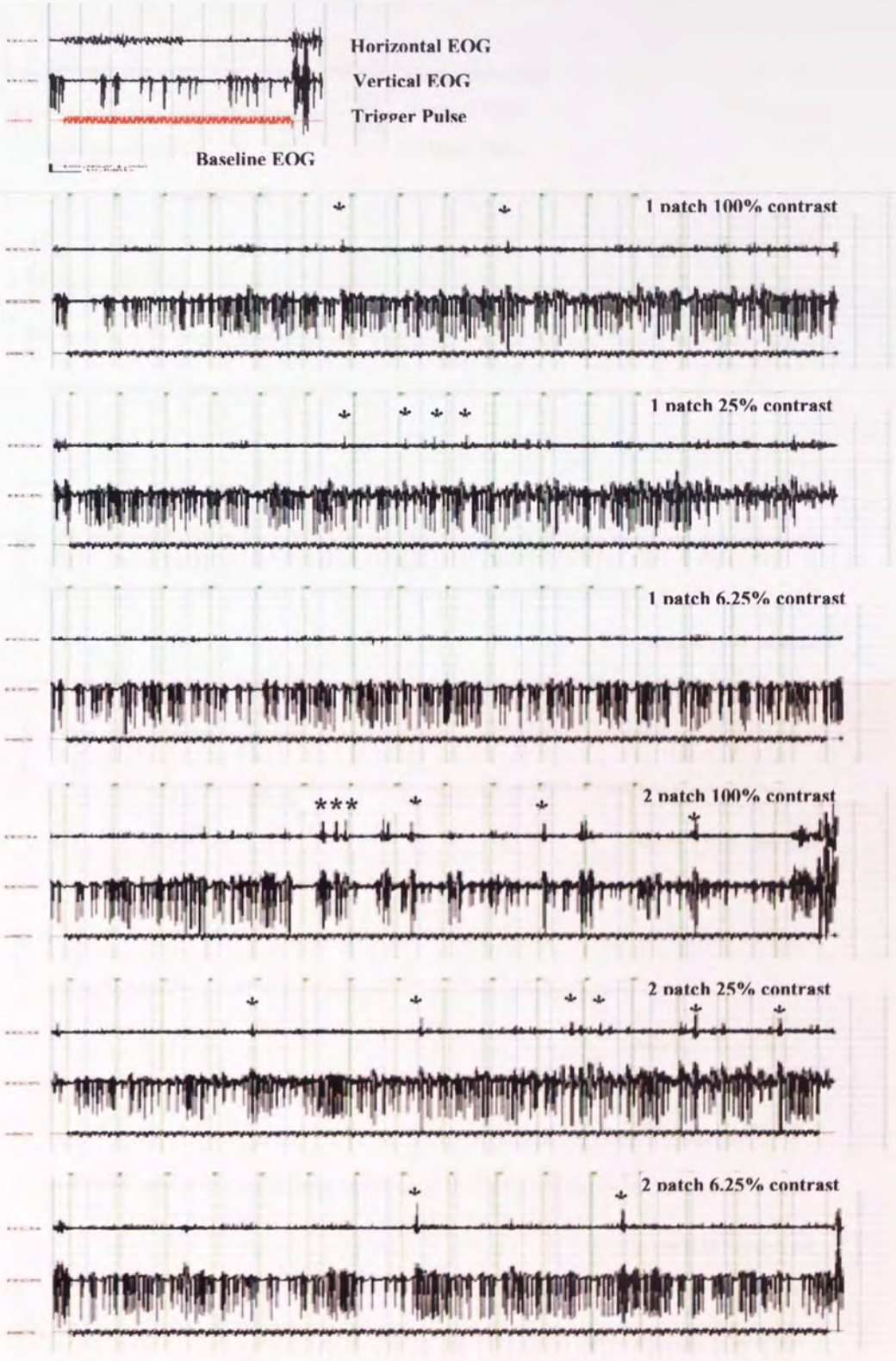

EOG recording from subject 2

Appendix X

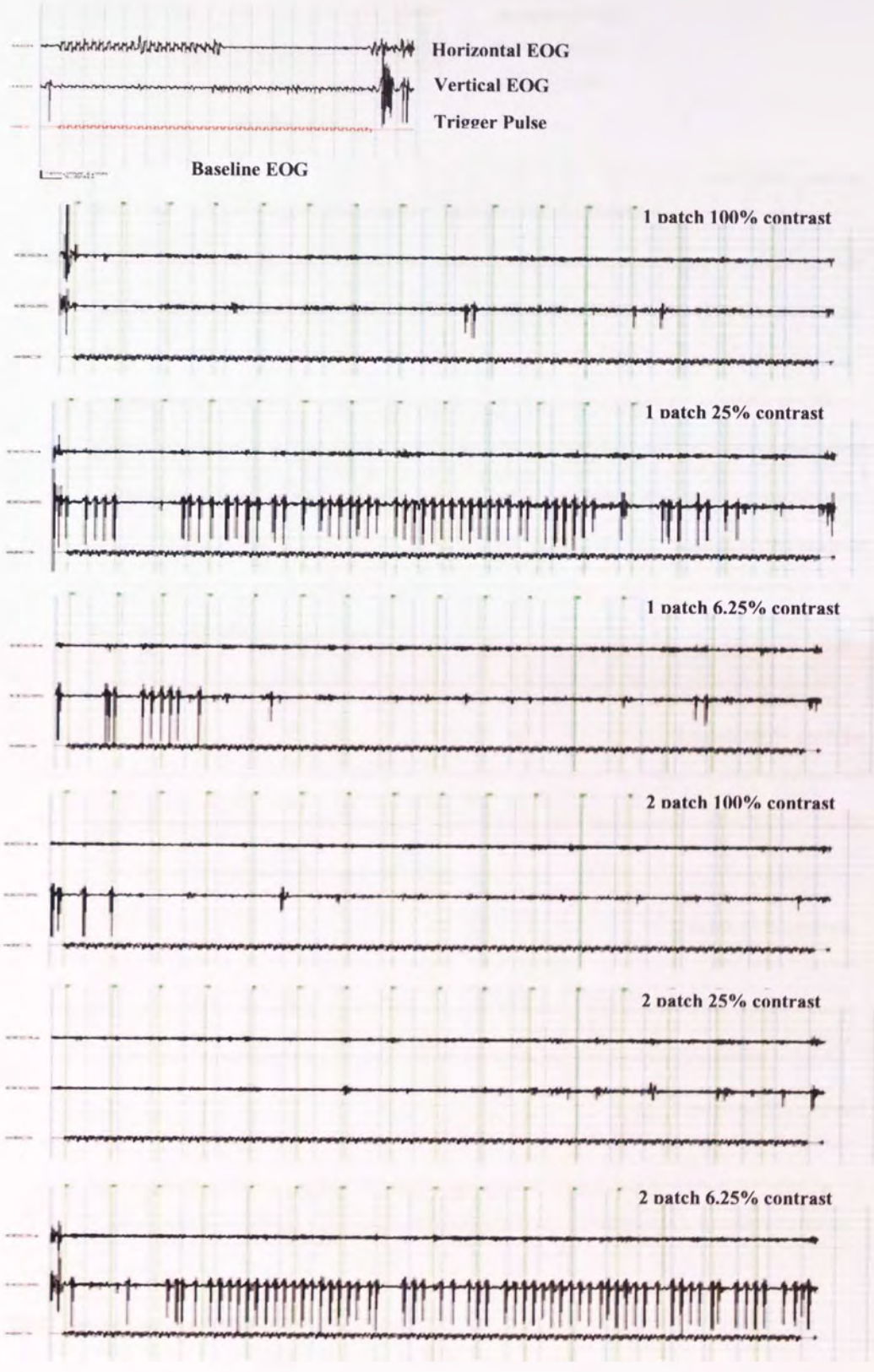

EOG recording from subject 3

Appendix XI

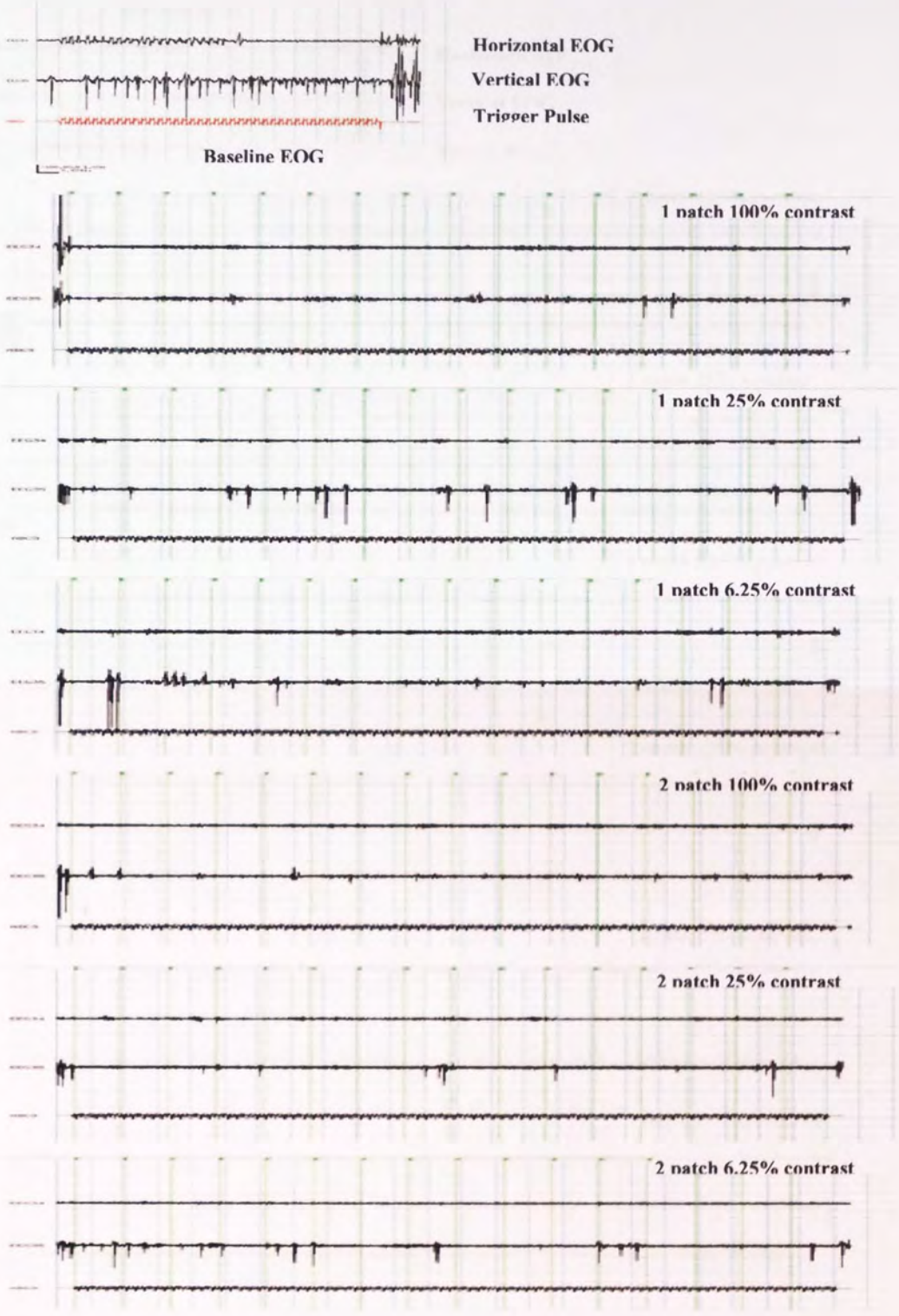

EOG recording from subject 4

Appendix XII

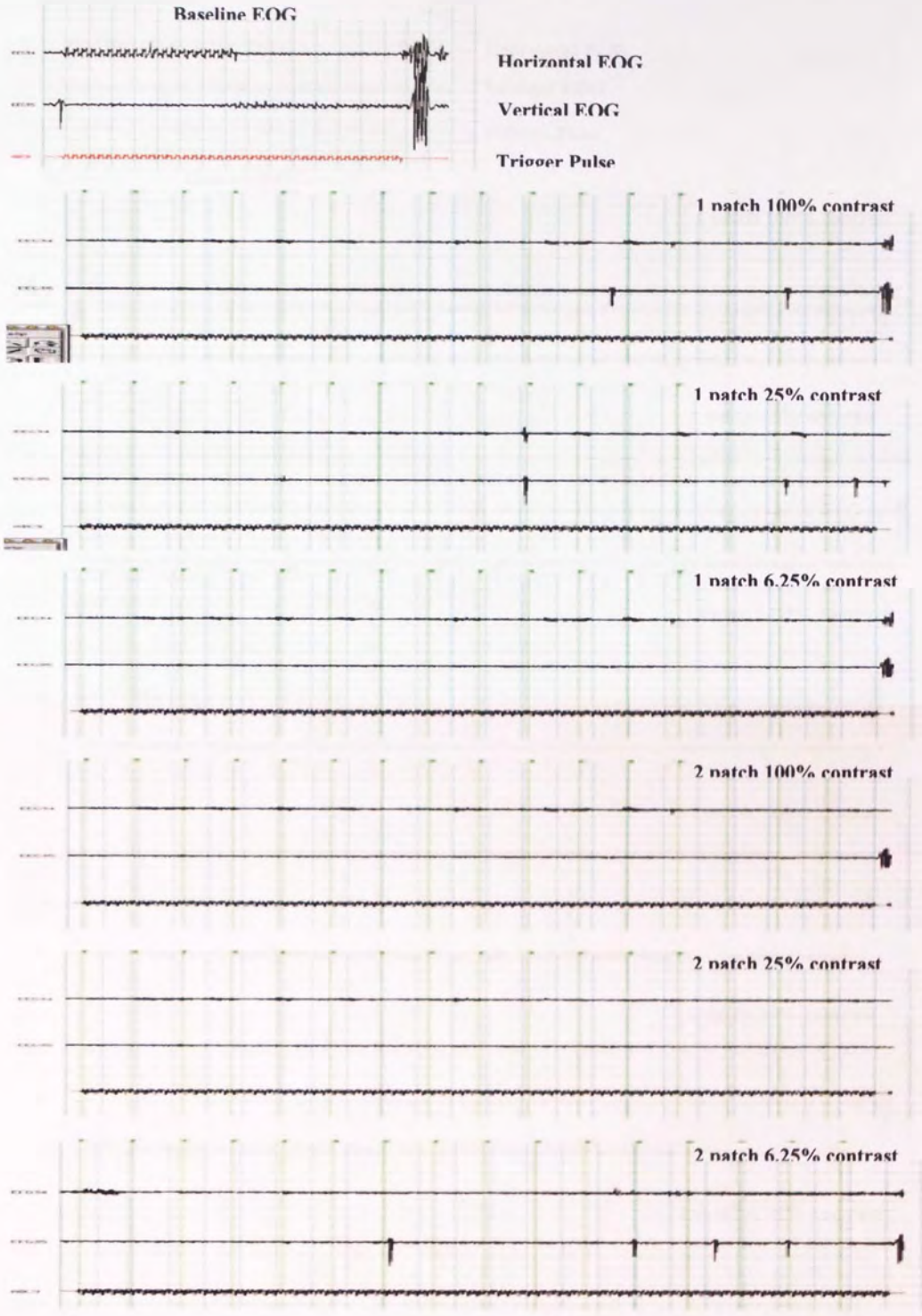

EOG recording from subject 5

Appendix XIII

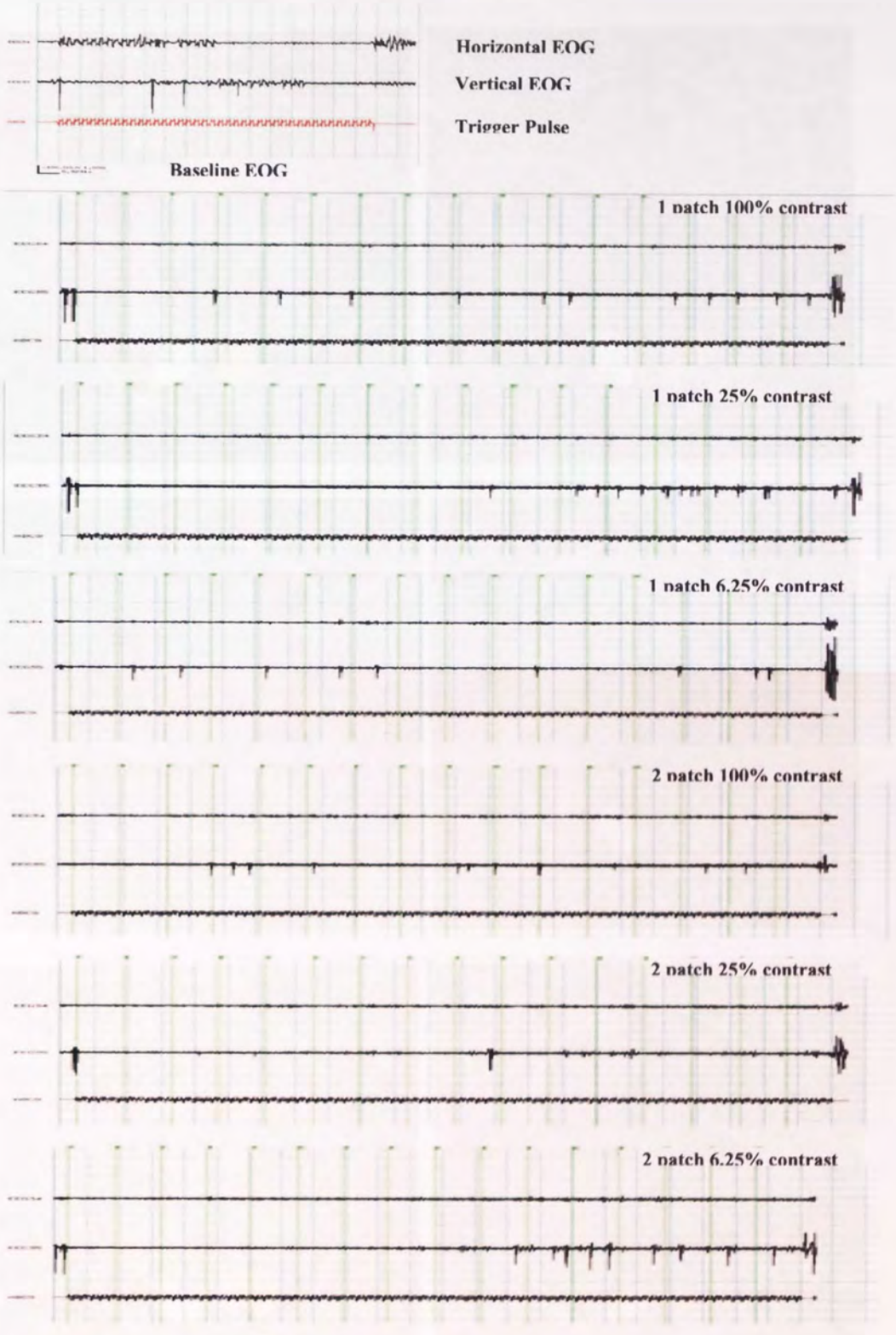

EOG recording from subject 6

Appendix XIV

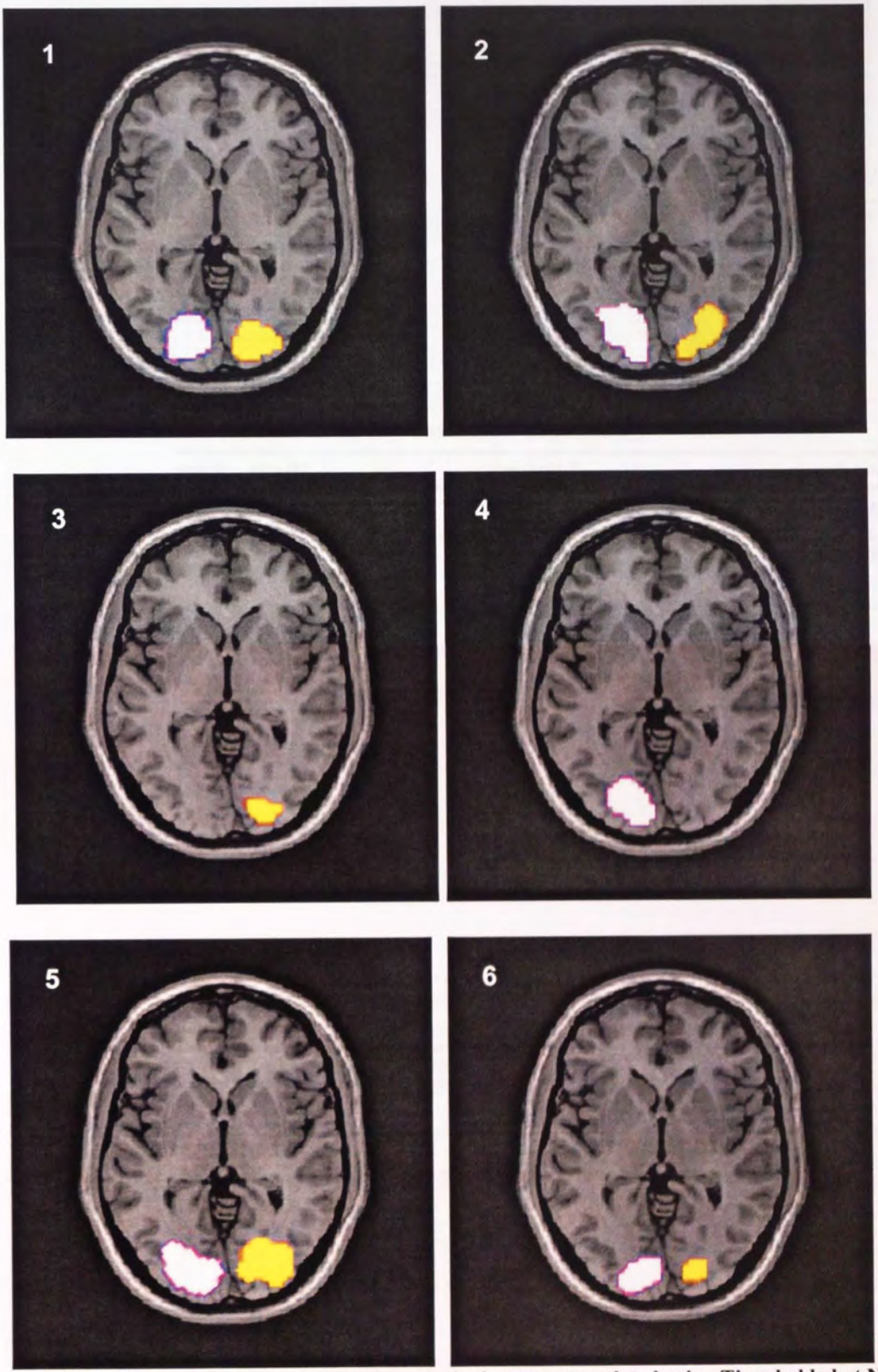

Individual responses from 1-patch block analysis shown on template brain. Thresholded at NAI = 2. For an explanation of activation colours see Figure 5-6.

Appendix XV

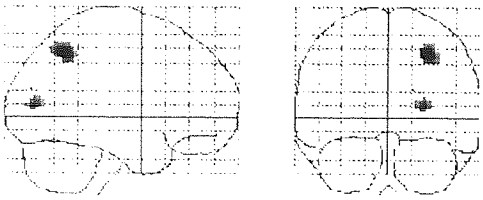

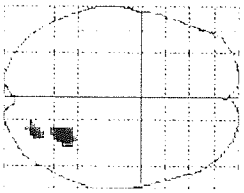

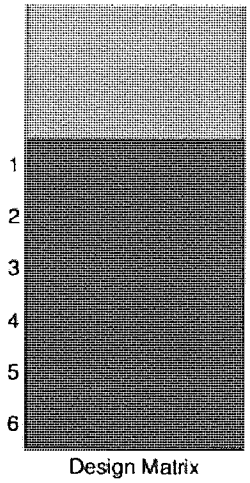

Design Matrix

P values & statistics: ./attention_snpm/100_1

region	size (k)	Pseudo-t (T_{max} >= u)	P(T_{max} >= u)	{x,y,z} mm
1	88	7.27	0.016	30 –57 48
2	29	6.75	0.016	27 –78 9
3	1	5.96	0.047	18 –81 21

alpha = 0.0500, df = 5 Critical threshold = 5.8648
Volume = 141893 3.00x 3.00x 3.00 mm voxels
Design: Multisubject, 1 scan per subj: 6(subj)
Perms: 64 permutations of conditions, bhPerms=1
Pseudo-t: Variance smoothed with FWHM [50x50x50] mm

SnPM output for the attend-right – attend-left block analysis in the 8-13Hz frequency band

Appendix XVI

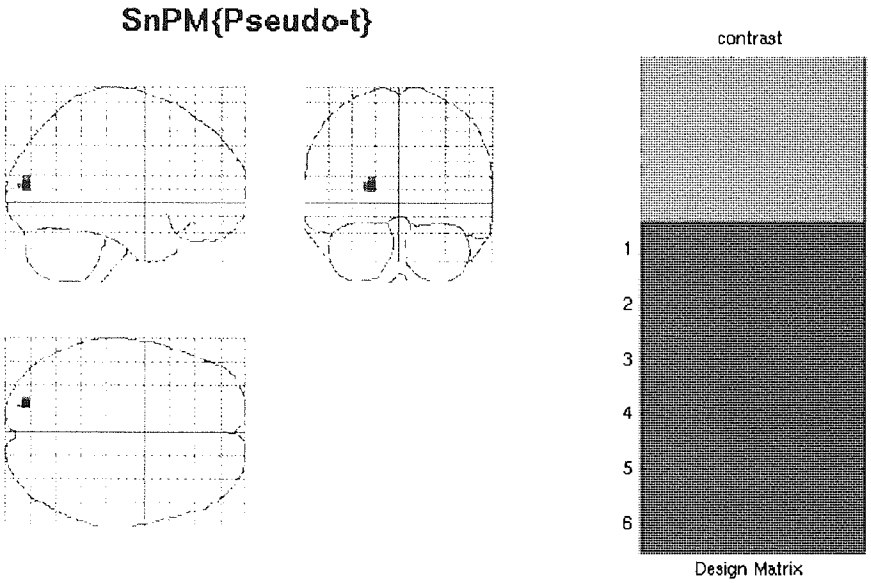

P values & statistics: ./attention/attention_snpm/100_1_8-13Hz

region	size {k}	Pseudo-t	P(T_{max} >= u)	{x,y,z} mm
1	21	7.74	0.031	-18 -87 15

alpha = 0.0500, df = 5 Critical threshold = 6.9869
Volume = 141893 3.00x 3.00x 3.00 mm voxels
Design: Multisubject, 1 scan per subj: 6(subj)
Perms: 64 permutations of conditions, bhPerms=1
Pseudo-t: Variance smoothed with FWHM [50x50x50] mm

SnPM output for attend-left – attend-right block analysis in the 8-13Hz frequency band

Appendix XVII

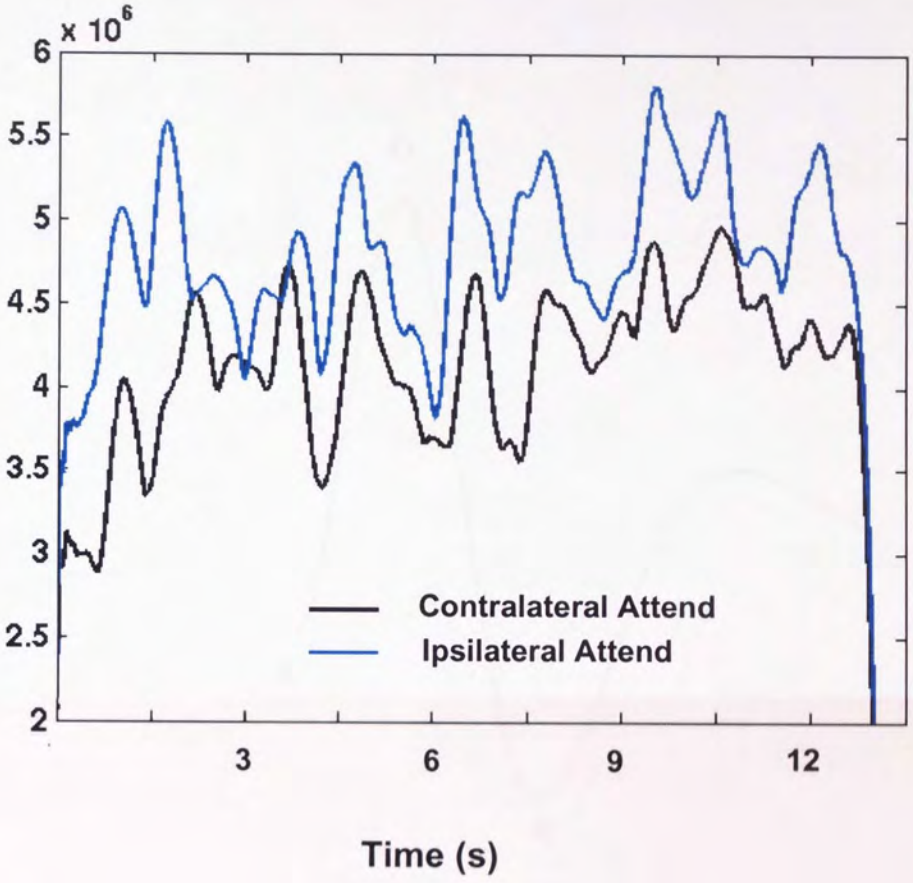

Measurement of mean induced cortical activity in the 8-13Hz frequency band, for the 2 patch condition block analysis, averaged across contrast conditions, hemispheres and subjects.

Appendix XVIII

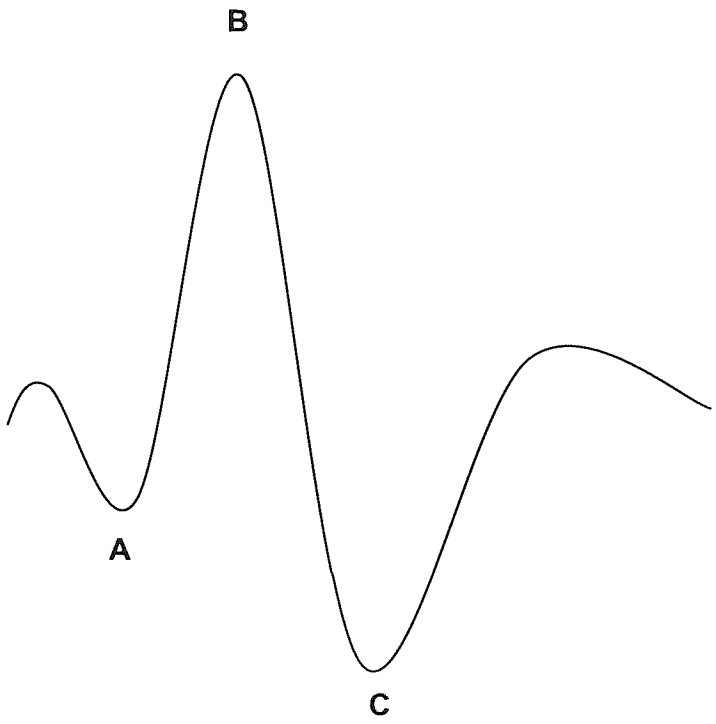

$$\text{Amplitude} = \frac{(B-A) + (B-C)}{2}$$

Schematic of evoked potential showing how amplitude was calculated in Figure 5-19

PUBLICATIONS

• Human Brain Mapping 23:120–127(2004) •

Realistic Spatial Sampling for MEG Beamformer Images

Gareth R. Barnes,* Arjan Hillebrand, Ian P. Fawcett, and Krish D. Singh

Neurosciences Research Institute, Aston University, Birmingham, United Kingdom

ELSEVIER

NeuroImage

www.elsevier.com/locate/ynimg
NeuroImage 21 (2004) 1542–1553

The temporal frequency tuning of human visual cortex investigated using synthetic aperture magnetometry

Ian P. Fawcett, Gareth R. Barnes, Arjan Hillebrand, and Krish D. Singh*

The Wellcome Trust Laboratory for MEG studies, Neurosciences Research Institute, Aston University, Birmingham B4 7ET, UK

Received 6 August 2003; revised 16 October 2003; accepted 31 October 2003